



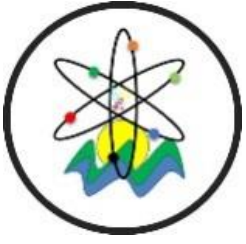
Black Sea Journal of Engineering and Science

Volume 7 | Issue 1



ISSN: 2619 - 8991


BS Journals



BLACK SEA JOURNAL OF ENGINEERING AND SCIENCE
(BSJ ENGIN SCI)


BS Journals

Black Sea Journal of Engineering and Science (BSJ Eng Sci) is a double-blind peer-reviewed, open-access international journal published electronically 6 times (January, March, May, July, September, and November) in a year by since January 2018. It publishes, in English and Turkish, full-length original research articles, innovative papers, conference papers, reviews, mini-reviews, rapid communications or technical note on advances in a wide range of scientific disciplines from all fields of engineering and science and from any source.

ISSN 2619 - 8991

Phone: +90 362 408 25 15

Fax: +90 362 408 25 15

Email: bsjsci@blackseapublishers.com

Web site: <http://dergipark.gov.tr/bsengineering>

Sort of publication: Periodically 6 times (January, March, May, July, September, and November) in a year

Publication date and place: January 15, 2024 - Samsun, TURKEY

Publishing kind: Electronically

OWNER

Assoc. Prof. Dr. Uğur ŞEN

DIRECTOR IN CHARGE

Prof. Dr. Hasan ÖNDER

EDITORIAL DECLARATION

Dear authors and readers,

First of all, we would like to thank you for being our travel companion by writing, evaluating, and reading us about this broadcasting life we started six years ago. With these thoughts, we are especially thankful for researchers and academicians honoring with the articles, valuable scientists involved in editorial boards, and reviewers for their contributions to the evaluation processes through their opinions/ideas/contributions/criticisms. With this article, we wanted to inform you, our valuable stakeholders, about the development of The Black Sea Journal of Engineering and Science (BSJ Eng Sci). The statistics of the BSJ Eng Sci for the last six years are given below. Hope you will be with us in future issues.

Year	Articles	Cites	Cite Index*	CNA	CNC	CCI
2018	20	1	0.05	20	1	0.05
2019	22	10	0.45	42	11	0.26
2020	29	40	1.38	71	51	0.72
2021	32	55	1.72	103	106	1.03
2022	24	95	3.96	127	201	1.58
2023	78	109	1.40	205	310	1.51

CNA= cumulative number of articles, CNC= cumulative number of cite, CCI= cumulative cite index

*according to Scholar Google

Rejection rate:

- 2020: 09%
- 2021: 18%
- 2022: 25%
- 2023: 14%

Average review time (days): 53

Average time from send to publish (days): 92

EDITOR BOARDS

EDITOR IN CHIEF

Prof. Dr. Hasan ÖNDER, Ondokuz Mayıs University, TÜRKİYE

Assoc. Prof. Dr. Uğur ŞEN, Ondokuz, Mayıs University, TÜRKİYE

SECTION EDITORS*

Prof. Dr. Ahmet UYANIK, Section Editor of Chemistry, Ondokuz Mayıs University, TÜRKİYE

Prof. Dr. Amila Sandaruwan RATNAYAKE, Section Editor of Geological Engineering, Uva Wellassa University, SRI LANKA

Prof. Dr. Berna KILIÇ, Section Editor of Fisheries Engineering, Ege University, TÜRKİYE

Prof. Dr. Çiğdem TAKMA, Section Editor of Statistics, Ege University, TÜRKİYE

Prof. Dr. Ertan BUYRUK, Section Editor of Mechanical Engineering, Sivas Cumhuriyet University, TÜRKİYE

Prof. Dr. Fahrul Zaman HUYOP, Section Editor of Biology, Universiti Teknologi Malaysia, MALAYSIA

Prof. Dr. Fauziatul FAJAROH, Section Editor of Chemical Engineering, Universitas Negeri Malang, INDONESIA

Prof. Dr. Fuad ALHAJOMAR, Section Editor of Electrical and Electronics Engineering, University of South Wales, UNITED KINGDOM

Prof. Dr. Gökhan CİVELEKOĞLU, Section Editor of Environmental Engineering, Akdeniz University, TÜRKİYE

Prof. Dr. Hasan TANAK, Section Editor of Physics, Amasya University, TÜRKİYE

Prof. Dr. Hasan TEMİZ, Section Editor of Food Engineering, Ondokuz Mayıs University, TÜRKİYE

Prof. Dr. Hojjat SADEGHİ-ALIABADI, Section Editor of Chemistry, Isfahan University, IRAN

Prof. Dr. İbrahim Özgür DENEME, Section Editor of Civil Engineering, Aksaray University, TÜRKİYE

Prof. Dr. İbrahim UĞUR, Section Editor of Mining Engineering, Süleyman Demirel University, TÜRKİYE

Prof. Dr. Jamrun EBBAH, Section Editor of Fisheries Engineering, Mindanao State University, PHILIPPINES

Prof. Dr. Messaoud SAIDANI, Section Editor of Civil Engineering, Coventry University, UNITED KINGDOM

Prof. Dr. Perarasu THANGAVELU, Section Editor of Aerospace Engineering, Anna University, INDIA

Prof. Dr. Sema PALAMUTCU, Section Editor of Textile Engineering, Pamukkale University, TÜRKİYE

Prof. Dr. Ümit Cafer YILDIZ, Section Editor of Forest Engineering, Karadeniz Technical University, TÜRKİYE

Assoc. Prof. Dr. Belgin KARABACAKOĞLU, Section Editor of Chemical Engineering, Eskişehir Osmangazi University, TÜRKİYE

Assoc. Prof. Dr. Bülent BOSTANCI, Section Editor of Geomatics Engineering, Erciyes University, TÜRKİYE

Assoc. Prof. Dr. Edit MİKÓ, Section Editor of Agricultural Engineering, University of Szeged, HUNGARY

Assoc. Prof. Dr. Ergün EKİCİ, Section Editor of Industrial Engineering, Çanakkale Onsekiz Mart University, TÜRKİYE

Assoc. Prof. Dr. Helal Uddin MOLLA, Section Editor of Physics, Rajshahi University of Engineering and Technology, BANGLADESH

Assoc. Prof. Dr. Kadyrbay CHEKİROV, Section Editor of Biology, Kyrgyz Turkish Manas University, KYRGYZSTAN

Assoc. Prof. Dr. Mehmet EBEOĞLUGİL, Section Editor of Metallurgical and Materials Engineering, Dokuz Eylül University, TÜRKİYE

Assoc. Prof. Dr. Nilüfer YURTAY, Section Editor of Computer Engineering, Sakarya University, TÜRKİYE

Assoc. Prof. Dr. Özgür Hakan AYDOĞMUŞ, Section Editor of Mathematics, Social Sciences University of Ankara, TÜRKİYE

Assoc. Prof. Dr. Rita ISMAİLOVA, Section Editor of Computer Engineering, Kyrgyz - Turkish Manas University, KYRGYZSTAN

Assoc. Prof. Dr. Samia Chehbi GAMOURA, Section Editor of Statistics, Strasbourg University, FRANCE

Assoc. Prof. Dr. Silvio DE OLIVEIRA JUNIOR, Section Editor of Mechanical Engineering, University of São Paulo, BRAZIL

Assoc. Prof. Dr. Sinan AKISKA, Section Editor of Geological Engineering, Ankara University, TÜRKİYE

Asst. Prof. Dr. Abdul JABBAR, Section Editor of Textile Engineering, National Textile University, PAKISTAN

Asst. Prof. Dr. Arsheed Ahmad RATHER, Section Editor of Forest Engineering, Annamalai University, INDIA

Asst. Prof. Dr. Ezenwanyi OCHULOR, Section Editor of Metallurgical and Materials Engineering, University Of Lagos, NIGERIA

Asst. Prof. Dr. Francis INEGBEDION, Section Editor of Industrial Engineering, University of Benin, NIGERIA

Asst. Prof. Dr. Haniyeh RASOULI PIROUZIAN, Section Editor of Food Engineering, Tabriz University, IRAN

Asst. Prof. Dr. Jun-wei LIM, Section Editor of Environmental Engineering, Universiti Teknologi Petronas, MALAYSIA

Asst. Prof. Dr. Mehmet GÜÇYETMEZ, Section Editor of Electrical and Electronics Engineering, Kırşehir Ahi Evran University, TÜRKİYE

Asst. Prof. Dr. Melahat CİHAN, Section Editor of Aerospace Engineering, Samsun University, TÜRKİYE

Asst. Prof. Dr. Muhammad GULİSTAN, Section Editor of Mathematics, Hazara University, PAKISTAN

Asst. Prof. Dr. Sedat KARADAVUT, Section Editor of Agricultural Engineering, Trakya University, TÜRKİYE

Asst. Prof. Dr. Seyedeh Narges SADATI, Section Editor of Mining Engineering, University of Mohaghegh Ardabili, IRAN

Asst. Prof. Dr. Xinyi WANG, Section Editor of Geomatics Engineering, Henan Polytechnic University, CHINA

* The ranking is arranged alphabetically within the academic title

EDITORIAL - ADVISORY BOARD*

Prof. Dr. Aglaia (Litsa) LIOPA-TSAKALIDI, Institute of Western Greece, GREECE

Prof. Dr. Ercan EFE, Kahramanmaraş Sutcu Imam University, TÜRKİYE

Prof. Dr. Mohammad Masood TARIQ, University of Balochistan, PAKISTAN

Prof. Dr. Mustafa Çağatay TUFAN, Ondokuz Mayıs University, TÜRKİYE

Prof. Dr. Özkan GÖRGÜLÜ, Ahi Evran University, TÜRKİYE

Assoc. Prof. Dr. Taner TUNÇ, Ondokuz Mayıs University, TÜRKİYE

Asst. Prof. Dr. Emil OMURZAK, Kyrgyz-Turkish Manas University, KYRGYZSTAN

Asst. Prof. Dr. Yılmaz KAYA, Ondokuz Mayıs University, TÜRKİYE

* The ranking is arranged alphabetically within the academic title

STATISTIC EDITOR

Prof. Dr. Mehmet TOPAL, Kastamonu University, TÜRKİYE

ENGLISH EDITOR

Asst. Prof. Dr. Betül ÖZCAN DOST, Ondokuz Mayıs University, TÜRKİYE

TURKISH EDITOR

Prof. Dr. Serkan ŞEN, Ondokuz Mayıs University, TÜRKİYE

REVIEWERS OF THE ISSUE*

Prof. Dr. Abbas GHASEMIZAD, University of Guilan, Department of Physics, Nuclear Energy Systems, IRAN

Prof. Dr. Hasan KORKMAZ, Ondokuz Mayıs University, Department of Biology, Ecology, TÜRKİYE

Prof. Dr. Nebile DAĞLIOĞLU, Department of Forensic Toxicology, Cukurova University, Türkiye

Prof. Dr. Recep Gökhan TÜRECI, Kırıkkale University, Department of Electronic and Automation, Nuclear Physics, TÜRKİYE

Prof. Dr. Salih YAZICIOĞLU, Department of Civil Engineering, Gazi University, TÜRKİYE

Prof. Dr. Şebnem ÖZÜPEK, Boğaziçi University, Department of Machinery, Finite Element Analysis, TÜRKİYE

Assoc. Prof. Dr. Ahmet TURAN, Yeditepe University, Department of Materials Science and Nanotechnology Engineering, Materials Science, TÜRKİYE

Assoc. Prof. Dr. Burcu ORALHAN, Nuh Naci Yazgan University, Department of Business Administration, Multiple Criteria Decision Making, TÜRKİYE

Assoc. Prof. Dr. Demet EROL, Gazi University, Department of City and Regional Planning, Urban Planning and Health, TÜRKİYE

Assoc. Prof. Dr. Edip ÇETKİN, Department of Mechanical Engineering, Batman University, TÜRKİYE

Assoc. Prof. Dr. Fatih KAR, Department of Biochemistry, Kütahya Health Sciences University, TÜRKİYE

Assoc. Prof. Dr. Hasan ARSLANOĞLU, Çanakkale Onsekiz Mart University, Department of Chemical Engineering, Polymer Science and Technologies, TÜRKİYE

Assoc. Prof. Dr. Kazım YILDIZ, Marmara University, Department of Computer Engineering, Data Mining and Knowledge Discovery, TÜRKİYE

Assoc. Prof. Dr. Mehmet Şeref SÖNMEZ, Istanbul Technical University, Department of Metallurgical and Materials Engineering, Materials Science and Technologies, TÜRKİYE

Assist. Prof. Dr. Ayşe Nilgün KAYADELEN, Kütahya Dumlupınar University, Department of Management Information Systems, Management Information Systems, TÜRKİYE

Assist. Prof. Dr. Bahadır DEMİREL, Department of Agricultural Machinery, Erciyes University, TÜRKİYE

Assist. Prof. Dr. Furkan GÜNDAY, Giresun University, Department of Civil Engineering, Structural Engineering, TÜRKİYE

Assist. Prof. Dr. Gökhan TIMAÇ, Department of Mechanical Engineering, Yalova University, TÜRKİYE

Assist. Prof. Dr. Hülya YALÇIN, Istanbul Technical University, Department of Machinery, Computer Vision, TÜRKİYE

Assist. Prof. Dr. Hüseyin BAYKAL, Recep Tayyip Erdoğan University, Department of Herbal and Animal Production, Medicinal and Aromatic Plants, TÜRKİYE

Assist. Prof. Dr. Hüseyin SAUK, Department of Agricultural Machinery, Ondokuz Mayıs University, TÜRKİYE

Assist. Prof. Dr. İpek ÇETINBAŞ, Eskişehir Osmangazi University, Department of Electrical and Electronics Engineering, Electrical Engineering, TÜRKİYE

Assist. Prof. Dr. Murat ALKAN, Dokuz Eylül University, Department of Metallurgical and Materials Engineering, Physics, TÜRKİYE

Assist. Prof. Dr. Nurullah ÖKSÜZER, Department of Civil Engineering, Karadeniz Technical University, TÜRKİYE

Assist. Prof. Dr. Orhan ECEMİŞ, Gaziantep University, Department of Computer Technologies, Quantitative Decision Methods, TÜRKİYE

Assist. Prof. Dr. Rukiye KOÇKAR TUĞLA, Department of Civil Engineering, Kastamonu University, TÜRKİYE

Assist. Prof. Dr. Seda BİÇE, Tokat Gaziosmanpaşa University, Department of Soil Sciences and Plant Nutrition, Plant Nutrition, TÜRKİYE

Assist. Prof. Dr. Yasin KIRELLİ, Kütahya Dumlupınar University, Department of Information Systems and Technologies, Multiple Criteria Decision Making, TÜRKİYE

Assist. Prof. Dr. Zehra Gülten YALÇIN, Çankırı Karatekin University, Department of Chemical Engineering, Composite and Hybrid Materials, TÜRKİYE

Dr. Abdurrahman BAYRAK, Hacettepe University, Department of Computer Engineering, Control Systems, TÜRKİYE

Dr. Ebru KARNEZ, Çukurova University, Department of Crop and Animal Production, Plant Nutrition and Soil Fertility, TÜRKİYE

Dr. Erkin ARSLAN, Middle East Technical University, Department of Electrical and Electronics Engineering, Control Systems, TÜRKİYE

* The ranking is arranged alphabetically within the academic title

Table of Contents

Research Articles

1. **YENİ BİR ÇOK KRİTERLİ KARAR VERME YAKLAŞIMI “OLABİLİRLİK DEĞERLENDİRME SİSTEMİ”: KATILIM FONLARI ÜZERİNE BİR UYGULAMA**
Furkan GÖKTAŞ, Fatih GÜÇLÜ.....1-8
2. **RADIATIVE TRANSFER EQUATION SOLUTION FOR MANY SCATTERING TYPES**
Dilek AYDIN, Halide KÖKLÜ.....9-15
3. **EFFECT OF CAF₂ ADDITIONS ON THE YIELD OF AZ63 MAGNESIUM CHIPS DURING REMELTING**
Pınar YÖRÜK, Mertol GÖKELMA.....16-20
4. **APPLICATION OF MULTI-CRITERIA DECISION MAKING METHODS FOR MENU SELECTION**
Semih Latif İPEK, Dilek GÖKTÜRK.....21-30
5. **PRODUCTION OF CHEMICALLY MODIFIED SHEAR THICKENING FLUIDS AND INVESTIGATION OF THEIR RHEOLOGICAL PROPERTIES**
Murat Yavuz SOLMAZ, Cenk YANEN, Celal KISTAK, Ercan AYDOĞMUŞ.....31-35
6. **KENDİNDEN TAHRİKLİ MİKRO ORGANİZMALARIN NEWTONYEN AKIŞKAN İÇİNDEKİ HAREKETİNİN SAYISAL MODELLENMESİ**
Hatice MERCAN, Tufan Tuna KÖSELER.....36-42
7. **ANATOMICAL, ECOLOGICAL AND TRICHOME MICRO-MORPHOLOGICAL FEATURES OF TWO MARRUBIUM L.TAXA (LAMIACEAE)**
Kamer Volkan KOÇAK, Nezahat KANDEMİR.....43-54
8. **SUGGESTIONS FOR URBAN TRANSFORMATION THROUGH TWO APPLICATIONS IN ANKARA, THE CAPITAL OF TÜRKİYE**
Varol KOÇ.....55-71
9. **DESIGN AND OPTIMIZATION OF VOLTAGE MODE PWM CONTROL OF DC-DC BUCK CONVERTER WITH A PI-LEAD COMPENSATOR USING THE SIMULATED ANNEALING ALGORITHM**
Kübra DOĞAN, Bülent DAĞ.....72-88
10. **PI-PD CONTROLLER DESIGN BASED ON WEIGHTED GEOMETRIC CENTER METHOD FOR TIME DELAY ACTIVE SUSPENSION SYSTEMS**
Abdullah TURAN, Hüseyin AGGUMUS, Mahmut DASKIN.....89-95
11. **AN INTEGRATED OVERVIEW OF BLASTING DAMAGE CRITERIA FOR ENGINEERING STRUCTURES**
Davut YILMAZ.....96-108
12. **VALORISATION OF THE EFFECT OF WASTE ALUMINUM SAWDUST ON CONCRETE: DURABILITY CHARACTERISTICS AND ENVIRONMENTAL IMPACTS**
Tuba DEMİR, Bahar DEMİREL, Melek ÖZTÜRK.....109-120

13. EFFECT OF DIFFERENT STEP-LAP JOINTS ON THE NATURAL FREQUENCIES OF DIFFERENT ADHESIVELY BONDED METALLIC MATERIALS: A NUMERICAL STUDY

Ali İhsan KAYA.....121-128

14. FALSE POSITIVES IN LUMINAL TESTING

Yakup GÜLEKÇİ, Fatma ÇAVUŞ YONAR.....129-138

Reviews

15. DOĞAL OLARAK BULUNAN KIRMIZI PİGMENT LİKOPEN VE SAĞLIĞA FAYDALI ETKİLERİ ÜZERİNE SİSTEMATİK BİR YOLCULUK

Güney AKINOĞLU, Arzu ERDAL.....139-154



YENİ BİR ÇOK KRİTERLİ KARAR VERME YAKLAŞIMI “OLABİLİRLİK DEĞERLENDİRME SİSTEMİ”: KATILIM FONLARI ÜZERİNE BİR UYGULAMA

Furkan GÖKTAŞ^{1*}, Fatih GÜÇLÜ¹

¹Karabük University, Faculty of Management, Department of Business, 78050, Karabük, Türkiye

Özet: Katılım hisse senedi şemsiye fonları, İslami finans ilkeleri çerçevesinde filtrelenmiş hisse senetlerine yatırım imkânı sağlayan bir yatırım alternatifidir. Olabilirlik teorisi karar vermede önemli bir araçtır. Bu çalışmada katılım hisse senedi şemsiye fonlarının karşılaştırılması gibi problemler için olabilirlik teorisine dayanan yeni bir çok kriterli karar verme (ÇKKV) yaklaşımı önerilmiştir. Bu yaklaşım Olabilirlik Değerlendirme Sistemi (PES) olarak adlandırılmıştır. PES, temel ÇKKV yöntemlerinden olan maksimin kuralı, ağırlıklı toplam yöntemi ve maksimaks kuralı ile ilişkilidir. Alternatiflerin öncelik vektörü PES ile tek olarak elde edilmektedir. Başka bir deyişle portföy seçimi problemi gibi çok amaçlı karar verme problemleri için tek bir çözüm vermektedir. PES, çok nitelikli karar verme problemleri için en yüksek önceliğe sahip alternatifin seçilmesine dayanmaktadır. PES, 31.07.2020 ve 30.12.2022 arasında Türkiye’de işlem gören beş farklı katılım hisse senedi şemsiye fonunun gerçek veri seti kullanılarak tanıtılmıştır. Yapılan uygulamada, PES’in bu temel yöntemlerden daha fazla bilgi ortaya koyduğu gözlemlenmiştir.

Anahtar kelimeler: Bulanık sayı, Çok kriterli karar verme, İslami finans, Katılım fonları, TOPSIS, Portföy seçimi


A New Multi-Criteria Decision Making Approach “Possibilistic Evaluation System”: An Application on Participation Funds


Abstract: Participation stock umbrella funds are an investment alternative that provides the opportunity to invest in stocks filtered within the framework of Islamic finance principles. Possibility theory is an important tool in decision making. In this study, we propose a new multi-criteria decision making (MCDM) approach based on possibility theory for problems such as comparing participation stock umbrella funds. We call this approach as the Possibilistic Evaluation System (PES). PES is related to the maximin rule, weighted sum method and maximax rule, which are the elementary MCDM methods. We uniquely derive alternatives’ priority vector with PES. In other words, it gives a unique solution for multi-objective decision making problems such as portfolio selection. It depends on selecting the alternative having the highest priority for multi-attribute decision making problems. We illustrate PES by using the real data set of five different participation stock umbrella funds traded in Türkiye between 31.07.2020 and 30.12.2022. In our application, we observe that PES reveals more information than these elementary methods.

Keywords: Fuzzy number, Multi-criteria decision making, Islamic finance, Participation funds, TOPSIS, Portfolio selection

*Sorumlu yazar (Corresponding author): Karabük University, Faculty of Management, Department of Business, 78050, Karabük, Türkiye

E mail: furkangoktas@karabuk.edu.tr (F. GÖKTAŞ)

Furkan GÖKTAŞ  <https://orcid.org/0000-0001-9291-3912>

Fatih GÜÇLÜ  <https://orcid.org/0000-0002-1007-4594>

Gönderi: 11 Ağustos 2023

Kabul: 27 Ekim 2023

Yayınlanma: 15 Ocak 2024

Received: August 11, 2023

Accepted: October 27, 2023

Published: January 15, 2024

Cite as: Göktaş F, Güçlü F. 2024. A new multi-criteria decision making approach “possibilistic evaluation system”: An application on participation funds. BSJ Eng Sci, 7(1): 1-8.

1. Giriş

COVID-19 pandemi sürecinin ardından tüm dünyada etkisini gösteren yüksek enflasyon, şirketlerin büyük bir kısmına pozitif anlamda yansımış, piyasada bollaşan para talebe dönüşerek şirketlerin finansal tablolarına olumlu anlamda etki etmiş, bu durum şirketlerin piyasa değerlerine de yansımıştır. Türkiye özelinde faizlerin düşüklüğü ve kur korumalı mevduat sisteminin etkisiyle altın ve döviz kurunun da sabit bir seyir izlemesi nedeniyle ellerindeki paranın alım gücünü korumak isteyen kişilerin hisse senedi piyasalarına olan ilgisi artmıştır. Türkiye’de 2020 Mart ayında yaklaşık 1 milyon 350 bin kişi olan hisse senedi yatırımcı sayısı, 2023 Eylül ayı itibarıyla yaklaşık 7 milyon 800 bine ulaşmıştır (MKK, 2023).

Hisse senedi yatırımları tasarruf sahipleri tarafından bireysel olarak yapılabileceği gibi, profesyonel fon yöneticileri tarafından yönetilen ve pek çok yatırımcıdan katılım belgeleri ile fon toplayan yatırım fonları aracılığıyla da gerçekleştirilebilir. Türkiye’de hisse senedi yatırım fonları, hisse senedi şemsiye fonları adı altında faaliyet göstermektedir. Hisse senedi şemsiye fonlarının bir türü de katılım hisse senedi şemsiye fonlarıdır. Portföyünün büyük bir kısmı, İslami finans ilkeleri uyarınca yapılan filtreleme sonucu İslami açıdan uygun olduğu belirlenen hisse senetlerinden oluşan bu fonlar, tahvil, bono ya da türev ürünler gibi konvansiyonel yatırım araçlarına portföylerinde yer verememektedirler. Hisse senetlerinin filtrelenmesi sürecinde, borsaya kote şirketler öncelikle faaliyet alanı açısından izlenmekte,



İslam finans ilkelerine göre faaliyette bulunulması yasak olan alanlarda (alkollü içecek, tütün ürünleri, faizli bankacılık, domuz ve domuz ürünleri vb.) faaliyet gösteren şirketlerin hisse senetleri dışarıda bırakılmaktadır. Sonraki süreçte ise faaliyet alanı açısından uygun olan şirketler, faizli borç, faizli alacak ve İslami açıdan uygun olmayan geliri ölçen oranlar aracılığıyla ikinci bir filtrelemeye tabi tutulmaktadır.

Portföy seçimi gibi birçok alanda oldukça geniş bir kullanım yelpazesi olan bulanık mantık Zadeh (1965)'in çalışmasında tanıtılmıştır. Bunlardan biri olan olabilirlik teorisi Zadeh (1978)'in çalışmasında önerilmiştir. Söz konusu teori, Dubois ve Prade (1988)'nin çalışmasında geliştirilmiştir. Diğer belirsizlik teorilerine oranla olabilirlik teorisinin kullanım kolaylığı vardır (Dubois, 2006). Bu nedenle söz konusu teori birçok alanda kullanılmaktadır. Bunlardan biri ÇKKV problemleridir (Fuller ve Harmati, 2018).

ÇKKV, yöneylem araştırmasının bir alt dalıdır ve bakış açısına göre tarihi eskiye veya yeniye dayanabilir. ÇKKV, sürekli problemler için çok amaçlı karar verme (ÇAKV) olarak adlandırılırken kesikli problemler için çok nitelikli karar verme (ÇNKV) olarak adlandırılır (Zavadskas ve ark., 2014). ÇKKV problemleri, satırlarında alternatifler olan sütunlarında kriterler olan bir karar matrisi ile temsil edilebilir (Taherdoost ve Madanchian, 2023). Karar matrisinin normalizasyonunda orana dayalı normalizasyon gibi çeşitli yöntemler kullanılabilir (Vafaei ve ark., 2017). ÇKKV problemleri için en çok kullanılan iki temel yöntem, ağırlıklı toplam ve ağırlıklı çarpım yöntemleridir (El Gibari ve ark., 2019). İyimser yaklaşıma dayanan maksimaks kuralı ve kötümser yaklaşıma dayanan maksimin kuralı da temel yöntemlerdendir (Moghaddam ve ark., 2011). Bu çalışmada olabilirlik teorisine dayanan yeni bir ÇKKV yaklaşımı önerilmiştir. Bu yaklaşım; maksimin kuralı, ağırlıklı toplam yöntemi, maksimaks kuralıyla ilişkilidir ve tanımı gereği söz konusu temel yöntemlere oranla daha fazla bilgi ortaya koymaktadır.

Literatürde olabilirlik teorisine dayanan birçok ÇKKV yaklaşımı önerilmiştir. Bulanık kümelerin oldukça kompleks uzantılarının kullanıldığı Wan ve Li (2013), Yi ve Li (2018), Garai ve ark. (2020), Foroozesh ve ark. (2022), Garai ve Gark (2022), Reig-Mullor ve Salas-Molino (2022) çalışmaları bunlara örnek olarak verilebilir. Bu çalışmada önerilen PES'in söz konusu çalışmalardan temel farkları bulanık kümelerin özel hali olan ve kullanım kolaylığına sahip olan bulanık sayılara dayanması ve söz konusu temel yöntemlerle ilişkili olmasıdır. PES'e benzer şekilde olabilirlik teorisi ve bulanık sayılardan yararlanarak TOPSIS yönteminin farklı uzantılarını oluşturan Ye ve Li (2014) ile Wang ve ark. (2015) ise söz konusu çalışmalardan ayrılmaktadır. Uygulama açısından bu çalışma ile benzerlik taşıyan Deng ve Yuan (2021) çalışmasında ise olabilirlik teorisi ve bulanık sayılardan yararlanarak ve hedef programlama kullanılarak portföy seçimi yapılmıştır. Bu çalışmanın devamı şu şekilde organize edilmiştir.

Bölüm 2'de, PES olarak kısaltılan Olabilirlik Değerlendirme Sisteminin teorik altyapısı oluşturulmuştur. Bölüm 3'te, 31.07.2020 ve 30.12.2022 arasında Türkiye'de işlem gören beş farklı katılım hisse senedi şemsiye fonunun gerçek veri seti kullanılarak PES tanıtılmıştır. Bölüm 4'teki son değerlendirmelerle çalışma sonuçlandırılmıştır.

2. Materyal ve Yöntem

Karar matrisinin (A) orana dayalı normalizasyonu aşağıda gösterilmiştir (Eşitlik 1). Burada a_{ij} , A matrisinin i. satır j. sütun elemanı iken β_j (α_j), A matrisinin j. sütununun eş değeri olarak j. kriterin en iyi (kötü) değeridir. Başka bir deyişle fayda (maliyet) yönlü kriter için β_j değeri, sütunun en yüksek (düşük) değeridir. Normalize edilmiş karar matrisinin (B) tüm elemanları [0,1] aralığında değer alır (Vafaei ve ark., 2017).

$$b_{ij} = \frac{|a_{ij} - \alpha_j|}{|\beta_j - \alpha_j|}, \forall i, j \quad (1)$$

Kriterlerin ağırlık vektörünü (x) belirlemek için birçok yöntem kullanılabilir. Analitik Hiyerarşi Süreci (AHS), bunlardan biridir (Odu, 2019). Bu yöntemle kriterlerin ağırlıklarını en doğru şekilde belirlemek için kriterlerin pozitif ikili karşılaştırma matrisinin Perron vektörü kullanılmalıdır. Perron vektörü, elemanları pozitif olan kare matrisin özvektörleri içinde tüm elemanları pozitif olan tek özvektördür. Bu özvektörle ilişkili olan özdeğer, bu matrisin en büyük özdeğeridir ve ikili karşılaştırmaların tutarlılığını belirlemede kullanılır (Saaty, 2003; Alonso ve Lamata, 2006).

Uyarı: Bu çalışmada kriterlerin ağırlık vektörü bulunurken bulanık AHS yerine orijinal AHS'nin kullanılmasının temel nedeni, ikili karşılaştırma matrislerini bulanıklaştırmanın değil iyi yargılarda bulunmanın kararın geçerliliğini artırmasıdır (Saaty ve Tiran, 2007). Kriterlerin ağırlık vektörünü bulmak için AHS'den farklı yöntemler de kullanılabilir.

Ağırlıklı toplam yönteminde, B matrisinin her bir satırı için ağırlıklı toplam değerleri bulunduktan sonra ağırlıklı toplam değeri en yüksek olan alternatif seçilir. Burada kriterlerin ağırlık vektörü olan x vektörü kullanılır (Sorooshian ve Parsia, 2019). Maksimaks kuralında, B matrisinin her bir satırı için satırın en yüksek değeri iyimserlik düzeyi olarak atanır ve en yüksek iyimserlik düzeyine sahip alternatif seçilir. ÇNKV için maksimin kuralı, B matrisinin her bir satırının en düşük değerinin güvenlik düzeyi olarak atanması ve en yüksek güvenlik düzeyine sahip alternatife seçilmesidir (Moghaddam ve ark., 2011). ÇAKV için maksimin kuralı, aşağıdaki doğrusal programlama ile verilebilir (Eşitlik 2). Burada w vektörü, alternatiflerin ağırlık vektörüdür (Sikalo ve ark., 2022).

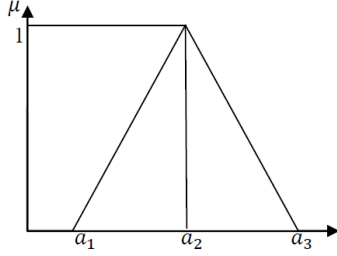
Üçgensel bulanık sayılar, üç parametre ile temsil edilir. (a_1, a_2, a_3) üçgensel bulanık sayısının üyelik fonksiyonunun grafiği Şekil 1'deki gibidir (Ali ve ark., 2016).

maks v

$$\text{öyle ki } \sum_{i=1}^n B_{ij} w_i \geq v, \forall j$$

$$\sum_{i=1}^n w_i = 1$$

$$w_i \geq 0, \forall i$$



Şekil 1. Üçgensel bulanık sayının üyelik fonksiyonunun grafiği.

Alternatifin güvenlik düzeyi ($b_{i,1}$), ağırlıklı toplam değeri ($b_{i,2}$) ve iyimserlik düzeyi ($b_{i,3}$) kullanılarak, i . alternatifin faydasının ($b_{i,1}, b_{i,2}, b_{i,3}$) üçgensel bulanık sayısı ile verilen olabilirlik dağılımı oluşturulsun. Fuller ve ark. (2011) çalışmasında verilen olabilirlik ortalaması ve varyansı tanımları ağırlık fonksiyonu 1'e eşit iken kullanıldığında, w vektörüne karşı gelen olabilirlik ortalaması ve varyansı sırasıyla Eşitlik 3'teki gibi bulunur (Göktaş ve Duran, 2019).

$$E_p \left(\sum_{i=1}^n w_i (b_{i,1}, b_{i,2}, b_{i,3}) \right) = \sum_{i=1}^n w_i \left(\frac{b_{i,1} + 2b_{i,2} + b_{i,3}}{4} \right)$$

$$Var_p \left(\sum_{i=1}^n w_i (b_{i,1}, b_{i,2}, 1) \right) = \sum_{i=1}^n w_i^2 \left(\frac{1 - b_{i,1}}{6} \right)^2$$

Uyarı: Bu tanımlar, Laplace'nin yetersiz neden prensibine ve sürekli düzgün olasılık dağılımına dayanmaktadır (Dubois, 2006; Fuller ve ark., 2011). Olabilirlik varyansının hesabında $b_{i,3}$ yerine 1 kullanılmasının nedeni, olabilirlik varyansının aşağı yönlü bir risk ölçüsüne benzer sonuç vermesini sağlamaktır.

Olabilirlik teorisi, olasılık teorisi ve bulanık küme teorisi ile ilişkilidir. Söz konusu teori, kesin olmayan olasılık için alt ve üst sınırları belirler (Dubois, 2006). Buna göre i . alternatifin faydasının, ($b_{i,1}, b_{i,2}, b_{i,3}$) üçgensel bulanık sayısı ile verilen olabilirlik dağılımının herhangi bir α -kesmesinde olmasının olasılığının alt ve üst sınırları sırasıyla $1-\alpha$ ve 1 olarak bulunur. Ayrıca faydanın $[b_{i,1}, b_{i,3}]$ kapalı aralığında olmasının olasılığı 1'dir (Göktaş ve Duran, 2019).

Bu çalışmada önerilen PES ile bulunan alternatiflerin öncelik vektörü (w^*), aşağıda verilen maksimizasyon probleminin optimal sonucudur. Başka bir deyişle w^* vektörü, olabilirlik ortalaması olabilirlik standart sapmasına bölüldüğünde elde edilen ve olabilirlik performansı olarak adlandırılan $P(w)$ fonksiyonunu maksimum yapar (Eşitlik 4).

$$\text{maks } P(w) := \frac{\sum_{i=1}^n w_i \left(\frac{b_{i,1} + 2b_{i,2} + b_{i,3}}{4} \right)}{\sqrt{\sum_{i=1}^n w_i^2 \left(\frac{1 - b_{i,1}}{6} \right)^2}}$$

$$\text{öyle ki } \sum_{i=1}^n w_i = 1$$

$$w_i \geq 0, \forall i$$

Eşitlik 4'teki negatif değer almayan amaç fonksiyonu, w vektörünün homojen fonksiyonu olduğundan Eşitlik 5'teki kesin konveks kuadratik minimizasyon probleminin tek optimal çözümü standardize edildiğinde yani elemanları toplamına bölüldüğünde Eşitlik 4'ün tek optimal çözümü elde edilir (Goldfarb ve Iyengar, 2003; Tütüncü ve Koenig, 2004).

$$\min \sum_{i=1}^n \frac{1}{2} w_i^2 \left(\frac{1 - b_{i,1}}{6} \right)^2$$

$$\text{öyle ki } \sum_{i=1}^n w_i \left(\frac{b_{i,1} + 2b_{i,2} + b_{i,3}}{4} \right) = 1$$

$$w_i \geq 0, \forall i$$

Eşitlik 5'in optimal çözümü MATLAB gibi paket programlarla bulunabilir. Burada w vektörünün elemanları için negatif olmama kısıdı kaldırıldığında aşağıdaki kesin konveks kuadratik minimizasyon problemi elde edilir. Eşitlik 6'nın tek optimal çözümü Lagrange çarpanları yöntemi yardımıyla bulunabilir. Eğer Eşitlik 6'nın optimal çözümünün tüm elemanları negatif olmayan değerler alıyorsa bu çözüm Eşitlik 5'in de optimal çözümüdür ve dolayısıyla alternatiflerin öncelik vektörü Eşitlik 6'nın optimal çözümünün standardize edilmiş halidir.

$$\min \sum_{i=1}^n \frac{1}{2} w_i^2 \left(\frac{1 - b_{i,1}}{6} \right)^2$$

$$\text{öyle ki } \sum_{i=1}^n w_i \left(\frac{b_{i,1} + 2b_{i,2} + b_{i,3}}{4} \right) = 1$$

λ , Lagrange çarpanı iken Eşitlik 6 için Lagrange fonksiyonu Eşitlik 7'deki gibi oluşturulur.

$$L(w, \lambda) = \frac{1}{2} \sum_{i=1}^n w_i^2 \left(\frac{1 - b_{i,1}}{6} \right)^2 - \lambda \left[\sum_{i=1}^n w_i \left(\frac{b_{i,1} + 2b_{i,2} + b_{i,3}}{4} \right) - 1 \right]$$

Eşitlik 6'nın tek optimal çözümü, λ 'ya bağlı olarak aşağıdaki gibi bulunur. Eşitlik 6'daki kısıdın sağlanabilmesi için λ 'nın pozitif olması gerektiği açıktır. Orana dayalı normalizasyon yöntemi ile elde edilen B matrisinin elemanları pozitif olduğundan tüm w_i 'ler de pozitifdir.

$$\frac{\partial L(w, \lambda)}{\partial w_i} = w_i \left(\frac{1 - b_{i,1}}{6} \right)^2 - \lambda \left(\frac{b_{i,1} + 2b_{i,2} + b_{i,3}}{4} \right) = 0, \forall i$$

$$\rightarrow w_i = 9\lambda \frac{(b_{i,1} + 2b_{i,2} + b_{i,3})}{(1 - b_{i,1})^2}, \forall i$$

Eşitlik 8 ile verilen, Eşitlik 6'nın tek optimal çözümü standardize edildiğinde aşağıdaki bilgi elde edilir. Buna göre i. alternatifin öncelik değeri Eşitlik 9'daki gibidir ve görüldüğü üzere $b_{i,1}$, $b_{i,2}$, $b_{i,3}$ parametrelerinin kesin artan fonksiyonudur.

$$w_i^* = \frac{1}{\sum_{i=1}^n \frac{b_{i,1} + 2b_{i,2} + b_{i,3}}{(1-b_{i,1})^2}}, \forall i \quad (9)$$

Bu çalışmada önerilen PES'in adımları şu şekildedir.

Adım 1: Karar matrisi (A) oluşturulur.

Adım 2: (1) ifadesi ile A normalize edilir ve normalize edilmiş karar matrisi (B) oluşturulur.

Adım 3: Kriterlerin ağırlıklı vektörü (x), AHS gibi bir yöntem ile belirlenir.

Adım 4: B matrisinin i. satırının güvenlik düzeyi ($b_{i,1}$), ağırlıklı toplam değeri ($b_{i,2}$) ve iyimserlik düzeyi ($b_{i,3}$) kullanılarak i. alternatifin faydası için ($b_{i,1}$, $b_{i,2}$, $b_{i,3}$) üçgensel bulanık sayısı ile verilen olabirlik dağılımı oluşturulur.

Adım 5: (4) ifadesinin optimal sonucu olan alternatiflerin öncelik vektörü (w^*) (9) ifadesi ile bulunur.

Adım 6: i. ÇNKV problemlerinde en yüksek önceliğe sahip alternatif seçilir.

ii. ÇAKV problemlerinde öncelik vektörü, kaynakların alternatiflere dağıtılmasında kullanılabilir. Öncelik vektörü, olabirlik performansını maksimum yapan kaynak dağıtım planına karşı gelir.

Öncelik vektörü (9) ile verilen PES'in; kötümser yaklaşıma dayanan maksimum kuralı, iyimser yaklaşıma dayanan maksimum kuralı ve en çok kullanılan temel yöntemlerden olan ağırlıklı toplam yönteminden elde edilen bilgileri olabirlik teorisinden ve üçgensel bulanık sayılardan yararlanarak sentezlediği söylenebilir.

3. Bulgular ve Tartışma

Çalışma kapsamına 31.07.2020 ve 30.12.2022 arasında Türkiye'de işlem gören Ziraat portföye ait ZPE fonu, Albaraka portföye ait RBH fonu, Mükafat portföye ait MPS fonu, KT portföye ait KPC fonu ve QInvest portföye ait ELZ fonu dahil edilmiştir. Söz konusu fonlar, katılım hisse senedi şemsiye fonlarının karşılaştırılması ÇKKV problemi için alternatiflerdir. Bu problem için kriterler ise Güçlü (2022)'nin çalışmasında olduğu gibi belirlenmiştir. Buna göre kriterler; ortalama getiri (K1), bilgi oranı (K2), Sharpe oranı (K3), Treynor oranı (K4), standart sapma (K5) ve beta katsayısı (K6) olarak sıralanabilir. Bunlardan ilk dördü fayda yönlü kriter iken son ikisi maliyet yönlü kriterdir. Söz konusu ÇKKV probleminin çözümünde PES kullanılmıştır.

Adım 1: Belirtilen tarihler arasında alternatiflerin haftalık getiri verileri kullanılarak oluşturulan karar matrisi (A) Tablo 1'deki gibidir.

Adım 2: Orana dayalı normalizasyon kullanılarak oluşturulan normalize edilmiş karar matrisi (B) Tablo 2'deki gibidir. K6 hariç tutulduğunda, RBH diğer alternatiflerden üstün iken KPC de RBH ve ZPE dışındaki alternatiflerden üstündür.

Adım 3: AHS'de kriterlerin ikili karşılaştırma matrisi Tablo 3'teki gibi oluşturulmuştur. Bu matrisin Perron vektörünü bulmak için MATLAB paket programı kullanılmıştır. Buna göre kriterlerin ağırlık vektörü (x) AHS ile (0,1291, 0,1291, 0,3185, 0,3185, 0,0524, 0,0524)^T sütun vektörü olarak bulunmuştur. İkili karşılaştırmaların tutarlılık oranı 0,0123 olarak hesaplanmıştır. Burada 0,0123 < 0,1 olduğundan yapılan ikili karşılaştırmalar tutarlıdır (Saaty ve Vargas, 2012).

Adım 4: Tablo 2'deki bilgiler doğrultusunda i. alternatif için güvenlik düzeyi ($b_{i,1}$), ağırlıklı toplam değeri ($b_{i,2}$) ve iyimserlik düzeyi ($b_{i,3}$) Tablo 4'teki gibi bulunmuştur.

Tablo 1. Karar matrisi

	K1	K2	K3	K4	K5	K6
ZPE	0,0133	-0,0025	0,3148	0,0127	0,0316	0,7844
RBH	0,0144	0,0333	0,3600	0,0161	0,0307	0,6840
MPS	0,0117	-0,0518	0,2586	0,0110	0,0323	0,7573
KPC	0,0135	0,0052	0,3169	0,0138	0,0321	0,7401
ELZ	0,0081	-0,1060	0,0965	0,0090	0,0495	0,5301

Tablo 2. Normalize edilmiş karar matrisi

	K1	K2	K3	K4	K5	K6
ZPE	0,8238	0,7431	0,8285	0,5134	0,9524	0
RBH	1	1	1	1	1	0,3950
MPS	0,5690	0,3893	0,6152	0,2814	0,9160	0,1064
KPC	0,8633	0,7986	0,8364	0,6665	0,9219	0,1743
ELZ	0	0	0	0	0	1

Tablo 3. Kriterlerin ikili karşılaştırma matrisi

	K1	K2	K3	K4	K5	K6
K1	1	1	1/3	1/3	3	3
K2	1	1	1/3	1/3	3	3
K3	3	3	1	1	5	5
K4	3	3	1	1	5	5
K5	1/3	1/3	1/5	1/5	1	1
K6	1/3	1/3	1/5	1/5	1	1

Tablo 4. PES için parametreler

	Güvenlik Düzeyi	Ağırlıklı Toplam D.	İyimserlik Düzeyi
ZPE	0	0,6796	0,9524
RBH	0,3950	0,9683	1
MPS	0,1064	0,4629	0,9160
KPC	0,1743	0,7507	0,9219
ELZ	0	0,0524	1

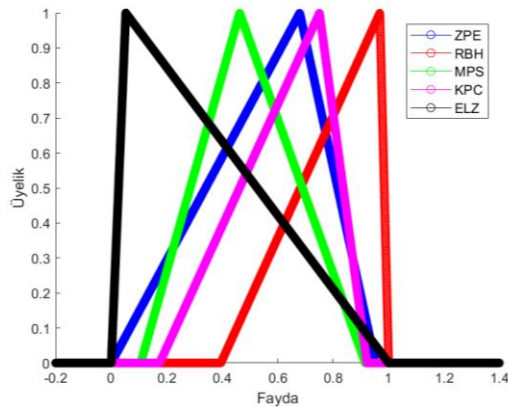
Tablo 5. Olabilirlik teorisine dayanan bilgiler

	Olabilirlik Ortalaması	Olabilirlik Varyansı	Ol Ort. / Ol. Var.
ZPE	0,5779	0,0278	20,80
RBH	0,8329	0,0102	81,92
MPS	0,4870	0,0222	21,96
KPC	0,6494	0,0189	34,29
ELZ	0,2762	0,0278	9,94

Tablo 4'teki bilgiler doğrultusunda alternatiflerin faydaları için aşağıdaki bilgiler verilebilir.

- ZPE için olabilirlik dağılımı (0, 0,6796, 0,9524) üçgensel bulanık sayısıdır.
- RBH için olabilirlik dağılımı (0,3950, 0,9683, 1) üçgensel bulanık sayısıdır.
- MPS için olabilirlik dağılımı (0,1064, 0,4629, 0,9160) üçgensel bulanık sayısıdır.
- KPC için olabilirlik dağılımı (0,1743, 0,7507, 0,9219) üçgensel bulanık sayısıdır.
- ELZ için olabilirlik dağılımı (0, 0,0524, 1) üçgensel bulanık sayısıdır.

Şekil 2'de bu üçgensel bulanık sayıların üyelik fonksiyonlarının grafikleri verilmiştir. Alternatiflerin renkleri sırasıyla mavi, kırmızı, yeşil, eflatun ve siyah olarak belirlenmiştir.



Şekil 2. Alternatiflerin faydaları için olabilirlik dağılımları.

Tablo 5'te, alternatiflerle ilgili bazı önemli bilgiler verilmiştir. (PES, (9) ifadesi ile öncelik vektörünü bulur. Eş değer olarak Tablo 5'in son sütunu standardize edildiğinde de aynı öncelik vektörü elde edilir). Görüldüğü üzere RBH, olabilirlik ortalama-varyans düzleminde diğer alternatiflere baskındır. Başka bir deyişle RBH, diğer alternatiflere göre daha yüksek olabilirlik ortalamasına ve daha düşük olabilirlik standart sapmasına sahiptir. KPC bu düzlemde RBH dışındaki alternatiflere baskındır. Bu değerlendirmeler, Tablo 2 için yapılan değerlendirmelerle uyumludur.

Tablo 5 için;

Adım 5: (9) ifadesi kullanılarak veya Tablo 5'in son sütunu standardize edilerek alternatiflerin öncelik vektörü (0,1232, 0,4850, 0,1300, 0,2030, 0,0589)^T olarak bulunmuştur.

Adım 6: Tablo 1'deki karar matrisi ve Tablo 3'teki ikili karşılaştırma matrisinde verilen bilgiler doğrultusunda PES ile bulunan en iyi kaynak dağıtım planı; ZPE için %12,32, RBH için %48,50, MPS için %13,00, KPC için %20,30 ve ELZ için %5,89 olarak belirlenmiştir.

İkili karşılaştırmalara ve öznel yargılara dayanan AHS'nin aksine TOPSIS yöntemi, Öklid uzaklığına dayanır (Chakraborty, 2022). Tablo 6'da maksimin kuralıyla, ağırlıklı toplam yöntemiyle, maksimaks kuralıyla, TOPSIS yöntemiyle ve PES yaklaşımı ile bulunan öncelik vektörleri verilmiştir. Maksimaks kuralı hariç, öncelik vektörleri tek olarak bulunmuştur. RBH ile ELZ'nin Tablo 4'te verilen iyimserlik düzeyleri aynı olduğundan bunların öncelikleri maksimaks kuralında eşit alınmıştır.

Tablo 6. Öncelik vektörleri

	Maksimin Kuralı	Ağırlıklı Toplam Yöntemi	Maksimaks Kuralı	TOPSIS	PES
ZPE	0	0	0	0,2437	0,1232
RBH	0,6231	1	0,5	0,3255	0,4850
MPS	0	0	0	0,1553	0,1300
KPC	0	0	0	0,2629	0,2030
ELZ	0,3769	0	0,5	0,0126	0,0589

Tablo 7. Kriterlerin farklı ağırlık vektörleri için PES ile bulunan öncelik vektörleri

	S0	S1	S2	S3	S4	S5	S6
ZPE	0,1232	0,1318	0,1289	0,1320	0,1112	0,1359	0,0701
RBH	0,4850	0,4703	0,4903	0,4692	0,5210	0,4413	0,4393
MPS	0,1300	0,1372	0,1192	0,1427	0,1115	0,1701	0,1139
KPC	0,2030	0,2099	0,2088	0,2054	0,2001	0,2051	0,1559
ELZ	0,0589	0,0507	0,0529	0,0506	0,0562	0,0476	0,2208

Tablo 8. Kriterlerin farklı ağırlık vektörleri için PES ile bulunan öncelik sıralamaları

	S0	S1	S2	S3	S4	S5	S6
ZPE	4.	4.	3.	4.	4.	4.	5.
RBH	1.	1.	1.	1.	1.	1.	1.
MPS	3.	3.	4.	3.	3.	3.	4.
KPC	2.	2.	2.	2.	2.	2.	3.
ELZ	5.	5.	5.	5.	5.	5.	2.

TOPSIS ile bulunan öncelik vektörü, TOPSIS ile bulunan genel tercih skor vektörü standardize edilerek yani elemanları toplamına bölünerek elde edilmiştir. Görüldüğü üzere PES ve TOPSIS ile bulunan öncelik sıralamaları neredeyse aynıdır. PES ile yapılan sıralama RBH, KPC, MPS, ZPE ve ELZ şeklindeyken, TOPSIS ile yapılan sıralama RBH, KPC, ZPE, MPS ve ELZ şeklindedir. ÇNKV problemleri için beş yöntem de RBH'yi seçer. ÇAKV problemleri için bulunan öncelik vektörü, kaynakların alternatiflere dağıtılmasında kullanılabilir. Örneğimizde bu durum Tablo 6'daki öncelik vektörleri ile portföy oluşturulmasına karşı gelmektedir. Maksimin ve maksimaks kuralları, diğer alternatiflere göre geride olduğu görülen ELZ için yüksek öncelik değeri verirken, en iyi ikinci alternatif olduğu görülen KPC için öncelik değerini sıfır olarak vermiştir. Ağırlıklı toplam yöntemi, en iyi alternatif olan RBH'ye tüm önceliği vermiştir. Öte yandan PES ile elde edilen öncelik vektörü dengelidir ve en iyi (ikinci) alternatif olan RBH'ye (KPC'ye) en yüksek (ikinci) önceliği vermiştir. Örneğimizde, normalize edilmiş karar matrisindeki veriyi işlemede daha başarılı olduğu için, PES'in söz konusu temel yöntemlere oranla daha fazla bilgi ortaya koyduğu söylenebilir. Yani örneğimizde verilen bilgiler doğrultusunda portföy oluşturmak isteyen bir yatırımcı, Tablo 6'daki öncelik vektörleri içinden TOPSIS ile bulunan hariç PES ile bulunanı tercih edebilir. PES ve TOPSIS arasındaysa herhangi bir üstünlük ilişkisi yoktur. Bu nedenle PES ya da TOPSIS ile bulunan öncelik vektörlerinden hangisinin portföy seçiminde kullanılacağı karar vericinin tercihinine bağlıdır.

PES ile bulunan sonuçlar kriterlerin ağırlık vektöründen

etkilenmektedir. PES için yapılan duyarlılık analizinin sonuçları Tablo 7 ve Tablo 8'de verilmiştir. Burada (0,1291, 0,1291, 0,3185, 0,3185, 0,0524, 0,0524)^T sütun vektörüyle verilen ve bu çalışmada kullanılan kriterlerin ağırlık vektörü S0 ile gösterilmiştir, SX ise X. kriterin ağırlığının %100 olduğu diğer kriterlerin ağırlığının %0 olduğu duruma karşı gelmektedir.

Tablo 8'de görüldüğü üzere RBH tüm durumlarda en yüksek önceliğe sahiptir. S6 dışındaki durumlarda KPC (ELZ) en yüksek ikinci (beşinci) önceliğe sahiptir. S3 ve S6 dışındaki durumlarda MPS (ZPE) en yüksek üçüncü (dördüncü) önceliğe sahiptir.

Tablo 7 ve Tablo 8'de görüldüğü üzere PES ile bulunan sonuçlar, kriterlerin ağırlık vektöründeki değişimlere karşı aşırı duyarlı değildir. Bu durumun temel nedeni, (9) ifadesindeki $b_{i,1}$, $b_{i,2}$ ve $b_{i,3}$ parametrelerinden sadece $b_{i,2}$ parametresinin kriterlerin ağırlık vektöründen etkilenmesidir.

4. Sonuç

Ülkemizde hisse senedi piyasasına duyulan ilgi hızla artmaktadır. Buna paralel olarak hisse senedi yatırım fonları, Borsa İstanbul'un önemli bir güç merkezi haline gelmiştir. Katılım hisse senedi şemsiye fonları, dini hassasiyetleri nedeniyle hisse senedi evrenindeki tüm hisse senetlerine yatırımda bulunamayan tasarruf sahiplerine, İslami finans ilkeleri çerçevesinde filtrelenmiş hisse senetlerine yatırım imkânı sağlayan bir yatırım alternatifidir. Nainggolan ve ark. (2016), Bayraktar ve Aksoy (2020), Climent ve ark. (2020), Güçlü ve Şekkeli (2020), Güçlü (2022) gibi çalışmalardan bilindiği üzere katılım hisse senedi şemsiye fonları, diğer

hisse senedi yatırım fonlarının büyük bölümünden daha kötü performans vermemektedir. Bu çalışmada katılım hisse senedi şemsiye fonlarının karşılaştırılması gibi önemli ÇKKV problemleri için Olabilirlik Değerlendirme Sistemi (PES) önerilmiştir. PES, temel ÇKKV yöntemleri olan Maksimin kuralı, ağırlıklı toplam metodu ve Maksimaks kuralı ile ilişkilidir. Maksimin kuralı kötümser yaklaşıma dayanırken, Maksimaks kuralı iyimser yaklaşıma dayanır. Ağırlıklı toplam değeriye, iş hayatına ek olarak günlük hayatta da sıklıkla kullandığımız bir referans noktasıdır. Yapılan uygulamada PES'in söz konusu temel yöntemlere oranla daha fazla bilgi ortaya koyduğu görülmüştür. Çünkü tanımı gereği PES, söz konusu temel yöntemlerden edilen bilgileri olabilirlik teorisinden ve üçgensel bulanık sayılardan yararlanarak sentezlemektedir. Bu nedenle PES müstakil bir ÇKKV yöntemi olarak değil, söz konusu temel yöntemlerle ilişkili olan yeni bir ÇKKV yaklaşımı olarak görülebilir. Bu ilişkinin, PES ile elde edilecek bilgi için bir sınırlılık oluşturduğu iddia edilebilir. PES'in; AHS, TOPSIS gibi diğer ÇKKV yöntemlerinden üstün olduğuna dair herhangi bir hipotez ise söz konusu değildir ve dolayısıyla bununla ilgili herhangi bir analiz yapılmamıştır. Kullanım kolaylığı olan PES, öncelik vektörünü tek olarak vermektedir. Sonuç olarak PES'in dikkate değer bir ÇKKV yaklaşımı olduğu söylenebilir. İlerideki çalışmalarda grup karar verme problemleri için PES genelleştirilebilir. Farklı ÇKKV problemlerinin incelendiği akademik çalışmalarda ve ÇKKV problemi olarak formalize edilebilecek herhangi bir işletme probleminin çözümünde PES kullanılabilir.

Katkı Oranı Beyanı

Yazar(lar)ın katkı yüzdesi aşağıda verilmiştir. Tüm yazarlar makaleyi incelemiş ve onaylamıştır.

	F.Gö.	F.Gü.
K	50	50
T	50	50
Y	50	50
VTI	50	50
VAY	50	50
KT	50	50
YZ	50	50
KI	50	50
GR	50	50
PY	50	50
FA	50	50

K= kavram, T= tasarım, Y= yönetim, VTI= veri toplama ve/veya işleme, VAY= veri analizi ve/veya yorumlama, KT= kaynak tarama, YZ= Yazım, KI= kritik inceleme, GR= gönderim ve revizyon, PY= proje yönetimi, FA= fon alımı.

Çatışma Beyanı

Yazarlar bu çalışmada hiçbir çıkar ilişkisi olmadığını beyan etmektedirler.

Etik Onay Beyanı

Bu çalışmada hayvanlar ve insanlar üzerinde herhangi bir çalışma yapılmadığı için etik kurul onayı alınmamıştır.

Kaynaklar

- Ali MY, Sultana A, Khan AFMK. 2016. Comparison of fuzzy multiplication operation on triangular fuzzy number. *IOSR J Math*, 12(4): 35-41.
- Alonso JA, Lamata MT. 2006. Consistency in the analytic hierarchy process: a new approach. *Int J Uncert Fuzzy Knowledge-bas Syst*, 14(04): 445-459.
- Bayraktar M, Aksoy M. 2020. Katılım esasına dayalı bireysel emeklilik fonlarının performans analizi. *Muhas Finan Derg*, 86: 153-184.
- Chakraborty S. 2022. TOPSIS and Modified TOPSIS: A comparative analysis. *Decis Analyt J*, 2: 100021.
- Climent F, Mollá P, Soriano P. 2020. The investment performance of U.S. Islamic mutual funds. *Sustainability*, 12(3530): 1-18.
- Deng X, Yuan Y. 2021. A novel fuzzy dominant goal programming for portfolio selection with systematic risk and non-systematic risk. *Soft Comput*, 25(23): 14809-14828.
- Dubois D. 2006. Possibility theory and statistical reasoning. *Computl Stat Data Analysis*, 51(1): 47-69.
- Dubois D, Prade H. 1988. Possibility Theory. Plenum Press, New York, US.
- El Gibari S, Gómez T, Ruiz F. 2019. Building composite indicators using multicriteria methods: A review. *J Busin Econ*, 89(1): 1-24.
- Foroozesh N, Mousavi SM, Mojtahedi M, Gitinavard H. 2022. Maintenance policy selection considering resilience engineering by a new interval-valued fuzzy decision model under uncertain conditions. *Sci Iranica*, 29(2): 783-799.
- Fullér R, Harmati IA. 2018. On possibilistic dependencies: A short survey of recent developments. *Soft Comput Based Optimiz Decision Models*, 2018: 261-273.
- Fullér R, Mezei J, Varlaki P. 2011. An improved index of interactivity for fuzzy numbers. *Fuzzy Sets Syst*, 165(1): 50-60.
- Goldfarb D, Iyengar G. 2003. Robust portfolio selection problems. *Math Operat Res*, 28(1): 1-38.
- Göktaş F, Duran A. 2019. A new possibilistic mean-variance model based on the principal components analysis: an application on the Turkish holding stocks. *J Multiple-Valued Logic Soft Comput*, 32(5-6): 455-476.
- Garai T, Dalapati S, Garg H, Roy TK. 2020. Possibility mean, variance and standard deviation of single-valued neutrosophic numbers and its applications to multi-attribute decision-making problems. *Soft Comput*, 24: 18795-18809.
- Garai T, Garg H. 2022. Multi-criteria decision making of water resource management problem (in Agriculture field, Purulia district) based on possibility measures under generalized single valued non-linear bipolar neutrosophic environment. *Expert Syst Appl*, 205: 117715.
- Güçlü F. 2022. Katılım hisse senedi şemsiye fonlarının performansının gri ilişkisel analiz yöntemi ile incelenmesi. *Finans Ekon Sos Araş Derg*, 7(1): 121-130.
- Güçlü F, Şekkel FE. 2020. Türkiye'deki İslami ve konvansiyonel hisse senedi yatırım fonlarının performans analizi ve karşılaştırılması. *Busin Manag Stud*, 8(5): 4463-4486.
- MKK. 2023. Uyrak bazında yatırımcı sayıları. Veri Analiz Platformu. URL: <https://www.vap.org.tr/uyruk-bazinda-yatirimci-sayilari> (erişim tarihi: 29 Eylül 2023).

- Moghaddam NB, Nasiri M, Mousavi SM. 2011. An appropriate multiple criteria decision making method for solving electricity planning problems, addressing sustainability issue. *Int J Environ Sci Technol*, 8(3): 605-620.
- Nainggolan Y, How J, Verhoeven P. 2016. Ethical screening and financial performance: The case of Islamic equity funds. *J Busin Ethics*, 137(1): 83-99.
- Odu GO. 2019. Weighting methods for multi-criteria decision making technique. *J Appl Sci Environ Manag*, 23(8): 1449-1457.
- Reig-Mullor J, Salas-Molina F. 2022. Non-linear neutrosophic numbers and its application to multiple criteria performance assessment. *Int J Fuzzy Syst*, 24(6): 2889-2904.
- Saaty TL. 2003. Decision making with the AHP: why is the principal eigenvector necessary. *European Journal of J Operat Res*, 145(1): 85-91.
- Saaty TL, Tran LT. 2007. On the invalidity of fuzzifying numerical judgments in the analytic hierarchy process. *Math Comput Model*, 46(7-8): 962-975.
- Saaty TL, Vargas LG. 2012. *models, methods, concepts & applications of the analytic hierarchy process*. Springer, New York, US, pp: 78.
- Sikalo M, Arnaut-Berilo A, Zaimovic A. 2022. Efficient asset allocation: Application of game theory-based model for superior performance. *Int J Finan Stud*, 10(1): 20.
- Sorooshian S, Parsia Y. 2019. Modified weighted sum method for decisions with altered sources of information. *Math Stat*, 7(3): 57-60.
- Taherdoost H, Madanchian M. 2023. Multi-criteria decision making (MCDM) methods and concepts. *Encyclopedia*, 3(1): 77-87.
- Tütüncü RH, Koenig M. 2004. Robust asset allocation. *Annals Operat Res*, 132: 157-187.
- Vafaei N, Ribeiro RA, Camarinha-Matos LM. 2016. Normalization techniques for multi-criteria decision making: Analytical hierarchy process case study. *Doctoral conference on computing, electrical and industrial systems*. Springer, Cham, New York, US, pp: 261-269.
- Wan SP, Li DF. 2013. Possibility mean and variance based method for multi-attribute decision making with triangular intuitionistic fuzzy numbers. *J Intell Fuzzy Syst*, 24(4): 743-754.
- Wang X, Yang F, Wei H, Zhang L. 2015. A new ranking method based on TOPSIS and possibility theory for multi-attribute decision making problem. *Optik*, 126(24): 4852-4860.
- Ye F, Li Y. 2014. An extended TOPSIS model based on the possibility theory under fuzzy environment. *Knowledge-Based Syst*, 67: 263-269.
- Yi ZH, Li HQ. 2018. Triangular norm-based cuts and possibility characteristics of triangular intuitionistic fuzzy numbers for decision making. *Int J Intell Syst*, 33(6): 1165-1179.
- Zadeh LA. 1965. Fuzzy sets. *Info Control*, 8(3): 338-353.
- Zadeh LA. 1978. Fuzzy sets as a basis for a theory of possibility. *Fuzzy Sets Syst*, 1(1): 3-28.
- Zavadskas EK, Turskis Z, Kildienė S. 2014. State of art surveys of overviews on MCDM/MADM methods. *Technol Econ Devel Econ*, 20(1): 165-179.



RADIATIVE TRANSFER EQUATION SOLUTION FOR MANY SCATTERING TYPES

Dilek AYDIN¹, Halide KÖKLÜ^{2*}

¹Iğdır University, Postgraduate Education Institute, Department of Mathematics, 76000, Iğdır, Türkiye


²Iğdır University, Vocational School of Health Services, Department of Medical Services and Techniques, 76000, Iğdır, Türkiye


Abstract: The radiative transfer equation is a mathematical equation that describes the changes in the number of photons within a specified volume of a medium over time, taking into account phenomena such as scattering, absorption, and re-emission resulting from photon interactions with the medium. In this study, the radiative transfer equation is considered for a finite slab which anisotropic scattering in a homogeneous medium. The equation solution is done by Legendre polynomials for linear anisotropic, pure quadratic and Rayleigh scattering types. The numerical results are displayed in the tables up to the 13th iteration of the Legendre polynomials. Tables are obtained using different scattering coefficients and single scattering albedo values. The results contain a wide range of data obtained from the method of solving the Legendre polynomial of the radiative transfer equation. Thus, with this study, the effect of different scattering types on the solution of the radiative transfer equation has been demonstrated.

Keywords: Radiative transfer equation, Legendre polynomial method, Anisotropic scattering

*Corresponding author: Iğdır University, Vocational School of Health Services, Department of Medical Services and Techniques, 76000, Iğdır, Türkiye

E mail: halidecelikten@gmail.com (H. KÖKLÜ)

Dilek AYDIN  <https://orcid.org/0009-0004-0026-285X>

Halide KÖKLÜ  <https://orcid.org/0000-0003-1787-6693>

Received: August 01, 2023

Accepted: November 07, 2023

Published: January 15, 2024

Cite as: Aydın D, Köklü H. 2024. Radiative transfer equation solution for many scattering types. BSJ Eng Sci, 7(1): 9-15.

1. Introduction

Radiative transfer theory can be applied to many fields in physics. The radiative transfer equation expresses the states of photons in a medium such as absorption, scattering and propagation. Radiative transfer (radiation emission) is known as a kind of physical energy transfer of electromagnetic radiation (Herman and Browning, 1965). Radiative transfer equation is an equation that depends on time, direction, energy and space variables. The concept of radiative transfer is widely used in many fields of physics such as astrophysics, optics, atmospheric physics, marine sciences and remote sensing systems (Stamnes et al., 2017).

In 1960, Chandrasekhar showed that statistical physics methods can obtain the Boltzmann equation for radiational transfer as photon gas transfer (Chandrasekhar, 1960). The eigenvalue calculations in one-dimensional geometry showed the applicability of the new scattering function to the radiative transfer equation (Anlı and Güngör, 2005). A Legendre polynomial approximation method has been developed to find approximate solutions of higher order Volterra type integro-differential equations by Güçlü (Güçlü İ. 2009). At the same time, he concluded that the method is a good method that can also be used to find the exact solutions of the equations of the mentioned property.

Elghazaly et al. (Elghazaly A, El-Konsol S, Sabbah AS, Hosni M. 2017) have solved the integral form of the radiative transfer equation in a two-layer inhomogeneous plate for

linear anisotropic scattering by using the Galerkin iterative method. Biçer and Kaşkaş (Biçer M, Kaşkaş A., 2018) solved the radiative transfer equation for Rayleigh scattering using the infinite medium Green's function. Tapimo et al. (R. Tapimo, H.T. Tagne Kamdem, & D. Yemele, 2018) used the discrete spherical harmonics method to calculate the discrete spherical harmonics method for radiative transfer in the scalar planar inhomogeneous atmosphere and extended the radiative density with a finite series of Legendre polynomials.

This study uses Legendre polynomial methods to discuss the radiative transfer equation solution for linear anisotropic, pure quadratic and Rayleigh scattering types. The scattering phenomena is efficient for the analyzing of the photon behavior in the medium. The discrete eigenvalues from the calculation of the equation are obtained for the 13th iteration of the method to approach the accurate roots of the equation. When the iteration steps are increased, the accuracy is increased to. The closeness of the roots is nearly one digit after comma. The calculated eigenvalues precision is accepted enough for the study.

2. Legendre Polynomial Solution Method

2.1 Linear Anisotropic Scattering Solution

The radiative transfer equation has used with the most convenient with some restrictions that are no thermal emission, plane-parallel atmosphere, phase function expandable in Legendre polynomial series and azimuthal



symmetry. After all the considerations of the RTE is written as given in Equation 1;

$$\mu \frac{d}{dx} I(x, \mu) + I(x, \mu) = \frac{\omega}{2} \int_{-1}^1 f(\mu, \mu') I(x, \mu) d\mu' \quad (1)$$

where $I(x, \mu)$ is the angular intensity, μ is the direction cosine of the propagating radiation, x is the optical variable, ω is the single scattering albedo and $f(\mu, \mu')$ is the scattering phase function. It can be shown as given in Equation 2;

$$f(\mu, \mu') = \sum_{n=0}^N (2n+1) f_n P_n(\mu) P_n(\mu') \quad (2)$$

here f_n represent the scattering coefficients belong to scattering type. The linear anisotropic scattering is known as the case of the $N=1$. So, the function becomes (Equation 3);

$$f(\mu, \mu') = f_0 P_0(\mu) P_0(\mu') + 3f_1 P_1(\mu) P_1(\mu') \quad (3)$$

Now the scattering function for the linear anisotropic case in Equation 3 is substituted in to the general form of the radiative transfer equation in Equation 1 so Equation 4.

$$\begin{aligned} \mu \frac{d}{dx} I(x, \mu) + I(x, \mu) \\ = \frac{\omega}{2} \int_{-1}^1 (f_0 P_0(\mu) P_0(\mu') \\ + 3f_1 P_1(\mu) P_1(\mu')) I(x, \mu) d\mu' \end{aligned} \quad (4)$$

The angular flux of the radiative transfer equation can be displayed through series expansion of the Legendre polynomials (Equation 5);

$$I(x, \mu) = \sum_{n=0}^N \frac{2n+1}{2} \phi_n(x) P_n(\mu) \quad (5)$$

here $\phi_n(x)$ is called as flux moments that are demonstrated as for $n=0$ and 1 (Equations 6 and 7);

$$\phi_0(x) = \int_{-1}^1 P_0(\mu') I(x, \mu) d\mu' \quad (6)$$

$$\phi_1(x) = \int_{-1}^1 P_1(\mu') I(x, \mu) d\mu' \quad (7)$$

After determining the angular flux in Equation 5, scattering function in Equation 3 and the flux moments in Equations 6 and 7, the radiative transfer equation in Equation 1 is composed again like;

$$\begin{aligned} \mu \frac{d}{dx} \left[\sum_{n=0}^N \frac{2n+1}{2} \phi_n(x) P_n(\mu) \right] \\ + \sum_{n=0}^N \frac{2n+1}{2} \phi_n(x) P_n(\mu) \\ = \frac{\omega}{2} [f_0 \phi_0(x) + 3\mu f_1 \phi_1(x)] \end{aligned} \quad (8)$$

By solving Equation 8 the recurrence relation of the Legendre polynomials is used and then the series is expanded for $n=0,1,2,3,\dots,N$. The resultant equation is multiplied by $\int_{-1}^1 P_m(\mu) d\mu$. The orthogonality relation of the Legendre polynomials is applied to obtain the discrete differential sets for $m=0,1,2,3,\dots$. (Equations 9a-9d)

$$m = 0; \quad \frac{d}{dx} \phi_1(x) + \phi_0(x) = \omega f_0 \phi_0(x) \quad (9a)$$

$$m = 1; \quad \frac{1d}{3dx} \phi_0(x) + \frac{2d}{3dx} \phi_2(x) + \phi_1(x) = \omega f_1 \phi_1(x) \quad (9b)$$

$$m = 2; \quad \frac{2d}{5dx} \phi_1(x) + \frac{3d}{5dx} \phi_3(x) + \phi_2(x) = 0 \quad (9c)$$

$$m = 3 \quad \frac{3d}{7dx} \phi_2(x) + \phi_3(x) = 0 \quad (9d)$$

The eigen-spectrum of the differential sets in Equations 9.a-d are obtained by employing the well-known ansatz;

$$\phi_n(x) = A_n(v) e^{x/v} \quad (10)$$

The Equation 10 is used to determine the eigenvalues of the radiative transfer equation by Legendre polynomial solution (Equations 11a-11c).

$$A_1(v) = -v A_0(v) (1 - \omega f_0) \quad (11a)$$

$$A_2(v) = (-3v A_1(v) (1 - \omega f_1) - A_0(v)) / 2 \quad (11b)$$

$$A_3(v) = (-5v A_2(v) - 2A_1(v)) / 3 \quad (11c)$$

with $A_0(v) = 1$, the eigenvalues of v can be found by solving the equation $A_{n+1}(v) = 0$, (Taşdelen, 2017). These eigenvalues are the roots needed to solve the equation. As the iteration steps increase in the method, convergence in the roots is increased. If N symbolizes the iteration step, $N+1/2$ eigenvalues are found for P_N iteration. For example, there are seven positive eigenvalues for the 13th iteration of the polynomial expressed as P_{13} .

2.2. Pure-Quadratic Anisotropic Scattering Solution

The scattering function is taken into account for the case of $N=2$ which is called as pure quadratic anisotropic scattering type. In this situation, the scattering coefficients are assumed as $f_1=0$ and $f_2 \neq 0$. Described the scattering function in Equation 2 takes the form of pure quadratic anisotropic scattering (Equation 12);

$$f(\mu, \mu') = f_0 P_0(\mu) P_0(\mu') + 5f_2 P_2(\mu) P_2(\mu') \quad (12)$$

The Equation 12 is used in Equation 1 (Equation 13);

$$\begin{aligned} \mu \frac{d}{dx} I(x, \mu) + I(x, \mu) \\ = \frac{\omega}{2} \int_{-1}^1 (f_0 P_0(\mu) P_0(\mu') \\ + 5f_2 P_2(\mu) P_2(\mu')) I(x, \mu) d\mu' \end{aligned} \quad (13)$$

The angular moments are applied (Equation 14).

$$\begin{aligned} \mu \frac{d}{dx} I(x, \mu) + I(x, \mu) \\ = \frac{\omega}{2} [f_0 P_0(\mu) \phi_0(x) \\ + 5f_2 P_2(\mu) \phi_2(x)] \end{aligned} \quad (14)$$

The mentioned angular flux Legendre polynomial expansion form in Equation 7 is substituted into Equation 15.

$$\begin{aligned} \mu \frac{d}{dx} \left[\sum_{n=0}^N \frac{2n+1}{2} \phi_n(x) P_n(\mu) \right] \\ + \sum_{n=0}^N \frac{2n+1}{2} \phi_n(x) P_n(\mu) \\ = \frac{\omega}{2} \left[f_0 \phi_0(x) \right. \\ \left. + \frac{5(3\mu^2 - 1)}{2} f_2 \phi_2(x) \right] \end{aligned} \quad (15)$$

The solution of the Equation 15 is done by using the recurrence relation of Legendre polynomials and then multiplying by $\int_{-1}^1 P_n(\mu) d\mu$. After some algebra the differentials sets are found as given in Equation 16a-16c;

$$\frac{1d}{3dx} \phi_0(x) + \frac{2d}{3dx} \phi_2(x) + \phi_1(x) = 0 \quad (16a)$$

$$\frac{2d}{5dx} \phi_1(x) + \frac{3d}{5dx} \phi_3(x) + \phi_2(x) = \omega f_2 \phi_2(x) \quad (16b)$$

$$\frac{3d}{7dx} \phi_2(x) + \phi_3(x) = 0 \quad (16c)$$

The differential equations are solved by applying to the Equation 10. The eigenfunctions obtained as given in Equations 17a-17c;

$$A_1(v) = -vA_0(v)(1 - \omega f_0) \quad (17a)$$

$$A_2(v) = (-3vA_1(v) - A_0(v))/2 \quad (17b)$$

$$A_3(v) = (-5vA_2(v)(1 - \omega f_0) - 2A_1(v))/3 \quad (17c)$$

2.3. Rayleigh Scattering Solution

Rayleigh scattering occurs when the incident wavelength is greater than the size of the scattering particles. Lord Rayleigh explained why the sky is blue and the sunset is red by using this scattering function. This scattering function can be used in astrophysics, oceanography and tissue optics. Chandrasekhar formulated the scattering function for the polarized case using the Stokes parameters (Chandrasekhar, 1950). The scattering function can be written for the unpolarized Rayleigh case in the following form with ($f_0 = 1$ ve $f_2 = 1/2$) (Sallah and Selim, 2008) (Equation 18).

$$f(\mu, \mu') = P_0(\mu)P_0(\mu') + \frac{1}{2}P_2(\mu)P_2(\mu') \quad (18)$$

The Rayleigh scattering function is applied to radiative transfer equation in Equation 1 and the same procedure is used to solve the eigenvalues of the Rayleigh scattered radiative transfer equation some of them are found as given in Equations 19a-19c;

$$A_1(v) = -vA_0(v)(1 - \omega) \quad (19a)$$

$$A_2(v) = (-3vA_1(v) - A_0(v))/2 \quad (19b)$$

$$A_3(v) = (-vA_2(v)(\frac{\omega}{2} - 5) - 2A_1(v))/3 \quad (19c)$$

3. Results and Discussion

The radiative transfer equation is solved by the P_N method with linear anisotropic scattering, pure quadratic anisotropic scattering and Rayleigh scatterings. The solutions are done to obtain the discrete eigenvalues of the radiative transfer equation solutions. The anisotropic scattering function comprises the scattering coefficient belonging to the type of anisotropy. The scattering coefficients are not arbitrary numbers. They are chosen from the numbers supplying the condition that the scattering function must be -1 to 1. The numerical results of the radiative transfer equation solution are demonstrated for many possibilities of the scattering coefficients and also single scattering albedo numbers. The discrete eigenvalues of the linear anisotropic scattering solution is tabulated in Table 1 for $f_1 = -0.3$ to 0.3 in 0.1 with the 13th iteration of the P_N method for the single scattering albedo numbers from 0.1 to 0.9 .

The series of the scattering function is expanded up to the second term called as the pure quadratic anisotropic scattering. So, it contains two scattering coefficients that have to be determined by verifying the condition of the scattering function. It occurs with many possibilities and complexity. That's why the first term is assumed zero. The conceivable numbers are selected for the second scattering coefficient. Table 2 shows the discrete eigenvalues of the solution of pure quadratic anisotropic scattering corresponding to the scattering coefficients $f_2 = -0.20, -0.14, -0.12, -0.08, 0.2, 0.4$ with the 13th iteration of the P_N method for the single scattering albedo numbers from 0.1 to 0.9 .

Physically, Rayleigh scattering is considered when the size of scattering particles of the stochastic media are much smaller than the incident radiation wavelength. On the other hand, if particles sizes are comparable to, or larger than, wavelength, the scattering is customarily referred to as Mie scattering. Frequently, these phenomena are related to the radiative transfer in astrophysical setting, Hussein and Selim 2012 (Hussein A, Selim MM., 2012). Rayleigh scattering occurs for particles that are smaller than the radiation's wavelength, Cherry et al. (Cherry SR, Sorenson JA, Phelps ME, 2012). The obtained discrete eigenvalues from the solution of the Rayleigh scattering are presented in Table 3. The numerical results are found for many single-scattering albedo numbers. The iteration of the method up to 13th are demonstrated in the Table 3.

Table 1. Discrete eigenvalues of the P_{13} iteration for linear anisotropic scattering

$w \setminus f_2$	-0.30	-0.20	-0.10	0.10	0.20	0.4
0.1	0.10922148	0.10922494	0.10922839	0.10923530	0.10923875	0.10922148
	0.32219243	0.32227921	0.32236568	0.32253769	0.32262323	0.32219243
	0.51918027	0.51952389	0.51986492	0.52053919	0.52087243	0.51918027
	0.69087793	0.69160299	0.69232224	0.69374250	0.69444314	0.69087793
	0.82966620	0.83069108	0.83171640	0.83376409	0.83478432	0.82966620
	0.92969277	0.93069121	0.93171344	0.93382459	0.93491039	0.92969277
	0.98670182	0.98725320	0.98784506	0.98916558	0.98990283	0.98670182
0.2	0.11041966	0.11042538	0.11043110	0.11044252	0.11044822	0.11041966
	0.32548166	0.32562806	0.32577344	0.32606112	0.32620344	0.32548166
	0.52371805	0.52431936	0.52491114	0.52606633	0.52662988	0.52371805
	0.69552988	0.69686517	0.69817373	0.70070702	0.70193025	0.69552988
	0.83342189	0.83542848	0.83741796	0.84131332	0.84320383	0.83342189
	0.93205500	0.93415408	0.93632627	0.94081361	0.94307785	0.93205500
	0.98769054	0.98897814	0.99046838	0.99421394	0.99656147	0.98769054
0.3	0.11164962	0.11165650	0.11166338	0.11167710	0.11168395	0.11164962
	0.32897040	0.32914907	0.32932593	0.32967430	0.32984584	0.32897040
	0.52886564	0.52962213	0.53036016	0.53178205	0.53246656	0.52886564
	0.70138335	0.70314689	0.70484696	0.70805365	0.70956018	0.70138335
	0.83885381	0.84169675	0.84445092	0.84961387	0.85199328	0.83885381
	0.93609830	0.93939343	0.94273627	0.94917588	0.95207554	0.93609830
	0.98975263	0.99224194	0.99535240	1.00405916	1.00996814	0.98975263
0.4	0.11291130	0.11291836	0.11292541	0.11293948	0.11294650	0.11291130
	0.33264081	0.33282569	0.33300823	0.33336642	0.33354213	0.33264081
	0.53457905	0.53537754	0.53615019	0.53762103	0.53832076	0.53457905
	0.70846781	0.71039809	0.71222317	0.71556824	0.71709547	0.70846781
	0.84629826	0.84960969	0.85269048	0.85810452	0.86043851	0.84629826
	0.94265997	0.94694311	0.95092772	0.95737025	0.95975642	0.94265997
	0.99426781	0.99916528	1.00561351	1.02420108	1.03661995	0.99426781
0.5	0.11420447	0.11421088	0.11421729	0.11423007	0.11423644	0.11420447
	0.336646549	0.33663373	0.33679955	0.33712414	0.33728298	0.336646549
	0.54074783	0.54147764	0.54217942	0.54350354	0.54412812	0.54074783
	0.71658598	0.71836771	0.72002196	0.72298041	0.72430106	0.71658598
	0.85564288	0.85875076	0.86150142	0.86603504	0.86788586	0.85564288
	0.95208742	0.95608654	0.95925044	0.96350908	0.96491653	0.95208742
	1.00559135	1.01571858	1.02861238	1.06285561	1.08426029	1.00559135
0.6	0.11552862	0.11553378	0.11553892	0.11554919	0.11555431	0.11552862
	0.34040673	0.34054095	0.34067316	0.34093177	0.34105822	0.34040673
	0.54718592	0.54775892	0.54830840	0.54934148	0.54982726	0.54718592
	0.72521422	0.72657054	0.72781700	0.73002022	0.73099495	0.72521422
	0.86573030	0.86792898	0.86981382	0.87283199	0.87404498	0.86573030
	0.96168007	0.96380309	0.96536066	0.96742550	0.96813127	0.96168007
	1.03618749	1.05500487	1.07695949	1.13072705	1.16309948	1.03618749
0.7	0.11688301	0.11688655	0.11689008	0.11689713	0.11690064	0.11688301
	0.34441690	0.34450741	0.34459666	0.34477148	0.34485709	0.34441690
	0.55364491	0.55401637	0.55437341	0.55504711	0.55536513	0.55364491
	0.73357939	0.73439339	0.73514427	0.73648133	0.73707809	0.73357939
	0.87464629	0.87576819	0.87673949	0.87832916	0.87898525	0.87464629
	0.96775833	0.96848696	0.96906062	0.96990133	0.97021734	0.96775833
	1.10928863	1.13815411	1.17050645	1.24766452	1.29390650	1.10928863
0.8	0.11826658	0.11826845	0.11827033	0.11827407	0.11827594	0.11826658
	0.34844029	0.34848697	0.34853312	0.34862389	0.34866852	0.34844029
	0.55985551	0.56003533	0.56020956	0.56054224	0.56070114	0.55985551
	0.74096975	0.74132138	0.74165184	0.74225611	0.74253295	0.74096975
	0.88128288	0.88168247	0.88204327	0.88266853	0.88294097	0.88128288
	0.97090984	0.97110548	0.97127502	0.97155402	0.97167012	0.97090984
	1.26976876	1.31072484	1.35638228	1.46564646	1.53196937	1.26976876
0.9	0.11967792	0.11967847	0.11967902	0.11968012	0.11968067	0.11967792
	0.35241654	0.35242970	0.35244277	0.35246865	0.35248146	0.35241654
	0.56558411	0.56563071	0.56567648	0.56576562	0.56580904	0.56558411
	0.74702582	0.74710576	0.74718308	0.74733038	0.74740058	0.74702582
	0.88581158	0.88588812	0.88596092	0.88609637	0.88615946	0.88581158
	0.97261221	0.97264393	0.97267370	0.97272807	0.97275295	0.97261221
	1.69054019	1.75321107	1.82353786	1.99446652	2.10042214	1.69054019

Table 2. Discrete eigenvalues of the P_{13} iteration for pure quadratic anisotropic scattering

$w \setminus f_2$	-0.20	-0.14	-0.12	-0.08	0.2	0.4
0.1	0.10895392	0.10903710	0.10906487	0.10912045	0.10951161	0.10979322
	0.32201417	0.32214493	0.32218862	0.32227616	0.32289470	0.32334281
	0.52011074	0.52013845	0.52014769	0.52016622	0.52029672	0.52039087
	0.69290065	0.69294127	0.69295478	0.69298174	0.69316867	0.69330025
	0.83156661	0.83192279	0.83204079	0.83227570	0.83387855	0.83497840
	0.93048130	0.93116489	0.93139274	0.93184832	0.93501871	0.93723967
	0.98673580	0.98723536	0.98740633	0.98775515	0.99047397	0.99274801
0.2	0.10986620	0.11003659	0.11009354	0.11020766	0.11101506	0.11160108
	0.32495100	0.32523853	0.32533485	0.32552820	0.32690883	0.32792482
	0.52518702	0.52527825	0.52530879	0.52537007	0.52580662	0.52612672
	0.69935152	0.69938262	0.69939296	0.69941358	0.69955607	0.69965587
	0.83760278	0.83814919	0.83832893	0.83868482	0.84104236	0.84258561
	0.93432490	0.93561159	0.93603769	0.93688475	0.94252263	0.94609498
	0.98814878	0.98925826	0.98964727	0.99045547	0.99738803	1.00393672
0.3	0.11079166	0.11105338	0.11114097	0.11131669	0.11256672	0.11348156
	0.32790610	0.32837809	0.32853664	0.32885560	0.33115919	0.33288348
	0.53038197	0.53058838	0.53065776	0.53079736	0.53180748	0.53256582
	0.70646993	0.70647376	0.70647503	0.70647757	0.70649526	0.70650779
	0.84544020	0.84595426	0.84612225	0.84645325	0.84859109	0.84993887
	0.94085982	0.94249134	0.94302123	0.94405804	0.95031347	0.95364596
	0.99166000	0.99367573	0.99439450	0.99590571	1.00953810	1.02291264
0.4	0.11173007	0.11208738	0.11220712	0.11244759	0.11416793	0.11543761
	0.33086075	0.33154597	0.33177685	0.33224233	0.33564520	0.33823878
	0.53557531	0.53596290	0.53609381	0.53635824	0.53831154	0.53982442
	0.71389426	0.71390952	0.71391462	0.71392486	0.71399764	0.71405082
	0.85461337	0.85489670	0.85498915	0.85517113	0.85634232	0.85707930
	0.95046649	0.95178904	0.95220399	0.95299571	0.95726743	0.95927194
	1.00080113	1.00431802	1.00556721	1.00818332	1.03111306	1.05288552
0.5	0.11268119	0.11313843	0.11329188	0.11360036	0.11581988	0.11747201
	0.33379479	0.33472229	0.33503577	0.33566928	0.34035956	0.34400147
	0.54063303	0.54127709	0.54149592	0.54193998	0.54530379	0.54801081
	0.72111740	0.72124622	0.72128972	0.72137757	0.72202612	0.72252810
	0.86377027	0.86381569	0.86383066	0.86386035	0.86405903	0.86419176
	0.96033036	0.96077981	0.96091991	0.96118665	0.96265017	0.96338561
	1.02534909	1.03060372	1.03243540	1.03622353	1.06802366	1.09782395
0.6	0.11364472	0.11420633	0.11439508	0.11477492	0.11752363	0.11958729
	0.33668724	0.33788546	0.33829171	0.33911470	0.34528653	0.35016755
	0.54542417	0.54640134	0.54673558	0.54741727	0.55273118	0.55719661
	0.72763575	0.72801650	0.72814666	0.72841203	0.73047791	0.73221463
	0.87135469	0.87137800	0.87138586	0.87140168	0.87151701	0.87160464
	0.96644071	0.96646801	0.96647691	0.96649442	0.96660713	0.96667832
	1.08063246	1.08657617	1.08864746	1.09293407	1.12950579	1.16537440
0.7	0.11462029	0.11529078	0.11551644	0.11597106	0.11928000	0.12178556
	0.33951717	0.34101295	0.34152170	0.34255478	0.35040039	0.35671175
	0.54983867	0.55121816	0.55169332	0.55266760	0.56049482	0.56736981
	0.73312078	0.73388027	0.73414348	0.73468582	0.73918112	0.74335675
	0.87676704	0.87699755	0.87707713	0.87724065	0.87857479	0.87978760
	0.96943100	0.96945724	0.96946621	0.96948447	0.96962642	0.96974573
	1.18621471	1.19181411	1.19378196	1.19788197	1.23442256	1.27312845
0.8	0.11560748	0.11639142	0.11665564	0.11718851	0.12108955	0.12406845
	0.34226450	0.34408221	0.34470238	0.34596460	0.35566459	0.36358118
	0.55380035	0.55563702	0.55627403	0.55758709	0.56845053	0.57837485
	0.73748263	0.73870282	0.73913142	0.74002392	0.74791525	0.75602992
	0.88033414	0.88088192	0.88107549	0.88148059	0.88519735	0.88933282
	0.97092928	0.97106182	0.97110871	0.97120694	0.97211711	0.97315890
	1.39020742	1.39487561	1.39652857	1.39999355	1.43220727	1.46920665
0.9	0.11660579	0.11750778	0.11781223	0.11842688	0.12295251	0.12643684
	0.34491088	0.34707162	0.34781100	0.34931913	0.36103194	0.37069121
	0.55727131	0.55960236	0.56041615	0.56210195	0.57642182	0.58986849
	0.74080919	0.74252347	0.74313315	0.74441517	0.75645303	0.76991088
	0.88261170	0.88349502	0.88381341	0.88449047	0.89142971	0.90081789
	0.97172777	0.97197493	0.97206474	0.97225708	0.97435412	0.97771060
	1.89084608	1.89412099	1.89528671	1.89774090	1.92130043	1.95026061

Table 3. Discrete eigenvalues of the P_{13} iteration for Rayleigh scattering

w	P_1	P_3	P_5	P_7	P_9	P_{11}	P_{13}
0.1	0.60858061	0.35222723	0.24488545	0.18718942	0.15136247	0.12699919	0.10937150
		0.88057190	0.67400993	0.53419630	0.43959504	0.37245332	0.32267262
			0.94430192	0.80710092	0.68740631	0.59356701	0.52024994
				0.96807914	0.87340830	0.77693402	0.69310227
					0.97940041	0.91082296	0.83331449
						0.98564509	0.93389202
							0.98944456
0.2	0.64549722	0.36571853	0.25158251	0.19113571	0.15395071	0.12882341	0.11072497
		0.90411068	0.68838211	0.54367652	0.44625702	0.37735381	0.32641023
			0.95942482	0.81897020	0.69627130	0.60039482	0.52564918
				0.97870361	0.88309100	0.78479704	0.69950555
					0.98739798	0.91880792	0.84022709
						0.99197218	0.94058014
							0.99463679
0.3	0.69006555	0.38062956	0.25874573	0.19528384	0.15664289	0.13070776	0.11211622
		0.93344599	0.70444820	0.55400685	0.45338796	0.38253161	0.33032203
			0.97953926	0.83228659	0.70601210	0.60780084	0.53143999
				0.99396365	0.89402772	0.79345871	0.70648897
					0.99982107	0.92791733	0.84786261
						1.00258591	0.94829321
							1.00402138
0.4	0.74535599	0.39714836	0.26641011	0.19964359	0.15944256	0.13265376	0.11354599
		0.97132057	0.72219072	0.56517951	0.46097677	0.38797673	0.33440022
			1.00754661	0.84673828	0.71654195	0.61574158	0.53759277
				1.01708559	0.90562266	0.80273881	0.71397142
					1.02027563	0.93730424	0.85594381
						1.02148094	0.95597296
							1.02196695
0.5	0.81649658	0.41546162	0.27460801	0.20422368	0.16235283	0.13466276	0.11501493
		1.02246601	0.74132376	0.57712215	0.46898805	0.39366829	0.33863169
			1.04860294	0.86151877	0.72764092	0.62411645	0.54404879
				1.05383918	0.91668860	0.81227652	0.72178754
					1.05509988	0.94558001	0.86398985
						1.05542533	0.96219727
							1.05551141
0.6	0.91287092	0.43572393	0.28336587	0.20903107	0.16537617	0.13673582	0.11652358
		1.09577468	0.76117560	0.58967609	0.47735621	0.39957261	0.34299714
			1.11237875	0.87545486	0.73894975	0.63276225	0.55071777
				1.11457086	0.92606913	0.82158858	0.72969547
					1.11489313	0.95192134	0.87147487
						1.11494159	0.96656875
							1.11494890
0.7	1.05409255	0.45800247	0.29269948	0.21407019	0.16851418	0.13887365	0.11807228
		1.21019870	0.78072693	0.60258799	0.48598262	0.40564231	0.34747085
			1.21886551	0.88757282	0.75002833	0.64146483	0.55748160
				1.21948640	0.93340591	0.83022719	0.73742020
					1.21953274	0.95651192	0.87805633
						1.21953620	0.96957269
							1.21953645
0.8	1.29099444	0.48219365	0.30260795	0.21934189	0.17176740	0.14107655	0.11966122
		1.41545544	0.79891941	0.61552907	0.49473821	0.41181688	0.35202086
			1.41868761	0.89756316	0.76047000	0.64999068	0.56420569
				1.41878191	0.93902530	0.83792883	0.74471844
					1.41878467	0.95988991	0.88366025
						1.41878475	0.97173843
							1.41878475
0.9	1.82574185	0.50792847	0.31306648	0.22484233	0.17513496	0.14334429	0.12129035
		1.91074772	0.81506202	0.62814655	0.50347343	0.41802545	0.35660993
			1.91130975	0.90566601	0.77000594	0.65812931	0.57075608
				1.91131339	0.94341956	0.84464332	0.75143000
					1.91131342	0.96249787	0.88839506
						1.91131342	0.97340607
							1.91131342

4. Conclusion

The radiative transfer equation is used to understand the behaviour of light within a medium. In this study we assumed homogeneous medium surrounded with a slab thickness x . The behaviour of the photons is examined with three different scattering types. The numerical results are obtained for each condition separately. By making calculations, The Wolfram Mathematica program is run to find the discrete eigenvalues of the radiative transfer equation by Legendre polynomial method. The P_N method is iterated up to 13th to observe the convergence. The results for all scattering types meet the expectations related with the eigenvalues of the radiative transfer equation. The presented study displays a wide range of numerical data about the radiative transfer equation solution with Legendre polynomial method. The single scattering albedo numbers and the scattering coefficients are taken into account a detailed spectrum. Being a large scale of calculated data causes a great source to compare their own method solutions.

Author Contributions

The percentage of the author(s) contributions is presented below. All authors reviewed and approved the final version of the manuscript.

	D.A.	H.K.
C	50	50
D	100	
S		100
DCP	50	50
DAI	50	50
L	50	50
W	50	50
CR	50	50
SR	50	50

C=Concept, D= design, S= supervision, DCP= data collection and/or processing, DAI= data analysis and/or interpretation, L= literature search, W= writing, CR= critical review, SR= submission and revision.

Conflict of Interest

The authors declared that there is no conflict of interest.

Ethical Consideration

Ethics committee approval was not required for this study because of there was no study on animals or humans.

References

- Anlı F, Güngör S. 2005. General eigenvalue spektrum in a one-dimensional slab geometry transport equation. Nucl Sci Eng, 150: 1-6.
- Biçer M, Kaşkaş A. 2018. Solution of the radiative transfer equation for Rayleigh scattering using the infinite medium Green's function. Astrophys Space Sci, 363: 46.
- Chandrasekhar S. 1950. Radiative transfer. Oxford University Press, London, UK.
- Chandrasekhar S. 1960. Radiative Transfer. Dover Publication, New York, US.
- Cherry SR, Sorenson JA, Phelps ME. 2012. Interaction of Radiation with Matter. J Nucl Med, 54(7): 63-85.
- Elghazaly A, El-Konsol S, Sabbah AS, Hosni M. 2017. Anisotropic radiation transfer in a two-layer inhomogeneous slab with reflecting boundaries. Int J Therm Sci, 120: 148-161.
- Güçlü İ. 2009. Legendre polynomial approach for solutions of higher order linear volterra integro-differential equations. MSc Thesis, Celal Bayar University, Insitute of Science, Manisa, Türkiye, pp: 84.
- Herman BM, Browning SR. 1965. A Numerical solution to the equation of radiative transfer. J Atmos Sci, 22(5): 559-566.
- Hussein A, Selim MM. 2012. Solution of the stochastic radiative transfer equation with Rayleigh scattering using RVT technique. Appl Math Comput, 218(13): 7193-7203.
- Sallah M, Selim MM. 2008. Continuous stochastic radiative transfer with Rayleigh scattering in semi-infinite atmospheric media. In Proceedings of the 3rd Environmental Physics Conference, 19-February 23, 2008, Aswan, Egypt.
- Stamnes K, Thomas GE, Stamnes JJ. 2017. Formulation of radiative transfer problems. Cambridge University Press, Cambridge, UK, pp: 186-226.
- Tapimo R, Tagne Kamdem HT, Yemele D. 2018. Homojen olmayan polarize düzlemsel atmosferde ışınım transfer analizi için ayrı bir küresel harmonik yöntemi. Astrofizik Uzay Bilim, 363(3): 52.
- Taşdelen M. 2017. Application SN method and AG phase functions to radiavite transfer equation of eigenvalue spektrum. MSc Thesis, Sütçü İmam University, Institute of Science, Kahramanmaraş, Türkiye, pp: 42.



EFFECT OF CaF_2 ADDITIONS ON THE YIELD OF AZ63 MAGNESIUM CHIPS DURING REMELTING

Pınar YÖRÜK¹, Mertol GÖKELMA^{1*}


¹*Izmir Institute of Technology, Department of Materials Science and Engineering, 35430, İzmir, Türkiye*

Abstract: Magnesium is one of the metals listed in European Union's critical raw materials list. Primary production of magnesium is a high energy demanding process which raised the necessity of recycling the magnesium alloys in an efficient way. Remelting those scraps under a salt flux consist of chlorides (NaCl , KCl , and MgCl_2) and fluorides (CaF_2) are a common process however, different alloys might behave differently when it comes to salt-metal-metal oxide interactions. Furthermore, the condition of the salt flux such as dry-mixed or pre-melted (fused) affects the coagulation and metal yield. This work presents results on the effect of CaF_2 concentration and pre-melting the salt flux on metal yield during remelting of chips. A yield up to 75% was observed in the case of remelting of chips under a fused salt flux with 5.5% CaF_2 concentration.

Keywords: Recycling, Machining waste, Salt flux, Fluoride

*Corresponding author: Izmir Institute of Technology, Department of Materials Science and Engineering, 35430, İzmir, Türkiye

E mail: mertolg kelma@iyte.edu.tr (M. GÖKELMA)

Pınar YÖRÜK  <https://orcid.org/0009-0008-5501-6620>

Mertol GÖKELMA  <https://orcid.org/0000-0002-0217-6013>

Received: September 08, 2023

Accepted: November 07, 2023

Published: January 15, 2024

Cite as: Yörük P, Gök elma M. 2024. Effect of CaF_2 additions on the yield of AZ63 magnesium chips during remelting. BSJ Eng Sci, 7(1): 16-20.

1. Introduction

Magnesium alloys are used in aerospace, automotive, electronics, construction, and medical industries due to their unique properties (Demirci, 2006). The demand for magnesium and its alloys has been increasing in the last decades due to the need of substitution of heavier materials in many applications. The European Union reported the risks and importance of sourcing 41 raw materials which are not produced sufficiently in Europe although they have high importance in European economy (Türe and Türe, 2020). Magnesium as a raw material is also included in the list of critical raw materials (Entr, 2014; Ostrovsky and Henn, 2007).

The primary production of magnesium is an energy intensive process as it must be extracted from ores at high temperatures with high electricity consumption. In many countries, strict environmental rules are set thus, the supply of magnesium may be constrained, and production costs might increase with rising energy prices and environmental concerns. Due to the environmental impact of primary metal production, recycling has been also rising to reduce the environmental effects (Lewicka et al., 2021).

Recycling of magnesium scraps are complex due to a thick layer of oxide (Mendis and Singh, 2013). Magnesium is a highly reactive to oxygen and moisture which results in exothermic reactions and forms magnesium oxide (Tenorio and Espinosa, 2002; Nie et al., 2016; Tan et al., 2019). The oxidation reactions of magnesium are given in equations 1 and 2 (Filotás et al. 2020).



AZ63 magnesium alloy is a suitable alloy for weight reduction in structural application and commonly used in magnesium industry. This alloy has high specific strength and stiffness. However, AZ63 has risk to oxidize especially in environments with high moisture. When exposed to air and moisture it goes through a similar oxidation process to that of pure magnesium (Filotás et al. 2020). It is typically coated or alloyed with rare earth elements to improve the corrosion resistance.

Due to the oxide layer on the scraps and high oxidation tendency at high temperature, remelting magnesium alloys is complex. Especially, chips generated during machining processes have a large surface area which increases the oxide amount per unit mass as well as oxidation speed. Remelting scraps are conducted under a salt flux which helps to remove the thick oxide layer, as well as enhances the coalescence of the metal droplets. Furthermore, the molten salt covers surface of the metallic melt and avoids interactions between the metal and air (Akbari and Friedrich, 2010). Salt fluxes typically consist of fluorides (CaF_2 and NaF) and chlorides (NaCl , KCl , and MgCl_2) which are used for promoting coagulation and generate a fluid flux respectively (Çağlar Yüksel et al., 2017). Leading research teams have chosen the chloride combination $\text{MgCl}_2/\text{KCl}/\text{NaCl}$ in recycling and remelting applications (Maksoud and Bauer, 2015; Ding et al., 2019; Vidal and Klammer, 2019; Sun et al., 2020).



This study investigates the recyclability of chips generated from AZ63 alloy as well as the effect of fluoride concentrations on the metal yield.

2. Materials and Methods

Chips were machined from AZ63 magnesium ingots to generate a high surface area (approximately 30x10 mm) and study its recyclability accordingly. Chips were analysed under Scanning Electron Microscopy (SEM- FEI QUANTA 250 FEG) and Energy Dispersive X-ray Spectroscopy to observe the alloying elements.

Additionally, chips were analysed by Thermogravimetric analysis (TGA-Perkin Elmer Diomand) to observe the oxidation behaviour of chips with increasing temperature. Table 1 presents the elemental composition of the ingot. The chips were remelted under the salt flux consisting of NaCl (24 wt.%), KCl (15 wt.%), MgCl₂ (56 wt.%), and CaF₂ (4-6 wt.%). A laboratory-scale resistance chamber furnace was used for the remelting experiments. The salt flux was used as dry-mixed and fused to observe the effect of pre-melted salt on the yield.

Table 1. Chemical composition of AZ63 magnesium alloy in wt.%.

Mg	Be	Fe	Mn	Al	Si	Ni	Cu	Zn
90.283	0.0012	0.0032	0.6628	5.6007	0.0033	0.0008	0.0003	3.4386

Dry-mixed salt was prepared by manually mixing the salt components in a mortar while the fused salt flux was prepared by melting the dry-mixed salt mixture at 750 °C and crushing after cooling down. 4 grams of AZ63 magnesium chips shown in the Figure 1 and was charged with the salt mixture in a clay-bonded crucible and heated up to 850 °C and kept at the temperature for 15 minutes. 40 grams of salt mixture was used for each experiment to ensure a full coverage and interaction of the salt with the scrap. Each experiment was carried out three times to define a standard deviation.



Figure 1. AZ63 chips used for the remelting experiments.

CaF₂ was added into the chloride mix in five different concentrations from 4 to 6 wt.% presented in Table 2. CaF₂ was varied to observe the effect of the fluoride content on the metal yield of AZ63 scraps which is missing in the literature. After remelting, the dross and metal in the crucible were separated manually and metal yield was calculated after drying and weighing the samples. The metal yield was calculated according to equation 3.

$$\text{Metal Yield(\%)} = \frac{m_{\text{recovered metal}}}{m_{\text{scrap}}} \times 100 \quad (3)$$

where $m_{\text{recovered metal}}$ is the total amount of recovered magnesium after remelting, m_{scrap} is the total amount of scrap charged for remelting.

Table 2. Experimental parameters

Exp. Nr.	CaF ₂ (wt. %)	Preparation method of the salt flux
1-3	4	Dry-mixed
4-6	4.5	
7-9	5	
10-12	5.5	
13-15	6	
16-18	4	
19-21	4.5	Fused
22-24	5	
25-27	5.5	
28-30	6	

3. Results and Discussion

SEM/EDS results of the AZ63 chips are presented in Figure 2. The results show that the alloy is mainly composed of magnesium, aluminium, and zinc. Aluminium zinc intermetallic precipitation is also seen in the SEM image.

The chip samples were also analysed by TGA under oxygen atmosphere up to 800°C (5°C/min). It was observed that the oxidation rate was approximately 1% weight gain per 50°C until 450 °C, however the oxidation rate increased significantly after 450 °C up to 30% weight gain per 50°C. This transition of oxidation behaviour indicates the first liquid formation of the alloy (solidus) which increases the oxidation and shows the necessity of using salt fluxes during remelting.

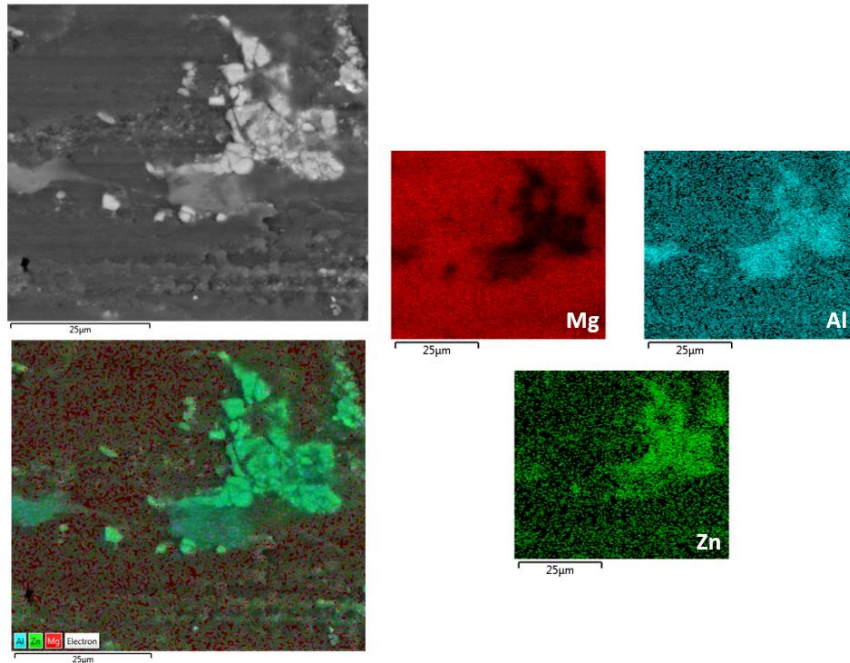


Figure 2. SEM Analysis and EDX mapping for AZ63 magnesium chips.

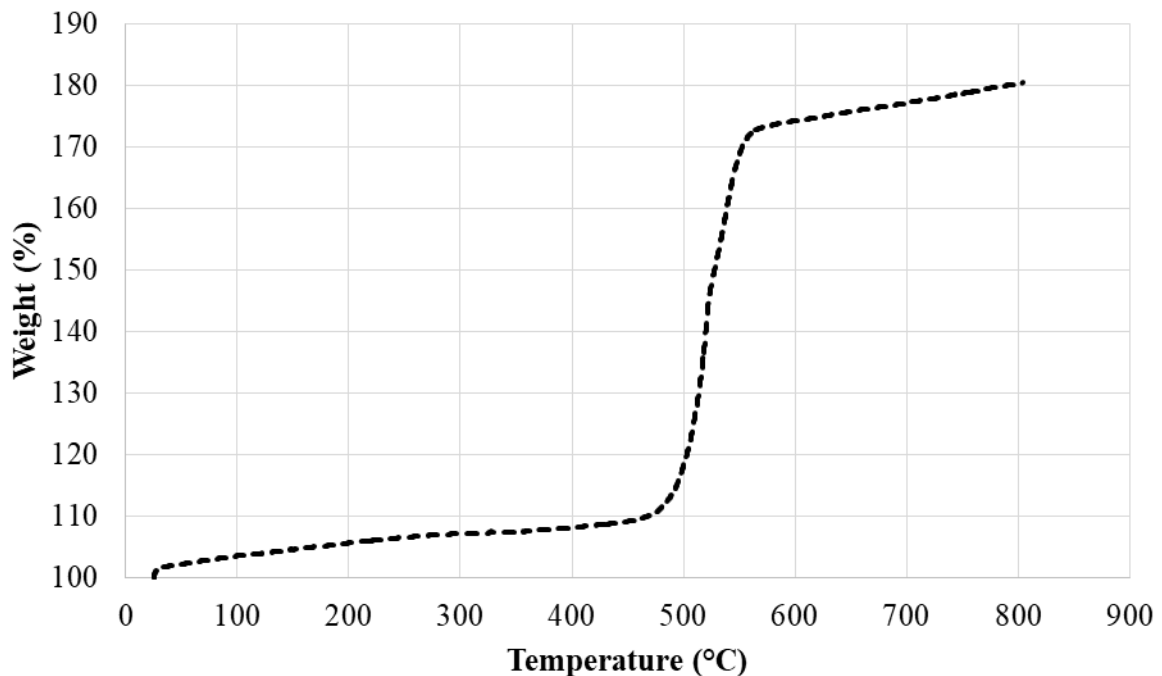


Figure 3. TGA analysis of AZ63 magnesium chips under oxygen flow.

Chips were remelted under dry-mixed and fused salt having CaF_2 concentrations from 4 to 6 wt. %. Figure 4 presents the metal yield of ten different conditions each with three repetitions. In both conditions increasing CaF_2 concentrations increased the magnesium yield until 5.5 wt.% of CaF_2 and decreased after this concentration. 5.5 wt.% showed the highest yield (av. 69% for dry-mixed, av. 73% for fused) which was found in different works as 5 wt.% for pure magnesium (Yörük and Göknelma, 2023) and AZ31 (Akbari et al., 2009) which indicates that different amount of fluoride additions might work different for different alloys. Fused salt showed a higher

yield than dry-mixed in all fluoride conditions. The reason for the fused salt worked better is mainly because of its homogeneity which allows it to melt before the chips melt while dry-mixed salt generates a liquid phase at one of the melting points of the components. Early melting protects the metal better from high temperature oxidation.

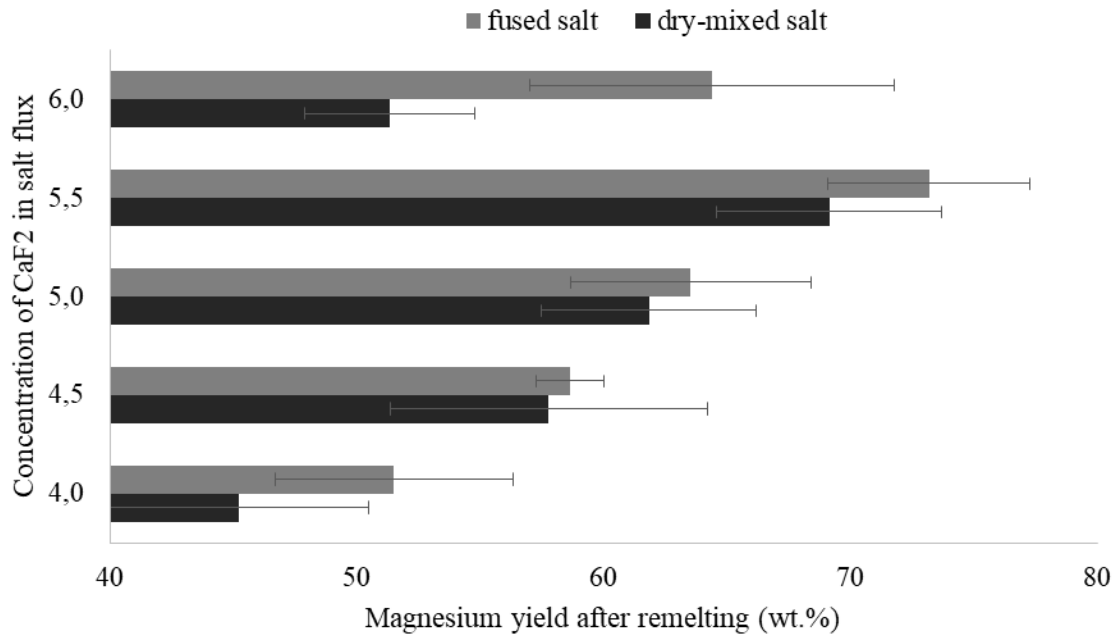


Figure 4. Effects of CaF₂ concentrations and salt pre-melting on metal yield.

Figure 5 presents the recovered magnesium droplets after remelting under dry-mixed and fused salt fluxes. Two size and shape of the droplets are important parameters to understand the coagulation. An efficient coagulation is required to overcome the metal yield issues mainly originating from metal entrapment in the dross. In the lab scale experiments the dross is washed on a sieve so all metals can be included in the yield however, in industrial scale dross is separated to be sold or disposed. Therefore, it is important to achieve an efficient metal-dross separation. The droplets formed in the dry-mixed salt flux are smaller and less spherical in comparison with the droplets formed in the fused salt flux. The main reason for low sphericity is the insufficient removal of the oxide layer due to homogeneity issues. The sphericity of droplets indicates that the salt-oxide interactions were sufficient. Fused salt worked more efficiently since the flux was homogeneous in terms of the melting and F⁻ concentration in the flux.

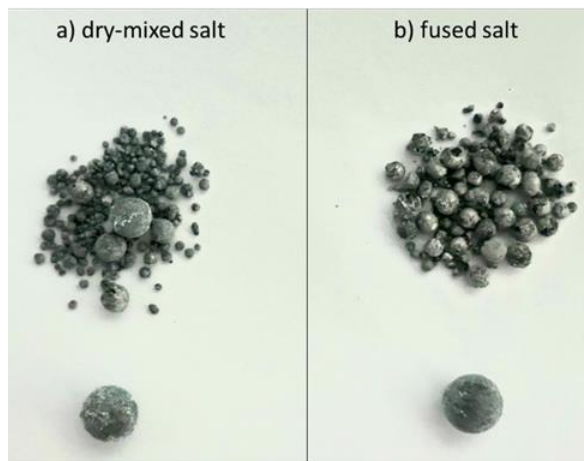


Figure 5. Metal droplets obtained after remelting under (a) dry-mixed and (b) fused salt

4. Conclusions

The effects of premelting the salt flux and CaF₂ content in the salt were studied in this work and the following conclusions could be drawn:

- 5.5 wt.% of CaF₂ showed the highest metal yield for AZ63 alloys.
- Fused salt increases the metal yield significantly. Metal yield increased with increasing sphericity of droplets.

Author Contributions

The percentage of the author(s) contributions is presented below. All authors reviewed and approved the final version of the manuscript.

	P.Y.	M.G.
C	25	75
D	50	50
S		100
DCP	50	50
DAI	50	50
L	75	25
W	75	25
CR	25	75
SR	50	50
PM		100
FA		100

C=Concept, D= design, S= supervision, DCP= data collection and/or processing, DAI= data analysis and/or interpretation, L= literature search, W= writing, CR= critical review, SR= submission and revision, PM= project management, FA= funding acquisition.

Conflict of Interest

The authors declared that there is no conflict of interest.

Ethical Consideration

Ethics committee approval was not required for this study because of there was no study on animals or humans.

Acknowledgements

This research was funded by the Scientific and Technological Research Council of Türkiye (TÜBİTAK) under the BİDEB-2232 program with grant number 118C311. Center for Materials Research at İzmir Institute of Technology is gratefully acknowledged for the sample analyses.

References

- Akbari S, Friedrich B. 2010. Salt-Metal interaction in magnesium recycling. In Proceedings of International Workshop on Metal-Slag Interaction, September 14-19, Yalta, Crimea, Ukraine, pp: 71.
- Akbari S, Gökelma M, Friedrich B, Recycling M. 2009. Potential of minimizing magnesium losses in black dross through optimization of salt fluxes. In Proceedings of European Metallurgical Conference, June 28 - July 1, Innsbruck, Austria, pp: 1-19.
- Çağlar Yüksel ÖT, Erzi E, Dışpınar D, Çiğdem M. 2017. Melt quality change with different fluxes in secondary A356 alloy. In Proceedings of European Congress and Exhibition on Advanced Materials and Processes, September 17-22, Athens, Greece, pp: 1-5.
- Demirci G. 2006. Electrolytic magnesium production using coaxial electrodes. PhD thesis, Middle East Technical University, The Graduate School of Natural And Applied Sciences, Ankara, Türkiye, pp: 170.
- Ding W, Gomez-Vidal J, Bonk A, Bauer T. 2019. Molten chloride salts for next generation CSP plants: Electrolytical salt purification for reducing corrosive impurity level. *Solar Energy Mater Solar Cells*, 199: 8-15.
- Entr D. 2014. Report on critical raw materials for the EU. European Commission, Brussels, Belgium, pp: 124.
- Filotás D, Fernández-Pérez B, Nagy L, Nagy G, Souto R. A novel scanning electrochemical microscopy strategy for the investigation of anomalous hydrogen evolution from AZ63 magnesium alloy. *Sensors Actuat B: Chem*, 308: 127691.
- Lewicka E, Guzik K, Galos K. 2021. On the possibilities of critical raw materials production from the EU's primary sources. *Resources*, 10(5): 50.
- Maksoud L, Bauer T. 2015. Experimental investigation of chloride molten salts for thermal energy storage applications. In Proceedings of 10th International Conference on Molten Salt Chemistry and Technology, May 22 - 25 Seattle, USA, pp: 751-760.
- Mendis CL, Singh A. 2013. Magnesium recycling: to the grave and beyond. *Jom*, 65: 1283-1284.
- Nie H, Schoenitz M, Dreizin EL. 2016. Oxidation of magnesium: implication for aging and ignition. *J Physical Chem*, 120(2): 974-983.
- Ostrovsky I, Henn Y. 2007. Present state and future of magnesium application in aerospace industry. In Proceedings of International Conference "New challenges in aeronautics", August 19-22, Moscow, Russia, pp: 19-22.
- Sun H, Wang JQ, Tang Z, Liu Y, Wang C. 2020. Assessment of effects of Mg treatment on corrosivity of molten NaCl-KCl-MgCl₂ salt with Raman and Infrared spectra. *Corrosion Sci*, 164: 108350.
- Tan Q, Yin Y, Mo N, Zhang M, Atrens A. 2019. Recent understanding of the oxidation and burning of magnesium alloys. *Surface Innovat*, 7(2): 71-92.
- Tenorio JAS, Espinosa DCR. 2002. Effect of salt/oxide interaction on the process of aluminum recycling. *J Light Met*, 2(2): 89-93.
- Türe Y, Türe C. 2020. An assessment of using Aluminum and Magnesium on CO₂ emission in European passenger cars. *J Cleaner Prod*, 247: 119120.
- Vidal JC, Klammer N. 2019. Molten chloride technology pathway to meet the US DOE sunshot initiative with Gen3 CSP. In AIP Conference Proceedings, 4-8 September, Bodrum, Türkiye, pp: 2126.
- Yörük P, Gökelma M, Derin B. 2023. Effect of compaction and fluoride content on the remelting efficiency of pure magnesium chips. *Canadian J Metallur Mat Sci*, <https://doi.org/10.1080/00084433.2023.2262189>.



APPLICATION OF MULTI-CRITERIA DECISION MAKING METHODS FOR MENU SELECTION

Semih Latif İPEK^{1*}, Dilek GÖKTÜRK²

¹Adana Alparslan Türkeş Science and Technology University, Department of Food engineering, 01250, Adana, Türkiye


²Adana Alparslan Türkeş Science and Technology University; Department of Bioengineering, 01250, Adana, Türkiye


Abstract: Nutritional information on menus can assist customers in making healthier eating choices. One technique being utilized to tackle the rise of overweight and obesity is the use of nutritional information on menus. Menu engineering strategies can be used to improve sales of generally healthier and higher margin items. For today's food and beverage companies, menu engineering has become essential. Companies must continually evaluate their menus in order to keep up with changing customer demands and the conditions of the competitive market. Menu engineering's core involves comparing the effectiveness of each menu. At this point, correct decision-making under numerous factors is thought to be a very challenging procedure. To evaluate alternatives according to many features, several Multi-Criteria Decision-Making (MCDM) approaches have been created. The main novelty of this paper is that four MCDM methods, including Technique for Order Preference by Similarity to an Ideal Solution (TOPSIS), Fuzzy TOPSIS, VlseKriterijumska Optimizacija I Kompromisno Resenje (VIKOR), and Fuzzy VIKOR, are employed to evaluate menu options. Comparative analysis of MCDM methods is another contribution of this study. The process of evaluating and selecting healthier menu alternatives can become challenging and time-consuming. This study pointed out how crucial it is to conduct comparative analysis using various MCDA methods and to carefully determine the right ones when addressing the issue of selecting the best menu, taking into account the values of the criterion in fuzzy numbers.

Keywords: Menu engineering, Menu selection, Multi-criteria, Decision-making approaches

*Corresponding author: Adana Alparslan Türkeş Science and Technology University, Department of Food engineering, 01250, Adana, Türkiye

E mail: slipek@atu.edu.tr (S. L. İPEK)

Semih Latif İPEK  <https://orcid.org/0000-0002-4661-7765>

Dilek GÖKTÜRK  <https://orcid.org/0000-0002-1195-5828>

Received: September 12, 2023

Accepted: November 07, 2023

Published: January 15, 2024

Cite as: İpek SL, Göktürk D. 2024. Application of multi-criteria decision making methods for menu selection. BSJ Eng Sci, 7(1): 21-30.

1. Introduction

Describing the most nutritious menu items in less appealing words may promote the idea that healthy foods aren't delicious or indulgent, undermining customers' choice of healthier eating options. Much can be done to make healthy selections appealing, and further research is needed to understand how changing descriptions in restaurant settings might impact food choice, metabolism, satisfaction, and overall attitudes about healthy eating (Turnwald et al., 2017). Efficient communication is critical in providing significant and relevant nutrition information that reflects the healthiness of a menu item. Moreover, offering more nutrition information may be necessary to foster positive perceptions of the promoted menu item and purchase intent among customers. Restaurant management can encourage consumers to choose healthier menu items by displaying calorie, fat, and cholesterol information on the menu board or through advertising healthy choices (Jeong and Jang, 2016).

Researchers should prioritize long-term prevention of chronic diseases such as cancer and cardiovascular disease among the general population (Detopoulou et al., 2022). For instance, menu calorie labeling may

contribute to public health promotion and the prevention of chronic diseases (Jia et al., 2023). Additionally, dietary fiber plays a crucial role in maintaining good health and preventing noncommunicable diseases (Sampaio et al., 2017). Excessive sodium consumption, often associated with restaurant foods, has been linked to an increased risk of cardiovascular disease (Wolfson et al., 2018). Many are unaware that reducing salt intake is one of the easiest and quickest ways to improve our health. In the UK alone, just 1 fewer "pinch" of salt per day can save almost 4,000 heart attacks and strokes annually (World awareness weeks). Alonso et al. (2021) presented that by 2050, there would be 87 870 fewer cases of premature ischemic heart disease and 126 010 fewer cases of premature stroke, compared to the health gains in the base-case analysis, if larger population salt intake reductions were achieved by 2030, as advised by the World Health Organization (WHO). Consequently, numerous researchers have investigated issues related to dietary habits. One of the main aims of this study is to evaluate the most preferred menus of a local restaurant according to six important criteria. It is very difficult to evaluate the six criteria, including calories, cholesterol, fiber, saturated fat, sodium, and sugar, for each menu at the same time. At this point, the advantages of using



MCDM methods are emphasized in this study.

Yamamoto et al. (2005) found that most adolescents' meal ordering behavior remained unchanged when calorie and fat content information was added to menus. Nevertheless, promoting the provision of nutrition information is advisable because it lead some adolescents to reduce their calorie and fat intake without imposing any adverse financial effects on the restaurants. Gerend (2009) examined the dietary choices of college students in relation to the availability of calorie information on fast-food menus. Elbel et al. (2009) investigated how menu calorie labels influence consumer decisions regarding fast food. In their study involving low-income and minority consumers, calorie labeling increased both the calorie information and the number of individuals reporting that this information influenced their food choices. Dumanovsky et al. (2010) assessed awareness of calorie content on fast-food menus. Obbagy et al. (2011) found that most chefs believed that restaurant dishes could be significantly reduced in calorie content without customers noticing. They emphasized the need for collaboration between chefs and public health experts to make appealing low-calorie menu options more accessible. Dowray et al. (2013) explored the impact of calorie content labeling, combined with information about the physical activity required to burn those calories, on meal choices from a fast-food menu. Respondents generally selected lower-calorie meals when presented with this information, suggesting that the distance-to-walk label was particularly effective.

Hobin et al. (2022) demonstrated that listing calories for both alcoholic and non-alcoholic beverages on restaurant menus increased customer awareness of calorie content. Jia et al. (2023) investigated the relationship between menu calorie labels, dietary quality, and weight status, exploring whether this relationship varied among different groups. While calories provide a measure of food consumption, they do not reflect nutritional value comprehensively. Considerations such as protein and fiber content, sugar, salt, and fat levels are equally important. For instance, reducing total fat intake without addressing saturated fat may not significantly impact low-density lipoprotein cholesterol (LDL-C) levels (Nicolosi et al., 2001). Therefore, it is advisable to consider multiple criteria when evaluating dietary choices.

In Hwang and Lorenzen (2008), the participants found menus that included calories, macronutrients, and fat content to be the most useful and reliable. They also perceived menus with more nutritional information as more appealing. Furthermore, the disclosure of nutritional information influenced participants' overall sentiments about menu items and their attitudes toward nutrition. Bruemmer et al. (2012) audited menu items to document changes resulting from King County's menu labeling regulation. Certain menu items were redesigned to improve nutrition profiles by reducing energy, saturated fat, and sodium content. Patel et al. (2016)

assessed restaurant companies and their recipes. They found that acceptable ingredient changes led to reductions of up to 26% in calories and up to 31% in sodium per serving. Most menu items in restaurants experienced slight decreases in calories, fat, saturated fat, and sodium, which were considered acceptable. Cantu-Jungles et al. (2017) conducted a meta-analysis on sodium, total fat, saturated fat, and carbohydrates, finding no significant impact of menu labeling on U.S. adults' nutrient choices in restaurants. Huang et al. (2022) observed that menu items at large chain restaurants in the USA contained higher absolute levels of energy, fat, saturated fat, and sugar compared to the UK. Inter-country variations were especially notable in children's meal items for sodium and saturated fat.

Scourboutakos et al. (2014) found that displaying sodium information on restaurant menus led to significantly lower salt intake among customers compared to those who only had access to calorie information. However, the extent of the reduction varied depending on the type of restaurant. These results suggest that menu labeling can influence the nutrient composition of diners' choices when eating out, particularly when sodium information is provided alongside calorie information. Rudelt et al. (2014) recommended that individuals aiming to limit their sodium intake should exercise caution when making menu choices at fast-food establishments. Hobin et al. (2016) conducted an experimental study to explore whether various menu labeling formats, which provide information on calorie and sodium content, influence parents' choices. Menu labeling that includes calorie and sodium information may reduce the demand for fast food children's meals and help parents choose healthier food options for their kids. Wolfson et al. (2018) demonstrated that although the sodium content of newly introduced items decreased on average, foods on U.S. chain restaurant menus still tend to have excessive sodium levels. In Byrd et al. (2018), customers' menu choices were assessed based on the calorie and sodium contents of the items. The study found that, even with taste preferences considered, the menu displaying the sodium warning symbol did not significantly differ from the other menu conditions. Byrd and Almanza (2021) indicated that policies mandating sodium menu labeling may not achieve the expected outcome of encouraging customers to choose lower-sodium items. Sisti et al. (2023) also demonstrated that the sodium content of menu items remained unchanged after the implementation of sodium warning icon legislation, underscoring the challenges associated with reducing sodium levels in restaurant offerings.

State and local governments can contribute to creating a healthier food supply and population by supporting efforts to reduce sodium levels through systemic and environmental reforms (Alexander et al., 2021). Bowers and Suzuki (2014) found that menu labeling, intended to encourage shifts in dietary and health behaviors, was associated with positive changes. Those who used menu

labels reported meeting recommended exercise guidelines, consuming more fruits, and drinking less soda compared to those who did not use menu labeling. Sigala et al. (2022) assessed the impact of menu added-sugar warning labels on customer behavior. Falbe et al. (2023) reported that the likelihood of ordering high-added-sugar menu items decreased with the presence of added-sugar warning labels, and participants' awareness of items containing more than 50% of the daily recommended added sugar amount improved.

This study contributes to a better understanding of menu selection and the most effective ways to evaluate six important criteria: calories, cholesterol, fiber, saturated fat, sodium, and sugar. This study also contributes to the literature by conducting a field experiment at a local restaurant to examine menu choices in a real-world environment. While this study deals with choosing the best menu by considering the criteria values, it has made a comparative analysis using various MCDM methods. For the problem of menu selection, two different fuzzy MCDM methods—fuzzy TOPSIS and fuzzy VIKOR—are proposed. In both cases, both quantitative and qualitative decision factors can be evaluated as subjectively as necessary. Tom et al. (2015) used calories, cholesterol, fiber, saturated fat, sodium, and sugar for restaurant menu evaluation. As in the study of Tom et al. (2015), six criteria, including calories, cholesterol, fiber, saturated fat, sodium, and sugar, are used. This study focuses on

- determine and evaluate alternatives considering six criteria,
- propose fuzzy TOPSIS and fuzzy VIKOR,
- present comparison analyses of proposed MCDM methods, TOPSIS, and VIKOR,
- analyze the results, considering six criteria for ten menu alternatives.

The paper is structured as follows: the proposed methods are explained in the "Proposed Methodology" section. The "Results and Discussion" section assesses the findings using four different methods. Finally, the "Conclusion" section summarizes the contribution of the study and offers suggestions for further research.

2. Materials and Methods

The food and beverage sector is among the fastest growing sectors due to economic developments. The rapid increase in the number of those operating in this sector worldwide has led to fierce competition in this field, and businesses have chosen to focus more on customer requests and needs day by day (İpek and Gökürk, 2021). At this point, one of the phenomena required to meet customer requests and needs in businesses is the menu engineering process (Mutlu et al., 2022).

Menu management took what enterprising chefs had used intuitively for years and turned it into a computerized, scientific model that everyone could understand. The gastronomic value and inventiveness of dishes are highly valued by all menu planners in menu

engineering (Morrison, 1996). Menu engineering is a methodological alternative that allows the analysis of the dishes offered by a restaurant, making it possible to determine the financial profitability and popularity of the gastronomic offer in order to correct, improve, and maintain the menu (Juliana et al., 2021; Hermida and Aráuz, 2023). Menu engineering may periodically make the decision to formulate a strategy based on the results of menu sales that occur within a given period of time. It is necessary to understand the solutions and follow-up to increase the sales of the next menu (Ardiansyah, 2020).

Kwong (2005) found that menu engineering and design were crucial in enhancing the profitability of Asian restaurants. Many of the evaluated main course products in the study were classified as unpopular and/or unprofitable, and it was discovered that the sampled menus had little commercial impact. To create a menu recommender, Tan et al. (2012) determined that the MCDM method was successful with a number of innovative algorithms and a database of client knowledge. The restaurant menu evaluation and selection problem has been successfully solved as an MCDM problem by Tom et al. (2015). To rank the menu items according to the customer-selected priority criteria, they created a fuzzy MCDM model. Tom and Annaraud (2017) determined that the fuzzy MCDM method can be successfully used to assess the contribution margin and popularity index and to choose the best strategy.

After implementing activity-based costing, Linassi et al. (2016) discovered that the majority of menu items have negative operational profits. Particularly in labor-intensive production systems, the adoption of activity-based costing improves the accuracy of the effective cost of each menu item. DiPietro (2017) examined the changing and evolving segments of the food service industry, restaurant operations, service quality in food service, restaurant financing, food service marketing, food safety and health, and the increasing role of technology in the industry. The results of Hamdallah and Srouji (2018) studies showed that the modified balanced scorecard approach, which includes both financial and non-financial perspectives, positively affects menu management in health-care centers in Jordan. Fang (2020) found that integrated a slack-based measure and data envelopment analysis model can be used to improve the financial performance and sustainability of the menu in chains of Chinese and Japanese restaurants. Hermida and Aráuz (2023) determined that menu engineering methodology in a restaurant located in the city of Ibarra can be used to increase the profitability of catering services, improve kitchen resources, and improve service quality. Lai et al. (2020) discussed the management of menu profitability in the restaurant industry. Technology advancement has led to the creation of methods that can be used to manage menu profitability.

Menu engineering describes particular methods for assessing the performance of individual menu items so

that strategic choices can be made. In order to choose imprecise and strategic options, decision makers utilize menu engineering against manually created target values (Tom et al., 2017). There are several methods for menu engineering, and companies have different preferences depending on what they need. In order to develop a more effective decision-making tool, this study used fuzzy

MCDM models to identify the options for a strategy. MCDM methods for menu management are given in Table 1. The comparative use of four different methods (TOPSIS, fuzzy TOPSIS, VIKOR, and fuzzy VIKOR) in menu management makes a significant contribution to the literature.

Table 1. MCDM methods for menu management

Author(s)	Fuzzy based MCDM	MAIRCA*	BWM*	TOPSIS	AHP*	VIKOR
Tom, Wibowo, and Grandhi (2015)	√					
Tom and Annaraud (2017)	√					
Nerisafitra and Putri (2017)				√		
Arsić et al. (2019)		√	√			
Ho et al. (2022)					√	
This study	√			√		√

*AHP= analytic hierarchy process, MAIRCA= multi attributive ideal-real comparative analysis, BWM= best-worst method

A precise understanding of the criterion weights and assessments is assumed in traditional MCDA approaches. However, there are some instances in the real world where it is impossible to use precise expressions. At this point, variables that are imprecisely expressed by fuzzy TOPSIS and fuzzy VIKOR can be created using linguistic values.

Unquestionably, one of the most critical actions a person can take is making decisions, encompassing a broad range of alternatives. The study of decision-making delves into how decisions are made and how they can be improved. Essentially, it involves determining the best alternative or ranking them by preference (Arora et al., 2022). Effective decision-making can be exceptionally challenging in various situations. When dealing with group decision-making, the complexity increases because it necessitates gaining consensus within the group. Therefore, numerous Multiple-Criteria Decision-Making (MCDM) techniques have been developed and are favored by decision-makers for evaluating options based on various criteria (Cevikcan et al., 2009). MCDM methods rely on engineering expertise, intuition, and past experiences. Fuzzy logic-based MCDM approaches are gaining popularity among researchers due to their capacity to compare multiple criteria and potential alternatives using natural language linguistic terms, which align with human subjective cognition (Alpar and Iphar, 2018).

The Technique for Order Preference by Similarity to an Ideal Solution (TOPSIS) is a straightforward and widely used method for addressing problems related to ranking and selecting alternatives. It excels at handling MCDM issues because it can accommodate decision-makers' fuzzy opinions and perceptions. Moreover, the TOPSIS method is adept at managing uncertainties that often arise in real-world scenarios characterized by fuzziness (Arora et al., 2022). The proposed approach is described as a sequence of sequential steps.

Step 1. Create a decision matrix and construct the normalized decision matrix

Decision matrix, which includes m alternatives connected to n criteria, is assessed using the TOPSIS approach. A_i denotes the i^{th} alternative considered. In order to enable comparison across the attributes, this procedure attempts to convert the various attribute dimensions into nondimensional attributes. It is possible to calculate an element r_{ij} of the normalized decision matrix R as (equation 1);

$$r_{ij} = \frac{x_{ij}}{\sqrt{\sum_{i=1}^m x_{ij}^2}} \tag{1}$$

The numerical result of the i^{th} alternative in relation to the j^{th} criterion is denoted by x_{ij} .

Step 2. Construct the weighted normalized decision matrix

A set of weights from the decision maker is incorporated into the decision matrix. The computation of this matrix involves multiplying each column of the matrix R by the corresponding weight, w_j . Weighted normalized decision matrix is denoted as v .

Step 3. Determine ideal and negative ideal solutions

The two created alternatives, A^* and A^- , stand for the ideal solution, which is the most preferred alternative, and the least preferable solution, which is the negative-ideal solution, respectively.

Step 4. Calculate the separation measure

The n -dimensional Euclidean distance can be used to calculate the distance between each alternative. Each alternative's distance from the ideal is provided by (equation 2);

$$s_{i^*} = \sqrt{\sum_{j=1}^n (v_{ij} - v_j^*)^2} \tag{2}$$

$i = 1, 2, \dots, m$

Each alternative's distance from the negative ideal is provided by (equation 3);

$$s_{i-} = \sqrt{\sum_{j=1}^n (v_{ij} - v_j^-)^2}$$

$$i = 1, 2, \dots, m$$

Step 5. Calculate the relative closeness to the ideal solution

The relative closeness of A_i with respect to A^* is defined as (equation 4);

$$c_{i^*} = \frac{s_{i-}}{(s_{i^*} + s_{i-})}$$

$$0 < c_{i^*} < 1, i = 1, 2, \dots, m$$

Step 6. Rank the preference order

The descending order of c_{i^*} can be used to rank a group of alternatives in order of preference. A detailed information of TOPSIS can be found in Hwang and Yoon (1981). Incorporating the steps mentioned above, the fuzzy extension of the TOPSIS method is depicted in Figure 1 (Papathanasiou and Ploskas, 2018).

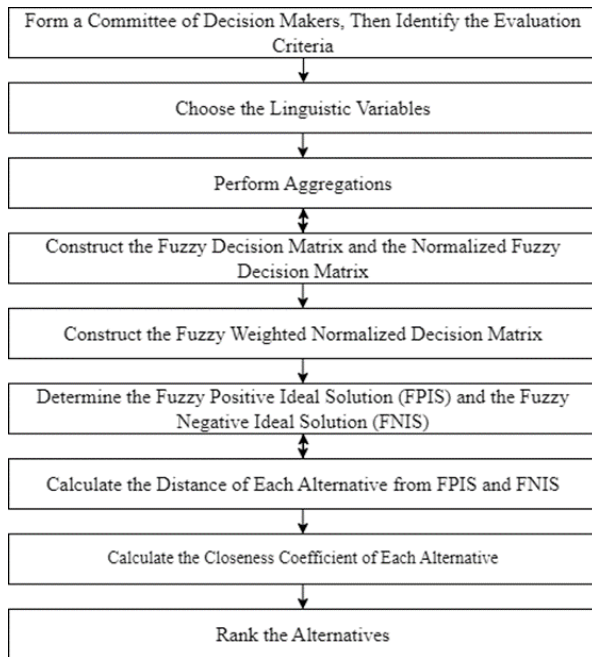


Figure 1. Fuzzy TOPSIS (Papathanasiou and Ploskas, 2018).

Each method has a separate procedure for normalizing. Vector normalization is used by TOPSIS, but linear normalization is used by VIKOR (Sari, 2018). On the other hand, both the TOPSIS and VIKOR methods operate on a fundamental principle: they employ an aggregating function to determine the proximity of a solution to the ideal one. The fuzzy TOPSIS method identifies a solution that is the closest to the ideal and furthest from the negative ideal solution. Meanwhile, the fuzzy VIKOR method seeks a compromise solution that maximizes group utility for the majority while minimizing it for the opponents (Umamaheswari and Kumari, 2014). The VIKOR and fuzzy VIKOR methodologies are outlined in

Figure 2 and Figure 3, including the maximum desirability (S_i), lack of desirability (R_i), and VIKOR index (Q_i).

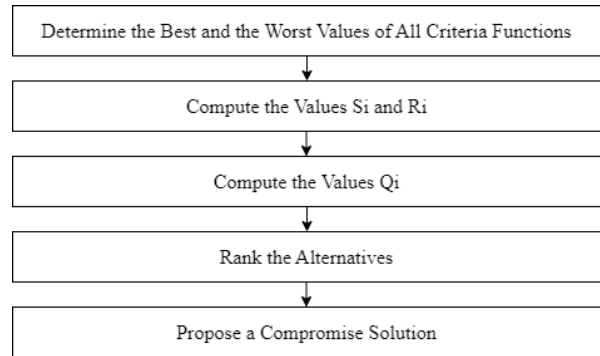


Figure 2. VIKOR (Papathanasiou and Ploskas, 2018)

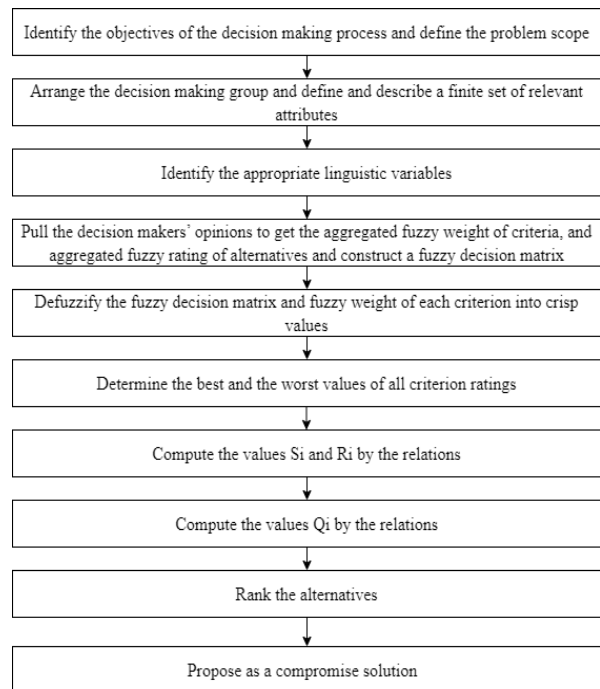


Figure 3. Fuzzy VIKOR (Sanayei et al., 2010).

The most important methods for resolving issues in the real world are TOPSIS and VIKOR, which are applied to discrete alternative challenges. They are capable of identifying the right alternative right away. They reduce the need for pairwise comparisons, and the process may not be greatly impacted by the capacity limitation. They can be applied to a wide range of alternatives and attributes. When objective or quantitative data are available, they are suitable to use. Based on an aggregating function that stands for "closeness to the ideal," they are created (Alsalem et al., 2018). TOPSIS and VIKOR methods were used in this study due to their many advantages. The real world occasionally presents situations in which using precise expressions is not possible. At this point, fuzzy TOPSIS and fuzzy VIKOR can be used to provide a better solution. This study contributes to the literature by comparing these four methods.

3. Results and Discussion

A "healthy menu" has emerged as a crucial idea for the survival and success of the restaurant industry. Given the growing significance of healthiness in the restaurant sector, it has emerged as one of the most difficult academic problems (Hur and Jang, 2015). In this paper, four MCDM methods are used to evaluate ten alternatives, considering six important criteria, including calories, cholesterol, fiber, saturated fat, sodium, and

sugar. The menu content of ten alternatives is presented in Table 2. The most preferred menu content by the local restaurant was taken into account. Menu contents were designed for university students and employees. Alternatives were evaluated by four different dietitians, considering six criteria. The importance of the criteria weights for TOPSIS and VIKOR is given in Table 3. In Table 3, calorie weight is greater than other criteria.

Table 2. Menu content of alternatives

	Menu content
Alternative 1	Lentil Soup, Chicken Leg, Pasta With Sauce, Ayran
Alternative 2	Beef Stew, Rice, Cacik, Shambali Dessert
Alternative 3	Roast Meatballs, Bulgur Rice, Salad, Seasonal Fruit
Alternative 4	Creamy Carrot Soup, Minced Potatoes, Noodle, Yogurt
Alternative 5	Chickpea Stew, Tavern Rice, Yogurt, Pickle
Alternative 6	Tomato Soup, Chicken Döner, Rice, Ayran
Alternative 7	Moussaka, Bulgur Rice, Cacik Sekerpare Dessert
Alternative 8	Lentil Soup, Stuffed Peppers, Yogurt, Seasonal Fruit
Alternative 9	Haricot Bean, Rice, Yogurt, Turkish Doughnuts
Alternative 10	Forest Kebab, Bulgur Rice, Cacik, Pickle

Table 3. The importance of the criteria weight for TOPSIS and VIKOR

	Decision Maker 1	Decision Maker 2	Decision Maker 3	Decision Maker 4
Criteria	Weights	Weights	Weights	Weights
Calories	0.3	0.4	0.3	0.4
Cholesterol	0.2	0.2	0.1	0.2
Fiber	0.1	0.1	0.1	0.1
Saturated fat	0.2	0.1	0.2	0.1
Sodium	0.1	0.1	0.1	0.1
Sugar	0.1	0.1	0.2	0.1

Linguistic terms are utilized to make it easier for nutritionists to make subjective judgments about the various criteria. Fuzzy numbers are used to approximate these linguistic terms for computational simplicity. Linguistic expressions for criteria are very unsatisfactory (VU), unsatisfactory (US), satisfactory (S), high satisfactory (HS), and very satisfactory (VS). Their values are (1, 1, 3), (1, 3, 5), (3, 5, 7), (5, 7, 9), and (7, 9, 9), respectively (Tom et al., 2015). Linguistic expressions for criteria importance are very unacceptable (VA), unacceptable (UA), just acceptable (JA), acceptable (A), and highly acceptable (HA). Their values are (1, 1, 3), (1, 3, 5), (3, 5, 7), (5, 7, 9), and (7, 9, 9), respectively (Tom et al., 2015). The importance weight of the criteria for fuzzy TOPSIS and fuzzy VIKOR is given in Table 4.

Four MCDM methods, namely TOPSIS, VIKOR, fuzzy VIKOR, and fuzzy TOPSIS, were employed to rank the alternative menus. The distances from the positive ideal and negative ideal are given in Figure 4 for TOPSIS and fuzzy TOPSIS. The maximum desirability (Si) and the lack of desirability (Ri) are given in Figure 5 for VIKOR and Fuzzy VIKOR. VIKOR indices for the VIKOR and fuzzy VIKOR methods and closeness coefficients for TOPSIS and fuzzy TOPSIS are presented in Figure 6 for each

alternative. If an alternative's closeness coefficient is closer to 1, it indicates better performance in TOPSIS and fuzzy TOPSIS compared to other alternatives. The alternative with the minimum VIKOR indices score is the best for VIKOR and fuzzy VIKOR. According to the results from VIKOR and TOPSIS, alternative 2 emerges as the best menu when compared to the others. According to the results from fuzzy VIKOR and fuzzy TOPSIS, alternative 3 is the best menu.

The food industry's growing concerns about sustainability have made creative approaches to culinary operations imperative. Designing the menus and recipes from a sustainable perspective is a good way to decrease the environmental impact of restaurants (Coskun, Genç, & Coskun, 2023). Future studies might look at sustainable menu and recipe planning techniques to support sustainable food services in restaurants. To develop novel methods for reducing the environmental effects of food services, more study is required. In addition, big data can make it possible to track the eating and drinking habits of customers and provide them with more individualized menus. Big data analytics may be utilized in future studies to comprehend consumer preferences and tastes.

Table 4. The importance weight of the criteria for fuzzy TOPSIS and fuzzy VIKOR

	Decision Maker 1	Decision Maker 2	Decision Maker 3	Decision Maker 4
Criteria	Weights	Weights	Weights	Weights
Calories	A	A	A	A
Cholesterol	UA	JA	A	UA
Fiber	A	JA	JA	A
Saturated fat	UA	JA	JA	UA
Sodium	UA	A	VA	UA
Sugar	A	A	UA	A

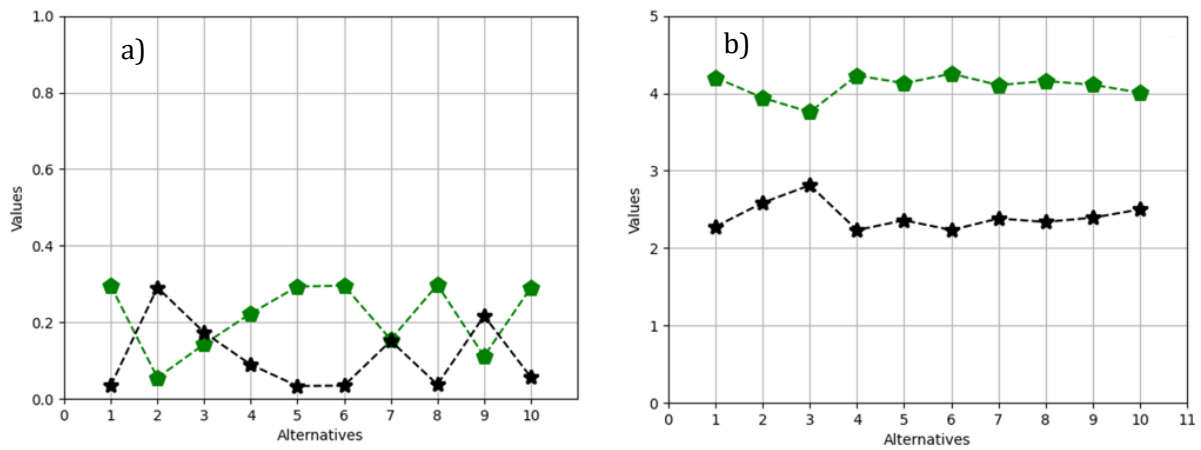


Figure 4. TOPSIS (a) and Fuzzy TOPSIS (b) results (distance from positive ideal solution is green and distance from negative ideal solution is black).

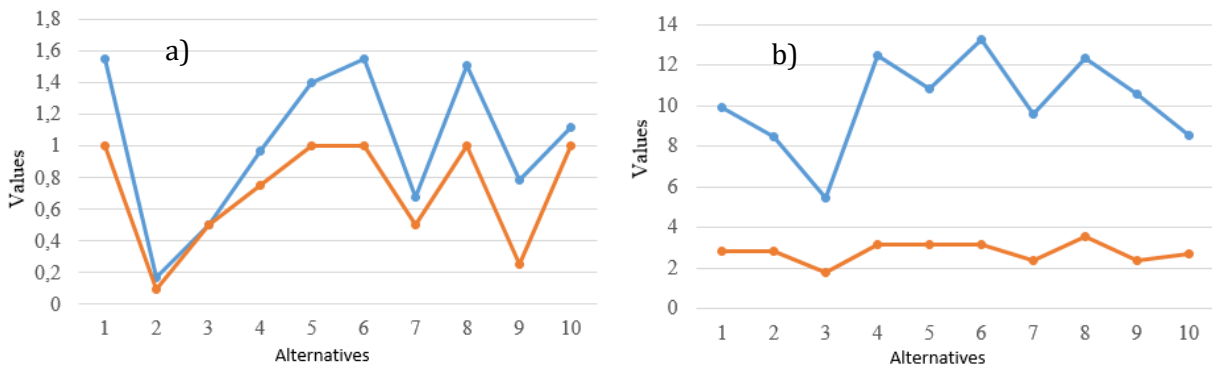


Figure 5. VIKOR (a) and Fuzzy VIKOR (b) results (S_i is blue and R_i is orange).

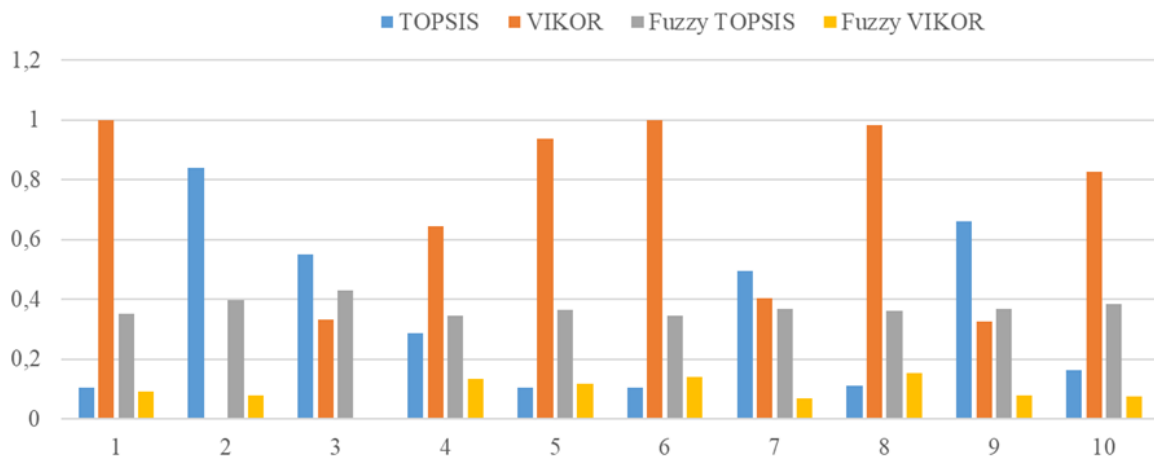


Figure 6. Final results for menu selection

4. Conclusions

Fuzzy MCDM strategies can be employed to address decision-making problems in uncertain environments. One such challenge is menu choice. One such challenge is menu selection, where explicit data determination is difficult. Many people struggle with the problem of deciding on a menu. Several parameters are not clearly defined by numerical values. In such cases, fuzzy numbers can be utilized. This study addresses the menu selection problem through various MCDA approaches, including TOPSIS, VIKOR, fuzzy TOPSIS, and fuzzy VIKOR. According to TOPSIS and VIKOR, Alternative 2 emerges as the best choice, while according to Fuzzy TOPSIS and Fuzzy VIKOR, Alternative 3 proves to be the most favorable option.

The menu plays a vital role in influencing customer behavior. Individuals' aspirations to maintain a healthy weight and cultivate a positive body image can motivate them to opt for healthier menu items. This study may contribute to enhancing the understanding of menu selection among researchers and restaurant owners. Furthermore, it underscores the need for future policies that hold restaurants accountable for offering healthier menu options and ensure that customers are informed about the calories, cholesterol, fiber, saturated fat, sodium, and sugar content of the meals they consume. In future research, this study could be expanded to explore other MCDM methods, and different menus could be evaluated by considering various restaurants.

Author Contributions

The percentage of the author(s) contributions is presented below. All authors reviewed and approved the final version of the manuscript.

	S.L.I.	D.G.
C	50	50
D	50	50
S	40	60
DCP	60	40
DAI	60	40
L	60	40
W	50	50
SR	50	50

C=Concept, D= design, S= supervision, DCP= data collection and/or processing, DAI= data analysis and/or interpretation, L= literature search, W= writing, SR= submission and revision.

Conflict of Interest

The authors declared that there is no conflict of interest.

Ethical Consideration

Ethics committee approval was not required for this study because of there was no study on animals or humans.

Acknowledgements

The authors sincerely acknowledge the nutritionists for answering the survey in this study.

References

Alexander E, Rutkow L, Gudzone KA, Cohen JE, McGinty EE. 2021. Sodium menu labelling: priorities for research and policy. *Public Health Nutr*, 24(6): 1542-1551.

Alonso S, Tan M, Wang C, Kent S, Cobiac L, MacGregor GA, He FJ, Mihaylova B. 2021. Impact of the 2003 to 2018 population salt intake reduction program in England: a modeling study. *Hypertension*, 77(4): 1086-1094.

Alpay S, Iphar M. 2018. Equipment selection based on two different fuzzy multi criteria decision making methods: Fuzzy TOPSIS and fuzzy VIKOR. *Open Geosci*, 10(1): 661-677.

Alsalem MA, Zaidan AA, Zaidan BB, Hashim M, Albahri OS, Albahri AS, Hadi A, Mohammed KI. 2018. Systematic review of an automated multiclass detection and classification system for acute Leukaemia in terms of evaluation and benchmarking, open challenges, issues and methodological aspects. *J Med Syst*, 42, 204.

Ardiansyah I. 2020. The application of menu engineering technique in determining marketing strategy at the den of kalaha restaurant jakarta. *J Bus Entrep*, 8(1): 18-39.

Arora HD, Naithani A, Gupta S. 2022. Distance measures of Pythagorean fuzzy TOPSIS approach for online food delivery apps. *Int J Eng*, 35(10): 1877-1886.

Arsić SN, Pamučar D, Suknovic M, Janošević M. 2019. Menu evaluation based on rough MAIRCA and BW methods. *Serb J Manag*, 14(1): 27-48.

Bowers KM, Suzuki S. 2014. Menu-labeling usage and its association with diet and exercise: 2011 BRFSS sugar sweetened beverage and menu labeling module. *Prev Chronic Dis*, 11: E02. doi: 10.5888/pcd11.130231.

Bruemmer B, Krieger J, Saelens BE, Chan N. 2012. Energy, saturated fat, and sodium were lower in entrées at chain restaurants at 18 months compared with 6 months following the implementation of mandatory menu labeling regulation in King County, Washington. *J Acad Nutr Diet*, 112(8): 1169-1176.

Byrd K, Almanza B, Ghiselli RF, Behnke C, Eicher-Miller HA. 2018. Adding sodium information to casual dining restaurant menus: beneficial or detrimental for consumers? *Appetite*, 125: 474-485.

Byrd K, Almanza B. 2021. Restaurant menu labeling for calories and sodium: Effect of consumer mindset of immediate versus future consequences. *J Foodserv Bus Res*, 24(3): 310-347.

Cantu-Jungles TM, McCormack LA, Slaven JE, Slebodnik M, Eicher-Miller HA. 2017. A meta-analysis to determine the impact of restaurant menu labeling on calories and nutrients (ordered or consumed) in US adults. *Nutrients*, 9(10): 1088.

Cevikcan E, Cebi S, Kaya I. 2009. Fuzzy VIKOR and fuzzy axiomatic design versus to fuzzy TOPSIS: an application of candidate assessment. *J Mult-Valued Log Soft Comput*, 15(2-3): 181-208.

Coskun A, Genç HU, Coskun A. 2023. How sustainable is your menu? Designing and assessing an interactive artefact to support chefs' sustainable recipe-planning practices. In *Proceedings of the 6th ACM SIGCAS/SIGCHI Conference on Computing and Sustainable Societies*, August 16-19, Cape Town, South Africa, pp: 90-98.

Detopoulou P, Al-Khelefawi ZH, Kalonarchi G, Papamikos V. 2022. Formulation of the menu of a general hospital after its conversion to a "COVID Hospital": a nutrient analysis of 28-

- day menus. *Front. Nutr*, 9: 833628.
- DiPietro R. 2017. Restaurant and foodservice research: A critical reflection behind and an optimistic look ahead. *Int J Contemp Hosp Manag*, 29(4): 1203-1234.
- Dowray S, Swartz JJ, Braxton D, Viera AJ. 2013. Potential effect of physical activity based menu labels on the calorie content of selected fast food meals. *Appetite*, 62: 173-181.
- Dumanovsky T, Huang CY, Bassett MT, Silver LD. 2010. Consumer awareness of fast-food calorie information in New York City after implementation of a menu labeling regulation. *Am J Public Health*, 100(12): 2520-2525.
- Elbel B, Kersh R, Brescoll VL, Dixon LB. 2009. Calorie labeling and food choices: a first look at the effects on low-income people In New York City: Calorie information on menus appears to increase awareness of calorie content, but not necessarily the number of calories people purchase. *Health Aff*, 28(Suppl1): w1110-w1121.
- Falbe J, Musicus AA, Sigala DM, Roberto CA, Solar SE, Lemmon B, Sorscher S, Nara D, Hall, MG. 2023. Online RCT of icon added-sugar warning labels for restaurant menus. *Am J Prev Med*, 65(1): 101-111.
- Fang CY. 2020. From the total-factor framework to food cost performance disaggregation—developing an innovative model to enhance menu performance. *Sustainability*, 12(22): 9552.
- Gerend MA. 2009. Does calorie information promote lower calorie fast food choices among college students? *J Adolesc Health*, 44(1): 84-86.
- Hamdallah ME, Srouji AF. 2018. Menu engineering in Jordanian health-care centers: a modified balanced scorecard approach. In 8th International Conference on Engineering, Project, and Product Management (EPPM 2017) Proceedings, pp: 109-118. URL: <https://link.springer.com/book/10.1007/978-3-319-74123-9#about-this-book> (accessed date, March 15, 2022).
- Hermida CEC, Aráuz MBB. 2023. Menu engineering: A benchmark methodology for improving the profitability of a restaurant company. *J Surv Fish Sci*, 10(3S): 3067-3079.
- Ho HP, Lin YC, Fu CJ, Chang CT. 2022. On the personal diet considering qualitative and quantitative issues. *Comput Ind Eng* 164: 107857.
- Hobin E, Lillico H, Zuo F, Sacco J, Rosella L, Hammond, D. 2016. Estimating the impact of various menu labeling formats on parents' demand for fast-food kids' meals for their children: An experimental auction. *Appetite*, 105: 582-590.
- Hobin E, Weerasinghe A, Schoer N, Vanderlee L, Shokar S, Orr S, Poon T, Hammond D. 2022. Efficacy of calorie labelling for alcoholic and non-alcoholic beverages on restaurant menus on noticing information, calorie knowledge, and perceived and actual influence on hypothetical beverage orders: a randomized trial. *Can J Public Health*, 113(3): 363-373.
- Huang Y, Burgoine T, Theis DR, Adams J. 2022. Differences in energy and nutrient content of menu items served by large chain restaurants in the USA and the UK in 2018. *Public Health Nutr*, 25(10): 2671-2679.
- Hur J, Jang SS. 2015. Consumers' inference-dynamics about healthy menu promotions in a bundle context. *Int J Hosp Manag*, 44: 12-22.
- Hwang J, Lorenzen CL. 2008. Effective nutrition labeling of restaurant menu and pricing of healthy menu. *J Foodserv*, 19(5): 270-276.
- Hwang CL, Yoon K. 1981. Multiple attribute decision making methods and applications, a state-of-the-art survey. Springer, London, UK, pp: 269.
- İpek SL, Göktürk D. 2021. Industry 4.0 approaches in food and bio industry: recent developments and future trends. *Adv Artif Intell Res*, 1(1): 29-42.
- Jeong E, Jang SS. 2016. Imagine yourself being healthy: The mental simulation effect of advertisements on healthy menu promotion. *Int J Hosp Manag*, 53: 81-93.
- Jia J, Van Horn L, Linder JA, Ackermann RT, Kandula NR, O'Brien MJ. 2023. Menu calorie label use and diet quality: a cross-sectional study. *Am J Prev Med*, 65(6): 1069-1077.
- Juliana J, Pramezwaray A, Nukak NA, Situmorang JMH. 2021. Using contribution of menu engineering in upscale restaurants to enhance sales volume. *Int J Soc Sci Manag Stud*, 2(4): 1-12.
- Kwong LYL. 2005. The application of menu engineering and design in Asian restaurants. *Int J Hosp Manag*, 24(1): 91-106.
- Lai HBJ, Karim S, Krauss SE, Ishak FAC. 2020. A review of approaches to manage menu profitability. *Int J Revenue Manag*, 11(3): 151-171.
- Linassi R, Alberton A, Marinho SV. 2016. Menu engineering and activity-based costing: an improved method of menu planning. *Int J Contemp Hosp Manag*, 28(7): 1417-1440.
- Morrison P. 1996. Menu engineering in upscale restaurants. *Int J Contemp Hosp Manag*, 8(4): 17-24.
- Mutlu H, Demirçakmak İL, Doğan M. 2022. Menu engineering in the restaurant business: A study on kitchen chefs. *J Tour Gastron Stud*, 10 (4): 3537-3553.
- Nerisafitra P, Putri PH. 2017. Establishing decision support system for determination healthy menu based in multi criteria and interatice approach. In Proceeding of 4th International Conference on Computer Applications and Information Processing Technology (CAIPT), August 8-1, Kuta, Bali, pp: 1-5.
- Nicolosi RJ, Wilson TA, Lawton C, Handelman GJ. 2001. Dietary effects on cardiovascular disease risk factors: beyond saturated fatty acids and cholesterol. *J Am Coll Nutr*, 20(sup5): 421S-427S.
- Obbagy JE, Condrasky MD, Roe LS, Sharp JL, Rolls BJ. 2011. Chefs' opinions about reducing the calorie content of menu items in restaurants. *Obesity*, 19(2): 332-337.
- Papathanasiou J, Ploskas N. 2018. Multiple criteria decision aid. Methods, examples and python implementations. Springer, London, UK, pp: 173.
- Patel A, Lopez NV, Lawless HT, Njike V, Beleche M, Katz DL. 2016. Reducing calories, fat, saturated fat, and sodium in restaurant menu items: Effects on consumer acceptance. *Obesity*, 24(12): 2497-2508.
- Rudelt A, French S, Harnack L. 2014. Fourteen-year trends in sodium content of menu offerings at eight leading fast-food restaurants in the USA. *Public Health Nutr*, 17(8): 1682-1688.
- Sampaio RM, Coutinho MBC, Mendonça D, da Silva Bastos D, Henriques P, Camacho P, Anastácio A, Pereira S. 2017. School nutrition program: Assessment of planning and nutritional recommendations of menus. *Rev Chil Nutr*, 44(2): 170-176.
- Sanayei A, Mousavi SF, Yazdankhah A. 2010. Group decision making process for supplier selection with VIKOR under fuzzy environment. *Expert Syst Appl*, 37(1): 24-30.
- Sarı F. 2018. Comparison of TOPSIS and VIKOR multi criteria decision analysis techniques. *Selcuk Univ J Eng Sci Tech*, 6, 825-831.
- Scourboutakos MJ, Corey PN, Mendoza J, Henson SJ, L'Abbé MR. 2014. Restaurant menu labelling: Is it worth adding sodium to the label? *Can J Public Health*, 105(5): e354-e361.
- Sigala DM, Hall MG, Musicus AA, Roberto CA, Solar SE, Fan S, Sorscher S, Nara D, Falbe J. 2022. Perceived effectiveness of added-sugar warning label designs for US restaurant menus: An online randomized controlled trial. *Prev Med*, 160,

- 107090.
- Sisti JS, Prasad D, Niederman S, Mezzacca TA, Anekwe AV, Clapp J, Farley SM. 2023. Sodium content of menu items in New York City chain restaurants following enforcement of the sodium warning icon rule, 2015–2017. *PLoS One*, 18(5): e0274648.
- Tan TH, Chang CS, Chen YF. 2012. Developing an intelligent e-restaurant with a menu recommender for customer-centric service. *IEEE Trans Syst Man Cybern Part C (Applications and Reviews)*, 42(5): 775-787.
- Tom M, Wibowo S, Grandhi S. 2015. A fuzzy multicriteria decision making model for restaurant menu ranking. In *Proceeding of IEEE 7th International Conference on Cybernetics and Intelligent Systems (CIS) and IEEE Conference on Robotics, Automation and Mechatronics (RAM)*, 15-17 July, Angkor Wat, Cambodia, pp: 104-108.
- Tom M, Annaraud K. 2017. A fuzzy multi-criteria decision making model for menu engineering. In *Proceeding of IEEE International Conference on Fuzzy Systems (FUZZ-IEEE)*, 9-12 July, Roma, Italy, pp: 1-6.
- Turnwald BP, Jurafsky D, Conner A, Crum AJ. 2017. Reading between the menu lines: Are restaurants' descriptions of "healthy" foods unappealing? *Health Psychol*, 36(11): 1034.
- Umamaheswari A, Kumari P. 2014. Fuzzy TOPSIS and fuzzy VIKOR methods using the triangular fuzzy hesitant sets. *Int J Comput Sci Inf Technol Res*, 4(3): 15-24.
- Wolfson JA, Moran AJ, Jarlenski MP, Bleich SN. 2018. Trends in sodium content of menu items in large chain restaurants in the US. *Am J Prev Med*, 54(1): 28-36.
- World awareness weeks. World Action on Salt, Sugar and Health (WASSH), <https://www.worldactiononsalt.com/awarenessweek/> (accessed date, March 15, 2022).
- Yamamoto JA, Yamamoto JB, Yamamoto BE, Yamamoto LG. 2005. Adolescent fast food and restaurant ordering behavior with and without calorie and fat content menu information. *J Adolesc Health*, 37(5): 397-402.



PRODUCTION OF CHEMICALLY MODIFIED SHEAR THICKENING FLUIDS AND INVESTIGATION OF THEIR RHEOLOGICAL PROPERTIES

Murat Yavuz SOLMAZ¹, Cenk YANEN^{1*}, Celal KISTAK¹, Ercan AYDOĞMUŞ²

¹Firat University, Faculty of Engineering, Department of Mechanical Engineering, 23119, Elazığ, Türkiye


²Firat University, Faculty of Engineering, Department of Chemical Engineering, 23119, Elazığ, Türkiye


Abstract: In this study, the rheological properties of shear thickening fluid, which are generally used as single solid phase in the literature, were investigated by chemical material reinforcement. Considering that the unique shear thickening effect of STF is used in many areas such as increasing the impact resistance of fabrics and energy dissipation, this study aims to provide guidance for investigating what STFs can do with chemical bonds as well as physical bonding. Methylene diphenyl diisocyanate (MDI) was used in varying proportions for chemical reinforcement. When the rheological properties of the suspensions reinforced with MDI as a chemical additive were evaluated, the initial viscosity values increased as the MDI ratio increased, while the solidification behavior under shear was observed significantly in the sample with 2.5% MDI ratio with increasing shear ratio.


Keywords: Shear-thickening fluid, Chemical reaction, Rheology


*Corresponding author: Firat University, Faculty of Engineering, Department of Mechanical Engineering, 23119, Elazığ, Türkiye

E mail: cyanen@firat.edu.tr (C. YANEN)

Murat Yavuz SOLMAZ  <https://orcid.org/0000-0001-6394-0313>

Cenk YANEN  <https://orcid.org/0000-0002-5092-8734>

Celal KISTAK  <https://orcid.org/0000-0003-4621-5405>

Ercan AYDOĞMUŞ  <https://orcid.org/0000-0002-1643-2487>

Received: September 27, 2023

Accepted: November 09, 2023

Published: January 15, 2024

Cite as: Solmaz YM, Yanen C, Kistak C, Aydoğmuş E. 2024. Production of chemically modified shear thickening fluids and investigation of their rheological properties. *BSJ Eng Sci*, 7(1): 31-35.

1. Introduction

High performance fabrics have been used extensively to provide protection without restricting the movement of personnel. In recent years, shear thickening fluids (STF) have been investigated to increase the energy absorbing capacity of these systems. Shear Thickening Fluids are non-Newtonian suspensions that exhibit a sudden increase in viscosity with increasing shear rate. This property of STFs is reversible. Thus, when the stress that increased the viscosity is removed, the liquids return to their initial state. Many studies have been conducted to understand the rheological properties of these fluids and to use them in engineering applications. (Hoffman, 1972; Hoffman, 1974; Bossis and Brady, 1989; Boersma et al., 1992). The rheological properties of STFs mainly depend on parameters such as the solid medium (shape, size, proportion, hardness, additional particles), the liquid medium (type, density) and the physical conditions of the suspension. It was observed that the viscosity of the suspension increased with increasing molecular weight of polyethylene glycol (PEG) used as a liquid medium (Baharvandi et al., 2016). In the study by Qin et al., three different PEGs with mole weights of 200, 400 and 600 were added at a ratio of 45% to STF produced using PS microspheres and PEG. PEG 600 was reported to be more effective in the solidification behavior of the added sample (Qin et al., 2017). The addition of additional

particles to the suspension in the production of STF significantly changes the rheological properties. In the study by Sha et al., CNT and GNP were added as additional particles to CACS produced using 650 nm diameter spherical silica and PEG 200 (Sha et al., 2013). Hasanzadeh et al. investigated the effect of multi-walled carbon nanotube (CNT) reinforced STF on the puncture resistance performance of high modulus polypropylene (HMPP) fabrics (Hasanzadeh et al., 2016). Li et al. investigated the energy dissipation mechanisms of clean and STF impregnated UHMWPE fabrics in dynamic impact tests with knife and nail tip (Li et al., 2016). Tan et al. investigated the effects of graphene nanoplate (GNP) reinforcement on the rheological properties of STF (Tan et al., 2018). Wang et al. investigated the rheological properties and inter-yarn friction properties of STF at temperatures between -15 °C and 35 °C to examine their properties in different climatic conditions (Wang et al., 2019).

In the literature review, there are many studies in which the rheological properties of single and multi solid phase shear thickening fluids are determined and their effect on the energy absorbing performance of high performance fabrics is examined. When the FTIR analysis of the STFs' produced in previous studies was examined, it was determined that no chemical bond was formed between the silica and PEG forming the suspension content



(Yanen et al., 2020). In the literature review, no study was found in which chemically bonded STF's were produced. Within the scope of this study, chemically modified shear thickening fluid (CSTF) was first produced and rheological properties were investigated.

2. Materials and Methods

The silica particles were oven dried at 150 °C for about 12 hours to remove moisture absorbed on the surface. To prepare the STF samples, polyethylene glycol and silica particles were mixed at 6000 rpm using a high speed mechanical mixer. During the mixing process, silica particles were gradually added to prevent agglomeration as suggested in previous studies (Zhang et al., 2008; Gürgen and Kuşhan, 2017; Wang et al., 2017). Stirring was continued until the mixture became homogeneous. The stirring was carried out in a temperature adjustable water bath to keep the suspension temperature constant (Figure 1). The same method was used in the production of nanoparticle reinforced STF. In the production of STF's

developed by chemical modification, PEG 400 and Aerosil 150 were first homogenized with a high speed mechanical mixer (Table 1). Diphenylmethane diisocyanate (MDI) at the rate of 5% by mass was added to the resulting mixture and stirred at room temperature for 1 hour.

The rheological properties of CSTFs were determined using Anton Paar MCR 102 voltage-controlled rheometer, pictured in Figure 2, as in previous studies (Yanen et al., 2020; Yanen et al., 2021). The tests were performed using a 25 mm diameter parallel plate apparatus. During the testing process, liquids were placed in the inner region between the upper and lower measuring plates. The gap between the plates was kept constant at 0.3 mm and all tests were performed at 25 °C. Rheological measurements were performed in the shear rate range of 0-1000 s⁻¹. FTIR analysis was performed using Shimadzu S11025C (QATR-S) instrument to study the bond formation in the suspensions produced to obtain CSTF.

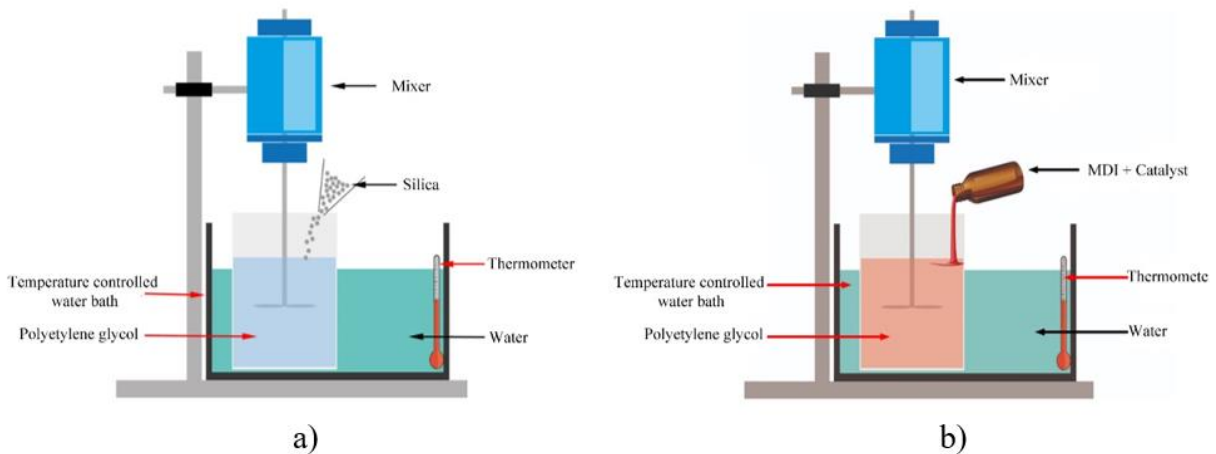


Figure 1. a) STF production b) CSTF production using STF.



Figure 2. Anton Paar MCR 102 Rheometer.

Table 1. Specimen nomenclature and properties used in the experiments

Specimen No	Factor investigated	STF	Silica Ratio	Chemical Ratio
1				0
2	Chemical Ratio	Aerosil 150 + PEG 400	25%	2.50%
3				5%
4				7.50%

3. Results and Discussion

Figure 3 shows the rheological properties of the suspensions reinforced with MDI as a chemical additive. All MDI reinforced samples exhibit non-Newtonian behavior. When pure STF and MDI reinforced samples were compared, it was observed that MDI additive reduced the critical shear rate. If the results are evaluated, while the initial viscosity values increase as the MDI ratio increases, the solidification behavior under shear is clearly observed in the sample with 2.5% MDI ratio with increasing shear rate. There is no significant difference between the critical shear rates with increasing MDI ratio. The final viscosity values change inversely proportional to the MDI ratio.

3.1. Chemical Reaction in the Production of CSTF

It is necessary to study the chemical reaction between polyethylene glycol and methylene diphenyl isocyanate (MDI) in the production of CSTF. Other components provide physical interactions among themselves. For example, aerosil, polyethylene glycol, fabric and nanoparticles do not make chemical bonds with each other. The chemical reaction described below shows that a chemical reaction takes place between the functional hydroxyl (-OH) groups in ethylene glycol and the cyanate

groups (-N=C=O) in methylene diphenyl isocyanate (Figure 4).

3.2. Fourier Transform Infrared Spectrophotometer (FTIR) Results

In the FTIR spectra, stress vibrations of hydroxyl bonds in polyethylene glycol are observed in the wavelength range of 3400-3550 cm^{-1} (Figure 5). In the wavelength range 2850-3000 cm^{-1} , stress vibrations of CH groups occur. Since methylene diphenyl diisocyanate gives chemical bonds with hydroxyl bonds in polyethylene glycol, it was determined that hydroxyl bonds decreased as the MDI ratio increased. However, free isocyanates that cannot undergo chemical reaction are seen at a wavelength of approximately 2225 cm^{-1} . In this study, polyethylene glycol reacts chemically at an optimum rate with about 2.5% MDI. The use of higher proportions of MDI indicates an increase in free isocyanates in the wavelength range 2215-2235 cm^{-1} . The highest rheological performance in the obtained CSTF samples was observed in 2.5% MDI reinforced samples. The use of high percentage of MDI decreases the rheological performance of the CSTF samples since it is present in the mixture without chemical reaction.

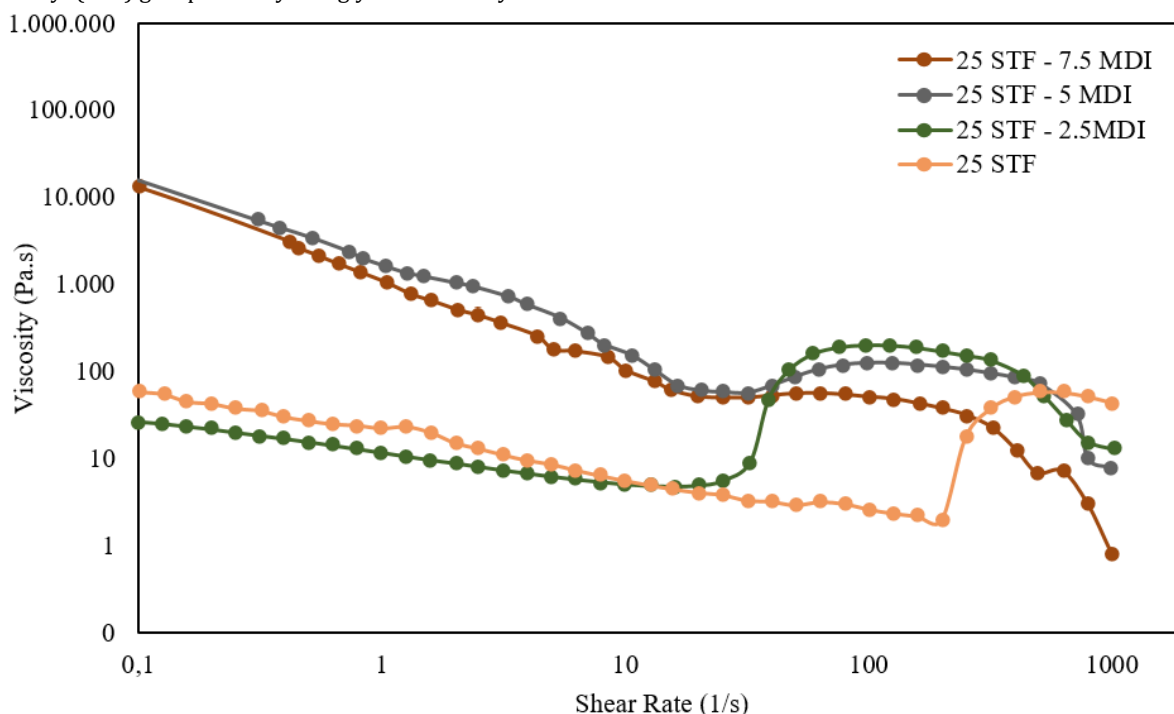


Figure 3. Effect of MDI ratios on rheological properties.

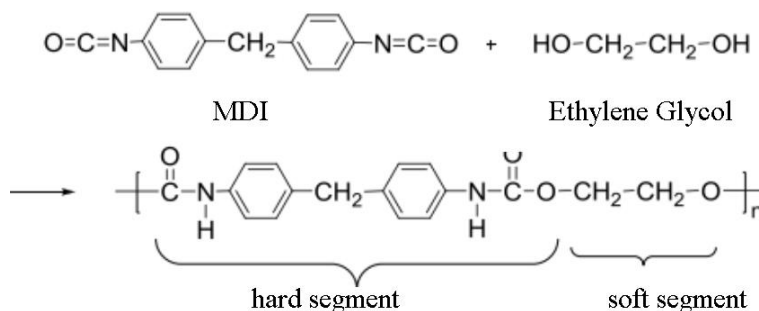


Figure 4. Chemical reaction between MDI and polyethylene glycol.

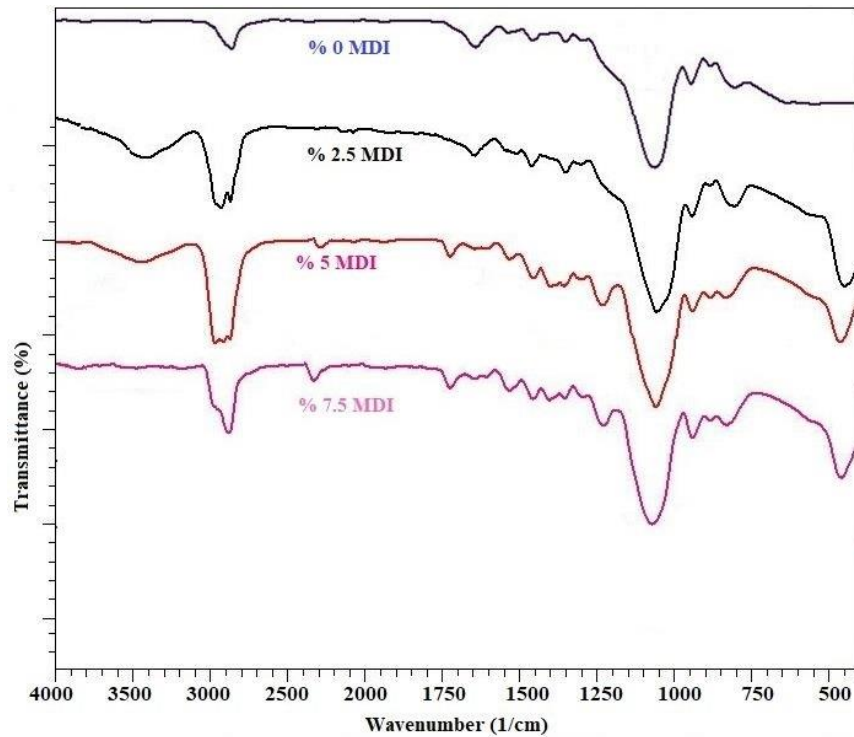


Figure 5. FTIR spectra of CSTF samples produced with different MDI ratios by mass.

4. Conclusion

In the suspensions produced within the scope of this study, solidification behavior under shear was observed and it was determined that properties such as critical shear rate and viscosity profile can be controlled by properties such as the ratio of reinforcement material. In the study, CSTF were impregnated into two different Twaron para-aramid fabrics. The effects of impregnating these high-performance fabrics with CSTF on their energy absorption capacities and low-speed impact tests were investigated. The information obtained as a result of the study can be summarized as follows;

- When the rheological properties of the suspensions reinforced with MDI as a chemical additive were evaluated, the initial viscosity values increased with increasing MDI ratio, while the solidification behavior under shear was observed significantly in the sample with 2.5% MDI ratio with increasing shear ratio. No significant difference was detected between the critical shear rates with increasing MDI ratio. The final viscosity values change inversely proportional to the MDI ratio.
- When FTIR peaks have been examined in this study, it is determined that the isocyanates in MDI are consumed. However, the use of high amounts of MDI indicates that free isocyanates are present in the mixture despite the chemical reaction taking place. It can be seen in the FTIR peaks that the hydroxyl bonds in PEG have decreased. When optimum 2.5 % MDI is used, peaks of free isocyanates are not observed in the wavelength range of 2215-2235 cm⁻¹. As a result, it has been determined that the chemically reacting components are consumed at

this optimum rate.

- All of the nanoparticle reinforced specimens exhibited solidification behavior under shear. As in the case of CSTF, the system consists of three stages: shear thinning, solidification under shear and the formation of a relative plateau.
- It is thought that the addition of MDI to the liquids solidified under shear creates a chemical reaction and may strengthen the connection between the fabric and the suspension in future studies.

Author Contributions

The percentage of the author(s) contributions is presented below. All authors reviewed and approved the final version of the manuscript.

	M.Y.S.	C.Y.	C.K.	E.A.
C	30	25	20	25
D	20	30	30	20
S	40	20	20	20
DCP	20	30	30	20
DAI	20	30	20	30
L	20	30	30	20
W	20	30	30	20
CR	20	30	20	30
SR	20	30	30	20
PM	30	20	30	20

C=Concept, D= design, S= supervision, DCP= data collection and/or processing, DAI= data analysis and/or interpretation, L= literature search, W= writing, CR= critical review, SR= submission and revision, PM= project management.

Conflict of Interest

The authors declared that there is no conflict of interest.

Ethical Consideration

Ethics committee approval was not required for this study because of there was no study on animals or humans.

Acknowledgements

This work was supported by the Scientific and Technological Research Council of Türkiye (TÜBİTAK) with project number 221M634.

References

- Baharvandi HR, Alebooyeh M, Alizadeh M, Khaksari P, Kordani N. 2016. Effect of silica weight fraction on rheological and quasi-static puncture characteristics of shear thickening fluid-treated Twaron® composite. *J Indust Textiles*, 46(2): 473-494. <https://doi.org/10.1177/1528083715589750>.
- Boersma WH, Laven J, Stein HN. 1992. Viscoelastic properties of concentrated shear-thickening dispersions. *J Colloid Interf Sci*, 149(1): 10-22. [https://doi.org/10.1016/0021-9797\(92\)90385-Y](https://doi.org/10.1016/0021-9797(92)90385-Y).
- Bossis G, Brady JF. 1989. The rheology of Brownian suspensions. *J Chem Physics*, 91(3): 1866-1874. <https://doi.org/10.1063/1.457091>.
- Gürgen S, Kuşhan MC. 2017. The effect of silicon carbide additives on the stab resistance of shear thickening fluid treated fabrics. *Mechan Advan Mater Struct*, 24(16): 1381-1390. <https://doi.org/10.1080/15376494.2016.1231355>.
- Hasanzadeh M, Mottaghitalab V, Babaei H, Rezaei M. 2016. The influence of carbon nanotubes on quasi-static puncture resistance and yarn pull-out behavior of shear-thickening fluids (STFs) impregnated woven fabrics. *Composites Part A: Appl Sci Manufact*, 88: 263-271. <https://doi.org/10.1016/j.compositesa.2016.06.006>.
- Hoffman RL. 1972. Discontinuous and Dilatant Viscosity Behavior in Concentrated Suspensions--1. Observation of a Flow Instability. *Trans Soc Rheol*, 16(1): 155-173.
- Hoffman RL. 1974. Discontinuous and dilatant viscosity behavior in concentrated suspensions. II. Theory and experimental tests. *J Colloid Interf Sci*, 46(3): 491-506. [https://doi.org/10.1016/0021-9797\(74\)90059-9](https://doi.org/10.1016/0021-9797(74)90059-9).
- Li W, Xiong D, Zhao X, Sun L, Liu J. 2016. Dynamic stab resistance of ultra-high molecular weight polyethylene fabric impregnated with shear thickening fluid. *Mater Design*, 102: 162-167. <https://doi.org/10.1016/j.matdes.2016.04.006>.
- Qin J, Zhang G, Shi X. 2017. Study of a shear thickening fluid: the suspensions of monodisperse polystyrene microspheres in polyethylene glycol. *J Dispers Sci Technol*, 38(7): 935-942. <https://doi.org/10.1080/01932691.2016.1216435>.
- Sha X, Yu K, Cao H, Qian K. 2013. Shear thickening behavior of nanoparticle suspensions with carbon nanofillers. *J Nanopart Res*, 15(7): 1816. <https://doi.org/10.1007/s11051-013-1816-x>.
- Tan Z, Li W, Huang W. 2018. The effect of graphene on the yarn pull-out force and ballistic performance of Kevlar fabrics impregnated with shear thickening fluids. *Smart Mater Struct*, 27(7): 075048. <https://doi.org/10.1088/1361-665X/aaca4b>.
- Wang QS, Sun RJ, Yao M, Chen MY, Feng Y. 2019. The influence of temperature on inter-yarns fictional properties of shear thickening fluids treated Kevlar fabrics. *Composit Part A: Appl Sci Manufact*, 116: 46-53. <https://doi.org/10.1016/j.compositesa.2018.10.020>.
- Wang S, Ma S, Xu C, Liu Y, Dai J, Wang Z, Liu X, Chen J, Shen X, Wei J, Zhu J. 2017. Vanillin-Derived High-Performance Flame Retardant Epoxy Resins: Facile Synthesis and Properties. *Macromolecules*, 50(5): 1892-1901. <https://doi.org/10.1021/acs.macromol.7b00097>.
- Yanen C, Aydoğmuş E, Solmaz MY. 2020. Determination of suitable rheological model for polyethylene glycols and silica particle mixtures. *Middle East J Sci*, 6: 57-67.
- Yanen C, Solmaz MY, Aydoğmuş E. 2020. Investigation of the effect of shear thickening fluid and fabric structure on inter-yarn friction properties in twaron fabrics. *European J Technic*, 10(2): 501-510. <https://doi.org/10.36222/ejt.823112>.
- Yanen C, Solmaz MY, Aydoğmuş E. 2021. Evaluation of rheological properties and distribution quality of shear thickening fluids. 1st International Conference on Applied Engineering and Natural Sciences, May 10-13, Konya, Türkiye, pp: 957.
- Zhang XZ, Li WH, Gong XL. 2008. The rheology of shear thickening fluid (STF) and the dynamic performance of anSTF-filled damper. *Smart Mater Struct*, 17(3): 035027. <https://doi.org/10.1088/0964-1726/17/3/035027>.



KENDİNDEN TAHRİKLİ MİKRO ORGANİZMALARIN NEWTONYEN AKIŞKAN İÇİNDEKİ HAREKETİNİN SAYISAL MODELENMESİ

Hatice MERCAN^{1*}, Tufan Tuna KÖSELER^{1,2}

¹Yıldız Technical University, Department of Mechatronics Engineering, 34349, İstanbul, Türkiye

²Martı Yazılım Danışmanlık Sanayi ve Ticaret A.Ş., 35170, İzmir, Türkiye

Özet: Mikro organizmaların hareketi gerek biyolojik davranışlarını anlamada gerekse mikro robot dizaynında önem taşımaktadır. Mikro yüzücü çoğu zaman durağan akışkanda oldukça düşük hızlarda kıvrınma hareketi ile yer değiştirmektedir, bu da düşük Reynolds sayısından dolayı viskozitenin domine ettiği bir akıştır. Kıvrınma hareketi yüzücünün sürüklenme kuvvetlerinin etkisini farklılaştırmaktadır. İleri, geri ve nötral moddaki hareketler için zamana bağlı periyodik kıvrınma hareketi ANSYS® yazılımı ile modellenmiştir. Sonuçlar durağan duruma erişildikten sonraki tam bir periyod için akış çizgileri, hız vektörü eş eğrileri ve yüzücü çeperindeki duvar kesme kuvveti, girdaplılık ve sürüklenme katsayısı değişimi olarak sunulmuştur. Kıvrınan yüzücünün yüzme verimliliğinin hem Reynolds sayısına hem de yüzücü moduna bağlı olduğu gösterilmiştir.

Anahtar kelimeler: Kendinden tahrikli akış, Düşük reynolds sayılı akış, Sürüklenme katsayısı, Hesaplamalı akışkanlar mekaniği, Biyomedikal akışkanlar mekaniği


Numerical Modeling of the Movement of Self-Propelled Microorganisms in Newtonian Fluid


Abstract: The movement of micro-organisms is important both in understanding their biological behavior and in micro-robot design. The micro swimmer is often displaced by squirming motion at very low speeds in stationary fluid, a flow dominated by viscosity due to the low Reynolds number. The squirming movement differentiates the effect of the drag forces of the swimmer. Time-dependent periodic squirming motion for forward, reverse and neutral mode movements is modeled by ANSYS® software. The results are presented as streamlines, velocity isocurves, and wall shear force, vorticity, and drag coefficient variation at the swimmer wall for a full period after steady state is reached. It has been shown that the swimming efficiency of a squirming swimmer is dependent on both the Reynolds number and the swimmer's mode.

Keywords: Self-propelled flow, Low Re flow Drag coefficient, Computational fluid dynamics, Biomedical fluid dynamics

*Sorumlu yazar (Corresponding author): Yıldız Technical University, Department of Mechatronics Engineering, 34349, İstanbul, Türkiye

E mail: hmercan@yildiz.edu.tr (H. MERCAN)

Hatice MERCAN  <https://orcid.org/0000-0002-3445-3441>

Tufan Tuna KÖSELER  <https://orcid.org/0009-0000-4138-6219>

Gönderi: 11 Eylül 2023

Kabul: 22 Kasım 2023

Yayınlanma: 15 Ocak 2024

Received: September 11, 2023

Accepted: November 22, 2023

Published: January 15, 2024

Cite as: Mercan H, Köselert T. 2024. Numerical modeling of the movement of self-propelled microorganisms in Newtonian fluid. BSJ Eng Sci, 7(1): 36-42.

1. Giriş

Dünya biyokütlesinin çoğu mikroplardan özellikle bakterilerden oluşur ve mikro organizmalar sıvılar içinde hareket ederler. Mikro ölçekli akışların dinamiği, bu tür canlıların davranışlarının belirli yönlerini anlamamıza yardımcı olur. Ayrıca mikro organizmaların sıvı ortamlardaki hareketinin modellenmesi medikal alanda hastalık tetkik-teşhis süreçlerinde ve tedavi protokollerinde kontrol edilebilir ilaç ulaştırma amaçlı kullanılacak mikro robotların dizaynında önem arz etmektedir. Yüzen canlıların akışkanlar mekaniği yöntemleri ile incelenmesi mikro ölçekte makro ölçeğe nazaran büyük farklılıklar gösterir. Karakteristik boylarının küçüklüğü (mikron mertebesinde) ve yine karakteristik hızlarının küçüklüğü (mikron/sn mertebesinde) akışı tanımlayan Reynolds sayısını da bir hayli küçük olmasına yol açar; öyleki tipik Reynolds sayısı 1 civarındadır. Bu durumda, viskoz etkiler akışı

domine ederken atalet kuvvetleri göz ardı edilebilecek kadar küçüktür ve bu sebeple mikro yüzücü hareketi Stokes denklemleri ile modellenebilir (Blake, 1971). Buna ek olarak kıvrınma hareketinin matematiksel olarak tanımlanmasında yüzücünün sınır koşulu klasik akışkanlar mekaniğinde olduğu gibi kaymanın sıfır olması olarak tanımlanmaz. Çünkü organizmaların tahrik için kullandıkları kamçı, sil veya şekil değiştirme hareketlerinden birinin veya bir kaçının ileri, geri veya durma (nötral) hareketi için tanımlanması gerekir (Blake, 1971; Pedley, 2006).

Literatürde kıvrınma hareketi için sınır koşulu ilk defa küresele yakın şekilli ve deformasyona uğrayabilecek organizmaların düşük Reynolds sayılı akışlarda Lighthill (1952) tarafından önerilmiştir. Bu model daha sonraki yıllarda çok sayıda çalışmada çeşitli versiyonlarla kullanılmıştır. Düşük Reynolds sayıları altındaki akışta, Blake (1971) sonsuz silindirik yüzeyindeki kaymazlık sınır koşulunu zarf içinde belirlenen sonlu bir hız ile



değiştirmiştir. Bu yeni sınır koşulu, mikro organizmaların şekil değiştirme yoluyla iki boyutta hareket etmesinin modellenmesini mümkün kılmıştır. Pedley (2016) sınır koşulunu yeniden ele almış ve kıvrancının yüzey hızını sabit teğet bileşene indirgemıştır. Yeni formülasyon mikro yüzücülerin yakınlardaki hidrodinamik akışların kesin olarak hesaplanabilmesini sağlamıştır. Datt ve ark. (2007) tarafından kompleks akışkanlar içindeki aktif partikül akışının modellenmesinde kullanılmıştır, sedimentasyondaki partikül davranışı kısmen modellenenmiştir. Hamilton ve ark. (2018), tek ferro manyetik partikülün hareket edebilen esnek kuyruğu ile makro hareketi modellemiştir. Bunun için salınan manyetik alan oluşturmuş ve kuyruk uzunluğunun ideal uzunluğunu farklı manyetik alan frekansları için belirlemiştir. Pedley (2016) mikro organizmaların hareketine ek olarak hücre çeperinden besin alımını da bu modele eklemiştir.

Daddi-Moussa-Ider ve ark. (2018), Newtonyen akışkan içinde nötr, itilen ve çekilen akış modları için üç küresel mikro yüzücüyü kanal içi akışta modellemiştir. Akışta salınımlı kayma durumu gözlemlenmişler ve bunun kanalın orta alanında ve duvarlardan birine daha yakın bir yerde meydana gelebileceğini raporlamışlardır. Çalışmada itici modundaki harekette salınımlı süzülme durumu kararsız olduğu raporlanmıştır. Çekici modundaki harekette ise bunun aksine, hareket tarzlarının geometrik özelliklerine güçlü bir şekilde bağımlı olduğu gösterilmiştir. Yüzücünün parametreleri değiştikçe, yakalama durumları kaybolabildiği ve yüzücülerin sabit bir oryantasyon ile sabit bir yükseklikte hareket ettiği kayma durumları ortaya çıkabildiği belirtilmiştir. Narinder ve ark. (2018) deneysel çalışmasında ışık enerjisi ile tahrik olan mikro yüzücünün viskoelastik akışkan içindeki hareketini deneysel olarak incelemiştir. Dönme hareketi yaparak ilerlemesi temin edilen yüzücülerin koloidal akışkanın içinde doğrusal olmayan bir şekilde itme hızına bağlı olan bir açılma hız ve bir eğrilik yarıçapı sergileyebildiğini raporlamışlardır. Bu denge dışı hareketin akışkanın Newtonyen olmamasından kaynaklandığı gösterilmiştir. Zöttl ve Stark (2014), ısılı gürültü ile kıvranan tarafından oluşturulan hidrodinamik akış alanını sayısal olarak modellemiştir. Çalışmalarında kolektif anlamda kıvranma sınırı ve çoklu kıvranma hareketleri arasındaki hidrodinamik etkileşimleri irdelemiş, yüksek yoğunlukta kıvrancıda ve nötr kıvrancıda küme benzeri faz oluşurken güçlü itici ve çekicilerde altıgen küme gözlemlendiği raporlanmıştır. Devam eden çalışmalarında, Zöttl ve Stark (2018) çoklu parçacık çarpışma dinamiği yöntemi kullanılarak küresel şekilli kıvrananların hidrodinamiğini ele almıştır. Doğrusal momentum transferinin, akış ve çarpışma adımını birleştirerek ve çözüm prosedürüne sanal parçacıklar ve termal gürültü ekleyerek değerlendirildiğini raporlamışlardır. Kuhr ve ark. (2017) yerçekimi kuvveti altında farklı türde kıvrananları içeren toplu çökelmeyi modellemiştir. Sedimentasyon profili, yoğunluğun yükseklik ve kıvranım

tipi ile üstel olarak değiştiğini göstermiştir. Dibe yakın bölge, çoğunlukla durgun yüzücüler veya zayıf itici ve çekiciler içeren yoğun bir şekilde paketlenmiş katmana sahiptir. Bununla birlikte üst bölge, sedimentasyonun üst tarafında dinamik profil ve konveksiyon akışları gösterir. Takip eden çalışmada Kuhr ve ark. (2019) yerçekimi kuvveti altındaki mikro yüzücü hareketine çoklu parçacık çarpışma dinamiği yöntemi uygulamış, bunun için mikro yüzücülerin kolektif dinamiklerini kıvranan tipine ve yoğunluğuna göre kategorize etmiş ve Wigner sıvısının hidrodinamiğinin akış alanının yapısında altıgen bir düzen oluşturduğunu bildirmiştir.

Biyolojik akışların pek çoğu Newtonyen olmayan özellik gösterse de özellikle kan vb. vücut sıvıları pek çok sayısal çalışmada Newtonyen olarak kabul edilmiş ve çeşitli akışlar için sonuçlar literatürde raporlanmıştır (Gijzen ve ark., 1999; Valencia ve Solis, 2006; Mercan ve Atalık, 2018). Ayrıca literatürde yer alan çalışmaların çoğunda kıvranan yüzücülerin hareketi geçirgenliği olmayan rijit organizma yüzeyinde durağan ve zarf içi yüzey hızı şeklinde tanımlı sınır koşulu kullanılarak modellenmiştir. Ancak bu durum özellikle sil hareketinin modellenmesinde sayısal çözümü kolaylaştırır da akış fiziğinin zamana bağlı değişim bilgisini verememektedir. Bu çalışmada geçirgen olmayan rijit silindirik yüzücünü kıvranma hareketi yeni önerilen zamana bağlı periyodik bir fonksiyonla tanımlanmıştır. Newtonyen akışkan için silli organizmanın özelliklerini taklit eden yeni bir sinüzoidal kıvranma modeli sunulmuştur. Düşük Reynolds sayılı Newtonyen akış içindeki mikro organizmanın hareketi sayısal olarak incelenmiş, sürüklenme katsayılarının değişimi gösterilmiştir. Mikro organizmanın iki farklı akış modu iki farklı akış hızı altında irdelemiştir.

2. Materyal ve Yöntem

Bu çalışmada rijit ve sonsuz silindirik şekilli bir mikro yüzücünün kıvranma hareketi ANSYS programı kullanılarak modellenmiştir. Yüzücü düşük ve çok düşük Reynolds sayılı ($Re=5$; $Re=0,0005$) akışların içinde zamana bağlı olarak tanımlanmış sil hareketi yapmaktadır. Çalışmada kullanılmış olan ana denklem takımları aşağıda detaylıca verilmiştir.

Kütle korunumu ve momentum dengesi denklemleri sırasıyla Denklem 1 ve 2'de verilmiştir;

$$\nabla \cdot u = 0 \quad (1)$$

$$\rho \frac{Du}{Dt} = -\nabla p + \nabla \cdot \tau \quad (2)$$

olup, burada p akışkan yoğunluğu, u hız vektörü, p basınç ve τ ekstra stres tensörüdür. Ekstra stres tensörü Newtonyen akışkan için Denklem 3'deki gibi ifade edilir:

$$\tau = 2\mu D \quad (3)$$

olup, burada μ dinamik viskozite ve D şekil değiştirme oranı tensörüdür. Reynolds sayısı (Denklem 4)

$$Re = \frac{\rho UD}{\mu} \quad (4)$$

burada U karakteristik hız, D yüzücünün çapıdır. Literatürde tanımlanmış kıvranma hareketi durağan durumda ve yarıçapı D/2 olan yüzücünün yüzeyinde tanımlı teğet hızlardan oluşmuş bir zarf fonksiyonudur. Analiz, kıvranma hareketinin zaman içinde periyodik olarak değiştiği bir teğetsel hız ile gerçekleştirilir. Bu yeni zamana bağlı hareket, yüzeyde kurbağalama benzeri hareket, silleri dövme veya kamçıyı itme gibi daha gerçekçi bir kıvranma hareketi sağlamıştır ve Denklem 5'deki gibi tanımlanır:

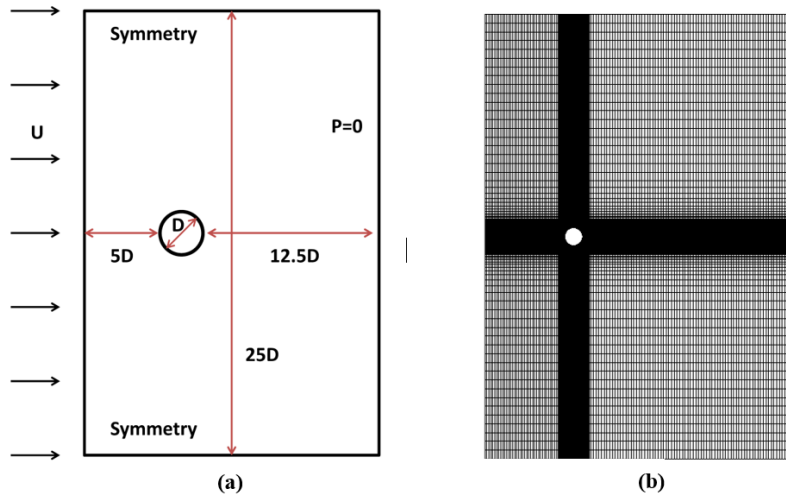
$$u_{\theta} \left(r = \frac{D}{2}, t \right) = \left[\sin\theta + \frac{1}{2r^3} \sin\theta + \frac{3}{2} \beta \frac{1}{r^4} \sin\theta \cos\theta \right] (\sin\omega t + 1) \quad (5)$$

burada t zamandır ve hesaplamalarda sabit açısal frekans $\omega = 1$ rad/sn şeklinde alınmıştır. θ yüzücünün yüzeyinde saat yönünün tersi istikametinde tanımlı açı, r yüzücünün yarıçapıdır ve β yüzücünün ileri geri veya nötral hareketini temsil eden boyutsuz sayıdır. $\beta > 0$ çeken, $\beta < 0$ iten ve $\beta = 0$ ne itici ne çekicidir. Nötral hareket ne itici ne çekicidir ve durağan durumdaki en yüksek enerji verimine sahip moddur (Pedley, 2016). Önerilmiş yeni zamana bağlı periyodik sil hareketi kıvranma hareketinin modunu değiştirmez. Zamana bağlı etkiler altında organizma itilen, çekilen veya nütür olarak

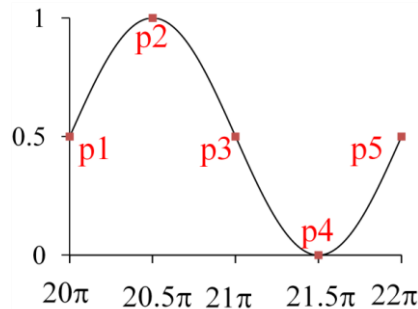
kalır.

Sayısal çözümleme ANSYS® programı ile yapılmıştır. Zamana bağlı ve durağan problemlerde hız ve basınç eşlemesi SIMPLE şeması ile gerçekleştirilmiştir (Şahin ve Atalık, 2019). Sınır koşulları klasik kaymazlık sınır koşulu olmadığından, kullanıcı tanımlı fonksiyon (UDF) kullanılarak ANSYS® programına tanımlanmıştır. Yüzücünün simetrik geometrisi sebebiyle 2 boyutta çözüm yapılmıştır. D çapındaki yüzücü girişten 5D, çıkıştan 12,5D mesafe uzaktadır. Dikdörtgen şeklindeki çözüm alanının yüksekliği 25D'dir, bakınız Şekil 1a. Kıvranma sınır koşulu yüzücü yüzeyinde, uniform hız girişte ve simetri sınır koşulu üst ve alt sınırlarda tanımlanmıştır. Çıkışta basınç değeri atmosferik basınca eşit olarak alınmıştır, o sebeple fark basınç 0'dır. Çözüm alanındaki ağ ANSYS® ICEM CFD program kullanılarak oluşturulmuştur. Çalışmada kullanılan örnek ağ, Şekil 1b'de verilmiştir.

Üç farklı ağ yoğunluğunda çözümlenmeler yapılmış ve eleman boyu küçültüldüğünde sonucun %0,1 den fazla değişmediği 46596 hücre sayılı ağ seçilmiştir. $Re = 40$ için kaldırma katsayısı değeri literatür ile karşılaştırılmış, farkın Şahin ve Atalık (2019) 'ın raporladığı değer olan %0,3'den küçük olduğu gözlemlenmiştir. Çözümün zamana bağlı periyodik durağan durumda olmasının sağlanması için sonuçlar 10'uncu periyottan sonraki periyotta sunulmuştur. Zamana bağlı sonuçlar Şekil 2'de gösterilen şemadaki noktalara karşılık gelen zamanda paylaşılmıştır.



Şekil 1. Çözümleme uzayı, (a) boyut ve sınır koşullarının şematik gösterimi, (b) simülasyonlarda kullanılan ağ.



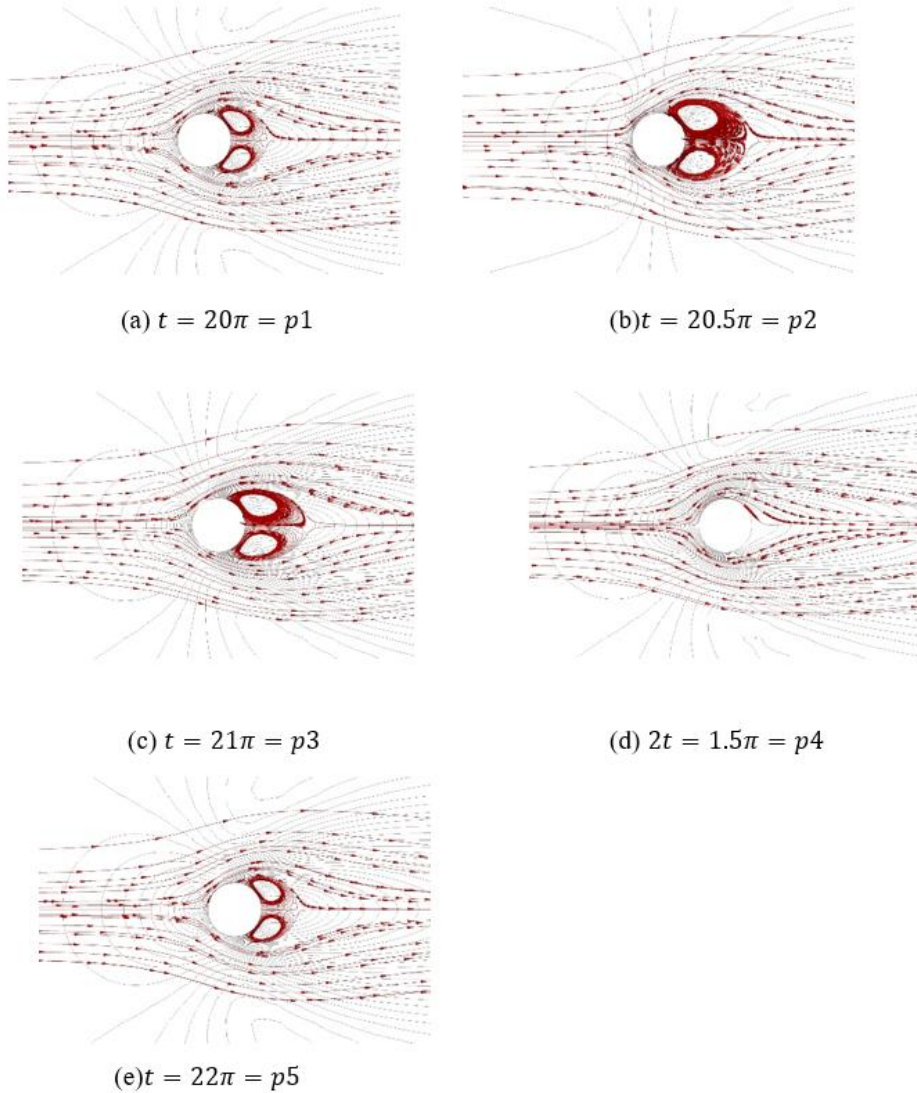
Şekil 2. Zaman bağlı periyodik hız değişiminin tam bir periyot boyunca karşılık geldiği değerlerin şematik gösterimi.

3. Bulgular ve Tartışma

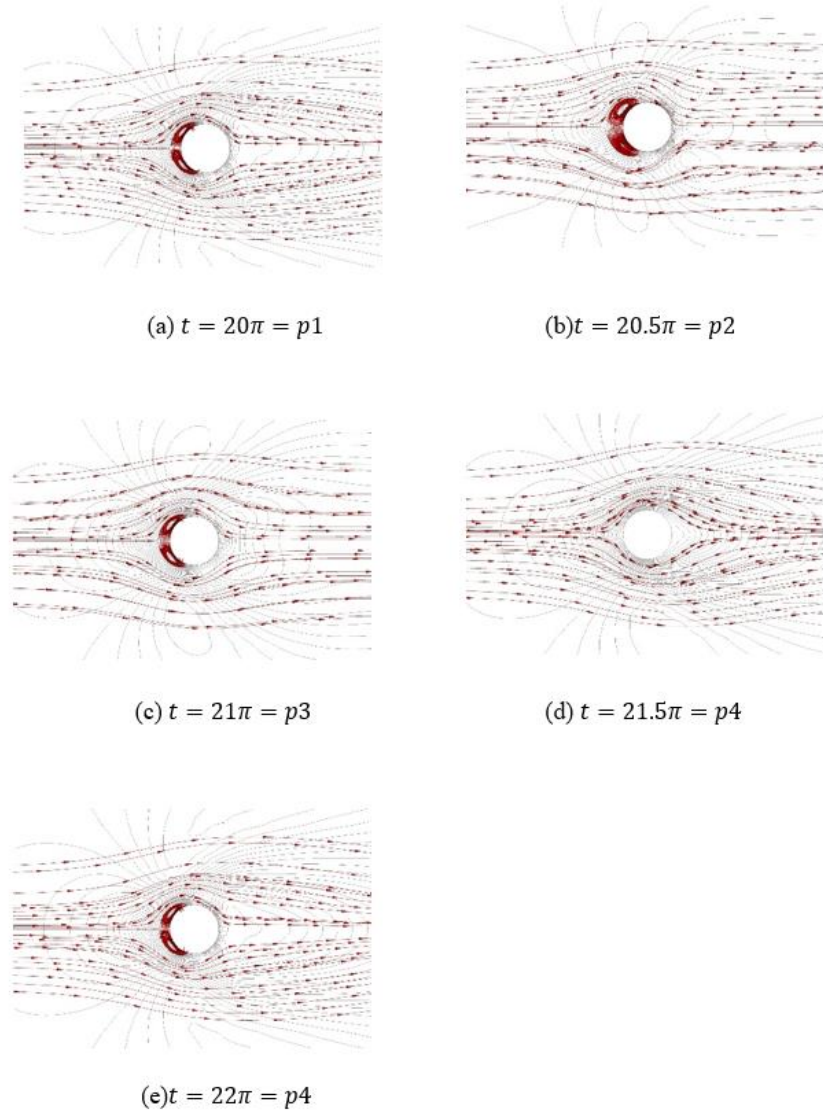
Bu çalışmada öncelikle yüzücünün periyodik olarak tanımlanmış sil hareketinin etkileri periyot süresince incelenmiştir. Bunun için 10'uncu tam periyot başlangıcından itibaren her çeyrek periyot zamanına denk gelen çözümler paylaşılmıştır. Seçilmiş noktalar Şekil 2'de gösterildiği gibidir. Sonuçlar itme ve çekme modlarında ve sabit $Re = 5$ değeri için gösterilmiştir. Öncelikle akış çizgileri ve eş hız eğrileri sonrasında da aynı zamana denk gelen duvar kayma gerilmesi ve girdaplılık değerleri incelenmiştir. Devamında bu sefer itme ve çekme modlarının ve Reynolds sayısının sürüklenme katsayılarına etkisi gösterilmiştir. Son olarak hareket modu ve Reynolds sayısının sürüklenme katsayısına etkisi araştırılmıştır.

Hareket modunun akış çizgilerine ve hız eşeğirilerine etkisi incelenmiştir. Mod etkisinin ($\beta < 0$ iken itme ve $\beta > 0$ iken çekme) kıvranan yüzücünün girdap oluşumuna belirgin etkileri gözlemlenmiştir. Mod

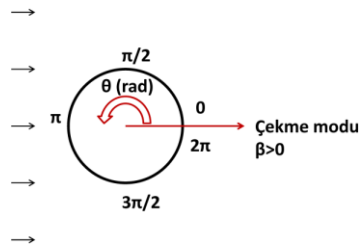
etkisinin belirgin şekilde gözlemlendiği iki farklı mod için tam bir periyot boyunca akış çizgileri ve hız eşeğirileri çekme modu $\beta = 5$ için Şekil 3'te ve itme modu $\beta = -5$ için Şekil 4'te gösterilmiştir. Yüzücü çekme modunda akış yönünde hareket etmekte olduğu için, girdap simetrik şekilde yüzücü arkasında oluşmuştur. Ancak itme modunda yüzücü akışa doğru kıvrandığı için simetrik girdaplar bu sefer yüzücünün ön tarafında oluşmuştur. İtme modundaki girdaplar çekme moduna göre küçüktür. Çekme ve itme modlarında benzer eğilim Ouyang ve ark. (2018) tarafından da raporlanmıştır. Periyodun $21,5\pi$ değerinde (Şekil 2'de p4 noktası) kıvranma hızı 0 olduğu için çekme veya itme modu akış çizgilerini ve hız eşeğirilerini etkilememiş, durum $Re = 5$ 'e karşılık gelen akışa indirgenmiştir, bakınız Şekil 3 ve 4. Her iki modda da en büyük girdaplılık periyodun $20,5\pi$ 'e eşit olduğu anda gözlemlenmiştir (Şekil 2'de p2 noktası).



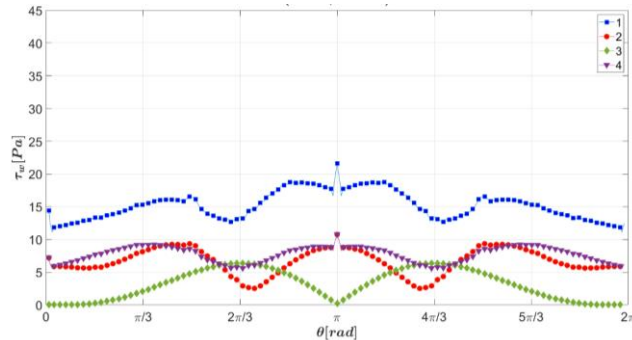
Şekil 3. Tam bir periyotta akış çizgileri (kırmızı çizgiler) ve eş hız eğrilerinin (siyah çizgiler) değişimi, $Re = 5, \beta = 5$, (a) 20π ; (b) $\frac{41\pi}{2}$; (c) 21π ; (d) $\frac{43\pi}{2}$; (e) 22π .



Şekil 4. Tam bir periyotta akış çizgileri (kırmızı çizgiler) ve eş hız eğrilerinin (siyah çizgiler) değişimi, $Re = 5, \beta = -5$, (a) 20π ; (b) $\frac{41\pi}{2}$; (c) 21π ; (d) $\frac{43\pi}{2}$; (e) 22π .



Şekil 5. Yüzücü çevresinde tanımlı açıların şematik gösterimi.



Şekil 6. Yüzücü çevresi boyunca duvar kesme kuvvetinin değişimi (çekme modu $\beta=5, Re = 5$).

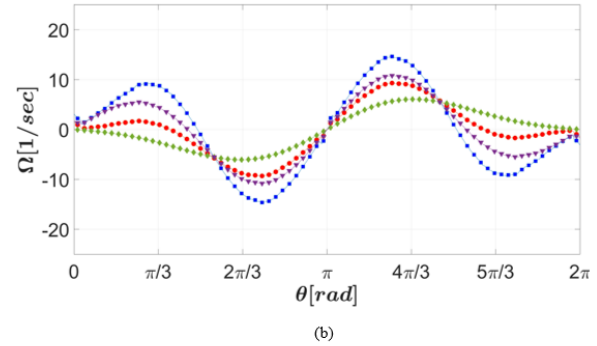
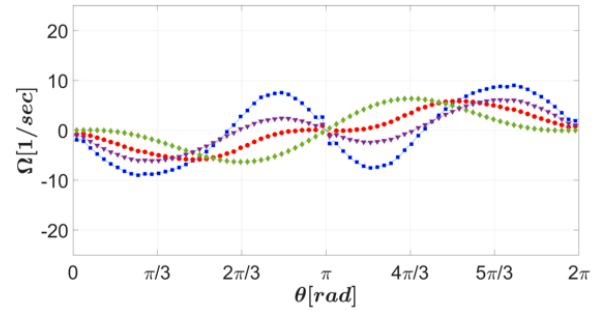
Periyot süresince ve çekme modundaki yüzücü çevresi boyunca kesme kuvveti incelenmiştir. Şekil 5'de şematik olarak gösterilen çekme modundaki yüzücü yüzeyindeki açılar pozitif θ yönünde tanımlanmıştır ve açının π radyan değeri gelen akış yönündeki uç noktaya denk gelmektedir. Çekme modundaki yüzücünün duvar kesme kuvvetindeki değişim Şekil 6'da p1 (mavi), p2 (kırmızı), p3 (yeşil) ve p4 (mor) noktalarına denk gelen zamanlar için gösterilmiştir, p5 noktası p1 noktası ile eşdeğer olduğu için şekilde gösterilmemiştir. Kesme kuvvetinin en yüksek olduğu zaman periyot başlangıcıdır ve maksimum değerini, beklendiği gibi uç noktada almaktadır.

Kıvrancı etrafındaki girdaplılık dağılımları Şekil 7'de gösterilmektedir. Girdap alanlarının üst yarısında, iticiler (çekiciler) yüzme yönlerinin ilerisinde (gerisinde) pozitif (negatif) girdap üretirler (Şekil 7 a çekici, Şekil 7 b itici). Girdaplılığın mutlak değerleri, kıvrancının hareket eksenine göre simetriktir. Kıvranma sınırı civarında, kesme kuvvetlerine maruz kalır ve bu da farklı akış davranışına neden olur. Kıvranan yüzücünün etrafındaki girdap düzeni doğrudan yüzme moduyla ilgilidir. İticilerin yüzeyindeki akış çizgileri girdabı aşağı yönde iter ve yönlendirirken, çekiciler yukarı ve aşağı yönlere yakın girdapları biriktirir. İticilerin yüzeyindeki akım çizgileri girdabı aşağı yönde iter ve yönlendirirken, çekiciler yukarı ve aşağı yönlere yakın girdapları biriktirir.

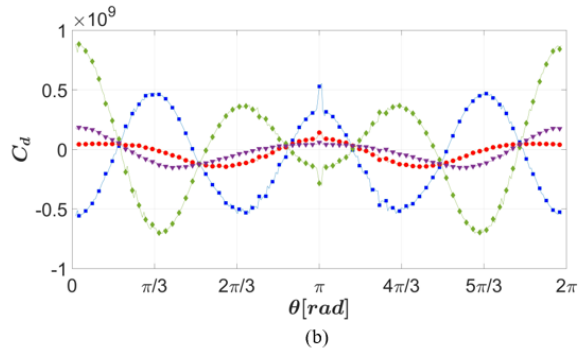
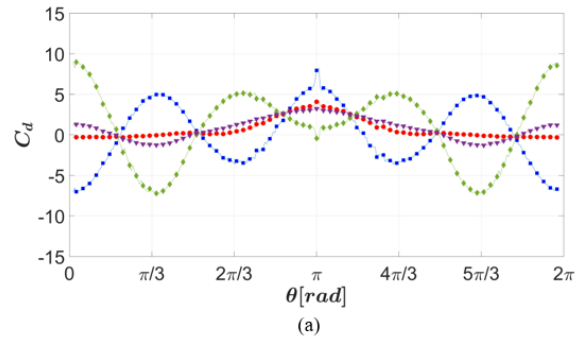
Son olarak hareket modunun ve Reynolds sayısının sürüklenme kuvvetlerine etkisi incelenmiştir. Sıvının kıvrancıya uyguladığı kuvvet, sürüklenme ve kaldırma olmak üzere iki bileşene ayrıştırılabilir. Toplam kuvvet, kıvranan cismin yüzeyi üzerindeki çekişin bir integralidir ve simülasyonumuzda, yüzey düğümlerindeki tüm birim kuvvetlerin toplamıdır. Sürüklenme kuvvetinin yüzey etrafındaki dağılımını elde etmek için sürüklenme katsayısı C_d Eşitlik 6'daki şekilde tanımlanır:

$$C_d = \frac{2F_x}{\rho U_0^2 D} \quad (6)$$

burada F_x yüzücü yüzeyindeki sürüklenme kuvveti; ρ sıvı yoğunluğu; U_0 sıvı hızıdır; ve D yüzücü çapıdır. Farklı Reynolds sayılarındaki yüzme modları için kıvrancı yüzeyi etrafındaki sürüklenme katsayıları Şekil 8'de gösterilmiştir. Şekil 8 a $Re = 5$ ve Şekil 8 b'de $Re = 0,0005$ içindir. Reynolds sayısı arttıkça sürüklenme katsayılarının azaldığı görülmektedir. Yüzücü yüzeyinde sürüklenme katsayısı dağılımları, kıvrancının hareket eksenine göre simetrik veya antisimetriktir. Kıvrananların yüzme özelliklerinin Reynolds sayısı ve yüzme modu ile yakından ilişkili olduğu sonucuna varılmıştır.



Şekil 7. Yüzücü çevresi boyunca girdaplılık değerinin değişimi, $Re = 5$, (a) çekme modu: $\beta = 5$, (b) itme modu $\beta = -5$.



Şekil 8. Farklı hareket modları için sürüklenme katsayılarının yüzücünün dış yüzeyi boyunca dağılımı (a) $Re = 5$, (b) $Re = 0,0005$. Hareket modları sırası ile çekme modu $\beta = 5$ mavi renk; $\beta = 0.5$ kırmızı renk; itme modu $\beta = -5$ yeşil renk; $\beta = -0.5$ mor renk.

4. Sonuç

Bu çalışmada, sonsuz silindir şeklindeki kıvrancının zamana bağlı periyodik sil hareketi sayısal olarak incelenmiştir. Önerilen periyodik sınır koşulu ile tek hücreli silli organizmaların kıvranma hareketi daha

gerçekçi olarak modellenmiştir. Newtonyen sıvı içinde yüzen bir kıvrancının hidrodinamik davranışı sistematik olarak analiz edilmiştir. Reynolds sayısı ve yüzme modunun hareket üzerindeki etkilerinin yanı sıra kıvrananların güç harcaması tartışılmıştır. Sonuçlar, Re değeri 0,0005 ile 5 arasında değişen (bu aralık çoğu mikroorganizmanın yüzmesi için uygundur) kıvranan yüzücünün yüzmesinin eylemsizlik kuvvetinden etkilendiğini göstermiştir. Sonuçlar aşağıdaki gibi özetlenebilir:

- Çok düşük Re 'de, Newtonyen akışkan için kıvranma hızı sabit kalmıştır. Nispeten yüksek Re 'de, kıvranma hızının değişme eğilimi gözlemlenmiştir.
- İtici hızı Re ve β değerinin artmasıyla artarken, çekicinin hızı Re 'nin artmasıyla azalır veya artar.
- Kıvranan yüzücünün yüzme verimliliği hem Re 'ye hem de β 'ye bağlıdır.

Son olarak, Newtonyen olmayan biyoakışkanlar içindeki periyodik kıvranma hareketleri ile sürüklenme ve kaldırma katsayılarının beraber incelenmesi gelecek çalışma olarak planlanmaktadır.

Katkı Oranı Beyanı

Yazar(lar)ın katkı yüzdesi aşağıda verilmiştir. Tüm yazarlar makaleyi incelemiş ve onaylamıştır.

	H.M.	T.T.K.
K	80	20
T	80	20
Y	100	
VTI	40	60
VAY		100
KT	60	40
YZ	90	10
KI	80	20
GR	80	20
PY	100	

K= kavram, T= tasarım, Y= yönetim, VTI= veri toplama ve/veya işleme, VAY= veri analizi ve/veya yorumlama, KT= kaynak tarama, YZ= Yazım, KI= kritik inceleme, GR= gönderim ve revizyon, PY= proje yönetimi.

Çatışma Beyanı

Yazarlar bu çalışmada hiçbir çıkar ilişkisi olmadığını beyan etmektedirler.

Etik Onay Beyanı

Bu çalışmada hayvanlar ve insanlar üzerinde herhangi bir çalışma yapılmadığı için etik kurul onayı alınmamıştır.

Kaynaklar

- Blake JR. 1971. Self propulsion due to oscillations on the surface of a cylinder at low Reynolds number. Bull Aust Math Soc, 5(2): 255-264.
- Daddi-Moussa-Ider A, Lisicki M, Mathijssen AJ, Hoell C, Goh S, Bławdziewicz J, Menzel AM, Löwen H. 2018. State diagram of a three-sphere microswimmer in a channel. J Phys Condens Matter, 30(25): 254004.
- Datt C, Natale G, Hatzikiriakos SG, Elfring GJ. 2017. An active particle in a complex fluid. J Fluid Mech, 823: 675-688.
- Gijsen FJH, Allanic E, Van de Vosse FN, Janssen JD. 1999. The influence of the non-Newtonian properties of blood on the flow in large arteries: unsteady flow in a 90 curved tube. J Biomechanics, 32(7): 705-713
- Hamilton JK, Gilbert AD, Petrov PG, Ogrin FY. 2018. Torque driven ferromagnetic swimmers. Phys Fluids, 30(9): 092001. <https://doi.org/10.1063/1.5046360>.
- Kuhr JT, Rühle F, Stark H. 2019. Collective dynamics in a monolayer of squirmers confined to a boundary by gravity. Soft Matter, 15(28): 5685-5694.
- Kuhr JT, Blaschke J, Rühle F, Stark H. 2017. Collective sedimentation of squirmers under gravity. Soft Matter, 13(41): 7548-7555.
- Lighthill MJ. 1952. On the squirming motion of nearly spherical deformable bodies through liquids at very small Reynolds numbers. Commun Pure Appl Math, 5(2): 109-118.
- Mercan H, Atalık K. 2018. Numerical investigation of blood flow features in intracranial saccular aneurysms. J Thermal Eng, 4(2): 1867-1878.
- Narinder N, Bechinger C, Gomez-Solano JR. 2018. Memory-induced transition from a persistent random walk to circular motion for achiral microswimmers. Physical Rev Lett, 121(7) : 78003.
- Ouyang Z, Lin J, Ku X. 2018. The hydrodynamic behavior of a squirmer swimming in power-law fluid. Physics Fluids, 30(8): 083301. <https://doi.org/10.1063/1.5045701>.
- Pedley TJ. 2016. Spherical squirmers: models for swimming micro-organisms. IMA J Appl Math, 81(3): 488-521.
- Şahin Ç, Atalık K. 2019. Comparison of inelastic and elastic non-Newtonian effects on the flow around a circular cylinder in periodic vortex shedding. J Non-Newtonian Fluid Mechanics, 263: 1-14.
- Valencia A, Solis F. 2006. Blood flow dynamics and arterial wall interaction in a saccular aneurysm model of the basilar artery. Comput Struct, 84(21), 1326-1337.
- Zöttl A, Stark H. 2014. Hydrodynamics determines collective motion and phase behavior of active colloids in quasi-two-dimensional confinement. Physical Rev Lett, 112(11): 118101.
- Zöttl A, Stark H. 2018. Simulating squirmers with multiparticle collision dynamics. European Physical J E, 41(5): 61.



ANATOMICAL, ECOLOGICAL AND TRICHOME MICRO-MORPHOLOGICAL FEATURES OF TWO *MARRUBIUM* L. TAXA (LAMIACEAE)

Kamer Volkan KOÇAK¹, Nezahat KANDEMİR^{2*}

¹Amasya University, Graduate School of Natural and Applied Sciences, Department of Biology, 05100, Amasya, Türkiye


²Amasya University, Faculty of Education, Department of Mathematics and Science Education, 05100, Amasya, Türkiye


Abstract: The anatomical, ecological and trichome micro-morphological features of two taxa (*Marrubium amasiensis* and *Marrubium parviflorum* subsp. *parviflorum*) belonging to the genus *Marrubium* were determined and these features were compared. *M. amasiensis* is endemic and is distributed only around Amasya in Türkiye. In anatomical examinations, cross sections were taken from the root, stem, petiole, leaves and surface sections were taken from stem, petiole, and the lower and upper surfaces of the leaves. When the anatomical findings were examined, multi-layered lamellar collenchyma layer was encountered at the corners of the stem. The studied taxa have equifacial leaves in terms of mesophyll structure. Stomata of *M. amasiensis* are anomocytic and rarely anisocytic type, while stomata of *M. parviflorum* subsp. *parviflorum* are anomocytic type. The margins of the adjacent cells of the stomata in both taxa are very undulate. E glandular and glandular trichomes were seen on vegetative organs of the two taxa. The glandular trichomes are stellate, dendroid, marrubioid and simple unicellular types, while glandular trichomes are capitate and peltate types. Dense stellate trichomes were found in the vegetative organs of the studied taxa. Since the head and stalk cell numbers of capitate trichomes showed variation, these trichomes were divided into subtypes. Three subtypes of capitate trichomes were found on the vegetative organs of *M. parviflorum* subsp. *parviflorum*, while four subtypes of capitate trichomes were found on the vegetative organs of *M. amasiensis*. Soil samples were taken during flowering periods of taxa, physical and chemical properties were determined. Some similarities and differences were detected in the anatomical, ecological and trichome micro-morphological features of the studied two taxa. It has been emphasized that these different features will be used as valuable taxonomic characters in distinguishing of the two taxa.

Keywords: *Marrubium* taxa, Anatomy, Ecology, Trichome micro-morphology, Lamiaceae, Türkiye

*Corresponding author: Amasya University, Faculty of Education, Department of Mathematics and Science Education, 05100, Amasya, Türkiye

E mail: nezahatkdmr@gmail.com (N. KANDEMİR)

Kamer Volkan KOÇAK  <https://orcid.org/0000-0003-0650-2661>

Nezahat KANDEMİR  <https://orcid.org/0000-0002-5428-4139>

Received: July 07, 2023

Accepted: November 24, 2023

Published: January 15, 2024

Cite as: Koçak KV, Kandemir N. 2024. Anatomical, ecological and trichome micro-morphological features of two *Marrubium* L. taxa (Lamiaceae). BŞJ Eng Sci, 7(1): 43-54.

1. Introduction

Marrubium L. genus belongs to the family Lamiaceae and includes annual and perennial plant species. The *Marrubium* taxa are mainly distributed in the Irano-Turanian and Mediterranean phytogeographic regions. The endemism rate of this genus in the Mediterranean phytogeographical region (88%) is higher than in the Irano-Turanian phytogeographical region (71%). The genus is represented by 27 taxa and 23 species in Türkiye and rate of endemism is 59% (Celep and Dirmenci, 2017).

Some members of the genus have medicinal and ethnobotanical importance. They are used to treat various diseases such as bronchitis, respiratory disorders, tuberculosis, asthma, skin damage, ulcers, boils, rheumatism, stomach disorders, cough, inflammation, myocardial infarction, edema, ear pain, appetizer, high blood pressure, spasm, flatulence, dyspepsia, and women infertility (Meyre-Silva and Cechinel-Filho, 2010; Yousefi et al., 2014; Okur et al.,

2019; Benzidane et al., 2020). In addition, the above-ground parts of *Marrubium* species, known as “dağ çayı, bozotu, kalartopu, yabaniderme, çalba, şapla, kukasotu” in Anatolia, are used as a pain reliever, antipyretic, expectorant and menstrual-reducing (Sargin et al., 2015; Tuzlacı, 2016; Selvi et al., 2022).

The genus is characterized by flowers arranged densely on the stems, leaves with toothed margins, having many lateral branches, the presence of stamens in the corolla tube, the beard of the calyx throat, the number of teeth in the calyx, the presence of hairs inside the corolla tube and stellate trichomes covering all organs (Ahvazi et al., 2016; Çalı, 2017; Koçak and Kandemir, 2023). The stellate trichomes are multicellular and branched at the tip of the stalk cell to form star shaped (Xiang et al., 2010). The branched glandular trichomes (dendroid) are branched along the stalk cell (El-Deen Osman, 2012). The glandular trichomes were reported on the vegetative and generative organs of the Lamiaceae taxa. These trichomes were divided into four types (simple



unicellular, simple multicellular, branched unicellular and branched multicellular) by Cantino (1990). On the other hand, two main types of glandular trichomes-peltate and capitate-were reported in some species of *Marrubium* genus (Dmitruk and Haratym 2014; Haratym and Weryszko-Chmielewska, 2017; Gyuzeleva et al., 2022; Koçak and Kandemir, 2023). Some taxa of the Lamiaceae family have the peltate trichomes with four, eight and twelve celled head in a single circle (Kamatou et al., 2006). The peltate trichomes were abundantly seen on the vegetative organs of some taxa in the Lamiaceae family. However, these trichomes were rarely seen on the reproductive organs of some taxa in this family (Serrato-Valenti et al., 1997; Kandemir, 2011). In capitate trichomes, head and stalk cell numbers are highly variable and these trichomes are subdivided into according to stalk and head cell numbers and head shape. The capitate ones were frequently found in the Lamiaceae taxa (Corsi and Bottega, 1999; Kandemir, 2011; El-Deen Osman, 2012). Both glandular and glandular trichomes are known as very significant taxonomic characters in the Lamiaceae family, since the structures of trichomes show variation in this family (El-Deen Osman, 2012; Seyedi and Salmaki, 2015; Haratym and Werszko-Chmielewska, 2017).

M. amasiensis Akgül and Ketenoglu is an endemic species limited distribution only around Amasya (Türkiye). This species is distributed in mixed forests and stony slopes. It has very important distinguishing characters such as stem is unbranched and dark green, the presence dense stellate trichomes on above of the stem, stem leaves being ovate to rounded, bracteoles being of equal in length to the calyx tube, calyx teeth having 10 equal or subequal. lengths and the corolla yellowish white, the pollen ornament reticulate, and the seeds oblong shaped (Akgül et al., 2017). In the areas where the species is distributed, activities such as road works and overgrazing have been encountered. This situation endangers the populations of the locally distributed and endemic species. Therefore, the species is placed in the CR category by Akgül et al. (2017). *M. parviflorum* Fisch. & Mey. subsp. *parviflorum* is a widely distributed taxon in Türkiye. The subspecies is distinguished from other *Marrubium* taxa with its morphological characters such as light green and grayish green color, dense lanate trichomes, protruding calyx teeth protruding outwards, teeth 1/3 spiny, 10 in number, cylindrical structure and no back-curving.

The aim of this study is to reveal the taxonomic importance of the anatomical, ecological and trichome micro-morphological features of two *Marrubium* taxa, which are morphologically similar to each other and to compare these features.

2. Materials and Methods

Plant and soil samples were taken from the areas where the taxa naturally spread. The taxonomic descriptions of these taxa were made according to Akgül et al. (2017)

and Cullen (1982). Some of the plant samples were dried up according to standard herbarium techniques and stored, some of them were fixed in 70 % alcohol for anatomical investigations. In anatomical examinations, the cross sections of root, stem, petiole and leaf and surface sections of stem, petiole and leaves were taken by hand. Sarture reagent was applied to cross and surface sections (Çelebioğlu and Baytop, 1949). Anatomical investigations were performed using an average of 15 plant specimens which were kept in 70% alcohol. Photographs were viewed using the 10X and 40X lenses of the Leica ICC50 HD microscope. Determining the micro-morphology of trichomes on the vegetative organs of studied taxa were made using 40X magnification of the Leica ICC50 HD microscope. Trichomes were classified according to Navarro and El Oualidi (2000), El-Deen Osman (2012) and given in Tables 1 and 2. Soil samples were taken 1-2 kg from 0-20 cm depth and brought to the laboratory in polyethylene bags. These samples were dried in the laboratory and passed through a 2 mm sieve and made ready for physical and chemical analysis. Physical and chemical analyzes of soil samples were performed in Amasya University Central Research and Application Laboratory Application and Research Center. Soil texture, total salinity, calcium carbonate, pH, nitrogen, phosphorus, potassium and organic matter contents of the soil samples were determined according to standard methods (Kaçar, 1995). Mean and standard deviation values of soil analysis results were shown in Tables 3 and 4. The localities where the taxa were collected were listed below;

Marrubium amasiensis;

A5 Amasya: Direkli Village, Northern slopes of Sakarat Mountain, Karanlıkönü location, clearings in mixed and *Quercus* forest slopes, 1100-1400 m., 09.07.2020, Koçak and Kandemir.

A5 Amasya: Roadsides in Direkli Village, 1225m., 05.07.2020, Koçak and Kandemir.

A5 Amasya: Surroundings of Direkli Village, calcareous rock slopes, 1200m., 05.07.2020, Koçak and Kandemir.

A5 Amasya; Open areas between Direkli Village and Sulugöl, 1400 m., 05.07.2020, Koçak and Kandemir.

Marrubium parviflorum subsp. *parviflorum*;

A5 Amasya: Next to the TV tower, above Ormanözü Village, open areas and roadsides, 1500 m., 14.07.2020, Koçak and Kandemir.

A5 Amasya: Ormanözü Village, stony slopes by the roadside, 1250 m., 14.07.2020, Koçak and Kandemir.

A5 Amasya: Roadsides in Direkli Village, 1225m., 05.07.2020, Koçak and Kandemir.

A5 Amasya: Above Direkli Village, open areas, 1300 m., 05.07.2020, Koçak and Kandemir.

A5 Amasya: Aydınca Şehzade Village open spaces, 1100 m., 09.07.2020, Koçak and Kandemir.

A5 Amasya: Between Sultançayırı Gümüş Town, roadsides Sultançayırı, 1000 m., 14.07.2020, Koçak and Kandemir.

2.1. Statistical Analysis

The Mann Whitney U test was used to determine whether there was a difference between the results of the soil analysis of the studied taxa (Büyükoztürk, 2001). However, no statistical difference was found between the soil analysis results of the two taxa ($P > 0.05$) (Table 5).

3. Results

3.1. Anatomical Features of *Marrubium amasiensis*

3.1.1. Root

It is observed that the root of the studied taxon has a secondary thickening. The periderm layer on the outermost surface is 6-7 layered (Figure 1 A). The cortex is beneath the periderma and consists of 9-11 layered, oval or rectangular shaped parenchyma cells. Phloem elements are obvious. Small groups of phloem sclerenchyma cells were located above the phloem (Figure 1 B). Cambium is distinguishable and 2-4 layered. The secondary xylem consisted mostly of sclerenchymatic cells and tracheids (Figure 1 C). The pith region is completely filled with primary xylem elements.

3.1.2. Stem

Cross-section of the stem is obviously quadrangular in shape. The epiderma consists of uniseriate, square shaped and small cells. The cuticle is thick and with dense micropapillae. Lamellar collenchyma is located immediately beneath the epiderma. The lamellar collenchyma at the corners is 8-10 layered (Figures 1 D, E). In the other parts of the stem, the lamellar collenchyma is 3 layered. Parenchyma is 3-4 layered, oval and elongated shaped, thin walled (Figure 1 F). Beneath of the cortex parenchyma, small groups of phloem sclerenchyma cells are located. The sclerenchyma is 3 layered. Phloem is in narrow region and its elements are clearly seen. Vascular cambium is 4-5 layered. The xylem is in large region and the tracheas are chain-shaped and quite large. Xylem elements are thick-walled. The pith region is composed of large, hexagonal and round shaped cells (Figure 1 G). Needles and solitary crystals were found in pith region.

3.1.3. Petiole

The cuticle is thick and with dense micropapillae. The epidermis cells are rectangular shaped and large. Collenchyma is 2-3 layered and parenchyma is 5-6 layered, large and hexagonal shaped (Figures 1 K, L). Both crystal granules and solitary crystals were obtained in the cortex (Figure 1 L). The endoderma layer around the vascular bundles contains of one layered, large and flattened cells. Phloem and xylem elements are clearly visible. The tracheas of the xylem are large and chain shaped. There are four vascular bundles in the petiole. Two of the vascular bundles are in the middle of petiole and quite large (Figures 1 H, K). The other two vascular bundles are at the margins of the petiole and smaller.

3.1.4. Leaf

In leaf cross sections, the upper and the lower epidermis cells are uniseriate, quadrangular shaped. However, upper epidermis cells are larger than lower epidermis

cells. Papillae were observed in both epidermis cells. On the epiderma, cuticle is thick and with micropapillae. Mesophyll is equifacial type (Figure 1 M). Palisade parenchyma beneath the upper epiderma is 1-2 layered (usually 1-layered), long, cylindrical shaped and with abundant chloroplast. The palisade parenchyma in the lower epiderma is 1-2 layered, cylindrical and shorter. Spongy parenchyma is composed of 2-3 layered, round or irregular shaped and with large intercellular spaces. Vascular bundles in the middle of the mesophyll are uniseriate and collateral type. The walls of the adjacent epidermis cells around the stomata are clearly undulate. Stomata are generally anomocytic type and rarely anisocytic type (Figure 1 O). The numbers of the adjacent epidermis cells are 3-4, usually 4. A large vascular bundle was observed in cross-sections taken from the leaf midrib (Figure 1 N).

3.1.5. Micro-morphology and localizations of eglandular and glandular trichomes on the vegetative organs of *Marrubium amasiensis*

Both eglandular and glandular trichomes were seen on the epiderma of the stem, petiole and leaves of *M. amasiensis* (Table 1). The eglandular trichomes are simple unicellular, stellate, dendroid and marrubioid types. The simple unicellular trichomes were obtained only in the petiole. This kind of trichomes has only one cell and is unbranched structure. The marrubioid trichomes are generally 3 celled, elongated and curved. This kind of the eglandular trichomes was obtained on the stem and leaves (Figure 1 P). The dendroid trichomes are multicellular branched along the stalk cell. Dense dendroid trichomes were observed on the upper and lower surfaces of the leaves of this species (Figures 1 R, X, Y, Z). However, dendroid trichomes were not found on the stem and petiole of *M. amasiensis*. The third type of eglandular trichomes is stellate ones. Dense stellate trichomes were seen on the stem, petiole, both the lower and upper surfaces of the leaves of *M. amasiensis* (Figures 1 S, T). Some of the stellate trichomes are less branched, the middle branch is two-celled, long and curved, other branches are approximately equal in length, unicellular, thin and curved. The middle branches of the stellate trichomes on the upper epiderma of leaves are quite long and multicellular, the lateral branches are thin, usually unicellular. On the lower epiderma, the stellate trichomes are few and finely branched, the middle branch is longer and all unicellular. Also, dense stellate trichomes were detected on calyx teeth, calyx surface and corolla of this species. Glandular trichomes are peltate and capitate types. The peltate trichomes have a mainly with short stalk and a large four or eight-celled head. This kind of glandular trichomes was dense detected on both upper and lower of leaves (Figures 1 V, Y). But, 4-celled head kind of peltate trichomes was observed on the stem and petiole. The capitate trichomes were divided into four subtypes: I. unicellular short-stalked and with unicellular or bicellular head, II. unicellular long-stalked and with unicellular or bicellular head, III. unicellular long-stalked,

with bicellular head and unicellular short neck. IV. unicellular short-stalked and with a cup-shape unicellular head. The unicellular short stalked and with unicellular or bicellular head capitate trichomes (type I) were rare observed on the stem and petiole, while these trichomes were dense observed on the upper and lower

surfaces of leaves (Figures 1 W, X, Y, Z). On the other hand, type II capitate trichomes were only found on the petiole and upper and lower surfaces of leaves. The types III and IV capitate trichomes were dense found on the upper and lower surfaces of leaves.

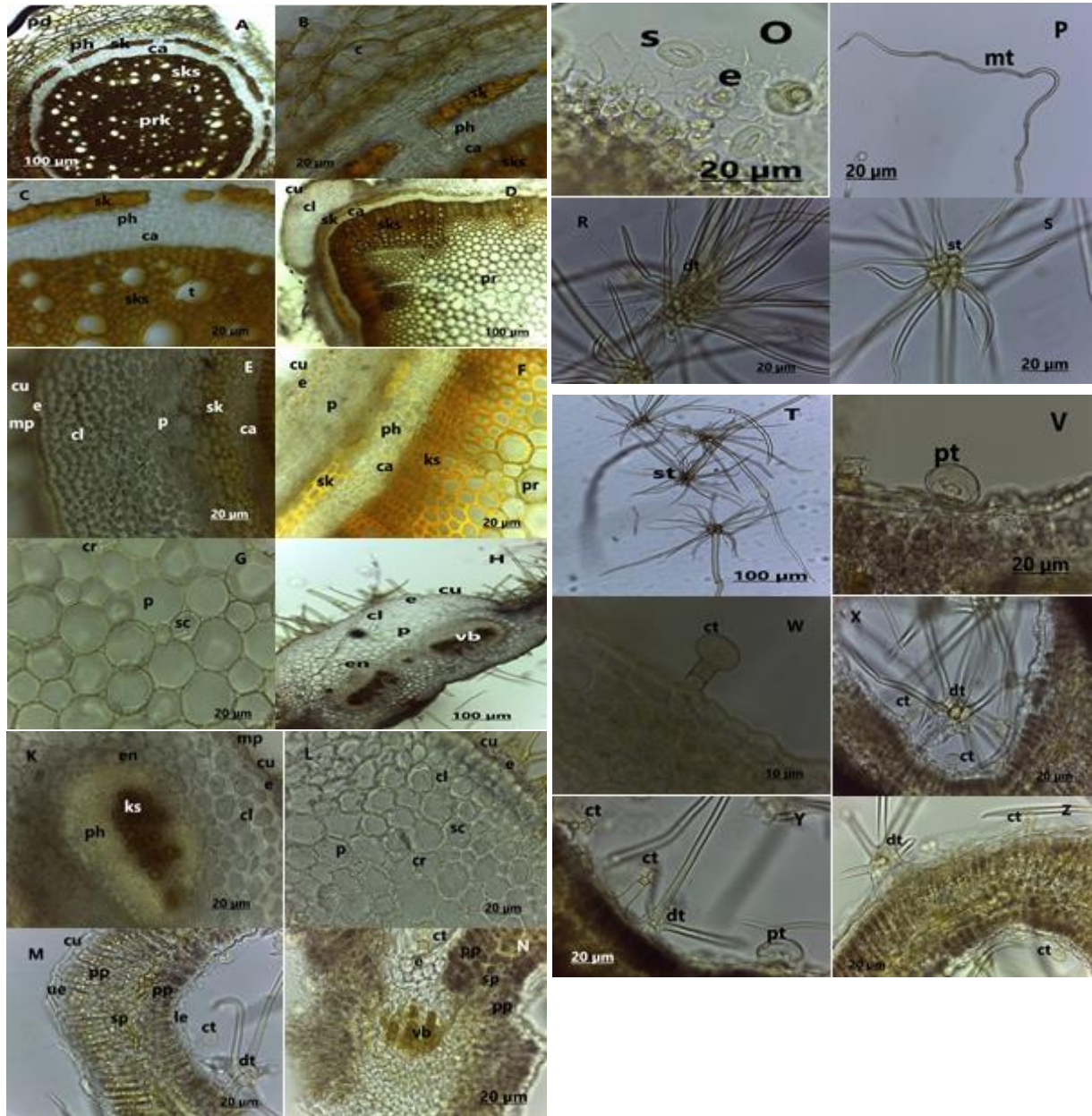


Figure 1. Root, stem and leaf anatomical structures and trichome types of *Marrubium amasiensis*. A=General structure of root, B=Cortex and phloem regions of root, C=Secondary xylem and phloem regions of root, D=General structure of stem, E=Cortex region of stem, F=Cortex, xylem and phloem regions of stem, G=Pith region of stem, H=General structure of petiole, K=Vascular bundle of petiole, L=Crystals in the petiole, M=General structure of leaf, N=Cross section of the leaf midrib, O=Stomata in surface section of leaf (lower surface), P=Marrubioid trichome in the leaf, R=Dendroid trichome in the leaf, S=Stellate trichome in the leaf, T=Stellate trichome in the stem, V=Peltate trichome in the leaf, W=Capitate trichome in the petiole, X=Dendroid and capitate trichomes in the leaf, Y=Dendroid, capitate and peltate trichomes in the leaf, Z=Dendroid and capitate trichomes in the leaf. pd= periderma, ph=phloem, t=trachea, sk=sclerenchyma, ca=cambium, sks=secondary xylem, prk=primary xylem, c=cortex, cu=cuticle, cl=collenchyma, p=parenchyma, pr=pith region, e=epiderma, mp= micropapillae, ks=xylem, cr=crystal granules, sc=solitary crystal, en=endodermis, ue=upper epiderma, pp=palisade parenchyma, sp=spongy parenchyma, le=lower epiderma, vb=vascular bundle, s=stoma, ct=capitate trichome, dt=dendroid trichome, mt=marrubioid trichome, st=stellate trichome, pt=peltate trichome.

Table 1. Trichome types and distributions on organs of *Marrubium amasiensis*

Organs of <i>M. amasiensis</i>	Type I capitate	Type II capitate	Type III capitate	Type IV capitate	Peltate trichomes	Simple eglandular	Stellate eglandular	Dendroid eglandular	Marrubioid eglandular
Stem	+	-	-	-	+	-	+++	-	+
Petiole	+	+	-	-	+	+	+++	+	-
Margin and veins of leaf	+++	++	++	++	++		+++	++	+
Lamina of leaf	+++	++	++	++	++		+++	++	+
Calyx teeth	++	-	-	-	+	+	++	+	-
Outer surface of calyx	++	+	-	-	+	+	++	-	-
Corolla	+	-	-	-	+	++	++	-	-

-absent, +scarce, ++ dense, +++ abundant

Type I capitate= unicellular short stalked and with unicellular or bicellular head, Type II capitate= unicellular long stalked and with unicellular or bicellular head, Type III capitate= unicellular long-stalked, with bicellular head and unicellular short neck, Type IV capitate= unicellular short-stalked and with a cup-shape unicellular head, Peltate trichomes= short stalked and a large four or eight-celled head, Stellate= star shaped trichome, Dendroid= multicellular branched trichome, Marrubioid= unicellular or multicellular and curly in the tip trichome

3.2. Anatomical Features of *Marrubium parviflorum* Subsp. *parviflorum*

3.2.1. Root

Periderma layer is located at the outermost part of the root (Figure 2 A). It is 5-6 layered. The cortex beneath the periderma layer is composed of large and ovoid parenchyma cells. Cambium consists of flat cells and it is 3 layered. Phloem is distinguishable and in a narrow region. It contains small sclerenchyma cell groups. Xylem is composed of tracheary elements. Tracheas are sparse and rather large (Figure 2 B). Dense sclerenchymatic cells were seen in the xylem. In the center of root, there are primary xylem elements.

3.2.2. Stem

Cuticle layer is thick and with dense micropapillae. The stem is apparent quadrangular shaped (Figure 2 C). Epiderma is uniseriate, small celled and rectangular shaped. Papillae were obtained in the epidermis cell. Lamellar collenchyma was observed at the corners of the stem. This collenchyma is 8-11 layered and covers a large area at the corners (Figure 2 D). Parenchyma cells beneath the epiderma are 5-6 layered, small and with chloroplasts. Crystal granules were observed in these parenchymatic cells. Other parenchyma cells are 3-4 layered (generally 4 layered), oval shaped, large and without chloroplast. Sclerenchyma is 4 layered (Figure 2 E). Phloem elements are conspicuous and consist of small cells. The cambium between the xylem and phloem is 1-3 layered and small celled. Xylem elements are evident and in a wide region. Dense sclerenchymatic cells were found in the xylem. There is a large pith region in the centre of the stem (Figures 2 C, F). The pith regions consist of large and orbiculate shaped parenchymatic cells. Pith parenchyma cells are smaller towards the xylem. In the pith region, there are needles and solitary crystals.

3.2.3. Petiole

The epiderma is uniseriate, quadrangular and with rare papillae. The cuticle is thick and with very dense micropapillae. On the xylem, 4-6 layered lamellar collenchyma and 4-5 layered parenchyma were seen (Figure 2 H). The parenchyma consists of hexagonal and round shaped cells. Chloroplasts do not have in the parenchyma cells. On the phloem, 4 layered lamellar collenchyma and 4 layered, oval shaped, large celled parenchyma were found. There are two large vascular bundles in the middle of petiole (Figure 2 G). In the margins of the petiole, smaller vascular bundles were observed. The parenchyma cells around the vascular bundles in the margins are small. Dense chloroplasts were observed in 3-4 layered of these parenchyma cells, while chloroplasts were not observed in 1-2 layered of parenchyma cells. The parenchyma cells around the large vascular bundles are rather large. These cells rarely contain crystal granules. Xylem and phloem elements were clearly seen. The endoderma layer around the vascular bundles consists of a single layered and large cell.

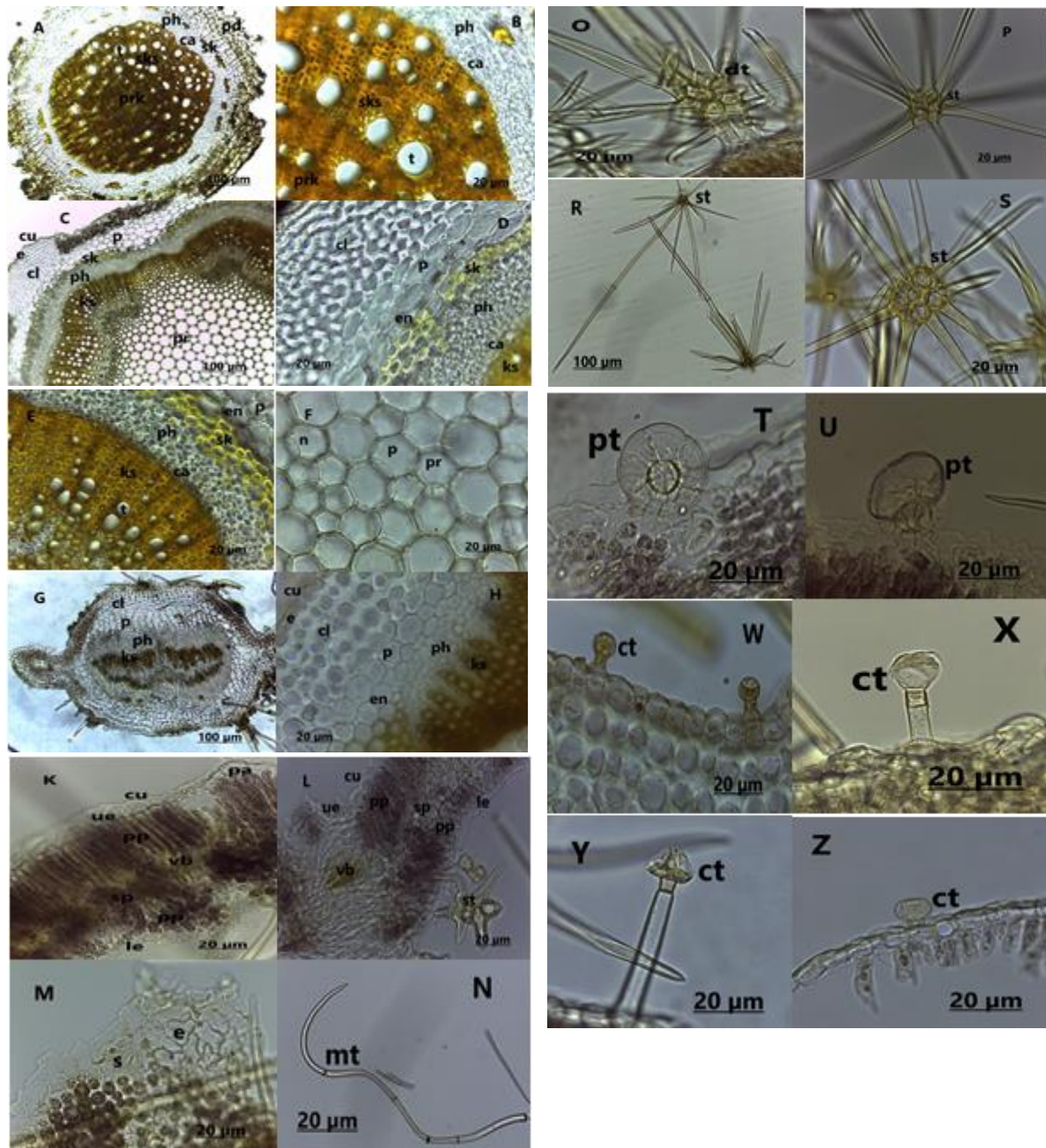


Figure 2. Root, stem and leaf anatomical structures and trichome types of *Marrubium parviflorum* subsp. *parviflorum*. A=General structure of root, B=Secondary xylem and phloem region of root, C=General structure of stem, D=Cortex and phloem regions of stem, E=Xylem and phloem regions of stem, F=Pith region of stem, G=General structure of petiole, H=Vascular bundle and cortex region of petiole, K=General structure of leaf, L=Cross section of the leaf midrib, M=Stomata in surface section of leaf (lower surface), N=Marrubioid trichome in the leaf, O=Dendroid trichome in the leaf, P=Stellate trichome in the stem, R,S=Stellate trichome in the leaf, T,U=Peltate trichomes in the leaf, W=Capitate trichome in the stem, X,Y,Z=Capitate trichome in the leaf. pd= periderma, ph= phloem, t=trachea, sk= sclerenchyma, ca=cambium, sks=secondary xylem, prk= primary xylem, c=cortex, cu=cuticle, cl=collenchyma, p=parenchyma, pr=pith region, e=epiderma, mp=micropapillae, ks=xylem, cr=crystal granules, sc=solitary crystal, en=endoderma, ue=upper epiderma, pp=palisade parenchyma, sp=spongy parenchyma, le=lower epiderma, vb=vascular bundle, pa=papillae, n=needles, s=stoma, ct=capitate trichome, dt=dendroid trichome, mt=marrubioid trichome, st=stellate trichome, pt=peltate trichome.

3.2.4. Leaf

In cross section of the leaf, the upper and lower epidermis cells are uniseriate and rectangular shaped. Upper epidermis cells are larger than the lower ones. The cuticle layer is very thick. Mesophyll layer of the leaf is of

the equifacial type (Figure 2 K). The palisade parenchyma beneath the upper epiderma consists of 1 layered, very long cylindrical parenchyma cells. On the lower epiderma, palisade parenchyma is 1-2 layered (usually 1-layered) and short cylindrical shaped. Sponge

parenchyma is 2-3 layered and usually 2 layered. Vascular bundles are collateral type. The stomata are anomocytic type and they are mostly occur on the lower surface of leaf. The walls of the adjacent epidermis cells around the stomata are clearly undulate (Figure 2 M). The numbers of the adjacent epidermis cells are 4-5, usually 5. Crystal granules were seen in the epidermis cells. In the cross sections taken from the main vein, there are 3-4 layered of lamellar collenchyma layer on the phloem and xylem side. The vascular bundle in the leaf midrib is single and rather large (Figure 2 L).

3.2.5. Micro-morphology and localizations of eglandular and glandular trichomes on the vegetative organs of *Marrubium parviflorum* subsp. *parviflorum*

The eglandular trichomes on the vegetative organs of *M. parviflorum* subsp. *parviflorum* were simple, stellate, multicellular branched (dendroid) and marrubioid types (Table 2). The simple eglandular trichomes are unicellular or bicellular, long. These trichomes were observed on the stem, petiole and leaves. On the stem, the upper and lower surfaces of the leaves of this subspecies, rarely dendroid and marrubioid trichomes were detected (Figures 2 N, O). The marrubioid trichomes are usually bicellular and curved trichomes (Figure 2 N). There are dense stellate trichomes on the

stem, petiole, both leaf surfaces (Figures 2 P, R, S). The middle and lateral branches of stellate trichomes on the lower and upper surfaces of the leaves are almost equal in length. However, the middle branches of the stellate trichomes on the stem and petiole are longer than the lateral branches. Also, there are abundant stellate trichomes on calyx teeth, calyx surface and corolla of this subspecies. The peltate trichomes in *M. parviflorum* subsp. *parviflorum* were rarely found on the stem and petiole. However, the peltate trichomes were densely observed on the both leaves (Figures T, U). The capitate trichomes in this taxon are of three subtypes: I. unicellular short stalked and with a unicellular or bicellular head and II. unicellular long stalked and with unicellular or bicellular head, III. unicellular long-stalked, with bicellular head and unicellular short neck. The unicellular short stalked and with unicellular or bicellular head capitate trichomes (type I) were densely seen on the petiole, upper and lower surfaces of leaves, while these capitate trichomes were rarely seen on the stem between eglandular trichomes (Figure 2 W, Z). The type II capitate trichomes were rarely encountered on the petiole and both surfaces of leaves of this taxon, whereas the type III capitate trichomes were encountered on both surfaces of leaves (Figure 2 X, Y).

Table 2. Trichome types and distributions on organs of *Marrubium parviflorum* subsp. *parviflorum*

Organs of <i>M. parviflorum</i> subsp. <i>parviflorum</i>	Type capitate	Type I	Type II	Type III	Peltate trichomes	Smiple eglandular	Stellate eglandular	Dendroid eglandular	Marrubioid eglandular
Stem	+	-	-	+	+	+++	+	+	
Petiole	++	+	-	+	+	+++	+	+	
Margin and veins of leaf	+++	++	+	++	+	+++	+	+	
Lamina of leaf	+++	++	+	++	+	+++	+	+	
Calyx teeth	+	-	-	-	-	++	-	-	
Outer surface of calyx	+	-	-	-	-	++	-	+	
Corolla	+	-	-	-	-	++	-	-	

3.3. Physical and Chemical Characteristics of Soil Samples of *Marrubium* Taxa

3.3.1. *Marrubium amasiensis*

Soil samples of *M. amasiensis* were taken from 4 different localities (Amasya). The pH, salinity and CaCO₃ values of the soil samples varied between 7.54-7.94, 0.36-0.65 % and 12.60-15.50 %, respectively. The species is distributed in sandy and sandy-salty textured soils. The organic matter and nitrogen values of the soil samples were determined as 3.75-4.20 % and 0.18-0.98 %. Phosphorus and potassium values of soil samples were found to be 32.80-42.22 mg/kg and 102.4-195.3 mg/kg (Table 3).

3.3.2. *Marrubium parviflorum* subsp. *parviflorum*

M. parviflorum subsp. *parviflorum* were taken from 6 different localities (Amasya). The CaCO₃, pH and salinity values of the soil samples were observed as 1.50-15-50

%, 6.50-8.06 and 0.46-0.69 %, respectively. The texture of the soil is sandy and sandy-salty. Nitrogen and organic matter values of soil samples were determined as 0.15-0.66 % and 3.30-4.95 %. Phosphorus and potassium values in soil samples were found as 32.65-48.59 mg/kg and 102.4-213.8 mg/kg (Table 4).

3.3.3. Statistical analysis of soil analysis results of the studied taxa

Mann Whitney U test was applied to soil analysis results of the these taxa. However, no statistical difference was found between the soil analysis results of the two taxa (p>0.05) (Table 5). This is due to the fact that the taxa grow in habitats with similar ecological conditions.

Table 3. Soil analysis results of *Marrubium amasiensis*

Localities	Texture	Salinity (%)	CaCO ₃ (%)	pH	Organic matter (%)	N (%)	K (mg/kg)	P (mg/kg)
Sakarat Mountain	Sandy-salty	0.36	14.80	7.80	4.20	0.76	120.7	38.12
Direkli Village	Sandy-salty	0.56	15.50	7.54	3.93	0.18	102.4	42.22
Surroundings of Direkli Village	Sandy-salty	0.45	13.80	7.35	3.75	0.37	195.3	34.25
Between Direkli Village and Sulugöl	Sandy	0.65	12.60	7.90	4.01	0.98	182.5	32.80
Mean±Sd.	-	0.50±0.13	14.17±1.26	7.64± 0.25	3.97±0.18	0.57±0.36	150.2±45.57	36.8±4.22

Table 4. Soil analysis results of *Marrubium parviflorum* subsp. *parviflorum*

Localities	Texture	Salinity (%)	CaCO ₃ (%)	pH	Organic matter (%)	N (%)	K (mg/kg)	P (mg/kg)
Ormanözü Village	Sandy-salty	0.69	14.35	6.70	4.25	0.66	187.9	32.65
Above Ormanözü Village	Sandy-salty	0.46	1.50	6.50	4.95	0.45	172.8	40.2
Direkli Village	Sandy-salty	0.56	15.50	7.54	3.93	0.18	102.4	42.22
Above Direkli Village	Sandy-salty	0.58	13.80	7.95	3.30	0.34	156.6	36.82
Aydınca Şeyhsadi Village	sandy	0.64	12.73	7.37	3.46	0.15	132.67	41.80
Sultançayırı Gümüş Town	Sandy-salty	0.48	3.12	8.06	3.58	0.21	213.8	48.59
Mean±Sd.	-	0.57±0.09	10.2±6.17	7.35±0.64	3.91±0.61	0.33±0.19	161±397	40.4±5.39

Table 5. Mann Whitney U Test results of the studied taxa

	Salinity (%)	CaCO ₃ (%)	pH	Organic matter (%)	N (%)	K (mg/kg)	P (mg/kg)
Mann-Whitney U	7.500	8.000	10.500	9.500	6.500	10.500	8.500
Z	-.962	-.858	-.321	-.535	-1.176	-.321	-.748
p	.336	.391	.748	.593	.240	.748	.454

4. Discussion

In the present study, the taxonomically valuable anatomical, ecological and trichome micro-morphological features of two *Marrubium* taxa were determined and these features were compared. It has been observed that these two taxa collected from the Amasya region are

close to each other in terms of anatomical, ecological and trichome micro-morphological features. However, some anatomical, ecological and trichome micro-morphological features were appeared to be different in the studied taxa.

When the root cross-sections of the studied taxa were

examined, periderma were determined to have 6-7 layered in *M. amasiensis*, 5-7 layered in *M. parviflorum* subsp. *parviflorum*. The layer number of cambium is 2-4 in *M. amasiensis*, 3 in *M. parviflorum* subsp. *parviflorum*. The centers of roots of both taxa were filled with primary xylem elements. Similar anatomical features were also found in the roots of *Marrubium bourgaei* Boiss and *Marrubium heterodon* (Benth) Boiss. Meit. Ball. (Büyükkartal et al., 2016). Our results are in agreement with the data of the study mentioned above.

Stem anatomical examinations showed that the stem had well-defined collenchyma in the corners. This collenchyma is 8-10 layered in *M. amasiensis* and is 8-11 layered in *M. parviflorum* subsp. *parviflorum*. Metcalfe and Chalk (1972) stated that in each of the stem corners of many the Lamiaceae species have multilayered collenchyma as a characteristic features. The collenchyma between the corners is 2 layered in *M. amasiensis* and 2-3 layered in *M. parviflorum* subsp. *parviflorum*. The parenchyma in the cortex is 3-4 layered (generally 3 layered) in both taxa. Although these parenchyma cells are without chloroplasts in *M. amasiensis*, these cells are with chloroplasts in *M. parviflorum* subsp. *parviflorum*. Sclerenchyma is 2 layered in *M. amasiensis* and is 3-4 layered (generally 4 layered) in *M. parviflorum* subsp. *parviflorum*. The mentioned stem anatomical features (collenchyma, parenchyma and sclerenchyma layers in the cortex) were also found in some members of the Lamiaceae family distributed in Western Azerbaijan (Hatamneia et al., 2008), *M. bourgaei* and *M. heterodon* (Büyükkartal et al., 2016), *Marrubium lutescens* Boiss. and *M. cephalanthum* Boiss. & Noë subsp. *akdaghicum* (Tuylu et al., 2017), some *Marrubium* taxa distributed in Iranian (Talebi et al., 2019a), *Marrubium friwaldskyanum* Boiss. and *Marrubium peregrinum* L. (Gyuzzeleva et al., 2022). However, the number of layers of collenchyma, parenchyma and sclerenchyma in the cortex differ both in other members of the Lamiaceae family and in the studied two *Marrubium* taxa. For this reason, we think that these anatomical features in the cortex can be used to distinguish these two taxa. The importance of these anatomical features were reported in some *Marrubium* taxa by Hatamneia et al., (2008), Büyükkartal et al. (2016), Talebi et al. (2019a). In addition, Kandemir et al. (2020) in *Heliotropium* L. taxa, Kandemir et al. (2022) in *Fritillaria* L. taxa suggested that the presence of different numbers of collenchyma, parenchyma and sclerenchyma layers in the cortex were important anatomical characters in the separation of taxa. In the studied taxa, there are sclerenchyma cells groups on the phloem of vascular bundles. The presence of sclerenchyma cell groups in phloem were detected in some taxa of the Lamiaceae family (Metcalfe and Chalk, 1979; Anhar et al., 2018; Koçak and Kandemir, 2023). Needles and solitary crystals were found in the pith region of stem of both taxa. These crystals were also seen in the stem of *M. vulgare* and other the Lamiaceae taxa (Anhar et al.,

2018). In addition, Anhar et al. (2018) suggested that crystals are of great importance in identification and taxon delimitation. Ryding (2010) recorded that calcium oxalate crystals are in needle shaped or polyhedral, druses and prismatic forms in the vegetative and generative organs of the Lamiaceae family species. However, similar crystal types were found in stem of these two taxa. Therefore, the types of crystals in the stem were not an important feature in the separation of these taxa.

Outline aspects of the petiole is half circle with wings in both taxa. When the petiole cross-sections of these taxa are compared, the epidermis cells in *M. amasiensis* are rectangular shaped and without papillae, while epidermis cell in *M. parviflorum* subsp. *parviflorum* are quadrangular shaped and rarely papillae. In *M. amasiensis*, cuticle is thick and with dense micropapillae, the cuticle is thick and with very dense micropapillae in *M. parviflorum* subsp. *parviflorum*. The collenchyma in *M. amasiensis* is 2-3 layered, while the collenchyma in *M. parviflorum* subsp. *parviflorum* is 4-5 layered. The number of parenchyma layer is 5-6 in *M. amasiensis*. However, parenchyma is 4 layered in *M. parviflorum* subsp. *parviflorum*. In the parenchymatic cells of *M. parviflorum* subsp. *parviflorum*, crystal granules were determined. The ends of the petiole are found curved slightly upwards in *M. amasiensis* and *M. parviflorum* subsp. *parviflorum*. Metcalfe and Chalk (1979), Kandemir (2003), Shahri et al. (2016) emphasized that the petiole anatomical structure was value in species characterization in the Lamiaceae family. The two *Marrubium* taxa in this study can be distinguished according to the differences in the number of collenchyma and parenchyma layers in the petiole, whether or not there are micropapillae on the cuticle, the presence or absence of crystal granules in parenchyma cells and the epidermis cell shape.

Although leaf anatomical features are similar in both taxa, there are some differences in leaf anatomical features. When the leaf cross-section findings of the taxa are examined, the upper and lower epidermis cells of *M. amasiensis* are rectangular shaped. But, upper and lower epidermis cells in *M. parviflorum* subsp. *parviflorum* are quadrangular shape. The mesophyll is equifacial (isolateral) structure and almost similar in both taxa. In the surface sections of the leaves, anomocytic and rarely anisocytic stomata were observed in *M. amasiensis*. The numbers of adjacent cells of the stomata are 3-4 (usually 4) in *M. amasiensis*. Stomata are anomocytic structure in *M. parviflorum* subsp. *parviflorum* and the numbers of cells adjacent of the stomata are 4-5. Although crystal granules were seen in the epidermis cells of *M. parviflorum* subsp. *parviflorum*, the crystal granules were not seen in the epidermis cells of *M. amasiensis*. Kandemir et al. (2019), Kandemir (2019) reported that the presence of crystal granules in the epidermis cells of the leaves could be used as important characters in the taxonomy of plant species. There are not variable in

aspects of midrib region of two taxa. This region is characterized by presence of parenchyma cells. However, the midrib shape is half circular shaped in *M. parviflorum* subsp. *parviflorum* and midrib shape is circular shaped in *M. amasiensis*. Some differences were observed in vascular system aspects; rounded in *M. parviflorum* subsp. *parviflorum* and crescent shaped in *M. amasiensis*. In the midrib region, the numbers of vascular bundles are one in these taxa. The results of this study showed to be different in the studied taxa regarding in dermal system, midrib region and crystals of leaves. These parameters were used to identify the relationships among species of the Lamiaceae family (Inyama et al., 2016). Looking at the data of the cross-sections of the leaves, similar anatomical results were determined in the leaves of other *Marrubium* taxa (Anhar et al. 2018; Talebi et al., 2019 b; Gyulezeva et al., 2022). The data obtained from the leaf cross sections in this study show parallelism with the results of the studies mentioned above.

The presence of four types of eglandular trichomes was detected on the vegetative organs of studied both taxa (Tables 1, 2). The simple eglandular trichomes in *M. parviflorum* subsp. *parviflorum* are unicellular or bicellular, long, while these trichomes in *M. amasiensis* are unicellular. This kind of trichomes in *M. parviflorum* subsp. *parviflorum* was observed on the stem, petiole and leaves. But, simple eglandular trichomes in *M. amasiensis* were obtained only in the petiole. Dense dendroid trichomes were observed on the upper and lower surfaces of the leaves of *M. amasiensis*, while rarely dendroid trichomes were observed on the stem, the upper and lower surfaces of the leaves of *M. parviflorum* subsp. *parviflorum*. However, the dendroid trichomes were not seen on the stem of *M. amasiensis*. Marrubiod trichomes were detected on the leaves and stems of both taxa. There are dense stellate trichomes on the stem, petiole, both leaf surfaces of the studied two taxa. In *M. amasiensis*, the middle branches of the stellate trichomes on the upper epiderma of leaves are quite long and multicellular, the lateral branches are thin, usually unicellular. On the lower epiderma, stellate trichomes are few and finely branched, the middle branch is longer and all unicellular. In *M. parviflorum* subsp. *parviflorum*, the middle and lateral branches of stellate trichomes on the lower and upper surfaces of the leaves are almost equal in length. However, the middle branches of the stellate trichomes on the stem and petiole of *M. parviflorum* subsp. *parviflorum* are longer than the lateral branches. Moreover, there are abundant stellate trichomes on calyx teeth, calyx surface and corolla of two taxa. The multicellular branched and unbranched eglandular trichomes were also recorded in other members of the genus *Marrubium* (Dmitruk and Haratym, 2014; Ahvazi et al., 2016; Anhar et al., 2018; Gyulezeva et al., 2022; Koçak and Kandemir 2023; Akbulut and Baykan, 2023). The peltate and capitate glandular trichomes were determined on the leaves, petiole and stems of both taxa (Tables 1,2). Peltate trichomes were rarely found on the

stem and petiole of *M. parviflorum* subsp. *parviflorum* and *M. amasiensis*. Whereas this kind of trichomes are dense on the leaves of both taxa. The capitate trichomes on the vegetative organs of *M. amasiensis* were seen four subtypes, whereas these trichomes on the vegetative organs *M. parviflorum* subsp. *parviflorum* were seen three subtypes. In *M. amasiensis*, the subtype I were rarely obtained on the stem and petiole, while this kind of capitate trichomes was dense obtained on the upper and lower surfaces of leaves. In *M. parviflorum* subsp. *parviflorum*, the subtype I was densely seen on the petiole, upper and lower surfaces of leaves, while this kind of capitate trichomes were rarely seen on the stem. The subtype II capitate trichomes are found only on the petiole and upper and lower surfaces of leaves in these taxa. On the other hand, the subtype III capitate trichomes were encountered on both surfaces of leaves of these two taxa. This kind of capitate trichomes (subtype III) is more dense on the leaves of *M. parviflorum* subsp. *parviflorum*. Although the subtype IV capitate trichomes are densely seen on the upper and lower surfaces of leaves of *M. amasiensis*, this kind of capitate trichomes was not seen in other organs and leaves of *M. parviflorum* subsp. *parviflorum*. This difference in the capitate trichomes is seen as an important distinguishing feature between two taxa.

Recently, the presence of eglandular and glandular trichomes has been reported in trichome micro-morphology studies on *Marrubium* taxa (Dmitruk and Haratym, 2014; Ahvazi et al., 2016; Çalı, 2017; Haratym and Weryszko-Chmielewska, 2017; Anhar et al., 2018, Gyulezeva et al., 2022, Koçak and Kandemir 2023). Also, both eglandular and glandular trichomes were found to be common in the other members of the Lamiaceae family and these trichomes were recorded to be very value taxonomic characters (Navarro and El Qualidi, 2000; Kandemir, 2003; Kandemir, 2011; El-Deen Osman, 2012; Seyedi and Salmaki, 2015; Koçak and Kandemir, 2023). We think that these features mentioned can be used as important taxonomic characters in the differentiation of these two taxa, since there are variations in their features such as eglandular and glandular trichome types, branching shapes, localization on organs, long and short branch lengths in stellate trichomes, sparseness and density. On the other hand, it was revealed that environmental conditions, especially altitude and arid areas, were effective in the morphological variations and density of trichomes (Ahvazi et al. 2016).

Based on soil analysis results, we suggested that *M. amasiensis* and *M. parviflorum* subsp. *parviflorum* were independent taxa with close relationships. The similarities in ecological features of the taxa were supported by statistical analysis. Because no statistically a significant difference was found between the soil analysis results of the taxa. This may be due to the fact that taxa are distributed in habitats with similar ecological characteristics.

5. Conclusion

To sum up, two *Marrubium* taxa collected from Amasya vicinity (*M. amasiensis* is endemic and *M. parviflorum* subsp. *parviflorum* is common) appeared as closely related taxa in terms of anatomical, ecological and trichomes micro-morphological features, distinct taxa. However, some differences were seen such as the number of periderma layer in the root, the number of collenchyma layer in the corners of the stem, the number of collenchyma, parenchyma and sclerenchyma layers in the cortex, the presence or absence of dendroid trichomes on the stem, the number of collenchyma and parenchyma layers in the petiole, the presence of crystals in the leaves and the shape of the epidermis cells in the leaves, midrib region of leaves, differences in the capitate glandular trichomes, the number of cells adjacent to the stoma and stoma type. These characters were stated to be valuable taxonomic characters in distinguishing of these two taxa. Moreover, anatomical and trichome micro-morphological data obtained from this study may be useful for future taxonomic studies in *Marrubium* genus. No significant differences were found in the soil analysis results of these two *Marrubium* taxa.

Author Contributions

The percentage of the author(s) contributions is presented below. All authors reviewed and approved the final version of the manuscript.

	K.V.K.	N.K.
C	20	80
D	20	80
S	10	90
DCP	50	50
DAI	20	80
L	60	40
W	20	80
CR	30	70
SR	20	80
PM	20	80
FA	50	50

C=Concept, D= design, S= supervision, DCP= data collection and/or processing, DAI= data analysis and/or interpretation, L= literature search, W= writing, CR= critical review, SR= submission and revision, PM= project management, FA= funding acquisition.

Conflict of Interest

The authors declared that there is no conflict of interest.

Ethical Consideration

Ethics committee approval was not required for this study because of there was no study on animals or humans.

Acknowledgements

This study was produced from Kamer Volkan Koçak's master's thesis.

References

- Ahvazi M, Jamzad Z, Balali GR, Saeidi H. 2016. Trichome micro-morphology in *Marrubium* L. (Lamiaceae) in Iran and the role of environmental factors on their variation. *Iran J Bot*, 22: 39-58.
- Akbulut TD, Baykan S. 2023. Morphological and micromorphological investigation of *Marrubium* L. (Lamiaceae) taxons distributed in the Aegean Region. *J Fac Pharm*, 47(1): 51-75.
- Akgül G, Ketenoğlu O, Doğan M. 2017. A new species of *Marrubium* L. (Lamiaceae) from Turkey. *J Herb Syst Bot*, 24: 37-46.
- Anhar AY, Soad AH, Zeinab AE, Hassan MI, Omayma AE. 2018. Morphological and anatomical studies on selected Lamiaceae medicinal plants in Bani Matar district, Sana'a (Yemen). *Taekholmia*, 38: 17-39.
- Benzidane N, Smahi R, Zabouche B, Makrouf A, Arrar L. 2020. Phytochemical study and antimicrobial activity of Algerian *Marrubium vulgare* leaf and stem extracts. *J Drug Deliv Ther*, 10(5):70-74.
- Büyükkartal HN, Çölgeçen H, Akgül G. 2016. Comparative leaf, stem and root anatomy of taxa *Marrubium bourgaei* and *Marrubium heterodon* (Lamiaceae). *Aust J Crop Sci*, 10(11): 1516-1522.
- Büyükköztürk, Ş. 2001. Data analysis for social science research design and statistical manual SPSS applications and review. Pegem Publication, Ankara, Türkiye, pp: 216.
- Cantino PD. 1990. The phylogenetic significance of stomata and trichomes in the Labiatae and Verbenaceae. *J Arnold Arbor*, 71(3): 323-370.
- Celep F, Dirmenci T. 2017. Systematic and biogeographic overview of Lamiaceae in Turkey. *Nat Vol Essent Oil*, 4(4): 14-27.
- Corsi G, Bottega S. 1999. Glandular hairs of *Salvia officinalis*: new data on morphology, localization and histochemistry in relation to function. *Ann Bot*, 84: 657-664.
- Cullen J. 1982. *Marrubium* L. In: Davis PH, Edmondson JR, Mill RR, Tan K, editors. *Flora of Turkey and the East Aegean Islands*. Edinburgh University Press, Edinburgh, 7th, pp: 165-178.
- Çalı İÖ. 2017. Glandular trichomes in *Marrubium cephalanthum* ssp. *montanum* (Lamiaceae) growing in Turkey. *Int J Agric and Biol*, 19(4): 697-700.
- Çelebioğlu S, Baytop T. 1949. A new reagent for microscopical investigation of plant. Publication of the Institute of Pharmacognosy, İstanbul, Türkiye, pp: 301.
- Dmitruk M, Haratym W. 2014. Morphological differentiation of non-glandular and glandular trichomes on *Marrubium vulgare* L. *Mod Phytomorphol*, 6: 85.
- El-Deen Osman AK. 2012. Trichome micromorphology of Egyptian *Ballota* L. (Lamiaceae) with emphasis on its systematic implication. *Pak J Bot*, 44(1): 33-46.
- Gyuzuleva DP, Stoyanov P, Bivolarska AV, Mladenov RD, Mladenova TR, Petkov VH, Todorov KT. 2022. Anatomical investigation of *Marrubium friwaldskyanum* Boiss. and *Marrubium peregrinum* L. (Lamiaceae) from Bulgaria. *Ecol Balk*, 14(1): 87-101.
- Haratym W, Weryszko-Chmielewska E. 2017. Ultrastructural and histochemical analysis of glandular trichomes of *Marrubium vulgare* L. (Lamiaceae). *Flora*, 231: 11-20.

- Hatamneia AA, Khayami M, Mahmudzadeh A, Sarghein SH, Heidari M. 2008. Comparative anatomical studies of some genera of Lamiaceae family in West Azarbaijan in Iran. *Bot Res J*, 1(3):63-67.
- Inyama C, Mbagwu F, Duru C. 2016. Taxonomic relationship on some *Chrysophyllum* species based on anatomical studies. *Med Aromat Plants*, 5(2):1-5.
- Kaçar B. 1995. Chemical analysis of plants and soil. Ankara University Faculty of Agriculture Education, Research and Development Foundation Publications, Ankara, Türkiye, pp: 705.
- Kamatou GP, Van Z, Van-Vuuren RL, Viljoen SF, Figueiredo AM, Barroso AC, Pedro JG, Tilney PM. 2006. Chemical composition, leaf trichome types and biological activities of the essential oils of four related *Salvia* species indigenous to Southern Africa. *J Essent Oil Res*, 18:72-79.
- Kandemir N. 2003. The Morphological anatomical and karyological properties of endemic *Salvia hypargeia* fisch. & meyer. (Lamiaceae) in Turkey. *Pak J Bot*, 35 (2): 219-236.
- Kandemir N. 2011. Trichomes on *Salvia pomifera* (Lamiaceae) in Turkey, *Bot Lith*, 17(1): 3-11.
- Kandemir, N. 2019. Comparative morphological and anatomical studies on *Iris peshmeniana* Güner & T. Hall. and *Iris aucheri* (Baker) Sealy (Iridaceae). *Trak Univ J Nat Sci*, 20(2): 105-113.
- Kandemir N, Çelik A, Ullah F, Shah SN, Zaman W. 2019. Foliar epidermal anatomical characteristics of taxa of *Iris* subg. *Scorpiris* Spach (Iridaceae) from Turkey, *Microsc Res Tech*, 82(6): 764-774
- Kandemir N, Çelik A, Shah SN, Razzaq A. 2020. Comparative micro-anatomical investigation of genus *Heliotropium* (Boraginaceae) found in Turkey. *Flora*, 262: 151495.
- Kandemir N, Çelik A, Ullah F. 2022. Comparative micro-anatomical features of endemic *Fritillaria* taxa growing in the Mediterranean region (Turkey). *Flora*, 290 (2): 152049.
- Koçak KV, Kandemir N. 2023. Taxonomic importance of anatomic, ecological and trichome features of *Marrubium astracanicum* subsp. *astracanicum* Jacq. (Lamiaceae). *BSJ Eng Sci*, 6 (3): 199-209.
- Metcalf CR, Chalk L. 1972. Anatomy of the dicotyledons. Oxford University Press, Oxford, UK, pp: 1459.
- Metcalf CR, Chalk L. 1979. Anatomy of the dicotyledons. Oxford University press, Oxford, UK, 2nd, pp: 276.
- Meyre-Silva CH, Cechinel-Filho V. 2010. A review of the chemical and pharmacological aspects of the genus *Marrubium*. *Curr Pharm Des*, 16: 3503-3518.
- Navarro T, El Oualidi, J. 2000. Trichome morphology in *Teucrium* L. (Labiatae). A taxonomic review. *An Jard Bot Madr*, 57(2): 277-297.
- Okur ME, Karakaş N, Karadağ AE, Yılmaz R, Demirci F. 2019. In vitro cytotoxicity evaluation of *Marrubium vulgare* L. methanol extract. *J Res Pharm*, 23(4): 711-718.
- Ryding O. 2010. Crystals in calyces of Lamiaceae and their phylogenetic and adaptive significance. *Plant Syst Evol*, 290:201-215.
- Sargin SA, Selvi S, López V. 2015. Ethnomedicinal plants of Sarigöl district (Manisa), Turkey. *J Ethnopharmacol*, 171: 64-84.
- Selvi S, Polat R, Çakılcıoğlu U, Celep F, Dirmenci T, Ertuğ ZF. 2022. An ethnobotanical review on medicinal plants of the Lamiaceae family in Turkey. *Turk J Bot*, 46(4): 283-332.
- Serrato-Valanti G, Bisio A, Cornara L, Ciarallo G 1997. Structural and histochemical investigation of the glandular trichomes of *Salvia aurea* L. leaves and chemical analysis of the essential oil *Ann Bot*, 79: 329-336.
- Seyedi Z, Salmaki Y. 2015. Trichome morphology and its significance in the systematic of *Phlomis* (Lamiaceae; Lamioideae; Phlomideae). *Flora*, 213: 40-48.
- Shahri S, Jafari A, Mahmoodzadeh H. 2016. Comparative anatomical studies on petioles of *Nepeta* L. Species (Lamiaceae) in NE Iran. *Adv Stud Biol*, 8(3): 119-126.
- Talebi S, Sheidai M, Ariyanejad F, Matsyura A. 2019a. Stem anatomical study of some Iranian *Marrubium* L. species. *Biodiversitas*, 20(9): 2589-2595.
- Talebi SM, Sheidai M, Ariyanejad F. 2019b. Investigation of leaf anatomical structure variation among different populations of *Marrubium anisodon* C. Koch in Iran. *J Cell Tiss*, 9(4): 388-397.
- Tuyulu M, Büyükkartal HN, Akgül G, Kalyoncu H. 2017. Comparing stem and leaf anatomy of *Marrubium lutescens* Boiss. and *M. cephalanthum* Boiss. & Noë subsp. *akdaghicum* (Lamiaceae). *SDU J Nat Appl Sci*, 21(1): 113-117.
- Tuzlacı E. 2016. Traditional medicinal plants of Turkey. Istanbul Medical Bookstores, İstanbul, Türkiye, pp: 286.
- Xiang C, Dong Z, Peng H, Lui Z. 2010. Trichome micromorphology of the East Asiatic genus *Chelonopsis* (Lamiaceae) and its systematic implications. *Flora*, 205: 434-441.
- Yousefi K, Fathiazad F, Soraya H, Rameshrad M, Maleki-Dizaji N, Garjani A. 2014. *Marrubium vulgare* L. methanolic extract inhibits inflammatory response and prevents cardiomyocyte fibrosis in isoproterenol-induced acute myocardial infarction in rats. *Bioimpacts*, 4(1): 21-27.



SUGGESTIONS FOR URBAN TRANSFORMATION THROUGH TWO APPLICATIONS IN ANKARA, THE CAPITAL OF TÜRKİYE

Varol KOÇ^{1*}


¹*Ondokuz Mayıs University, Faculty of Engineering, Department of Civil Engineering, 55139, Samsun, Türkiye*

Abstract: Cities resembling living organisms are dynamic places that constantly change, either positively or negatively. Urban transformation is a multifaceted process with economic, social, and cultural impacts, and it should trigger socio-economic change and transformation in a positive direction. This interaction between the city and urban transformation has also been integrated with relevant laws regulating the transformation. Urban transformation, which is a complex process in itself, draws from various related processes that have been ongoing since the past. The aim of the study is to examine the factors that play a role in the change and transformation of cities, their historical development, and legal regulations by analyzing the subject through two urban transformation examples in Ankara. In this context, Altındağ, which is the first region where gecekondu settlements began in Türkiye and the North Ankara Entrance Urban Transformation Projects, which marked the first urban transformation initiated by a law, were examined.

Keywords: Urban transformation, Urban design, Urban space, Urban transformation legislation, Squatting

*Corresponding author: Ondokuz Mayıs University, Faculty of Engineering, Department of Civil Engineering, 55139, Samsun, Türkiye

E mail: varol@omu.edu.tr (V. KOÇ)

Varol KOÇ  <https://orcid.org/0000-0003-4810-3845>

Received: February 04, 2023

Accepted: November 25, 2023

Published: January 15, 2024

Cite as: Koç V. 2024. Suggestions for urban transformation through two applications in Ankara, the capital of Türkiye. BSJ Eng Sci, 7(1): 55-71.

1. Introduction

Cities can be thought of as living mechanisms in which human life and activities are woven into their tissues. These mechanisms are the basis for almost everything related to human beings, from commercial and industrial activities to social and cultural activities (Özel and Kılıçaslan, 2021). As activities increase, cities become more complex. The increase in activities is directly proportional to the development of humanity in history and the increase in population. In this context, the phenomenon of migration from rural to urban after the industrial revolution, which has an important place in the development of humanity in Europe, has increased the population of cities. In Türkiye, on the other hand, in parallel with the delay in industrialization, population agglomerations began to be observed in the cities at later times, especially in the Republican Period that started in 1923 and afterwards. In some other developing countries, similar situations started to be seen only towards the end of the last century. Therefore, it is possible to compare the early models of these countries on the subject by analyzing Türkiye and Ankara, the first city where squatting started in Türkiye.

However, this article aims not only to examine urban transformation projects in Ankara but also to provide an international perspective and learn from international experiences. Comparing Ankara with major cities in other countries and understanding different approaches to urban transformation experiences in different geographical regions are important. After all, urban

transformation involves common challenges encountered in many regions of the world. For example, various population censuses conducted at different times in Ghana have shown that the urban population has been steadily increasing since the 1960s. The 1960 population census revealed that out of Ghana's 6.7 million population, 1.5 million lived in urban areas (Oosterbaan et al., 2012). By 2005, the proportion of people living in urban areas had increased to 47.8%, and it is estimated to reach approximately 60% by 2025 (United Nations, 2007). Understanding how different countries with different geographical locations, such as Türkiye and Ghana, have tackled similar problems can provide internationally shareable knowledge. Both Ankara and the capital of Ghana, Accra, face challenges related to their growing populations and urban sprawl. Therefore, both regions require urban transformation projects. Both Ankara and Accra have common issues like infrastructure deficiencies. Urban transformation projects in both regions involve public resources, and both believe that state institutions should support and finance these projects. All of this is also applicable to India's National Capital Territory (NCT), which, in addition to being similar to Ankara in terms of being a major capital region, had a significant rural-urban divide. At the beginning of the century, the NCT with a 62.5% urbanization rate was one of the largest rural-urban regions in the world. While India's gross domestic product (GDP) increased by 52% from 2005 to 2010, the NCT's GDP increased by 67% (NCRPB, 2013). Despite



having a 3.8% share of the population and occupying only 1% of the land area, the NCT contributed 7.1% to India's GDP from 2009 to 2010 (NCRPB, 2013). The NCT is an attractive destination for migrants due to various employment opportunities it offers. A similar situation was true for Ankara, especially in the early years of the Republic. Despite these similarities, Ankara is the capital of Türkiye and is located in the interior regions, while India's NCT is located in the northern part of India. Ghana, on the other hand, is a country in West Africa, and its capital, Accra, is located on the coast of the Atlantic Ocean. These three capitals are situated in entirely different geographical regions. The fact that all these capitals have different cultural and social dynamics may lead to differences in the implementation of urban transformation projects. Project sizes and scopes can also influence differences among projects in each region. However, providing a comparative perspective is beneficial for better understanding urban transformation practices and drawing lessons for future projects. Such comparisons are essential for addressing the universal challenges of urban transformation. Especially the fact that Türkiye's capital, Ankara, played a significant role in solving the "gecekondu" (shanty town) problem with Türkiye's first housing cooperative and urban transformation applications, as well as being the place where the first law on urban transformation was enacted, makes the examination of Ankara on this subject important. These examinations will also be significant for capitals, metropolises, and megacities around the world, which exhibit both similar and different characteristics.

Urban transformation practices, which gained value with the many legal regulations put into effect especially after 2004 in Türkiye, are important in terms of ensuring the peace and welfare of the people and the correct use of the public budget. Land and zoning regulations are needed in terms of legal and technical aspects for urban transformations that will provide solutions to urban problems in Türkiye. Providing economic resources, making applicable zoning plans, equitable distribution and registration of new properties are important for urban transformations (Ülger, 2011). In addition, urban transformation aims to respond to the needs of cities, to use the existing space efficiently, to increase urban welfare, to ensure sustainability and to create social participation for all of these. Urban transformation, which is a multi-actor process, requires the partnership of not only the public and private sectors, but also the local people for the success of a project, together with new technologies and developments in scope. For these reasons, urban transformation is an important phenomenon not only economically, but also socially and culturally.

Since urban transformation projects are supported by both national and international funds, it is necessary to determine the basis of the projects and to determine the needs for transformation correctly. Making these determinations and determinations depends on the deep

assimilation of the city and urban transformation culture. Such an internalization is possible with technically and legally specialized staff who can criticize the relevant issues. Because urban transformation is a multidisciplinary field with important extensions both in social sciences and in various branches and sub-branches. Real success with the least possible mistakes in all reflections can only be achieved by having a complete and clear understanding of the subject. Knowing the history of urban transformation and the relevant legislation makes an important contribution to developing this understanding. In this context, Nigel Taylor (1998) discusses urban planning theories and practices from 1945 to the present day. He provides comprehensive information about the historical development and theoretical foundations of urban transformation. Peter Roberts and Hugh Sykes (1999) aimed to provide a broad perspective on urban renewal and addressed various aspects of urban transformation. This work, composed of chapters by different authors, focuses on the revitalization, transformation, and improvement processes of cities. Topics include urban planning, social issues, economic factors, environmental sustainability, and public policies. The book is designed as a resource for academics, planners, policymakers, and urban development professionals who want to understand the processes from the design to the implementation of urban renewal projects. It explains key concepts, discusses different approaches, and presents real-world examples. It also examines the societal impacts and outcomes of these processes. Hoch et al. (2000) discussed the planning processes of local governments and provided practical applications and examples related to urban transformation projects. Beatley and Wheeler (2004) organized studies focusing on sustainable urban transformation and planning, addressing environmental and social sustainability perspectives. In his work, Moughtin (2007) deals with the physical aspect of urban transformation, urban design. He examines the planning and design of squares and public spaces and provides ideas on how these areas can be rearranged. The work by LeGates and Stout (2011), which includes a compilation of articles on urban planning and urban transformation, serves as a versatile source due to the different perspectives of various authors on the topic. Sclar et al. (2013) examines how urban transformation projects can be related to health, housing, and climate change. Fainstein (2014) addresses the concept of justice in urban planning. She explores how urban transformation projects can affect social justice and how planning processes can contribute to this goal. Leigh and Blakely (2016) focus on the economic dimension of urban transformation, providing information on local economic development strategies and planning. Fawcett (2016) examines the effects of urban transformation on human health and well-being, as well as the relationships between health and planning. Ratcliffe et al. (2021) discuss how urban planning and

real estate development work together and address topics related to the financing and execution of urban transformation projects. Jacobs (2011) focuses on the impact of urban transformation projects on neighborhood life and resident participation.

In the literature, the critical approaches of Jacobs (2011), a prominent scientist who lived between 1916 and 2006, still hold value. Escapes from the city center and the dynamics of change and transformation are her fundamental areas of interest. Jacobs has contributed to urban planning literature with her views on topics such as the organic growth of cities, local economy, community interaction, and street design. By criticizing traditional urban planning approaches, she emphasizes factors such as street design, diversity, and urban density for the healthy growth and sustainability of cities. Jacobs (2011), who has a critical perspective on urban transformation projects, often focuses on how urban planning processes affect local communities and how interventions are made in the organic growth of cities. According to her, urban transformation projects often reduce diversity, negatively impacting the liveliness and sustainability of cities. She emphasizes the need for projects to be planned according to the needs and expectations of the affected communities, and suggests that the active involvement of community members in the process can contribute to the success of projects. Nevertheless, urban transformation projects often hinder organic growth and can artificially shape cities. She highlights the importance of street design and pedestrian-focused planning in urban transformation. She argues that large projects pose the risk of disrupting the local fabric, dispersing communities, and compromising the unique character. The historical and cultural heritage of cities should not conflict with urban transformation projects but should be preserved. Jacobs (2011) views have laid the foundation for modern approaches in urban planning that focus on participation, diversity, and sustainability. However, it is important to remember that each city is unique, and the success of urban transformation projects is possible when approached in accordance with local conditions and community needs.

Contrary to Jacobs (2011) critical perspective, some scholars and experts who advocate for large-scale urban renewal projects have often argued that urban transformation projects can be advantageous for cities by focusing on factors such as urban restructuring, growth control, infrastructure improvements, and economic revitalization. However, it is important to note that urban renewal projects are complex and multidimensional, encompassing various views from different experts and communities. Therefore, there may be many scholars expressing supportive or advocacy views on the subject, but these views generally vary depending on the specific context and goals of the project. For example, Robert Moses, an influential city planner in New York, led major infrastructure projects and advocated for urban

transformation (Caro, 1975). Le Corbusier (1923), a renowned French architect and urban planner, is known for his modernist design and views on large-scale urban renewal projects. Economist and urban planning expert Glaeser (2011) has supported urban renewal projects that promote city growth and economic revitalization. Economist Romer (1990) emphasized city planning and infrastructure projects to encourage urban growth and demonstrated how such projects could contribute to economic development. American economist and urban planning expert Florida (2002) is recognized for his views supporting the attraction of creative classes and encouraging urban renewal in cities. Danish architect and urban planner Gehl (2010) approached urban areas with a perspective highlighting the importance of human-centered planning. Lerner (2014), a Brazilian architect and urban planner, is a pioneering figure in urban renewal projects and sustainable urban designs. Known as a Colombian politician and urban planner, Peñalosa (2012) advocated for urban renewal by emphasizing the importance of public spaces and supporting sustainable solutions such as bicycle lanes. Koolhaas (1997), a Dutch architect and theorist, is known for his views on how large urban projects can contribute to the transformation of cities.

Urban transformation is a process that has direct social and cultural effects. For this reason, legal legislation is shaped by relevant social and cultural influences. Urban transformation is not only limited to rehabilitating existing structures, but also includes the creation of new settlements. In this context, in this study, the relationship between urban transformation and urban planning has been tried to be embodied through the examples in the city of Ankara. The aim of the study is to analyze the historical development and legislation of urban transformation in Türkiye with projects made specifically for Ankara, and to contribute to the assimilation of urban transformation and to increase the understanding of urban transformation. For this purpose, the issues to be considered and done in urban transformation studies have been tried to be summarized in short articles through the projects examined.

In this context, the main aim of this article is to examine the concept of urban transformation, particularly in the context of Türkiye's capital city, Ankara, and to analyze factors such as historical developments contributing to change and transformation in cities and legal regulations associated with urban transformation. Essentially, the article aims to provide insights into the complex process of urban transformation and its multifaceted impacts on economic, social, and cultural aspects. Within this scope, this study emphasizes the dynamic nature of cities, which resemble living organisms and play a central role in various activities, while also addressing the historical background of urbanization in Türkiye, with a focus on the repercussions of population growth in Ankara as an example reflecting global trends. The historical context of urban transformation in Ankara is examined,

emphasizing the emergence of slum issues as a phenomenon and subsequent legal and cooperative initiatives to address this problem. The importance of legal and zoning regulations, as well as proper planning and resource allocation, is significant in urban transformations that have economic and social impacts. Urban transformation exhibits a multidisciplinary nature, drawing contributions from various social sciences and technical disciplines. This study underscores the need for expertise and a comprehensive understanding to grasp the essence of the subject. In this context, the interaction between urban transformation and urban planning is examined, highlighting their interconnectedness and importance in achieving sustainable urban development. Global trends in urban transformation are briefly mentioned, with examples from other countries such as India, Ghana, and China, underscoring the common challenges faced by cities in the Global South and East. The challenges resulting from rapid urbanization encompass issues related to housing, infrastructure, and public spaces. Dealing with urban sprawl requires active participation from individuals, and government institutions often play a critical role in facilitating this participation, particularly in terms of financing and regulation. This study advocates for considering cultural and social aspects alongside market-oriented activities in urban transformation, promoting a holistic approach that respects the spirit and identity of the city. This article focuses on Ankara as a case study while aiming to provide an examination of urban transformation that extracts insights from global experiences. Therefore, it addresses the multidimensional aspects of urban transformation, including legal, economic, social, and cultural factors.

This study analyzes the Atıfbey, Hıdırlıktepe, İsmetpaşa Urban Transformation and Development Projects, as well as the North Ankara Entrance Urban Transformation Project, in Ankara through various parameters and success criteria, aiming to assess the successes and weaknesses of these projects. The selection rationale, similarities, and differences of these projects can be summarized as follows:

Both projects are of great importance because they are carried out in Ankara, the capital and a major metropolitan city in Türkiye, where urban transformation projects hold significant significance. Both projects address the transformation of suburban areas and slum areas, involving common challenges such as infrastructure deficiencies, social issues, and environmental problems. Both projects are fundamentally related to the city's growth and increased housing demand due to rapid population growth and migration in Ankara. Both projects prioritize urban transformation with the aim of revitalizing the city by transforming suburban areas. Both projects involve public resources, with government institutions supporting and financing these projects. While the Atıfbey, Hıdırlıktepe, İsmetpaşa projects are smaller in

scale, the North Ankara Entrance project covers a larger area, representing a significant difference in project size. Although the North Ankara Entrance project covers a larger transformation area, it faces fewer property ownership issues compared to the Atıfbey, Hıdırlıktepe, İsmetpaşa projects. Both projects involve public resources, but the North Ankara Entrance project has more participation from the private sector, making its financing more complex. Public participation and the collection of public opinions differ between the two projects, with the North Ankara Entrance project placing more emphasis on considering public views, resulting in higher public satisfaction. These projects address similar fundamental problems but differ in aspects such as size, property structure, financing approach, and public participation.

Some conclusions drawn from this study can be summarized as follows:

Results of the Atıfbey, Hıdırlıktepe, İsmetpaşa Projects: These projects faced initial problems due to insufficient planning and comprehensive public participation. The absence of private sector involvement and heavy reliance on public funds increased costs and delayed returns on investments.

The projects' lengthy duration and unresolved issues indicate their lack of success.

Results of the North Ankara Entrance Project: This project, initiated by a unique law in Türkiye, aimed to transform the northern entrance of Ankara, significantly improving the city's appearance and infrastructure by reducing the distance between the city and the airport. However, the project's heavy reliance on public funds and limited private sector participation increased costs and delayed returns. The project has been criticized for favoring certain segments of the population and disregarding environmental impacts.

Both projects underscore the importance of urban transformation but also exhibit shortcomings and failures. Factors such as public participation, private sector integration, and consideration of environmental impacts should be taken into account for future urban transformation projects to be more successful.

2. The Transformation of the Urban Concept in the Global South and East

Sennett (2007) defines the city as a human settlement where individuals can come together constructively, proactively and without creating a long-term relationship. Even in this environment, the shyness and indifference displayed by the city dwellers in their relationships can be seen as a way to defend themselves against the demands and expectations of others. (Salomone and Messina 2011). In the Global South and East, people are accustomed to living in small-scale settlements in a tighter web of relationships, influenced by the past rural and nomadic culture. For example, with the new century, rapid growth is observed in small urban

settlements in the Indian state of Delhi. Under the influence of the megacity, small settlements record the highest growth. The growth of small settlements shows that these settlements are not competing, but rather the Capital New Delhi has completed its growth. Due to the high cost of living, people live in neighboring settlements and travel to the Capital to work (Jain 2018). The growth of residential areas close to the state of Delhi complements Delhi's growth by providing cheap land and rental areas. In Ankara, the lands close to the center were not cheap, they were completely free. The first squatters started in the hilly areas close to the city center and formed small settlements of their own. With subsequent amnesties, these lands were donated to the slum owners. The implementation of the Delhi metro in the last fifteen years has further accelerated the pace of developments in these settlements. In Ankara, the occupied areas were already within walking distance of the city center. In Delhi state, the region is also preferred by companies, as there is low taxation compared to other states. Also, the administrative capital is concentrated in this region (Jain 2018). Industrialization had not even begun in Ankara, only being the capital city and being at the center of the administrative mechanism was enough to attract migration.

In Ghana, too, the urban built environment has changed significantly since the country began implementing macroeconomic reform policies in the 1980s. There is extensive conversion of residential units to commercial uses such as service workshops, retail and wholesale stores, especially in city centers and along major roads (Oosterbaan et al., 2012). For today's "fluid society" cities (Mazzette 2006) are reduced to "a place for the organization of individual desires fueled by the market and its rules" (Bauman 2002). As the philosopher Nancy (2002) writes, the city is perhaps the epitome of "liquidity": The city is primarily circulation, transport, oscillation, vibration. It refers from anywhere to anywhere and beyond itself: the outside is the receding, indefinite exterior of the city itself. Every urban space refers to other places and its presence is immanent in its reference. As urban anthropologist Hannerz (2001), the city is precisely for this reason, it is "the place where you find one thing and find another". However, the scarcity of public spaces for socializing in the city only increases the feeling of socialization (Salomone and Messina 2011). This is one of the issues to be considered in urban transformation. The shanty settlements, which started on the peripheries of the city and were outside, gradually began to be inside. These settlements must now be transformed according to the character of the city. However, this transformation cannot be constructed independently of the spirit of the city and the public space needs that will keep this spirit alive. In other words, a successful urban transformation must be able to get in touch with the spiritual realm of the human being. It is essential for the transformation to eliminate the lack of spirit that results from reducing the city to material

elements, to some places.

In reality, the big city offers the opportunity to experience different situations than we are accustomed to every day. Thus, the city enables an educational and cultural exchange of listening and participation (Salomone and Messina 2011). The city is essentially the creativity of homo civicus, whose strong individuality fosters frequent and deep interdependence relations with fellow humans and collective history. It is a living space for individuals who know how to embrace larger temporal gaps (Cesareo and Vaccarini 2006). There is a greater longing for personal fulfillment, for individual self-creation, all over the world today (Salomone and Messina 2011). Creative people love complexity. Therefore, creativity contradicts reductionism; and because it is the ability to find new questions and invent new solutions, it corresponds to a way of thinking that has been defined as the "discovery or invention of problems" (Monceri 2004). For this reason, reducing the transformation of the city to market activities and finance will always have unsuccessful and problematic results.

All areas of social and political governance that directly affect the lives of many people in the developing world have now long been covered by international institutions (Gopakumar, 2015). Today, increasing urban sprawl in most cities in developing countries continues to attract the attention of national and international organizations. However, efforts to control the spread are not fruitful. All strategies for controlling the spread will fail without the participation of people. Therefore, Olujimi (2009) proposed a people-oriented strategy to control urban sprawl in Nigerian cities, expecting it to be facilitated by government planning officials. In addition, it should be reminded that closing the housing deficit and urban transformation activities in Developing Countries are mostly done by borrowing from international organizations. For example, Soederberg (2015) shows how the Mexican state effectively created the mortgage-backed securities market in the early 2000s through a series of legal reforms and emerging institutions. In parallel, many studies point to the state-directed nature of financialization processes. For example, in Brazil, it has been reported that the State is trying to realize urban transformations through the financialization of housing (Klink and Denaldi, 2014; Pereira, 2017). It has been shown that banking activities feed urban renewal projects in Singapore (Lai and Daniels, 2015). It has been argued that the State has become a shareholder with the activities of urban transformation and creating mega-city zones in China (Wang, 2015). According to Yeşilbağ (2020), the state in Türkiye is directly involved in the housing-finance link by undertaking multiple functions. It does this through a public administration endowed with vast land resources and overarching powers. In this respect, the state acts not only as a regulator, but also as a developer and financier in housing markets. As Bayat (2012) says, neoliberalization, unlike its emergence in the West, has emerged through authoritarianism by

“non-liberal states” in many countries of the Middle East. Macroeconomic reforms and open-door policies have significantly impacted the built environments in countries in the Global South and East. This is most evident in the political and administrative capitals, which often serve as the economic centers of these countries (Oosterbaan et al., 2012). For example, the initiation of reform efforts in China accelerated urbanization rates (Zhang, 2002). Since reform programs began in developing countries, major cities have received investments in wholesale, retail and construction to meet the growing demand for commercial space (Oosterbaan et al., 2012). Bangkok's growth has brought with it negative environmental impacts (Setchell 1995). While Lagos, the former capital of Nigeria, grew significantly with the implementation of macroeconomic policies, it had to face sustainability issues (Barredo and Demicheli, 2003). Major cities of the Developing Countries have witnessed a significant physical-spatial expansion with their reform programs including urban renewal projects (Cohen, 2004). Dar es Salaam, the former capital of Tanzania, has grown significantly with land joining urban areas (Kombe, 2005). The major cities of the Middle East witnessed intense urban growth (Mitchell 1999). Bahria Town, the largest real estate development project in Pakistan, provided mass housing to high-income segments of the population. Bahria Town has built new luxury urbanized areas on the peripheries of Pakistan's major cities (Karachi, Lahore, Islamabad, etc.), taking away the livelihoods of local populations (Khan and Karak 2018). Most dispossessed people live in the slums of Karachi. Thus, urban development processes have also created a new class of dispossessed who are self-sufficient, previously engaged in subsistence farming and farming (Khan and Karak 2018). The Indonesian central government has offered local cities and urban areas greater autonomy to formulate their own policy ideas and manage their own natural and financial resources (Tarigan et al., 2016). External organizations such as the Housing Rights and Eviction Center (COHRE) and Human Rights Watch have extensively documented displacement in Chinese settlements (Leon 2021). Gentrification, especially for mega-events such as the 2008 Olympics in the capital Beijing, has led to numerous displacements. Gentrification is a global force. Powerfully revising cities, this planning motif includes unique bursts of public housing construction. It targets the working class or marginalized populations who are reluctantly forced to modernize (Leon 2021).

Throughout this section, examples have been chosen from newly developed and developing countries. The common feature of these examples is the emergence of excessive migrations towards growing centers of attraction in the countries, the informal occupation of land to meet the housing needs arising from population growth, and the initial tolerance of governments due to political and economic concerns, as well as planning and implementation failures. As the situation becomes

increasingly complex and the occupied lands gain value through urban growth, distorted systems consisting of a mixture of gentrification and unjust claims are established, both as a solution and for political or economic gain. In these aspects, these examples parallel the gecekondu development in Ankara that began as early as the 1920s and the subsequent attempts at urban renewal in later years.

Based on the examples examined in this section, the following recommendations and findings can be made to make urban development processes more equitable and sustainable:

In newly developed and developing countries, urban growth planning should be carried out in a sustainable manner. Long-term urban development strategies should be created instead of haphazard urbanization and land occupations. Governments should improve land ownership regulations and reduce uncertainties regarding land ownership. This will help prevent informal land occupations. Social housing projects should be developed to meet the increasing housing demand accompanying population growth. These projects can offer affordable housing options to the poor and disadvantaged groups. Measures should be taken against the unjust consequences of gentrification. It is important to protect and support the local population living in redeveloped areas. The public should be informed about and educated on how urban transformation processes work and how to protect their rights. Therefore, public awareness and education programs should be organized. Participation in urban development planning should be encouraged among the public. Participatory planning processes can better reflect local needs. Governments should implement strict controls against corruption during urban development projects. Corruption can be one of the main reasons for unfair claims. The habit of shanty town construction has become a historical and cultural heritage in some countries. However, it is also true that this necessity or habit is unjust towards citizens who did not participate in shanty town construction. Therefore, instead of granting rights to those who have carried out land occupations for arbitrary or compulsory reasons, states should focus on resolving the problem in a manner consistent with social justice and equality. In this regard, developing countries should share their experiences with other countries facing similar problems and seek solutions through international cooperation, planning, cultural enrichment, and financing from developed countries.

3. An Overview of the History and Legislation of Urban Transformation in Türkiye

During the Republic period, which was established in 1923, priority was given to agriculture and animal husbandry, and farmers were supported with the regulations made in this context. Therefore, in the early

years of the Republic, migration was mainly concentrated in Ankara, primarily due to its status as the capital, and the first shantytowns began to emerge in Ankara as early as the 1920s. Şenyapılı (2004) has described this process in detail in her study. In the first years of the Republic, there was no intense wave of migration from rural to urban areas in Türkiye, except Ankara. In some provinces, urban transformation practices have been carried out in line with the plans prepared for modernization. These practices were aimed at the rehabilitation of buildings damaged and destroyed in the war and the existing infrastructure facilities in the city. The law numbered 5218, published in the Official Gazette in 1948, aimed to address the housing problem in Ankara. It is Türkiye's first law related to shantytowns. With this law, unlicensed structures within the municipal boundaries of Ankara were legalized (Cengiz, 2022). Through the law, treasury lands were transferred to Ankara Municipality at an appropriate cost, and the Municipality, in turn, granted permits free of charge to the structures built by citizens through land occupation. Following this law, a similar law, numbered 5228 in 1948, applicable throughout Türkiye, was enacted. The law encompasses both amnesty and planning. Treasury-owned lands not included in any planning in cities and towns were transferred to municipalities at cheap prices (tax value) to be paid in installments over 10 years (Cengiz, 2022). It can be said that these laws were politically motivated, reflecting the transition to multiparty elections in Türkiye in 1946. Shantytown amnesties will later be seen as a way to gain political support in Turkish politics.

Since the 1960s, an intense migration movement from rural to urban has started, mainly in big cities, with serious industrialization movements and the need for labor force. The said movement has led to some unplanned, inadequate infrastructure, faulty and incorrect constructions in terms of urban planning, and the majority of these buildings have created an unqualified and unprepared building stock for natural disasters and fires due to the insufficient development of the building and material sector (Yenice, 2014). The concept of "slums" emerged with the migration from rural to urban areas, and in 1966, the Gecekondu Law No. 775, which can be considered the first law in the field of urban transformation in Türkiye, came into force in order to solve the problems created by the slums. As it is clearly stated in Article 1 of the law, it is desired to regulate the improvement and liquidation of the slum areas, the prevention of the construction of new slums and the measures to be adapted for this purpose, with a legal framework (Genç, 2014).

The construction and materials sector started to develop with the opening of the construction sector after 1980, and as a result of these developments, the production of durable materials required restructuring and infrastructure changes in the real estate sector (Sür, 2014). In 1984, Amnesty Law No. 2981 came into effect.

In accordance with Article 4 of the relevant law, some principles regarding the buildings that do not comply with the zoning and slum laws have been determined, and as a result of the evaluation to be made according to these principles, the buildings to be protected or improved have been granted a building permit and a building occupancy permit if they fulfill the necessary obligations (Genç, 2008).

After 2004, legal regulations gained momentum in order to ensure that urban transformation is carried out with a fast and effective program, in accordance with the idea that natural disasters and fire risks will cause social, cultural and psychological problems and the principle of social state. In 2004, Law No. 5216 on Metropolitan Municipalities and Law No. 5226 on the Protection of Cultural and Natural Assets entered into force. Thus, municipalities were provided with the opportunity to participate in the practices, albeit partially, and preliminary preparations were made for the Law No. 5366 on the Renewal, Protection and Survival of Worn Historical and Cultural Heritage, enacted in 2005. The purpose of both laws is to continue the improvement practices that have been going on since the Ottoman period by arranging them with a legal framework. Another important law that came into force in 2005 is the Municipality Law No. 5393.

In 2012, the Government of Türkiye enacted the Law on the Transformation of Areas under Disaster Risk in order to determine the procedures and principles for the rehabilitation, cleaning and renewal of urban areas and disaster-prone buildings (Official Gazette, 2012). In Article 1 of this Law No. 6306, which is still in effect and is subject to urban transformation practices, the purpose of the relevant law is clearly defined. According to this; Methods and principles related to rehabilitation, liquidation and renewal in order to create healthy and safe living spaces in accordance with technical and artistic rules and standards, in places where there are risky structures in terms of structural features, even if they were built in disaster risk areas and risk-free areas, are regulated by the relevant law. The cultural and psychological impact of natural disaster and fire risk has an important role in the enactment of the law. After the Van Earthquake, it was understood that the legal regulations were clearly inadequate, and the relevant law came into force. Within the scope of this law, it is clearly stated that the old buildings should be rehabilitated, if they are not in a condition that can be rehabilitated, they should be liquidated, and the procedures and principles on which the new buildings should be built.

The Ministry of Environment and Urbanization, which is an important authority in urban transformation, announced in 2017 that approximately half of 15 million houses are at risk of disaster. Therefore, the government has an ambitious plan to rebuild 500,000 residences annually, 200,000 of which are in Istanbul, within the scope of urban transformation (Habertürk, 2017). As of May 2018, a total of 188 risky areas were declared by the

Ministry of Environment and Urbanization (Hurriyet, 2018). The legal framework and the practices realized so far show that the urban transformation processes in Türkiye consist of three basic steps: (1) declaring areas at risk, (2) evacuation and demolition of buildings, and (3) restructuring. Five main actors play an active role in urban transformation: Ministry of Environment and Urbanization, municipalities or mass housing administration (TOKİ), design and planning teams, residents and contractors (Gün et al., 2021). By law, the Ministry has the authority to regulate urban transformation actions. District municipalities, metropolitan municipalities and special provincial administrations can also carry out urban transformation studies with the approval of the ministry (Gün et al., 2021). Design and planning teams prepare planning and urban design projects that take into account the basic needs of the urban area, and these projects must be approved by the Ministry. Then, negotiations are held between the responsible authorities and the citizens, and when an agreement is reached, the buildings are evacuated and construction is carried out by the contractors (Gün et al., 2021).

4. Material and Method

Within the scope of the study, various urban transformation applications in Ankara were examined in line with the field studies, municipality decision and activity reports. In this section, the Atıfbey, Hıdırlıktepe, İsmetpaşa Urban Transformation and Development Projects and the partially successful Northern Ankara Entrance Urban Transformation Project, which have some deficiencies and shortcomings, are discussed in

terms of being good examples of unsuccessful urban transformation applications. Below, the problems identified after the information given about the historical development, actual problems and urban transformation practices in the areas, which make urban transformation mandatory in the areas, are discussed; and in the "Results, Discussion and Recommendations" section, some suggestions for urban transformation projects are presented within the scope of the lessons learned from these projects.

4.1. Atıfbey, Hıdırlıktepe, İsmetpaşa Urban Transformation and Development Projects

After being declared the capital city on October 13, 1923, Ankara, due to being the center of the country's administration, has received intense immigration compared to other cities in Türkiye and its population has increased rapidly. When this period is examined, it will be seen that sufficient housing has not been built in the face of intense migration. The uncontrolled growth of the city after the Second World War accelerated with the emergence of slum areas (Batuman, 2013). In this period, with the effect of the economic crisis that emerged all over the world, the inability of the contractors such as the state and private sector to make sufficient investments to meet the housing needs, caused the formation of slum areas since the beginning of the 1930s. The housing construction cooperatives that emerged from 1934 could not be effective in solving the problem. Close to the city center; Slum settlements have started in regions such as the steep hills (Altındağ, Hisar) and the creek bed (Bentderesi, Aktaş) next to it (Bostanoğlu, 2008) (Figure 1).

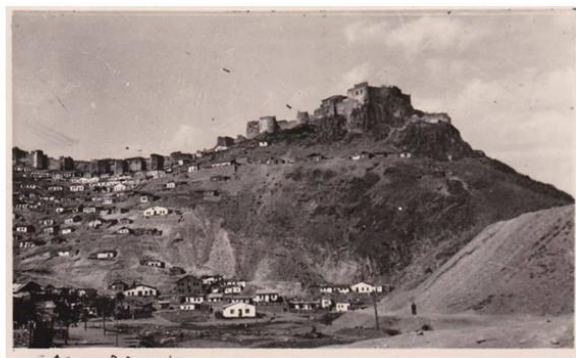
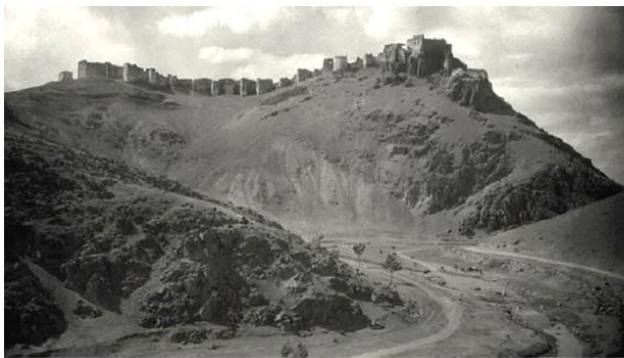


Figure 1. Ankara Castle, 1925 and 1934 (Sonmez, 2020).

At the beginning of the 1930s, the first irregular slums began to form on the steep slopes where the stones used in the Republican period structures were removed, and on the rugged Altındağ Hill and its surroundings. People who came to the region from various parts of Anatolia continued their lifestyles in the regions where they migrated, in this place where they settled. The inability to adapt to city life due to lack of education, ongoing social and technical infrastructure problems have caused the region to become a focus of crime and tension throughout the city. The slums in Altındağ Hill Slum Area

have worn out over time and have been sold or rented to people from lower income groups. The region has turned into a kind of collapse area due to the indifference of the central and local governments in providing the necessary social and technical infrastructure services (Bektaş and Türkün, 2017).

Bektaş and Yücel (2013) examined the social, economic, and spatial inequalities and divisions arising from migration movements in the Ankara-Altındağ Tepesi Gecekondu area. Spatial division was analyzed from both physical and socio-economic dimensions. Migration,

economic disparities, settlement patterns, and socio-economic factors were identified as the main causes of this division. It was emphasized that such divisions could exacerbate social and economic inequalities and deepen urban problems. After the proclamation of the Republic, Ankara became a city greatly affected by the gecekondu problem due to large-scale migrations. Altındağ Tepesi Gecekondu Region is an area where unplanned settlements have emerged, marking the beginning of gecekondu life. According to United Nations data, this region is one of the world's 30 largest mega gecekondu neighborhoods. When population changes in Ankara Province and Altındağ District are examined, it is observed that large-scale migrations occurred, especially during the periods of 1960-1970 and 1970-1980. Altındağ District stood out with its growth rate during these periods (Bektaş and Yücel, 2013). Türkiye, especially between the years 1940-1980, experienced an increase in the gecekondu problem, with Ankara and particularly the Altındağ region being significantly affected. Şenyapılı (2014) indicates that during this period, gecekondu areas grew and significantly influenced the urban space due to economic and political factors. The gecekondu phenomenon evolved over time, providing cheap, mobile, and hopeful labor to the economic space. In Ankara, especially in Altındağ, the adoption of the import substitution model in the early 1960s played a critical role in the transformation of gecekondu population. During this period, the gecekondu population integrated into the city and made economic demands. In 1966, a law was enacted officially recognizing the existence of gecekondu and introducing legal regulations to enable their settlement in the city. Uncontrolled and unjust sharing of rents shaped the urban texture where gecekondu were located,

influencing urban transformation (Şenyapılı, 2014). Physically, the Altındağ Tepesi (Hill) Gecekondu Region is characterized by old and irregular structures. The region faces problems related to infrastructure and services, especially in terms of inadequate drinking water and sewage services. The people living in the area faced problems such as inadequate infrastructure, security issues, unemployment, unplanned development, and transportation problems. Socioeconomically, it was observed that as the income levels of gecekondu owners increased, they moved to other parts of the city, leading to an increase in rental rates in the region. Additionally, crime rates increased. Furthermore, ethnic groups concentrated in different neighborhoods, leading to tensions. Spatial division in the Altındağ Tepesi Region can be associated with factors such as educational inequality, low income levels, changes in the nature of migration, and informal settlement patterns. This division has had a destructive impact on social relations throughout the city, creating a new sense of belonging instead of urbanity and citizenship. Local governments are implementing urban transformation projects to address these issues, but there is a need for projects that go beyond physical improvement and take into account the region's social, economic, and cultural characteristics. Therefore, rehabilitation and renewal efforts in the region need to be designed to address all these factors (Bektaş and Yücel, 2013).

Atıfbey - Hıdırlıktepe - İsmetpaşa settlements in Altındağ- Bentderesi Region were declared as urban transformation zones with the decision of the Metropolitan Municipality dated 17.02.2006, and then the border coordinates of the project area were determined and approved (Figure 2).

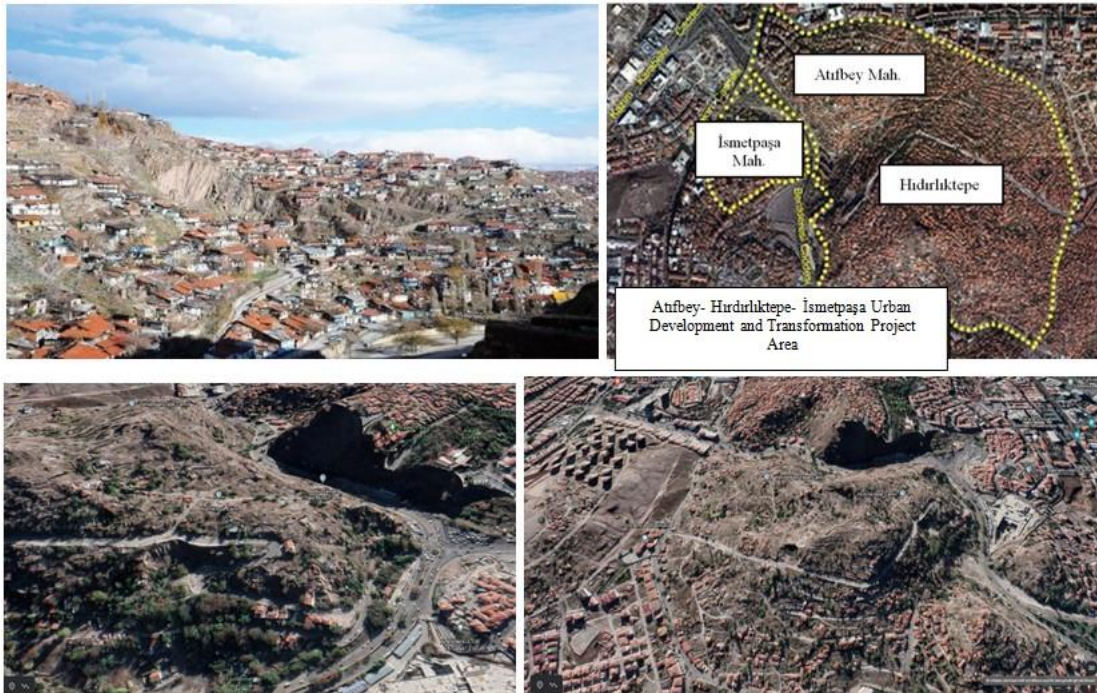


Figure 2. Construction of the region in 2006, project area (Sonmez, 2020) and Google Earth view (October 30, 2021).

103 Ha in Atıfbey – Hıdırlıktepe section. There are 9,947 independent sections in approximately 6,000 buildings covering the area. In İsmetpaşa, there are 1,682 independent sections in 574 buildings covering an area of 13 Ha. The buildings in the Project Area are in private, public and foundation ownership; it is used as residence, workplace, education, public service buildings. The Urban Transformation Project covers the area including Çandarlı, Hacıbayram, Atıfbey, Fatih, Öncüler, Yıldırım Beyazıt, Orhangazi and Yavuz Selim Neighborhoods (Sonmez, 2020).

The process that started with the inclusion of the region in the scope of the urban transformation project in 2006, due to the specific conditions of the said neighborhoods; it could not be completed except for the renovation of some buildings around the Hacı Bayram Mosque. The process is slow due to the fact that many structures in the region have multi-shareholder ownership due to succession and crime security problems. Despite the demolition of the slums in the current situation, the project has not been completed yet as other problems have not been resolved. Another negative aspect regarding the project area is that the entire project has to be implemented with public resources, since the private sector does not see the region as a profitable investment area (Sonmez, 2020).

Before the implementation of the Atıfbey, Hıdırlıktepe, İsmetpaşa Urban Transformation and Development Projects (AHİUTDP), detailed interviews and information, requests and suggestions were not exchanged with the people of the region in a systematic way. However, the participation of the right holders and even the local people in a wider area is the most important element of the urban transformation projects. For example, for the Hiroshima Danbara project, which is one of the successful urban transformation projects in the world, 21 organizations were established by the local people and 12 of them played an active role in the project decisions (Şişman and Kibaroglu, 2009). In addition, in terms of the execution of these projects, the problems of power sharing between the general and local governments were started to be implemented without being resolved from the beginning. Legislation has not been formed by planning the legal infrastructure and municipal decisions from the beginning to the smallest details. The fact that urban transformation project implementations have not reached satisfactory results, even if they have spread over many years, is the most important failure indicator in terms of urban transformation projects. Due to the mentioned determinations in the projects and applications discussed, this is exactly the case. In addition, legal decisions were taken without reaching a full consensus with the right holders, resulting in unsolved grievances. Projects that could ensure the participation of the private sector could not be designed, which, in addition to increasing the public cost, caused the process to be prolonged and the project implementations are still

unfinished.

Urban transformation projects are part of urban plans. The Hıdırlıktepe, Atıfbey, İsmetpaşa Urban Transformation and Development Project were designated as a Risky Area within the scope of Law No. 6306, based on the decision of the Ankara Metropolitan Municipality Council dated 11.09.2012 and numbered 1400. The area was declared a Risky Area by the Council of Ministers on 17.12.2012, in accordance with Law No. 6306, the "Law on the Transformation of Areas under the Risk of Disaster." The removal of derelict structures within the area, as stipulated by Article 39 of Law No. 3194 and Article 7, paragraph z of Law No. 5216, has been approved by the Ankara Metropolitan Municipality Council. However, more importantly, the decision of the Ankara Metropolitan Municipality Council dated 08.06.2023 and numbered 786 outlines all processes related to Hıdırlıktepe. Planning processes related to Hıdırlıktepe are still subject to legal disputes and are among the debated topics within the discipline of planning.

4.2. North Ankara Entrance Urban Transformation Project

Starting from the middle of the 1970s to the end of the 90s, dense slums were built around the Ankara Esenboğa Airport road. The difficult access to the airport from Ankara through a valley, and the uneven landscape during the journey created a negative image, especially when hosting guests from foreign countries. The Protocol Road, which connects Ankara with the whole world, was a winding, winding road and was surrounded by slums scattered on the valley slopes (Figure 3) (Genç, 2014).

For years, these lands were almost completely occupied by slum areas (Çalışkan, 2010). Within the scope of the urban transformation project in the region that includes the Ankara North entrance and its surroundings, it is aimed to increase the urban life standard by improving the current situation, making landscape design and creating a healthier residential area. For this reason, the region has been declared as the North Ankara Entrance Urban Transformation Project (NAEUTP) area with the law numbered 5104 with the approval date of 04.03.2004 (TBMM, 2004). Thus, for the first time in Türkiye, an urban transformation project was implemented with its own law. The law states that the only authority in the region that cannot be restricted by other smaller municipalities with legal rights is Ankara Metropolitan Municipality. In addition, the municipality was allowed to use the central national budget to finance the project. This gave a clear signal that the airport is not a local issue, but a national urban project in terms of entry into the Capital (Çalışkan 2010).

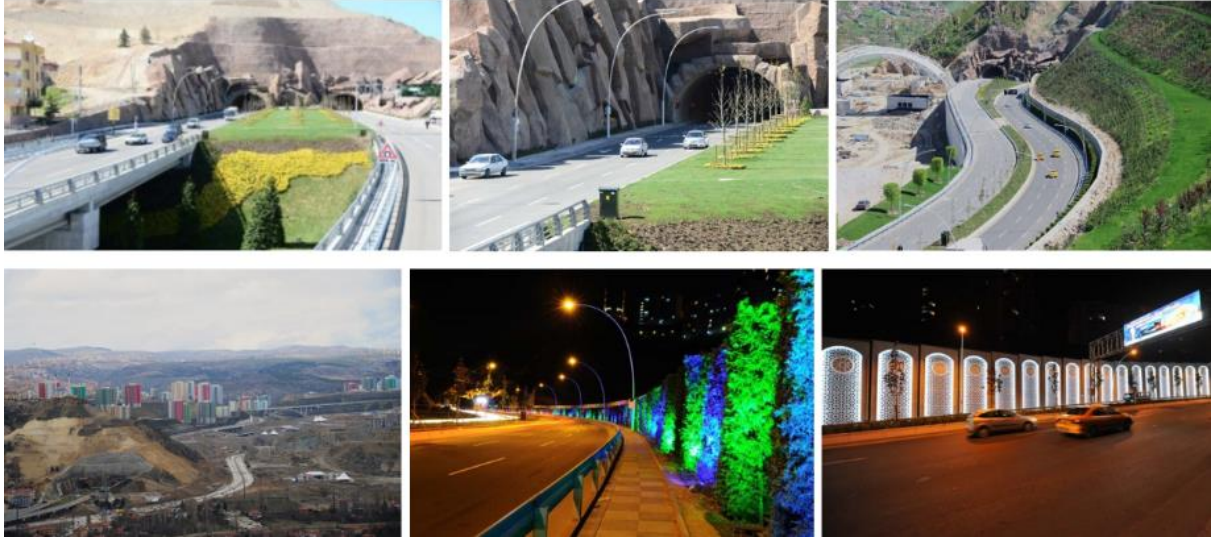


Figure 3. 2005 and 2018 view of the Protocol Road and a view from Kuzey Ankara Project (<https://www.ankara.bel.tr>).

In the project area, the boundaries of which are determined by law, of 10,500 slums, 1,520 Ha. was found on the total area. The Housing Development Administration and Ankara Metropolitan Municipality were assigned to the realization of the project. A part of the monetary resource was transferred to the Municipality and Administration budget with special regulations in the amount specified in the budget laws of the relevant year. In addition, it has been decided in the relevant law to provide the Project with all kinds of project income, including the appropriations and sales revenues to be transferred from the Municipality and the Administration's own resources.

Opening of Esenboğa Airport in the 1950s increased the importance of the northern axis of the city and led to the creation of Protokol Road. The relocation of the Turkish Grand National Assembly (TBMM) to its new building in İnönü Square in 1960 further elevated the significance of this axis. Starting from the 1970s, the rapid construction of shantytowns became concentrated in this area, and in 1983, Esenboğa- Protokol Road was expanded to a dual-lane road, further fueling shantytown construction. Particularly during election periods, zoning laws were enacted, and by the 1990s, there were 9,000 shantytowns covering 60% of this area of the city, diminishing the perceivability of the planned areas. This situation prompted the North Ankara Entry Urban Renewal Project to be proposed as a solution to this problem (İnce 2006).

According to the 2005 North Ankara Entry Urban Renewal Project Priority Project Area (Phase 1) 1/5000 Scale Master Zoning Plan Description Report, the irregular construction in the mentioned area made perception difficult. The presence of the Fruko Factory, resembling a typical Anatolian town, and the 4-story buildings in the Keçiören region, receiving services from Protokol Road, made traffic complex. The same problems, even though regulated in terms of zoning, were also applicable to the Pursaklar settlement, which failed to

provide coherence and a sense of belonging to Ankara. Irregularities in perception elements such as color, texture, and lighting of the buildings caused perceptual confusion. The existing connection form of the intersection point in front of the Fruko Factory and the entry points to the Pamuklar and Senyuva neighborhoods were causing traffic issues and also obfuscating the entrance to the Çubuk Dam recreation area. In this context, the project aimed to define Ankara's existing image and emphasize the concepts of the 21st century, taking into account the unique topography, historical and cultural heritage of the city.

With the project, only in the 1st Stage, in an area of 4 million square meters, social facilities and recreation areas were built. Within the scope of the project, a total of 18,000 residences are planned to be built. The open sale of shops and residences under the ownership of the administration in the completed stages of the project still continues. Owners of slums and unlicensed buildings were accepted as beneficiaries and 2,478 residences were delivered to the owners of illegal buildings from the Karacaören Stage (AMM Annual Report, 2018). For this, it was necessary to benefit from the Law No. 2981 on "Some Transactions to be Applied to Buildings Contrary to the Zoning and Slum Legislation" and the laws numbered 3290 and 3366, which amended some articles of this law. If this could not be achieved, it was sufficient to make use of the Law No. 6785 on the Amendment of an Article of the Zoning Law. If none of them could be used, it was necessary to prove that the shanty house was built before 01.01.2000. A house of a size determined by the Municipal Assembly was given to the beneficiaries who have a title deed or 400 m² land with Title Deed Allocation Certificate within the scope of Law No. 2981 and do not have any land debt. In the allocated lands, for the missing land ratios of the owners whose allocation amount is less than 400 m², the price to be calculated over the construction cost rate of the housing area to be determined by the housing contract and the Municipal

Assembly, by adding the land debt, if any, belonging to the slum, from the total; The cost of debris belonging to the facility and outbuilding was deducted and debited. A total of 8,152 residences were delivered to these beneficiaries from different stages within the project.

Within the scope of the 16- stage project, two five-star hotels, a congress center, a mosque, five trade centers and a 70,000- person recreational facility will be built (Akın 2007). At the end of the project, 12,000 new residences will be built in the same area, including a 25-floor smart housing complex in the former slum. These luxury homes will create a sort of gated community for the approximately 32,000 new residents. The program of the project also includes a hotel building and a recreation center of 650 000 m². Priority in the implementation of the project has been given to the houses located on the outskirts of the site (Metropolitan Ankara, 2005). Jessop (2016) portrays this project as an example of the future-oriented policies of neoliberal regimes. According to the plan, the reclaimed valley will provide a two-way view along the entire highway leading to the airport. The plan envisions the entire area as the 'gate' to the city and aims to transform the old traditional low- rise old and neglected 'rural' environment into a gorgeous modern high- rise urban fabric (Çalışkan 2010). In addition, the owners of the properties used as workplaces in the region have been granted rights from the commercial units in different stages, if their status is compatible with the current legislation, based on their applications. The new route change, consisting of tunnels, bridges, underpasses and crossroads, of the 3.50 km part of the Protocol Road, which passes through the project area, has been completed. With the new route change, the journey from Ankara city center to Esenboğa Airport, which used to take approximately one hour, has decreased to approximately 30 minutes. Within the framework of the urban transformation project implementation studies, the construction of rain water, sewage, drinking water, electricity, telecommunication, natural gas, road and asphalt manufacturing, education, social and commercial equipment in the general infrastructure has been completed.

Urban transformation projects are carried out to plan cities and focus on raising their residents in terms of quality of life, economy and social life, revitalizing and solving the problems (Aydın and Çamur, 2016). From this point of view, the NAEUTP is successful. In addition, rehabilitating an area that has accumulated problems for many years and seriously damaged the physical appearance of the city and making significant contributions to transportation are among the successful aspects of the project. However, the failure of the project stems from the heavy use of public resources and the fact that the return of funds that should be returned to the public is still not fully achieved. The reason for this is the failure to plan proposals and measures that will enable the private sector to be included in project implementations, and the lack of effective, fast and

efficient returns from projects and practices that can replace the resources spent by the public and generate income. However, the most important thing to consider when involving the private sector in urban transformation projects is to make arrangements that will not allow unfair rent. Landscaping and construction activities to be carried out in order to ensure financial recycling that will tolerate public costs should also be carried out with the consent of the local and city people.

NAEUTP, due to its unique law, is structurally different from other projects. Despite this, it has been the subject of Administrative Court Cases several times, and its phases have been canceled. The implementation of the NAEUTP Law (5140) has led to the cancellation of previous zoning plans, and consequently, building permits and occupancy permits, which are related to these plans, have been partially or entirely left to the authority of Ankara Metropolitan Municipality. This situation may have led to the loss of acquired rights and property rights (Ertaş, 2011). Many property owners, including those with title deeds, those with allocated title deeds, or those with adobe shanties, and those with 4-story reinforced concrete houses, have not been satisfied with their residences and have resorted to legal processes (Poyraz, 2021).

The transformation project, taking place in Keçiören and Altındağ districts, also includes Pursaklar and Çubuk districts. Initially covering a vast area of 1583 hectares, the project is divided into three phases: Phase I (Priority Area) 400 hectares, Phase II (Çubuk Dam Basin) 573 hectares, and Karacaören Region 650 hectares. In Phase I, there was land acquisition from roads, bridges, etc., increasing the project area to 1623 hectares. Public-initiated urban transformation in Phase II and Karacaören Phase was canceled by the Council of State Decision on 12.11.2014, mainly due to its proximity to the dam area and its unsuitability for urban transformation. In Phase I, housing was initially built for property owners with title deeds or allocated title deeds, with the condition of exchanging a certain area of land. Later, within the framework of financing these houses, financing houses were built. On the other hand, for those who built shanties on treasury land without title deeds, houses were built in the Karacaören Phase to be sold through credit (ABB Report, 2014).

The project area, being extensive and rugged, faced challenges during the construction and sale of residential units. Before the project, the Esenboğa-Ankara Protocol road passed through the valley. The region had unfavorable settlement areas due to slopes, excavation (stone quarries), especially the steep slopes of the south and east, despite having both planned and unplanned shanties. Much of the region, with limited infrastructure, was designated as a disaster zone unsuitable for construction. Additionally, old stone quarries were present in the field, known locally as Ankara stone. The project area, situated in a valley known as a riverbed, is within the boundaries of Keçiören and Altındağ districts.

According to the geological report of the project area, most of it is not suitable for settlement due to its geological and topographic structure. The region consists of Quaternary-age units, including hilly terrain, slopes, ridges, valleys, low plateaus, high ridges, low ridges, and valley bottom plains. The most common disaster type in the project area is rockfall, attributed to random cooling cracks in andesites. Particularly, in high cliffs and abandoned stone quarries without rehabilitation measures, the risk of rockfall is higher (Poyraz, 2021).

Under Law No. 5104, a new protocol road passing through Altındağ, Keçiören, and Pursaklar districts was constructed, as the previous protocol road financing housing area remained in place. The new protocol road, passing through the project area, was completed with the construction of a 3.5 km-long road consisting of 2 bridged intersections, 2 viaducts, and tunnels, with changes in its route. Moreover, the newly opened protocol road became operational as the only and longest heated road in Türkiye, featuring a substation, panel, and a system that can be controlled 24 hours a day (Poyraz, 2021).

The North Ankara Recreation area, once characterized as the outskirts of Ankara due to having the highest rate of informal settlements before urban transformation (constructed between 2011-2014), undergoes a distinct transformation. This transformation includes not only the necessary recreational resting areas from a topographic perspective but also the addition of greenery, wetlands, and an illuminated system compatible with landscape and residential integration. In such a transformation, the interaction between teams working on architecture and engineering specific to the area and teams from various interactive fields such as biologists, botanists, and landscape designers becomes inevitable. Environmental arrangements create a living texture consisting of greenery, trees, and special plants suitable for the climate and soil structure of the region, imitating natural/nature areas. When delving into the details of the harmony between these green areas and structures, particularly in the North Ankara example, it is noteworthy. While ecological balance often alleviates the heavy concrete appearance, the lack of greenery is supported aesthetically and ecologically by plant species with rapid climate adaptation in the region. Areas that are topographically inclined and unsuitable for settlement have been made suitable for environmental/spatial design through afforestation practices, unlike traditional landscape forms. Each intervention has been designed to provide spatial integrity with ecological data, forming a harmonious style with the created nature. In conclusion, the sample taken integrates city structure with ecological data, reflecting a comprehensive and successful planning approach. However, despite being processed in detail and aestheticized with ecological data, this urban transformation and recreation area does not carry concerns or attitudes towards issues related to ecological

art or environmental art. On the other hand, with its innovative environmental designs and its structure that reinforces the perception of "new nature," the North Ankara example can be considered exemplary in terms of urban ecology, urban aesthetics, and ecological recreation within its own field (Burçin, 2020).

4.3. Comparative Evaluation of Examined Urban Transformation Projects

In this study, urban transformation projects were compared over two basic parameter groups. As the first parameter group, the satisfaction of the projects and implementations in the beneficiaries, the people of the region and the residents of the city who have a relationship with the project area, the residents of other cities or people from different countries, and the possible grievances caused by the projects were taken into account. In all of these parameters, AHİUTDP were unsuccessful and NAEUTP was successful. With this, for NAEUTP, Caliskan (2010) says: "After the state amnesties, the municipality made a contract with the families who bought the title deeds. According to the contract, the shareholders will buy a new house in proportion to their existing land shares (Metropolitan Ankara, 2005). However, it is unlikely that these families will afford to live in such a noble urban environment in the near future." However, it should not be forgotten that the slums in the region were built by their owners without paying for the land. With the amnesty applied by the state, slum owners became land owners. This situation is not compatible with social equality and justice. Because only some people benefit from public goods. In the eyes of other citizens who did not go to squatting on state lands, the situation means unjustified gain. However, with this project, slum owners were given the rights to acquire new housing. Considering multifaceted, it should be said that the project did not cause grievances.

As the other parameter group, the cost of realizing the projects to public resources and whether this cost can be amortized, whether it can provide additional income to the public and if all these are realized, how long it can take are discussed. According to these parameters, both projects were found unsuccessful. For, according to Topal et al. (2019), the NAEUTP increased the concentration of state power, thus making it the main determinant of rent generation and allocation. This model can be considered as a manifestation of the authoritarian tendencies of the state in the contemporary stage of neoliberalism. However, there should be no problem in the state's ability to generate rent and evaluate it in favor of the society. The problem is that the state can choose to evaluate the rent created by the government in favor of only certain segments. Another important problem is that states can ignore environmental sensitivities in the way of generating rent. In my opinion, these are the 2 important issues that should be supervised by international organizations when necessary in urban transformation projects. Because these two issues are in

positions that exceed the freedom of choice of the rulers of a state in terms of global environmental effects and global problems that will reflect economic injustice. In addition, in the project discussed, the state does not seem to be very successful in generating rent. On the contrary, state resources have been spent for this project and no return has been provided. Various parameters inherent in and related to these two basic parameter groups, 4.1. and 4.2. It is mentioned during the examination of the project applications in chapters. Some suggestions for assimilation of all these criteria in a way to create an urban transformation culture are presented in the section below.

5. Results and Discussion

It can be said that the people of the city provide the blood circulation that provides the vitality of the urban organism and keeps the mechanism alive. Urban transformations are large-scale, important operations to improve the organism. The fact that these interventions can bring considerable satisfaction to the inhabitants of the city is the most important indicator of unequivocal success. Otherwise, as seen in the AHİUTDP, the project may be disrupted, as seen in Ankara and most regions of Türkiye. There may be situations such as the spread of projects over many years, the increase in grievances, the failure of the projects or the interruption of the project. In these cases, the urban transformation project can have the opposite effect on the issues of increasing safety, social life standard, city image and economic benefit. In addition, it is very important to direct the private sector in order to ensure the success of the project with minimum use of public resources. Otherwise, as seen in the NAEUTP, public costs increase and the principle of contributing to the economy, which is one of the objectives of urban transformation, is delayed or cannot be realized. In general, while the construction sector assumed the role of growth engine in the Turkish economy in the 2000s, certain financial mechanisms of housing supply show that it is a debt-based growth regime (Bahçe and Köse, 2016). Such debt-driven housing provision leads to gentrification of the urban built environment on the one hand and further marginalization of the least advantageous on the other (Topal et al., 2019). The recommendations drawn from the projects examined in the study can be summarized as follows:

- 1- Before the actual initiation of urban transformation projects, all details should be planned from the very beginning in terms of legal legislation, local government decisions and especially agreements with citizens residing in the area to be converted, and deficiencies should not be left.
- 2- A consensus should be reached between the public and private sector works and the owners of the land and building in the area to be converted, so that the beneficiaries can be entitled to the new project at an appropriate rate without investing. At this point, the

entrepreneurial support of the private sector gains importance. However, it is necessary to ensure control over the private sector, to adapt the legal regulations and municipal decisions in a way that does not create injustice, and to focus on projects that can achieve the profit target for the private sector. In addition, urban transformation projects should not be seen as a source of income, but should be aimed at solving problems. However, the solved problems should be able to return as a profit to the private sector, which has taken risks in solving these problems. Due to the difficulty of providing all these conditions in harmony, it may be necessary for the beneficiaries and the public to make investment costs at certain levels. In this case, it may be necessary to provide advantages such as interest-free or low-interest loans, especially to beneficiaries. If projects that can create their own resources for the area to be transformed can be developed, the solution of all these problems can be much easier, reducing the costs of the public and right holders and attracting the private sector.

- 3- Projects that will ensure the effective and efficient use of urban transformation areas should be produced; because the need for urban transformation itself is formed by the uncontrolled spread of urban life to the outside of the center and sometimes to the unplanned spaces in the center, as a result of the inability to use the urban areas effectively and efficiently. Therefore, so to speak, treatment should not contradict the diagnosis; the problematic approaches that created the negative situation should not be repeated in the solutions carried out to eliminate the negative situation. The transformation should not only address the physical structure of the city, but also its spirit and spiritual existence, so to speak. The soul of the city is formed by the life of its inhabitants. Therefore, urban transformation requires addressing the residents of the city as well. The real transformation of the city should be in a way that creates satisfaction, not victimization, in the context of the needs, wishes and economic concerns of the residents.
- 4- It is necessary to ensure that not only political forces such as central and local governments, but also social segments such as non-governmental organizations, professional chambers and universities, and the people of the city directly participate in urban transformation projects.

Urban transformation projects may cause significant damage to the environment. With urban transformation projects, only certain segments may be favored. Environmental impacts and economic injustices are practices that can have significant global repercussions. For this reason, it is necessary to provide supervision, suggestions and guidance by internationally competent and impartial organizations.

Author Contributions

The percentage of the author contributions is presented below. The author reviewed and approved the final version of the manuscript.

	V.K.
C	100
D	100
S	100
DCP	100
DAI	100
L	100
W	100
CR	100
SR	100

C=Concept, D= design, S= supervision, DCP= data collection and/or processing, DAI= data analysis and/or interpretation, L= literature search, W= writing, CR= critical review, SR= submission and revision.

Conflict of Interest

In the study, research and publication ethics were complied with. The author report there are no competing interests to declare. The author declares that the manuscript complies with ethical standards. No funding was received to assist with the preparation of this manuscript. The author declares that there are no conflicts of interest (financial or non-financial) in the manuscript. The author is confident that all data and materials as well as software application or custom code support their published claims and comply with field standards.

Ethical Consideration

Ethics committee approval was not required for this study because of there was no study on animals or humans.

References

- Akın E. 2007. Kentsel gelişme ve kentsel rantlar: Ankara örneği. Doktora Tezi, Ankara Üniversitesi, Sosyal Bilimler Enstitüsü, Ankara, Türkiye, pp: 292.
- AMM Anual Reports. 2018. Ankara Büyükşehir Belediyesi Faaliyet Raporu. Ankara Büyükşehir Belediyesi. Kentsel Dönüşüm Şube Müdürlüğü, ss: 125.
- Ankara Büyükşehir Belediyesi. (Metropolitan Ankara) 2005-2007-2009-2010-2015. Kuzey Ankara kentsel dönüşüm projesi uygulama raporları. Kentsel Dönüşüm Şube Müdürlüğü, ss: 125.
- Ankara Büyükşehir Belediyesi. 2014. Kuzey Ankara kentsel dönüşüm projesi raporu. Kentsel Dönüşüm Şube Müdürlüğü, ss: 125.
- Aydın AH, Çamur Ö. 2016. Kentsel dönüşüm uygulamalarında başarılı dünya örnekleri: Danbara, Solidere, Rio de Janeiro. Kahramanmaraş Sütçü İmam Üniv İktisad İdari Bilim Fak Derg, 6(1): 53-68.
- Bahçe, S., & Köse, A. H. (2016). Financialisation/borrowing circle as a solution to an unpleasant conundrum: Observations from the mature neoliberalism in Turkey.

- Research and Policy on Turkey, 1(1), 63-74.
- Barredo JI, Demicheli L. 2003. Urban sustainability in developing countries' megacities: modelling and predicting future urban growth in Lagos. *Cities*, 20(5): 297-310.
- Batuman B. 2013. City profile: Ankara. *Cities*, 31: 578-590.
- Bauman Z. 2002. *Modernità liquida*. Robinson / Letture, Bari-Roma, Italy, pp: 310.
- Bayat A. 2012. Politics in the city-inside-out. *City Soc*, 24(2): 110-128.
- Beatley T, Wheeler SM. 2004. *The sustainable urban development reader*. Routledge, London UK, pp: 540.
- Bektaş Y, Türkün A. 2017. mixed income housing strategy in urban transformation and Türkiye-specific dynamics: Ankara Altındağ-Gültepe case. *Megaron*, 11(2): 263-279.
- Bektaş Y, Yücel C. 2013. Ankara-Altındağ tepesi gecekondular bölgesi'nde mekânsal ayrışmanın gözlenmesine yönelik bir araştırma. *Megaron*, 8(2): 115-129.
- Bostanoğlu Ö. 2008. Ankara-İstanbul başkentlik çekişmesi: Cumhuriyet Ankara'sından Gökçek Ankara'sına. *Mülkiye Derg*, 32(261): 89-117.
- Burçin Ü. 2020. Kentsel ekoloji üzerinden estetik tasarımlar ve kuzey ankaralı örneklemi. *Sanat Tasarım Derg*, 25: 323-339.
- Caro RA. 1975. *The power broker: Robert Moses and the fall of New York*. Vintage Books, New York, USA, pp: 1344.
- Cengiz E. 2022. Meclis tutanaklarında imar affi tartışmaları. *J Inter Sci Res*, 7: 66-81.
- Cesareo V, Vaccarini I. 2006. *La libertà sorumlu*. Soggettività e mutamento sociale Milano. Vita e Pensiero, Milano, Italy, pp: 360.
- Cohen B. 2004. Urban growth in developing countries: a review of current trends and a caution regarding existing forecasts. *World Develop*, 32(1): 23-51.
- Çalışkan O. 2010. Urban gateway: Just a symbol or more? Reappraising an old idea in the case of Ankara. *J Urban Design*, 15(1): 91-122.
- Ertaş M. 2011. Kentsel dönüşüm çalışmalarında sosyal boyutun incelenmesi Ankara ve Londra örnekleri. *Selcuk Univ J Engin Sci*, 10(1): 1-18.
- Fainstein SS. 2014. The just city. *Inter J Urban Sci*, 18(1): 1-18.
- Fawcett P. 2016. *The routledge handbook of planning for health and well-being: shaping a sustainable and healthy future*. *Town Planning Rev*, 87(6): 736-739.
- Florida R. 2002. *The rise of the creative class*. Basic Books, New York, USA, pp: 512.
- Gehl J. 2010. *Cities for people*. Island Press, Washington, USA, pp: 285.
- Genç FN. 2008. Türkiye'de kentsel dönüşüm: Mevzuat ve uygulamaların genel görünümü. *Yönetim Ekon Derg*, 15(1): 115-130.
- Genç FN. 2014. Gecekonduyla mücadelede kentsel dönüşüm Türkiye'de kentleşme politikaları. *Adnan Menderes Üniv Sosyal Bilim Enstit Derg*, 1(1): 15-30.
- Glaeser EL. 2011. *Triumph of the City: How our greatest invention makes us richer smarter greener healthier and happier*. Penguin Books, London, UK, pp: 368.
- Gopakumar G. 2015. Intrusiveness of urban renewal in India: JNNURM as a development fix Canadian. *J Develop Stud*, 36(1): 89-106.
- Gün A, Pak B, Demir Y. 2021. Responding to the urban transformation challenges in Türkiye: a participatory design model for Istanbul. *Inter J Urban Sustain Develop*, 13(1): 32-55.
- Habertürk. 2017. Mehmet Özhasseki: Yeni yasanın eli kulağında 7.5 milyon bina yenilenecek [The minister of environment and urbanization: 7.5 million housing unit will be rebuilt].

- URL: <https://www.haberturk.com/gundem/haber/1600758-mehmet-ozhaseki-den-haberturk-tv-ye-aciklamalar#> (accessed date: August 20, 2022).
- Hannerz U. 2001. *Esplora la città. Antropologia della vita urbana* Bologna. Il Mulino, Bologna, Italy, pp: 554.
- Hoch C, Dalton LC, So FS. 2000. The practice of local government planning. *Intl City County Management Assn*, Washington, USA, pp: 496.
- Hurriyet. 2018. Yılda 500 bin konut yeniden üretilecek. 500000 housing unit will be reconstructed a year. URL: <http://www.hurriyet.com.tr/ekonomi/yilda-500-bin-konut-yeniden-uretilecek-40840334> (accessed date: August 20, 2022).
- İnce E K. 2006. Kentsel dönüşümde yeni politika yasa ve eğilimlerin değerlendirilmesi "Kuzey Ankara girişi protokol yolu. Kentsel dönüşüm projesi". Yüksek Lisans Tezi, Gazi Üniversitesi, Fen Bilimleri Enstitüsü, Şehir ve Bölge Planlama Anabilim Dalı, Ankara, Türkiye, ss: 213.
- Jacobs J. 2011. *The death and life of great American cities*. Modern Library, New York, USA, pp: 640.
- Jain M. 2018. The effect of distance on urban transformation in the Capital Region India. *Inter Planning Stud*, 23(1): 37-50.
- Jessop B. 2016. The heartlands of neoliberalism and the rise of the Austerity state. In Springer S, Birch K, MacLeavy J editors. *The handbook of neoliberalism*. Routledge, London, UK, pp: 410-421.
- Khan D, Karak A. 2018. Urban development by dispossession: planetary urbanization and primitive accumulation. *Studies Polit Econ*, 99(3): 307-330.
- Klink J, Denaldi R. 2014. On financialization and state spatial fixes in Brazil. A geographical and historical interpretation of the housing program My House My Life. *Habitat Inter*, 44: 220-226.
- Kombe WJ. 2005. Land use dynamics in peri-urban areas and their implications on the urban growth and form: the case of Dar es Salaam Tanzania. *Habitat Inter*, 29(1): 113-135.
- Koolhaas R. 1997. *Delirious New York: A retroactive manifesto for Manhattan*. The Monacelli Press, New York, USA, pp: 320.
- Lai KP, Daniels JA. 2015. Banking on finance in Singapore: The state-led financialization of banking firms. *GPN Working Paper Series*, Global Production Networks Centre Singapore, URL: <https://onlinelibrary.wiley.com/doi/epdf/10.1002/9781119051374.ch9> (accessed date: August 20, 2022).
- Le Corbusier. 1923. *Towards a new architecture*. Dover Publications, London, UK, pp: 413.
- LeGates RT, Stout F. 2011. *The city reader*. Routledge, London, UK, pp: 110-114.
- Leigh NG, Blakely EJ. 2016. *Planning local economic development: Theory and practice*. New York, USA, pp: 446.
- Leon JK. 2021. The global governance of housing: 1945-2016. *Planning Perspectiv*, 36(3): 475-494.
- Lerner J. 2014. *Urban acupuncture*. Island Press, Washington, USA, pp: 160.
- Mazzette A. 2006. *L'urbanità delle donne. Creare faticare altro*. FrancoAngeli, Milano, Italy, pp: 280.
- Mitchell T. 1999. *Dreamland: The neoliberalism of your desires*. *Middle East Report*, 29(1; ISSU 210): 28-33.
- Monceri F. 2004. *Il pensiero uyumsuz. Sulla creatività del filosofo*. *Elitler*, 4: 38-49.
- Moughtin C. 2007. *Urban design: street and square*. Routledge, London, UK, pp: 314.
- Nancy JL. 2002. *La città lontana. Ombre Corte*, Verona, Italy, pp: 75.
- NCRPB. 2013. *National Capital Region Planning Board. Draft Revised Regional Plan 2021: National Capital Territory*. URL: https://ncrpb.nic.in/policies_strategies.html (accessed date: August 20, 2022).
- Official Gazette. 2012. The law regarding transformation of areas under disaster risks. URL: <http://www.resmigazete.gov.tr/eskiler/2012/05/20120531-1.htm> (accessed date: August 20, 2022).
- Olujimi J. 2009. Evolving a planning strategy for managing urban sprawl in Nigeria. *J Human Ecol*, 25(3): 201-208.
- Oosterbaan C, Arku G, Asiedu AB. 2012. Conversion of Residential Units to Commercial Spaces in Accra Ghana: A Policy Dilemma. *Inter Plan Stud*, 17(1): 45-66.
- Özel N, Kılıçaslan H. 2021. Creative drama in the context of urbanization and urban planning from past to present. 2nd International Conference on Social Sciences and Humanities, July 09-11, Ankara, Türkiye, pp: 44-56.
- Peñalosa E. 2012. *Walkable city: how downtown can save America one step at a time*. Farrar Straus and Giroux, New York, USA, pp: 320.
- Pereira A. L. D. S. 2017. Financialization of housing in Brazil: New frontiers. *Inter J Urban Regional Res*, 41(4): 604-622.
- Poyraz E. 2021. Kentsel dönüşümün yarattığı ekonomik sonuçlar: Kuzey Ankara girişi kentsel dönüşüm projesi. *Doktora Tezi*, Ankara Üniversitesi, Sosyal Bilimler Enstitüsü, Ankara, Türkiye, ss: 162.
- Ratcliffe J, Stubbs M, Keeping M. 2021. *Urban planning and real estate development*. Routledge, London, UK p: 543.
- Roberts P, Sykes H. 1999. *Urban regeneration: a handbook*. Sage, New York, USA, pp: 257.
- Romer PM. 1990. Endogenous technological change. *J Politic Econ*, 98(5): 71-102
- Salomone M, Messina M. 2011. Complex ecological creative: The modern city and social change. *World Futures*, 67(2): 79-92.
- Sclar ED, Volavka-Close N, Brown P. 2013. *The urban transformation: health shelter and climate change*. Routledge, Abingdon, UK, pp: 238.
- Sennett R. 2007. *The culture of the new capitalism*. Yale University Press, New Haven, USA, pp: 241.
- Setchell CA. 1995. The growing environmental crisis in the world's mega cities: the case of Bangkok. *Third World Plan Rev*, 17(1): 1-18.
- Soederberg S. 2015. Subprime housing goes south: Constructing securitized mortgages for the poor in Mexico. *Antipode*, 47(2): 481-499.
- Sonmez H. 2020. Türkiye'de kentsel dönüşümün tarihesi ve Ankara'daki bazı kentsel dönüşüm uygulamaları. *Tezsiz Yüksek Lisans Projesi*, Ondokuz Mayıs Üniversitesi, Lisans Üstü Eğitim Enstitüsü, Taşınmaz Geliştirme Uzaktan Eğitim Programı, Samsun, Türkiye, ss: 38.
- Sür A. 2014. 1960'tan 2014'e kentsel dönüşüm serüveni. URL: <https://www.ekoyapidergisi.org>. (erişim Tarihi: 27 Mayıs 2020).
- Şenyapılı T. 2004. Barakadan gecekonduya Ankara'da kentsel mekânın dönüşümü. *İletişim Yayıncılık*, İstanbul, Türkiye, ss: 372.
- Şenyapılı T. 2014. Denetimsiz ve adaletsiz rant paylaşımının biçimlendirdiği kentsel dokuya örnek: Ankara-Yıldız. *İdealkent*, 5(11): 326-347.
- Şisman A, Kibaroglu D. 2009. Dünyada ve Türkiye'de kentsel dönüşüm uygulamaları. *TMMOB Harita ve Kadastro Mühendisleri Odası*, 12. Türkiye Harita Bilimsel ve Teknik Kurultayı, 11-15 Mayıs, Ankara, Türkiye, ss: 1-9.
- Tarigan AK, Samsura DAA, Sagala S, Wimbardana R. 2017. *Balıkpapan: Urban planning and development in anticipation of the post-oil industry era*. *Cities*, 60: 246-259.

- Taylor N. 1998. Urban planning theory since 1945. Sage, New York, USA, pp: 253.
- TBMM. 2004. North Ankara entrance urban transformation project law. URL: https://www5.tbmm.gov.tr/tutanaklar/KANUNLAR_KARARLAR/kanuntbmmc090/kanuntbmmc090/kanuntbmmc09005481.pdf. Accessed date: August 20, 2022).
- Topal A, Yalman GL, Çelik Ö. 2019. Changing modalities of urban redevelopment and housing finance in Türkiye: Three mass housing projects in Ankara. *J Urban Affairs*, 41(5): 630-653.
- United Nations. 2007. World urbanization prospects: 2007 revision data tables and highlights. United Nations, New York, USA, pp: 32.
- Ülger NE. 2011. Türkiye'de arazi düzenlemeleri ve kentsel dönüşüm. Nobel Akademik Yayıncılık, Ankara, Türkiye, ss: 360.
- Wang Y. 2015. The rise of the 'shareholding state': financialization of economic management in China. *Socio-Econ Rev*, 13(3): 603-625.
- Yenice MS. 2014. Türkiye'nin kentsel dönüşüm deneyiminin tarihsel analizi. *BAU Bilim Bil Öğr*, 16(1): 76-88.
- Yeşilbağ M. 2020. The state-orchestrated financialization of housing in Türkiye housing policy. *Debate*, 30(4): 533-558.
- Zhang KH. 2002. What explains China's rising urbanisation in the reform era? *Urban Stud*, 39(12): 2301-2315.



DESIGN AND OPTIMIZATION OF VOLTAGE MODE PWM CONTROL OF DC-DC BUCK CONVERTER WITH A PI-LEAD COMPENSATOR USING THE SIMULATED ANNEALING ALGORITHM

Kübra DOĞAN^{1*}, Bülent DAĞ²


¹Gazi University, Faculty of Engineering, Department of Electrical and Electronic Engineering, 06500, Ankara, Türkiye


Abstract: This paper presents a method for improving the performance of DC-DC Buck Converter Systems using voltage mode Pulse Width Modulation (PWM) control. We explore the effectiveness of Proportional-Integral (PI) and Lead Compensator controllers in enhancing system stability, minimizing voltage fluctuations, and improving load response. The system is modeled through transfer functions, and the controllers' impacts are analyzed both individually and in tandem. A key contribution of this work is the optimization of the PI-Lead Compensator parameters utilizing the Simulated Annealing Algorithm, which is fine-tuned to improve phase margin, gain crossover frequency, and steady state error. These parameters are critical for optimizing the system's output performance. Through MATLAB simulations, we demonstrate the iterative process of parameter optimization and validate the algorithm's efficacy in managing the DC-DC Buck Converter. The results highlight the enhanced performance achieved with the optimized parameters, providing a viable solution for effective control of DC-DC Buck Converter Systems.

Keywords: DC-DC Buck Converter, Voltage Mode PWM Control, PI-Lead Compensator, Simulated Annealing Algorithm

*Corresponding author: Gazi University, Faculty of Engineering, Department of Electrical and Electronic Engineering, 06500, Ankara, Türkiye

E mail: kubradogan@aselsan.com.tr (K. DOĞAN)

Kübra DOĞAN  <https://orcid.org/0009-0006-9099-9058>

Bülent DAĞ  <https://orcid.org/0000-0002-1404-232X>

Received: October 27, 2023

Accepted: November 27, 2023

Published: January 15, 2024

Cite as: Doğan K, Dağ B. 2024. Design and optimization of voltage mode pwm control of dc-dc buck converter with a pi-lead compensator using the simulated annealing algorithm. BSJ Eng Sci, 7(1): 72-88.

1. Introduction

In contemporary times, energy efficiency and power conversion are fundamental requirements in modern electronic systems. DC-DC converters encompass numerous topologies widely employed for power conversion purposes. These topologies are significant in achieving energy efficiency and power conversion in electronic systems. Power converter topologies transform a source voltage into a different voltage level and typically exhibit circuit structures characterized by high efficiency, low noise, and fast response time (Umanand, 2009; Rashid, 2010; Volkov, 2015; Rashid, 2017)

Generally, the operating principles of DC-DC Converters can be analyzed within two major categories: DC-DC linear and DC-DC switched-mode converters. DC-DC linear converters utilize the principle of linear regulation to control the input voltage and maintain the output voltage at a specific level, operating as active power-controlled converters. Energy flow is often controlled using a transistor or an electronic switch. The advantages of DC-DC linear converters include low power consumption, low cost, simple design requirements, and precise voltage regulation to maintain the desired output voltage. The disadvantage of DC-DC linear converters is

typically their low efficiency. Therefore, DC-DC linear converters are typically used to regulate the input voltage to a constant output voltage in low-power applications. On the other hand, DC-DC switched-mode converters or switched-mode power supplies are commonly preferred in applications requiring high power or where energy efficiency is critical. In these converters, switches such as transistors, MOSFETs, IGBTs, etc. control the energy flow. DC-DC switched-mode converters offer numerous advantages. In the presence of voltage oscillations, unbalanced loads, and similar situations, it provides high efficiency by utilizing feedback control mechanisms to maintain the desired output voltage. By rapidly switching the switches, energy losses are minimized, resulting in more effective energy conversion. These converters can be utilized in various power levels, from low-power to high-power applications. However, DC-DC switched-mode converters also have some disadvantages. The design, control, and implementation of DC-DC switched-mode converters can be complex. The correct timing and control of the switches may require additional electronic components or control algorithms (Middlebrook and Slobodan, 1976; Bose, 2002; Ogata, 2010; Rashid, 2010; Basso, 2014; Kazimierczuk, 2015; Erickson and Maksimović, 2020;



Bose, 2020).

Switched-Mode Power Supplies (SMPS) encompass different configurations, such as isolated and non-isolated configurations. Isolated converters basically include flyback converter, forward converter, and full-bridge converter. On the other hand, non-isolated converters consist mainly of Buck Converter, Boost Converter, and Buck-Boost Converter. In this paper, the Buck Converter, which is commonly used among non-isolated DC-DC SMPS, has been discussed. The DC-DC Buck Converter is an electronic circuit that efficiently steps down the energy from power sources to produce the desired output voltage at a lower voltage level (Moorthi, 2005; Ogata, 2010; Rashid, 2010; Rashid, 2017; Suntio and Messo, 2019).

In DC-DC Buck Converters, the output voltage must reach the desired value quickly and accurately, directly affecting the converter's performance. However, voltage fluctuations and load changes can cause the output voltage to deviate below or above the desired value. Therefore, various control methods are employed to optimize the converter's performance. Pulse-Width Modulation (PWM) and Frequency Modulation (FM) are the two main techniques used to control the output voltage of the DC-DC Buck Converter. In the PWM method, the converter's switches are turned on and off at a specific frequency, creating pulses. This method includes control methods such as voltage mode and current mode control. In the FM method, the switching frequency is continuously changed to achieve a constant pulse. Both of these control techniques are used to keep and control the output voltage of the DC-DC Buck Converter at the desired level. In this paper, the voltage mode PWM control method has been employed to adjust the output voltage of the DC-DC Buck Converter to the desired level (Middlebrook and Slobodan, 1976; Mohan and Tore, 2003; Umanand, 2009; Basso, 2014; Suntio and Messo, 2019; de 2021).

The voltage mode PWM control method is a widely used method in DC-DC converters to precisely adjust the desired output voltage by changing the pulse width of the switching signal. The output voltage is continuously measured and compared to the reference value. As a result of this comparison, an error signal is obtained, which is then fed back into the converter's switching circuit. The switching frequency and amplitude are adjusted based on the characteristics of this error signal. As a result, the output voltage is maintained at the desired level. The voltage mode PWM control method offers advantages such as superior voltage regulation, high precision, low output impedance, and stable operation. Additionally, its ability to respond rapidly to changes in output voltage makes it applicable to various applications (Mohan and Tore, 2003; Moorthi, 2005; Umanand, 2009; Basso, 2014; Kazimierczuk, 2015; Rashid, 2017; de Azpeitia, 2021).

In voltage mode PWM control, various control methods are employed to precisely adjust the pulse width of the

switching signal to achieve the desired output voltage: Proportional-Integral-Derivative (PID) Controller, Lead Compensator, Lag Compensator, Lag-Lead Compensator, etc. The PID Controller provides a fast response and appropriate settling times within the feedback loop. The P term rapidly adjusts the output voltage; the I term corrects steady-state errors; the D term enhances the system response speed. Similarly, compensator methods are control strategies that enable a DC-DC Converter to respond quickly to various load and input voltage conditions and ensure stability in the output voltage. This control system continuously measures the output voltage through a feedback loop and performs corrective actions. The Lead Compensator, one of the most commonly used, is typically employed to increase the Phase Margin (PM) value and speed up the system response. However, it might decrease the system's Gain Margin (GM) value. Conversely, the Lag Compensator is predominantly used to boost the Gain Margin value and diminish Steady-State Errors (SSE). However, it can reduce the Phase Margin value. Given the necessity to strike a balance between Phase and Gain Margin values, the Lag and Lead Compensator methods are usually used in conjunction. The term "Phase Margin" mentioned here indicates how close the phase of a control system is to -180 degrees at the frequency where the system's gain crosses 0 dB in the Bode Plot of the frequency response. In other words, it shows how close the phase is to -180 degrees when the system's frequency is at 0 dB. Systems with higher Phase Margins are typically more resilient to phase disturbances caused by external factors. Ideally, the Phase Margin should be between 45 to 60 degrees. On the other hand, "Gain Margin" indicates how close the magnitude of the system is to 0 dB at the frequency where the system's phase is at -180 degrees. In other words, it shows how close the magnitude is to 0 dB when the phase is at -180 degrees. A system with higher Gain Margin is generally more robust against magnitude disturbances caused by external factors. Ideally, the Gain Margin should be at least 6 to 10 dB (Franklin et al., 2002; Moorthi, 2005; Pressman, 2009; Ogata, 2010; Bishop and Dorf, 2011; Rashid, 2017; Nise, 2020; de 2021).

Various control methods can be combined to achieve desired performance objectives in voltage mode PWM control for DC-DC Converters. There are numerous studies related to combined control methods. In (Feng et al., 2023), a temperature control process was carried out using a PID Controller in conjunction with the PWM method (Qu et al., 2023), Fuzzy Logic and PWM methods were used together, and it was reported that this structure provided better performance than a PID controller. Amaral and Antonio (2022a), presented PWM signal generation in connection with a Type-II Controller for a non-isolated DC-DC Buck Converter. In Zebet et al. (2021), Adaptive-PI (A-PI) and Adaptive-Sliding Mode Controller (A-SMC) have been used together. Garg et al. (2015), PI Controller and Lead Compensator control

methods have been used together to regulate the output voltage based on frequency domain characteristics.

As mentioned in the previous paragraph, various advantages can be obtained when control methods are used together. Among these advantages are reaching the desired output voltage value quickly and accurately, reducing fluctuations in the output voltage, increasing stability, responding rapidly to load changes, and maintaining the output voltage at the desired level. Furthermore, the option to try different combinations of control methods provides design flexibility. However, combining multiple control methods can also lead to a complex design process that requires precise analysis and careful calibration to prevent potential instability (Franklin et al., 2002; Ogata, 2010; Rashid, 2017; Nise, 2020).

This paper aims to provide an effective and optimal approach for achieving the desired performance in DC-DC Buck Converters using voltage mode PWM control by combining PI Controller and Lead Compensator methods. This combination reduces output voltage fluctuations and enhances stability by enabling quick and precise attainment of the desired output voltage. The PI Controller measures the output voltage through a feedback loop and calculates the errors that need to be corrected. On the other hand, the Lead Compensator allows faster dynamic response by reaching the desired output voltage more quickly. During this integrated design process, obtaining the most appropriate settings to address instability issues and meet the desired performance goals effectively is crucial. In this integrated design process, obtaining the most suitable settings is crucial to address instability issues and effectively meet the desired performance goals. At this stage, utilizing heuristic algorithms, which is the most significant contribution of this publication, allows practical solutions and optimal adjustments for the complex design process (Franklin et al., 2002; Pressman, 2009; Bishop and Dorf 2011; Eiben and James, 2015; Erickson and Maksimović, 2020).

Heuristic algorithms are problem-solving algorithms that aim to obtain good results close to the desired values by evaluating various alternatives within a reasonable time without placing too much emphasis on the provability of the result. They do not guarantee that the best result will always be obtained because they are approximation methods. However, they generally reach a solution path that is quick, easy, and closest to the best possible outcome (Glover and Gary, 2006; Yang, 2020).

Different heuristic algorithms can be used in the controller design: Genetic Algorithm, Particle Swarm Optimization, Simulated Annealing, etc. These methods provide effective options for exploring and improving design parameters. It is important to note that each algorithm offers a different approach to optimize the complex design process and enhance performance by meeting design criteria. These algorithms have various advantages and disadvantages. Therefore, selecting a

suitable algorithm based on design requirements and priorities is crucial (Glover and Gary, 2006; Eiben and James 2015; Yang, 2020).

The most significant contribution of this paper is the utilization of the Simulated Annealing (SA) Algorithm to optimize the complex design process and enhance the performance of DC-DC Buck Converters. The SA Algorithm has facilitated the design process by optimizing the parameters of the PI-Lead Compensator used in the voltage mode PWM control method for fast and optimum adjustment of the desired output voltage in the DC-DC Buck Converter system.

The SA Algorithm is a search algorithm that seeks the best solution while navigating the potential solution space when determining an objective function that needs to be optimized. As the algorithm randomly traverses the solution space, it keeps the current solution open to changes and improvements for an acceptable period. In this way, by searching across a broad area of design parameters, it explores potential solutions for better performance (Glover and Gary, 2006; Chibante, 2010).

The SA Algorithm can offer numerous advantages when used in compensator design. First, its ability to explore design parameters by searching within an ample solution space can improve the output performance of the DC-DC Buck Converter. Another advantage of the algorithm is its flexible structure, which can be adapted to different design objectives. Furthermore, taking random steps in the complex design space can resist challenges such as balancing problems and adjusting difficulties while approaching the global optimum. However, using the SA Algorithm in compensator design can also entail certain disadvantages. For instance, in scenarios with many parameters to optimize, computational time and resource requirements may increase (Glover and Gary, 2006; Yang, 2020).

In the design of the DC-DC Buck Converter, for the SA Algorithm to function efficiently, it is essential to define the objective functions correctly. The need for a precise mathematical formula for the DC-DC Converters has been a complicating factor in their design. Therefore, in these converters, correct analysis and modeling of the system are essential to achieve the desired performance. This analysis can be conducted using various mathematical modeling methods, such as state-space models, transfer functions, small-signal linearization and compact models. These methods play a significant role in the design and optimization process of the converters (Bose, 2002; Mohan and Tore, 2003; Chibante, 2010; Rashid, 2010; Erickson and Maksimović, 2020).

Another contribution of this paper is using the duty-cycle-to-output-voltage transfer function method, obtained with the state-space averaging technique, for the mathematical model of DC-DC Buck converters. Considering the circuit's dynamics, this technique takes long-term averages at the circuit's operating frequency. Thus, the obtained transfer function describes the relationship between the circuit's duty cycle and the

output voltage. As a result, it becomes possible to obtain results that are close to the system responses. Due to its ease of use, the transfer function method is preferred over other mathematical modeling techniques, such as state-space representation, small-signal linearization, and compact models. It provides significant ease in the design and optimization process (Franklin et al., 2002; Pressman, 2009; Corradini, 2015).

Another significant contribution of this article is considering the parasitic components while deriving the transfer function of the DC-DC Buck Converter circuit. The goal is to obtain a more detailed mathematical model than the standard DC-DC Buck Converter transfer function to achieve accurate results that closely resemble the system responses (Franklin et al., 2002).

When the detailed extracted transfer function of the DC-DC Buck Converter system is analyzed for frequency and step response reactions, it is often observed that the PM value is low, and the Gain Crossover Frequency (GCF) or bandwidth remains constant at low frequencies. Additionally, the SSE value in an unregulated Buck Converter is generally very high. So, without a feedback loop or control algorithm, there can be a significant overshoot and some error in the output voltage. Therefore, designing the most suitable controller is of great importance to achieve the desired performance characteristics of the system. Thanks to the SA Algorithm, the error margin is almost reduced to zero, aiming to achieve a fast and accessible design (Mohan and Tore, 2003; Ogata, 2010; Rashid, 2010; Garg et al., 2015; Erickson and Maksimović, 2020).

The most significant contribution of this paper is the utilization of the Simulated Annealing Algorithm to optimize the PI-Lead Compensator parameters in a DC-DC Buck Converter system based on the accurate and detailed analysis of the mathematical model. In this optimization process, the PI-Lead Compensator parameters are optimized to bring critical values such as PM, GCF, and SSE to the desired levels, aiming to improve the system's performance accordingly.

The remainder of this paper is organized as follows. Section 0 presents a mathematical model of the Buck Converter system. This model incorporates parasitic components for realistic system response. The technique of state-space averaging is employed to derive the duty-cycle-to-output-voltage transfer function. Section 0 lays out the detailed design of a PI-Lead Compensator added to the Buck Converter system. This state facilitates Closed-Loop voltage mode PWM Control. In Section 0, the process of tuning the parameters of the PI-Lead Compensator using the Simulated Annealing Heuristic Optimization Algorithm is explicated. This process aims to improve values of the Buck Converter in both the frequency and time domain (PM, GCF or Bandwidth, the corner frequency of the PI Compensator, and SSE). Additionally, the open-source project, which enabled the optimization of PI-Lead Compensator parameters and performance analysis for DC-DC Buck Converters using

the SA Algorithm and developed in MATLAB, has been added as Buck-Converter-PI-Lead-Compensator-SA (2022). Section 5 features the performance outcomes obtained by adapting the optimized PI-Lead Compensator parameters to the DC-DC Buck Converter system using the Simulated Annealing Algorithm. Following these sections, the conclusion and discussion parts are presented.

The introduction should briefly place the study in a broad context and highlight why it is important. It should define the purpose of the work and its significance. The current state of the research field should be carefully reviewed and key publications cited. Please highlight controversial and diverging hypotheses when necessary. Finally, briefly mention the main aim of the work and highlight the principal conclusions. As far as possible, please keep the introduction comprehensible to scientists outside your particular field of research.

2. Materials and Methods

2.1. Transfer Function Mathematics Model of Dc-Dc Buck Converter

The transfer function of a DC-DC Buck Converter circuit is a function that expresses the mathematical relationship between the input and output. This function can be derived for both ideal and non-ideal cases (Ogata, 2010; Rashid, 2010).

When the DC-DC Buck Converter circuit is to be analyzed in the ideal case, the circuit's transfer function is derived as if there is a precise mathematical relationship between the input and output, disregarding all energy losses, parasitic effects, and delays. In this scenario, the converter is considered completely efficient and a perfect device that accomplishes the desired conversion. However, in practice, achieving such an ideal converter is not possible due to the limitations of real-world components. Nevertheless, ideal transfer functions are helpful for analysis and understanding fundamental principles (Ogata, 2010; Rashid, 2010; Garg et al., 2015; Erickson and Maksimović, 2020).

For non-ideal cases, the transfer functions of converters are derived by considering parasitic elements, energy losses, and other real-world effects. These transfer functions provide a more accurate representation of the behavior of real-world converters. Due to the limitations of real components, non-ideal transfer functions can be more complex, and mathematical calculations may be more challenging (Ogata, 2010; Rashid, 2010; Garg et al., 2015; Erickson and Maksimović, 2020).

The functioning modes of DC-DC Buck Converters significantly impact the transfer function's derivation and the control strategy's development. Generally, these converters function in two primary modes: Continuous Conduction Mode (CCM) and Discontinuous Conduction Mode (DCM) (Ogata, 2010; Rashid, 2010; Garg et al., 2015; Erickson and Maksimović, 2020).

The inductor current never falls to zero in the CCM. This mode is typically seen when the load is high. CCM is more

straightforward from a mathematical modeling perspective, assuming the continuity of the inductor current. On the other hand, in the DCM, the inductor current drops to zero for specific periods. This situation typically occurs when the load is lower. DCM is more complex from a mathematical modeling perspective as it needs to consider the discontinuity of the inductor current. Both operating modes can significantly affect the derivation of the transfer function and the overall performance and stability of the converter. Therefore, a detailed understanding of these operating modes is crucial for creating an effective control strategy (Ogata, 2010; Rashid, 2010; Garg et al., 2015; Erickson and

Maksimović, 2020; Nalepa, Karol and Błazej, 2020; Yang et al., 2020; Surya and Sheldon, 2021; Surya, Mohan and Sheldon, 2021; Wang, Bingwen and Hongdong, 2021; Amaral and Antonio, 2022b).

The schematic representation of a non-ideal DC-DC Buck Converter, functioning in CCM and considering its parasitic impedances, is illustrated in figure 1. The circuit includes a single switch (S) along with its parasitic resistance (r_{sw}), a single diode (D_d) and its forward resistance (r_d), an inductor (L) and its ESR parasitic resistance (r_L), a capacitor and its ESR parasitic resistance (r_c), and finally, a load resistor (R) (Ogata, 2010; Rashid, 2010; Erickson and Maksimović, 2020).

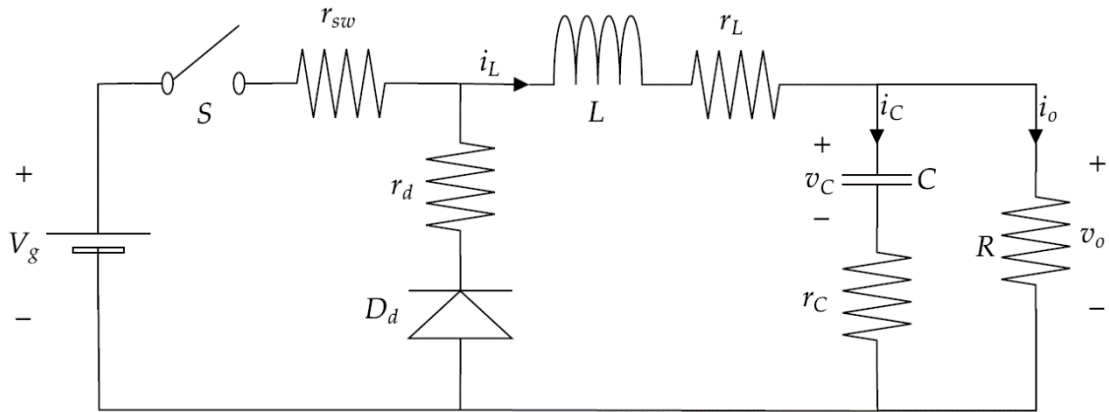


Figure 1. DC-DC buck converter circuit.

The duty-cycle-to-output-voltage transfer function of the DC-DC Buck Converter is derived from the equations formed based on the on and off states of the Switch in the CCM. The time intervals of $0 < t < dT$ when the Switch is on, the Diode is off, and $dT < t < T$ when the Diode is on and the Switch is off are analyzed. The variable 'd' represents the duty cycle, and 'T' denotes the Switch period (Ogata,

2010; Rashid, 2010; Erickson and Maksimović, 2020).

Firstly, as seen in figure 2 when the Switch is on, and the Diode is off, the equations 1, 2 and 3 obtained for the Inductor Current, Capacitor Voltage, and Output Voltage values are as follows (Ogata, 2010; Rashid, 2010; Garg et al., 2015; Erickson and Maksimović, 2020).

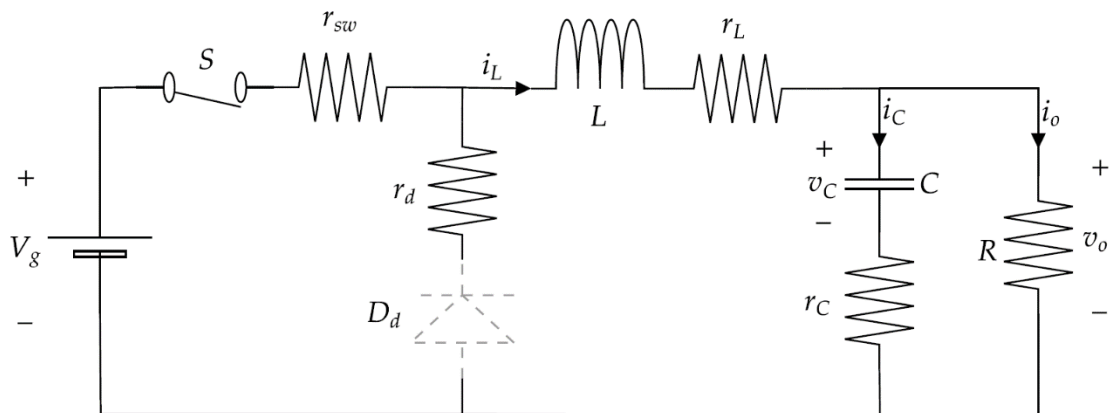


Figure 2. DC-DC buck converter circuit CCM switch on, diode off state analysis.

$$L \frac{di_L(t)}{dt} = -\left(r_{sw} + r_L + \frac{r_c R}{R + r_c}\right) i_L(t) - \frac{R}{R + r_c} v_c(t) + v_g(t) \quad (1)$$

$$C \frac{dv_c(t)}{dt} = \frac{R}{R + r_c} i_L(t) - \frac{1}{R + r_c} v_c(t) \quad (2)$$

$$v_o(t) = \frac{r_c R}{R + r_c} i_L(t) + \frac{R}{R + r_c} v_c(t) \quad (3)$$

As seen in figure 3 when the Switch is off, and the Diode is on, the equations obtained for the Inductor Current, Capacitor Voltage, and Output Voltage values are as

follows (Ogata, 2010; Rashid, 2010; Garg et al., 2015; Erickson and Maksimović, 2020).

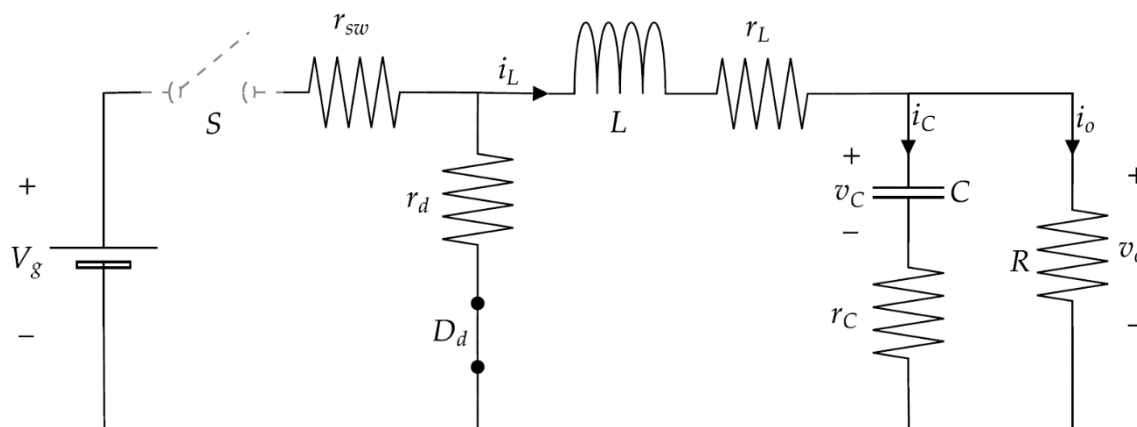


Figure 3. DC-DC buck converter circuit CCM switch off, diode on state analysis.

$$L \frac{di_L(t)}{dt} = -\left(r_d + r_L + \frac{r_c R}{R + r_c}\right) i_L(t) - \frac{R}{R + r_c} v_c(t) \quad (4)$$

$$C \frac{dv_c(t)}{dt} = \frac{R}{R + r_c} i_L(t) - \frac{1}{R + r_c} v_c(t) \quad (5)$$

$$v_o(t) = \frac{r_c R}{R + r_c} i_L(t) + \frac{R}{R + r_c} v_c(t) \quad (6)$$

The transfer function of the DC-DC Buck Converter essential for designing the PI-Lead Compensator will be derived using the State-Space Averaging (SSA) method and the equations mentioned in equations (1), 2, 3, 4, 5 and 6 mentioned earlier.

The equations in matrix form obtained during the Switch on; Diode off condition are as follows (Ogata, 2010; Rashid, 2010; Garg et al., 2015; Erickson and Maksimović, 2020). The equations in matrix form obtained during the Switch off; Diode on condition are as follows (Ogata, 2010; Rashid, 2010; Garg et al., 2015; Erickson and Maksimović, 2020).

Expanding upon the expressions in equations (7, 8, 9, 10 and 11 we obtain the following equalities (Ogata, 2010; Rashid, 2010; Garg et al., 2015; Erickson and Maksimović, 2020).

$$\dot{x}(t) = A_1 x(t) + B_1 u(t), \quad y(t) = C_1 x(t) \quad (7)$$

$$\dot{x}(t) = A_2 x(t) + B_2 u(t), \quad y(t) = C_2 x(t) \quad (8)$$

$$x(t) = \begin{bmatrix} i_L(t) \\ v_c(t) \end{bmatrix}, \quad u(t) = V_g, \quad y(t) = v_o(t) \quad (9)$$

$$A_1 = \begin{bmatrix} \frac{-1}{L} \left(r_{sw} + r_L + \frac{r_c R}{R + r_c} \right) & \frac{-R}{L(R + r_c)} \\ \frac{R}{C(R + r_c)} & \frac{-1}{C(R + r_c)} \end{bmatrix}, \quad B_1 = \begin{bmatrix} \frac{1}{L} \\ 0 \end{bmatrix}, \quad (10)$$

$$C_1 = \begin{bmatrix} \frac{r_c R}{R + r_c} & \frac{R}{R + r_c} \end{bmatrix}$$

$$A_2 = \begin{bmatrix} \frac{-1}{L} \left(r_d + r_L + \frac{r_c R}{R + r_c} \right) & \frac{-R}{L(R + r_c)} \\ \frac{R}{C(R + r_c)} & \frac{-1}{C(R + r_c)} \end{bmatrix}, \quad B_2 = \begin{bmatrix} 0 \\ 1 \end{bmatrix}, \quad C_2 = \begin{bmatrix} \frac{r_c R}{R + r_c} & \frac{R}{R + r_c} \end{bmatrix} \quad (11)$$

The formula for the transfer function that relates the BSJ Eng Sci / Kübra DOĞAN and Bülent DAĞ

duty cycle to output voltage is provided in equation (12) (Ogata, 2010; Rashid, 2010; Garg et al., 2015; Erickson and Maksimović, 2020). Equations (13) and (14) represent the steady-state values of the duty cycle (D), the inductor current (I_L), the output voltage (V_o), and the input voltage (V_g), respectively.

$$\frac{\tilde{v}_o(s)}{\tilde{d}(s)} = C(sI - A)^{-1} B_d \quad (12)$$

$$A = A_1 D + A_2 (1 - D), \quad C = C_1 D + C_2 (1 - D) \quad (13)$$

$$B_d = (A_1 - A_2) \begin{bmatrix} I_L \\ V_o \end{bmatrix} + (B_1 - B_2) V_g \quad (14)$$

Upon substituting the equations from equations (10), 11, 13 and (14) the following equalities are obtained (Ogata, 2010; Rashid, 2010; Garg et al., 2015; Erickson and Maksimović, 2020).

$$A = \begin{bmatrix} \frac{-1}{L} \left(r_x + r_L + \frac{r_c R}{R + r_c} \right) & \frac{-R}{L(R + r_c)} \\ \frac{R}{C(R + r_c)} & \frac{-1}{C(R + r_c)} \end{bmatrix}, \quad r_x = D r_{sw} + (1 - D) r_d \quad (15)$$

$$C = \begin{bmatrix} \frac{r_c R}{R + r_c} & \frac{R}{R + r_c} \end{bmatrix}, \quad B_d = \begin{bmatrix} \frac{-1}{L} ((r_d - r_{sw}) I_L + V_g) \\ 0 \end{bmatrix} \quad (16)$$

When equation (15) and (16) are substituted into equation (12), the duty cycle to output voltage transfer function is obtained as follows:

$$G_{ud}(s) = \frac{\tilde{v}_o(s)}{\tilde{d}(s)} = \frac{R((r_d - r_{sw}) I_L + V_g)(r_c C s + 1)}{(R + r_c) L C s^2 + [L + C(r_c R + (r_x + r_L)(R + r_c))] s + (R + r_x + r_L)} \quad (17)$$

2.2. Voltage Mode PWM Control with Pi-Lead Compensator of Dc-Dc Buck Converter

The closed-loop voltage mode PWM control diagram for the Buck Converter in the s-domain is depicted in Figur (Rashid, 2010; Erickson and Maksimović, 2020). In this diagram, $\tilde{v}_o(s)$ represents the actual output voltage of the Buck Converter in the s-domain; $\tilde{v}_{o,ref}(s)$ denotes the reference value for the output voltage; $\tilde{v}_e(s)$ signifies the error value between the reference and output voltage; $G_c(s)$ refers to the transfer function of the Compensator system; $\tilde{v}_{con}(s)$ indicates the output of the Compensator Controller; $G_{PWM}(s)$ corresponds to the transfer function

of the PWM modulator; $\tilde{d}(s)$ stands for the duty value produced by the PWM; $G_{vd}(s)$ expresses the duty-cycle-to-output-voltage transfer function of the Buck Converter circuit; and $H(s)$ represents the feedback sensor gain (Franklin et al., 2002; Ogata, 2010; Rashid, 2010; Garg et al., 2015; Erickson and Maksimović, 2020; Nise, 2020). In voltage mode PWM control, the value obtained from the output voltage of the Buck Converter is compared to the reference voltage value, and an error signal is

generated. This error value is compensated in the $G_c(s)$ block, producing the $\tilde{v}_{con}(s)$ output. This output is compared to a constant sawtooth frequency curve in the PWM block, and the required switching signal for the Buck Converter switch is generated based on the obtained duty (Franklin et al., 2002; Ogata, 2010; Rashid, 2010; Garg et al., 2015; Erickson and Maksimović, 2020; Nise, 2020).

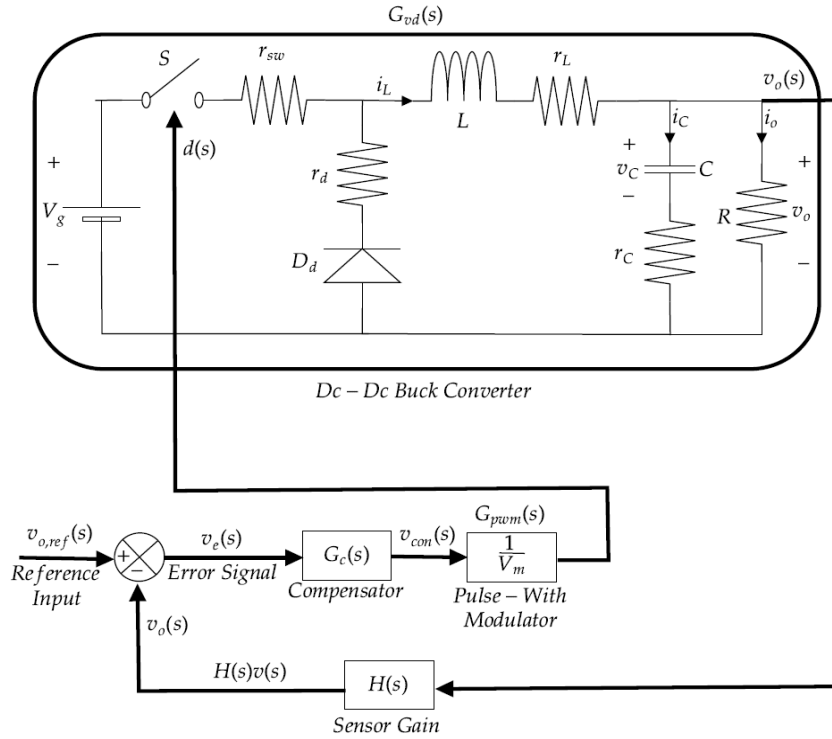


Figure 4. Closed-Loop control of DC-DC buck converter.

The open-loop transfer function of the system depicted in Figur is as follows (Ogata, 2010; Rashid, 2010; Garg et al., 2015; Erickson and Maksimović, 2020).

$$T(s) = G_c(s)G_{PWM}(s)G_{vd}(s)H(s) \quad (18)$$

In equation (18), G_{PWM} is defined as $G_{PWM}(s) = 1/V_m$. Here, V_m represents the peak voltage value of the sawtooth wave signal at the switching frequency. Therefore, $T(s)$ can be expressed as follows in equation 19 (Ogata, 2010; Rashid, 2010; Garg et al., 2015; Erickson and Maksimović, 2020).

$$T(s) = G_c(s)\frac{1}{V_m}G_{vd}(s)H(s) \quad (19)$$

2.2.1. PI-Lead compensator design

The PI-Lead Compensator is formed by cascading the PI and Lead Compensator systems together (Pressman, 2009; Ogata, 2010; Rashid, 2010; Bishop and Dorf, 2011; Basso, 2014; Corradini, 2015; Garg et al., 2015; Erickson and Maksimović, 2020; Nise, 2020; de Azpeitia, 2021).

2.2.1.1. PI compensator

Adding a PI Compensator, also known as a PI Controller, to a system allows for reducing the system's SSE and

increasing its gain in the low-frequency region (Pressman, 2009; Ogata, 2010; Rashid, 2010; Bishop and Dorf, 2011; Basso, 2014; Corradini, 2015; Garg et al., 2015; Erickson and Maksimović, 2020).

The method for the PI Compensator design involves adding a single pole to the origin. So, the PI Compensator transfer function, consisting of the K_p and K_i parameters, is as follows in equation 20 (Pressman, 2009; Ogata, 2010; Rashid, 2010; Bishop and Dorf, 2011; Basso, 2014; Corradini, 2015; Garg et al., 2015; Erickson and Maksimović, 2020; Nise, 2020; de Azpeitia, 2021).

$$G_{PI}(s) = \frac{K_p s + K_i}{s} \quad (20)$$

When deriving the closed-loop transfer function for the SSE, the following equation is obtained in equation 21 (Pressman, 2009; Ogata, 2010; Rashid, 2010; Bishop and Dorf, 2011; Basso, 2014; Corradini, 2015; Garg et al., 2015; Erickson and Maksimović, 2020; Nise, 2020; de Azpeitia, 2021).

$$\tilde{v}_e(s) = \frac{\tilde{v}_{o,ref}(s)}{1 + G_c(s)G_{PWM}(s)G_{vd}(s)H(s)} \quad (21)$$

When the PI Compensator transfer function composed of

K_p and K_i parameters from equation (20) is added to $G_c(s)$ in equation (21) the SSE is eliminated thanks to the pole at the origin (The $1/s$ term in the denominator). While the PI Compensator is crucial in reducing steady-state errors and improving the system's response, it brings along certain disadvantages. One of the primary concerns arises from adding a pole at the origin. The presence of this pole introduces a negative shift in the system's phase, affecting its phase response. The phase response is a critical aspect of system stability. Specifically, the Phase Margin, which is the difference in phase between the system's response and -180 degrees at the GCF, is a primary indicator of the system's stability. A larger PM corresponds to more excellent stability, while a smaller PM can lead to instability. When the PI Compensator induces a negative shift in the phase, the PM of the system is reduced. A lower PM indicates a system closer to instability, which is undesirable in a control system. As such, more than relying on the PI Compensator may be required to achieve the desired system performance and stability level. Other control strategies or compensator designs need to be considered to enhance the phase margin and maintain the system's stability (Franklin et al., 2002; Ogata, 2010; Rashid, 2010; Erickson and Maksimović, 2020; Nise, 2020; de Azpeitia, 2021).

2.2.1.2. Lead compensator

The Lead Compensator transfer function, composed of K_{Lead} , α and β parameters, is given as follows in equation 22 (Pressman, 2009; Ogata, 2010; Rashid, 2010; Bishop and Dorf, 2011; Basso, 2014; Corradini, 2015; Garg et al., 2015; Erickson and Maksimović, 2020; Nise, 2020; de Azpeitia, 2021).

$$G_{Lead}(s) = \frac{K_{Lead}(s + \alpha)}{(s + \beta)}, \quad (\alpha < \beta) \quad (22)$$

The Lead Compensator is another essential control component utilized for improving system stability and response. Unlike the PI Compensator, the Lead Compensator can introduce a positive shift in the system's phase. However, it is essential to note that this positive phase shift occurs around a particular frequency known as the GCF (Ogata, 2010; Rashid, 2010; Corradini, 2015; Erickson and Maksimović, 2020).

The GCF is a critical point in the frequency domain analysis of a system. It is the frequency at which the system's open-loop gain magnitude is 1 (or 0 dB). This frequency is important because it directly relates to the system's PM, a key indicator of system stability. The PM is the difference between the phase of the system's response at the GCF and -180 degrees. A larger PM indicates a more stable system (Pressman, 2009; Ogata, 2010; Rashid, 2010; Bishop and Dorf, 2011; Basso, 2014; Corradini, 2015; Garg et al., 2015; Erickson and Maksimović, 2020; Nise, 2020; de Azpeitia, 2021).

By positively shifting the system phase at the GCF, the Lead Compensator can increase the PM, thereby enhancing system stability. However, it does not contribute to reducing the SSE (Pressman, 2009; Ogata,

2010; Rashid, 2010; Bishop and Dorf, 2011; Basso, 2014; Corradini, 2015; Garg et al., 2015; Erickson and Maksimović, 2020; Nise, 2020; de Azpeitia, 2021).

The SSE measures the system's ability to accurately track a given reference signal. A smaller SSE corresponds to better tracking performance and, therefore, better system performance. A PI Compensator is typically used to reduce the SSE and increase the system's DC Gain. However, as we have discussed, relying solely on a PI Compensator can lead to stability issues due to a decreased PM. Therefore, a combined or cascaded PI-Lead Compensator can be an appropriate choice to balance these aspects. Such a configuration aims to exploit the advantages of both compensator types. The PI Compensator's ability to reduce SSE and increase DC Gain and the Lead Compensator's capacity to enhance the PM at the desired GCF ensure overall improved system performance and stability (Pressman, 2009; Ogata, 2010; Rashid, 2010; Garg et al., 2015; Erickson and Maksimović, 2020; Nise, 2020).

2.2.1.3. PI-Lead compensator

When a PI-Lead Compensator is added to the system, the PI Compensator part will eliminate the SSE in the output voltage and increase the DC Gain in the low-frequency region. The Lead Compensator part will increase the PM at the desired GCF, improving the system's transient response.

The PI-Lead Compensator transfer function can be obtained as follows by multiplying the equations in equation 23 (Garg et al., 2015).

$$G_{PI-Lead}(s) = \left(\frac{K_p s + K_i}{s}\right) * \left(\frac{K_{Lead}(s + \alpha)}{(s + \beta)}\right) = \frac{K_i K_{Lead} \left(\frac{s}{K_i} + 1\right) (s + \alpha)}{s(s + \beta)}, \quad (\alpha < \beta) \quad (23)$$

If in equation 24, we denote the $K_i * K_{Lead}$ expression as K and the K_i / K_{Lead} expression as ω_z , the $G_{PI-Lead}(s)$ transfer function can be expressed as follows (Garg et al., 2015).

$$G_{PI-Lead}(s) = \frac{K \left(\frac{s}{\omega_z} + 1\right) (s + \alpha)}{s(s + \beta)}, \quad (\alpha < \beta) \quad (24)$$

Step-by-step PI-Lead Compensator design for Buck converter is given below (Pressman, 2009; Ogata, 2010; Rashid, 2010; Bishop and Dorf, 2011; Basso, 2014; Corradini, 2015; Garg et al., 2015; Erickson and Maksimović, 2020; Nise, 2020; de Azpeitia, 2021).

- Step 1: In the first step, the transfer function of the uncompensated Buck Converter system is derived. As shown in equation 25, the Buck Converter can be seen as a system where the DC Gain remains consistently low in the low-frequency range. Additionally, it is characterized by having a low PM value.

$$G(s) = \frac{a_1 s + a_0}{b_2 s^2 + b_1 s + b_0} \quad (25)$$

As mentioned in earlier sections of this paper, to achieve a reduction in the SSE an increase in the DC Gain in the low-frequency region and an improvement in transient

response and overshoot values by increasing the PM at the desired GCF a PI-Lead Compensator will be designed. This compensator will consist of a PI section for SSE reduction and DC Gain enhancement and a Lead section for improving the PM at the selected GCF.

- Step 2: In the second step, a PI compensator is added to the system to increase the low-frequency gain and eliminate SSE. In equation 26, the PI Compensator equation, denoted by the corner frequency(ω_z) is as follows:

$$G_{PI}(s) = \frac{\frac{s}{\omega_z} + 1}{s} \quad (25)$$

ω_z is placed at an appropriate frequency lower than the GCF to increase the DC gain in the low-frequency region. The transfer function of the Buck Converter system with added PI Compensator and minimized SSE effect is as follows in equation 27.

$$G_{PI-Buck}(s) = G_{PI}(s)G(s) = \left(\frac{s}{\omega_z} + 1\right) \left(\frac{a_1s + a_0}{b_2s^2 + b_1s + b_0}\right) \quad (26)$$

$$= \frac{\frac{a_1}{\omega_z}s^2 + (a_1 + \frac{a_0}{\omega_z})s + a_0}{b_2s^3 + b_1s^2 + b_0s}$$

- Step 3: In the third step, for the Buck Converter system with PI Compensator which has reduced SSE and increased low-frequency DC Gain but has a poor transient response and reduced PM value, a Lead Compensator is added to improve transient response, increased PM, and reduced overshoot. The step-by-step method for adding the Lead Compensator is as follows: The magnitude and phase values of $G_{PI-Buck}(s)$ at the Gain Crossover Frequency (ω_{gc}) are determined in equation 28.

$$\varphi_{PI-Buck} = \angle G_{PI-Buck}(j\omega_{gc}), K_{PI-Buck} = |G_{PI-Buck}(j\omega_{gc})| \quad (27)$$

In order to obtain the necessary Phase Margin ($\varphi_{Desired}$) and Gain Crossover Frequency values for the system, the required magnitude and phase values for the Lead Compensator are provided below in equations 29 and 30.

$$K_{req} = \frac{1}{K_{PI-Buck}} \quad (28)$$

$$\varphi_{req} = -180 - \varphi_{PI-Buck} + \varphi_{Desired} \quad (29)$$

- Step 4: If the Lead Compensator transfer function in Equation (22) is expressed in terms of magnitude, phase angle, and frequency, the resulting equations are given in Equation (30) and Equation (31) below.

$$|G_{Lead}(j\omega)| = K_{Lead} \left(\frac{\sqrt{\omega^2 + \alpha^2}}{\omega^2 + \beta^2} \right) \quad (30)$$

$$\varphi_{Lead} = \angle G_{Lead}(j\omega) = \arctan\left(\frac{\omega}{\alpha}\right) - \arctan\left(\frac{\omega}{\beta}\right) = \arctan\left(\frac{\omega * (\beta - \alpha)}{\omega^2 + \alpha\beta}\right) \quad (31)$$

As stated in equation (22), since $\beta > \alpha$ in the Lead Compensator transfer function, the φ_{Lead} angle in equation (31) will always be positive.

The equation of the frequency (ω_m) at the maximum phase angle is as follows. To find the maximum phase

angle (φ_{Lead}) and maximum magnitude (K_m) values, substitute the formula from equation (32) for ω_m in place of ω in equation (31).

$$\omega_m = \sqrt{\alpha\beta} \quad (32)$$

If the maximum frequency value (ω_m) is expressed as the desired Gain Crossover Frequency (ω_{gc}), then the maximum phase angle (φ_m) becomes equal to the required phase angle (φ_{req}), and the maximum magnitude (K_m) becomes equal to the required magnitude (K_{req}).

$$\varphi_m = \frac{\omega_m(\beta - \alpha)}{\omega^2 + \alpha\beta} = \arctan\left(\frac{\beta - \alpha}{2\sqrt{\alpha\beta}}\right) \quad (33)$$

$$= \arcsin\left(\frac{\beta - \alpha}{\beta + \alpha}\right)$$

$$K_m = K_{Lead} \sqrt{\frac{\alpha}{\beta}} \quad (34)$$

To obtain the lead compensator parameters (K_{Lead} , α and β), one can utilize equations (35), 37, 38, 39, 40 and 41.

$$\omega_{gc} = \omega_m = \sqrt{\alpha\beta} \quad (35)$$

$$\varphi_{req} = \varphi_m = \arcsin\left(\frac{\beta - \alpha}{\beta + \alpha}\right) \quad (36)$$

$$K_{req} = K_m = K_{Lead} \sqrt{\frac{\alpha}{\beta}} \quad (37)$$

$$K_{Lead} = K_m \sqrt{\frac{1 + \sin \varphi_{req}}{1 - \sin \varphi_{req}}} \quad (38)$$

$$\alpha = \omega_{gc} \sqrt{\frac{1 - \sin \varphi_{req}}{1 + \sin \varphi_{req}}} \quad (39)$$

$$\beta = \omega_{gc} \sqrt{\frac{1 + \sin \varphi_{req}}{1 - \sin \varphi_{req}}} \quad (40)$$

PI-Lead Compensator Design process, as can be seen from the detailed equations above, it is necessary to optimally tune the Corner Frequency (ω_z) in the PI Compensator Section and the Phase Margin (φ_{margin}) and Gain Crossover Frequency (ω_{gc}) parameters in the Lead Compensator Section for the uncompensated Buck Converter system. However, no quantitative solution method or formula has been encountered in the literature for accurately adjusting these parameters. In the PI-Lead Compensator design, finding the best performance by trial and error for these three parameters at specific ranges may not be feasible. Even if possible, there would be more logical methods in terms of speed and time. Therefore, in this paper, the SA optimization algorithm, a type of artificial intelligence algorithm, has been utilized to find the most optimal values for ω_z , φ_{margin} , and ω_{gc} . This approach enables the attainment of performance close to, if not the best, the desired values for the PI-Lead Compensator quickly and easily (Pressman, 2009; Ogata, 2010; Rashid, 2010; Bishop and Dorf, 2011; Basso, 2014; Corradini, 2015; Garg et al., 2015; Erickson and Maksimović, 2020; Nise, 2020; de Azpeitia, 2021).

2.3. Optimally Designed PI-Lead Controller for Dc-Dc Buck Converter via Simulated Annealing Optimization Algorithm

2.3.1. Simulated annealing algorithm

The Simulated Annealing Algorithm is a meta-heuristic optimization algorithm developed based on the thermal treatment of metal solids at high temperatures. SA adopts a random search method to obtain the global best solution in optimization problems where the objective function has multiple local optima (Glover and Gary, 2006; Bose, 2020; Hekimoğlu and Ekinici, 2020; Yang, 2020; Magzoub and Thamer, 2022).

Annealing is a heating process that involves gradually heating the material from high to low temperatures. In the context of metals, this technique is used to enhance their properties. The metal is heated to a high temperature, causing the internal particles to move freely and in a disordered manner. As the temperature is gradually lowered, the particles within the metal begin to stabilize and organize, resulting in a more ordered and structured state (Fraga-Gonzalez et al., 2017; Duan et al., 2018; Hekimoğlu and Ekinici, 2020; Li et al., 2022; Magzoub and Thamer, 2022).

The SA Algorithm considers a situation similar to the annealing process of metals. The process begins at a high initial temperature, and at each iteration, it generates a new candidate solution by perturbing the current solution through a random move. The algorithm evaluates the candidate solution and decides whether to accept it based on a probability distribution dependent on the current temperature and the difference in objective function values between the current and candidate solutions. The temperature parameter controls the acceptance probability of worse solutions, thus enabling the algorithm to explore the search space while avoiding local optima. The temperature is gradually and slowly reduced according to a cooling schedule (Glover and Gary, 2006; Duan et al., 2018; Hekimoğlu and Ekinici, 2020; Yang, 2020; Li et al., 2022; Magzoub and Thamer, 2022).

As the temperature parameter decreases in the SA Algorithm, it gradually converges towards stability, potentially leading to a locally optimal solution. At this stage, the algorithm has a probability of outputting the local best solution while also increasing the chance of exploring the global best solution to some extent. The algorithm's effectiveness relies on carefully selecting the initial temperature, the cooling schedule, and the particular neighborhood structure employed to generate candidate solutions (Glover and Gary, 2006; Duan et al., 2018; Hekimoğlu and Ekinici, 2020; Yang, 2020; Li et al., 2022; Magzoub and Thamer, 2022).

In the SA Algorithm, the system's state represents the solution to the optimization problem while the energy function similar to physical annealing corresponds to the function value associated with that state. The algorithm's objective is to reach the optimal solution corresponding to the state with the lowest energy level (Duan et al.,

2018; Hekimoğlu and Ekinici, 2020; Yang, 2020; Li et al., 2022; Magzoub and Thamer, 2022).

The algorithm accepts a deteriorating solution during the solution search process with a certain probability "P" and performs the annealing operation. The mentioned probability "P" formula is as follows (Simulated Annealing Options-MATLAB, 2022).

$$P = \begin{cases} 1, & dy < 0 \\ \frac{1}{1 + \exp\left(\frac{dy}{T}\right)}, & dy \geq 0 \end{cases} \quad (41)$$

In Equation 42, dy represents the difference in cost function between the new solution and the current solution (dy = y(x2)- y(x1)). If dy<0, the probability of accepting the new solution P is 1. Otherwise, if dy≥0, the probability of accepting the new solution is given by

$$\frac{1}{1 + \exp\left(\frac{dy}{T}\right)}$$

In equation (41), T represents the annealing temperature, which varies depending on the initial annealing temperature, T₀. The relationship between them is as follows (Duan et al., 2018).

$$T_{k+1} = \alpha T_k \quad (42)$$

In equation (42), the parameter α is generally considered to be between 0.8 and 1. This paper considers the α value 0.95 (the default value). In this way, during the initial cooling stages, the temperature remains relatively high, allowing the possibility of escaping from the optimal solution (Fraga-Gonzalez et al., 2017; Duan et al., 2018; Simulated Annealing Options-MATLAB, 2022).

In this paper, the parameters of the SA Algorithm utilized for the optimization process of the PI-Lead Compensator parameters designed for the Buck Converter are presented in table 1 (Magzoub and Thamer, 2022). The variable n represents the number of variables for which the Simulated Annealing will find the optimum. In this paper, the value of n has been set to 3. These variables are for the PI-Lead Compensator to be designed for the Uncompensated Dc-Dc Buck Converter System: the corner frequency (ω_c) the bandwidth also known as Gain Crossover Frequency (GCF or ω_{gc}), and the Phase Margin parameters.

Table 1. Parameters of the simulated annealing algorithm

Parameter	Value
Max Iterations	Inf
Time Limit	Inf
Objective Limit	Inf
Annealing Function	Fast Annealing
Max Function Evaluations (3000 x n)	9000
Function Tolerance	1 x 10 ⁻⁶
Max Stall Iterations (500 x n)	1500
Reannealing Interval	100

2.3.2. PI-Lead controller optimization via simulated annealing

The open-source project, referenced as (Buck-Converter-PI-Lead-Compensator-SA, 2022), featuring performance analysis and identification of optimal PI-Lead Compensator parameters for DC-DC Buck Converters via the SA Algorithm, was developed using MATLAB within the scope of this paper.

The DC-DC Buck Converter circuit parameters, considered for conducting performance analysis and designing an appropriate PI-Lead Compensator, are provided in table 2.

Table 2. Parameters of Dc-Dc buck converter circuit

Parameter	Value
Input Voltage (V_{in})	60 V
Output Voltage (V_{out})	48 V
Output Power (P_{out})	2400 W
Inductance	6.2 μ H
Capacitance	45 μ F
Load Transient Response (\leq % of V_{out})	10
Inductance Current Ripple (D_{iL})	20
Switch Frequency (f_{sw})	200 kHz
Switch-on resistance (r_{sw})	14 m Ω
Diode forward resistance (r_d)	1 m Ω
Inductance ESR (r_L)	1.3 m Ω
Capacitance ESR (r_C)	1.72 m Ω
Sawtooth Peak (V_m)	1
Sensor Gain ($H(s)$)	1

In figure 4 the open-loop transfer function formula for the uncompensated DC-DC Buck Converter System is as follows.

$$T_{uncomp}(s) = \frac{1}{V_m} G_{vd}(s)H(s), \quad V_m = 1, \quad (43)$$

$$H(s) = 1(\text{from table 2})$$

$$r_x = Dr_{sw} + (1 - D)r_d \text{ (from equation 15)} \quad (44)$$

In Table, when the parameters are substituted into the equation for the open-loop transfer function of the DC-DC Buck Converter given in equations (43) and (44), the uncompensated system transfer function is obtained and presented in equation (45).

$$G_{vd}(s) = \frac{1.644 * 10^4 s + 2.123 * 10^{11}}{s^2 + 2.543 * 10^4 s + 3.625 * 10^9} \quad (45)$$

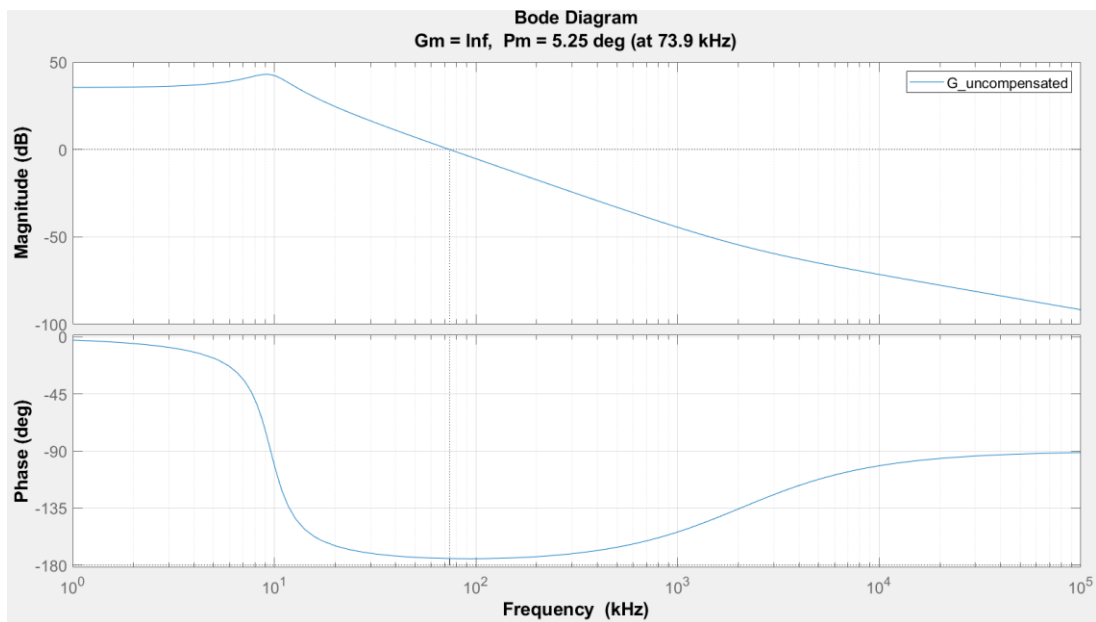


Figure 5. Frequency response of uncompensated DC–DC buck converter.

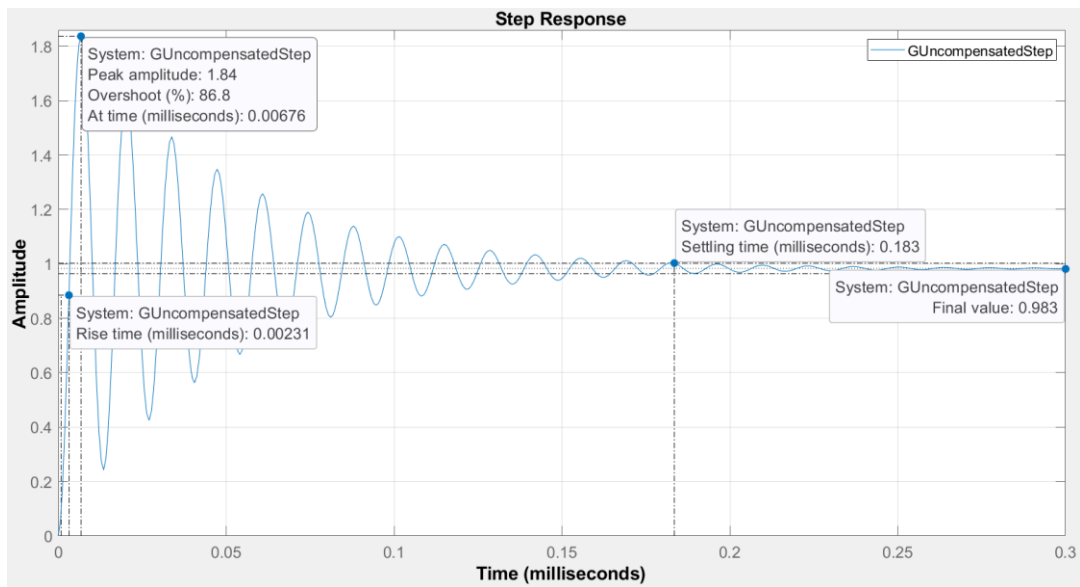


Figure 6. Step response of uncompensated DC-DC buck converter.

The frequency response (Bode plot) of the transfer function in Equation (45) is shown in Fig, while the step response is depicted in Fig.

If the frequency response and step response curves of the Uncompensated DC-DC Buck Converter System, which are located in Fig and Fig, are to be evaluated;

- PM is 5.25°, and the Overshoot (86.8%) and oscillation observed in the Step response curve in figure 6 are excessive. The transient response (settling time) value needs to be faster than 0.000183. In other words, the system response is slow. The system needs to be accelerated. For better transient response, the PM value should be at least 45° (Pressman, 2009; Ogata, 2010; Bishop and Dorf, 2011; Garg et al., 2015).
- As seen in figure 5, the Bandwidth, also known as GCF, is 73.9 kHz. The GCF value should be between Switch Frequency(f_{sw})/4 and Switch Frequency(f_{sw})/10 (i.e., according to the Switch Frequency value in table 2, it

should be between 50 kHz and 20 kHz) (Pressman, 2009; Ogata, 2010; Bishop and Dorf, 2011; Garg et al., 2015).

- The gain value in the low-frequency region is constant and low. Therefore, as shown in figure 6, the SSE could not be eliminated. For the SSE value to be reduced or eliminated in the range between 100Hz and 1kHz, the slope of the gain in the low-frequency region should preferably be -20 dB/decade (Pressman, 2009; Ogata, 2010; Bishop and Dorf, 2011; Garg et al., 2015). The block diagram for the DC-DC Buck Converter System, which includes a PI-Lead Compensator controller, can be seen in figure 7, as listed in table 2. The block diagram depicting the PI-Lead Compensator controller for the DC-DC Buck Converter System can be observed in figure 7. The DC-DC Buck Converter block within this diagram represents the transformed values of table 2 in the s-domain.

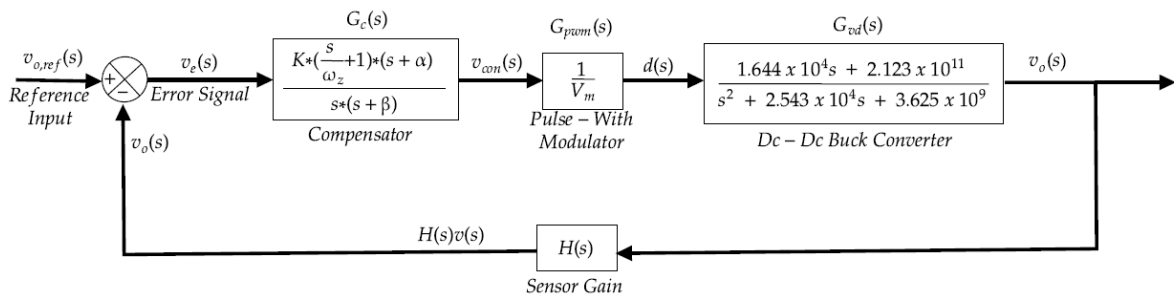


Figure 7. Buck converter system with PI-Lead compensator.

The SA optimization algorithm was utilized to determine the most optimal values for the parameters Corner Frequency (ω_z), bandwidth, also known as GCF (ω_{gc}), and PM for a PI-Lead Compensator that will be designed for the Uncompensated DC-DC Buck Converter (Pressman, 2009; Ogata, 2010; Rashid, 2010; Bishop and Dorf, 2011; Basso, 2014; Corradini, 2015; Garg et al., 2015; Erickson

and Maksimović, 2020; Nise, 2020; de Azpeitia, 2021). The detailed conceptual flow chart of the Simulated Annealing optimization approach is depicted in figure 8. The equation for the objective function (J), also known as the cost function, created for the error function represented in the flow chart in figure 8, is found by the equation below.

$$J(\text{CostFunction}) = (1 - e^{-\alpha})(E_{ss} + E_{\text{Overshoot}} + E_{\text{Undershoot}}) + e^{-\alpha}(T_s + T_r) \quad (46)$$

In the equation represented by Equation (46), the following terms are defined (Ogata, 2010; Rashid, 2010; Bishop and Dorf, 2011; Basso, 2014; Garg et al., 2015; Erickson and Maksimović, 2020; Hekimoğlu and Ekinci, 2020).

- E_{ss} = SSE (Steady State Error),
- $E_{\text{Overshoot}}$ = Percentage Overshoot,
- $E_{\text{Undershoot}}$ = Percentage Undershoot,
- T_s = Settling Time (Transient Response),
- T_r = Rise Time (Rise Time),
- α represents the coefficient factor.

In this paper, the maximum number of iterations, as

indicated in the flow chart in

Figure 8 has been taken as 5. Consequently, the outputs of each iteration in the optimization process of the PI-Lead compensator parameters, which will be added to the Buck Converter system presented in table 2, using Simulated Annealing, are provided in table 3. According to these outputs, the bode diagrams and step response graphs, obtained in both the frequency and time domain, are presented in figure 9 and 10.

In order to minimize the possibility of getting trapped in local minima, the Simulated Annealing algorithm is run multiple times from randomly chosen points. The Number of Restarts parameter defines the number of these reruns. The Number of Restarts is set to 5 for this study, and table 3 is generated.

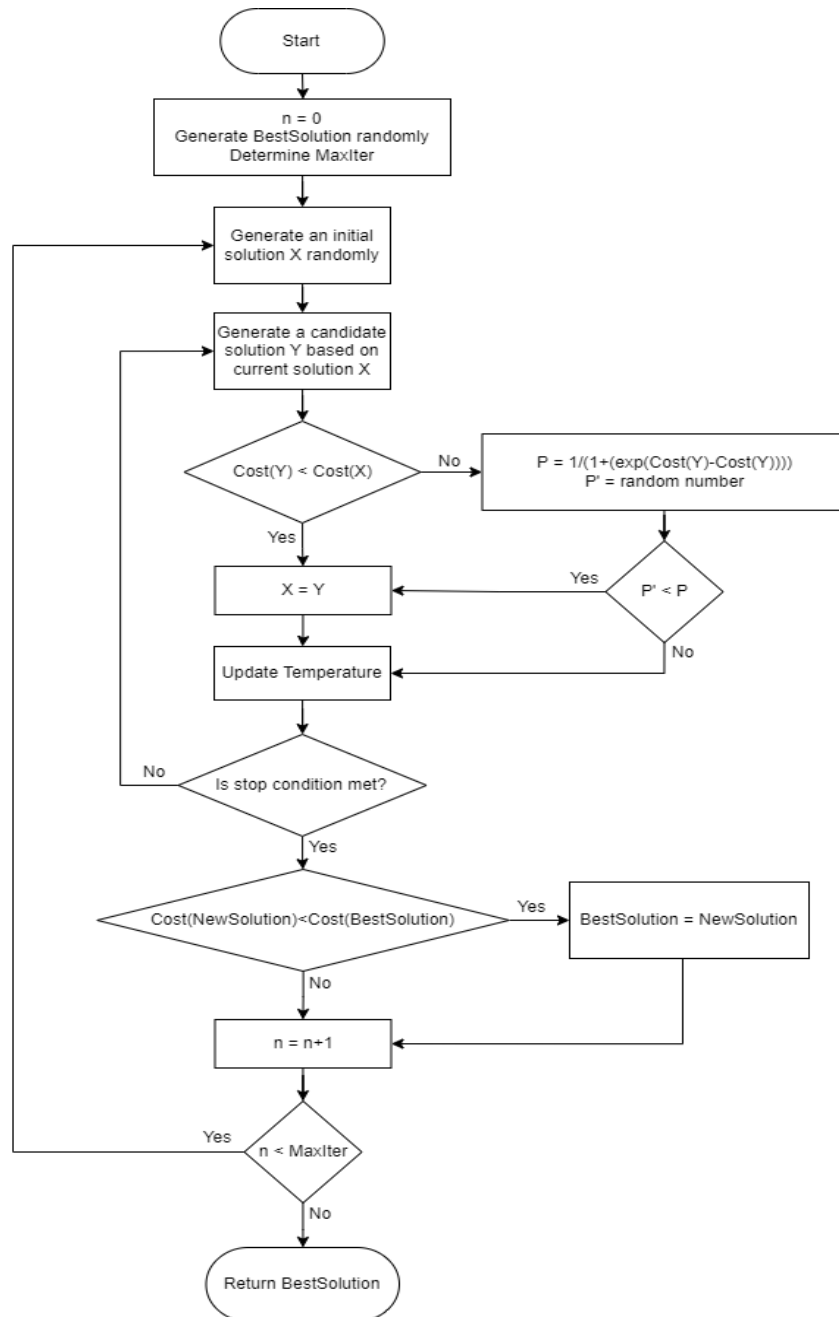


Figure 8. Flow chart of the simulated annealing optimization approach.

Table 3. Dc-Dc Buck converter system Pi-Lead compensator parameters: Outputs of Sa algorithm iterations

Number of Restart	Output of Cost Function	Corner Frequency (Hz)	Crossover Frequency (Hz)	Phase Margin
1	173.0030	1064	15174	55
2	0.1774	478	48172	62
3	0.2618	1172	26937	55
4	0.1243	1789	41900	61
5	0.0955	2153	48787	64

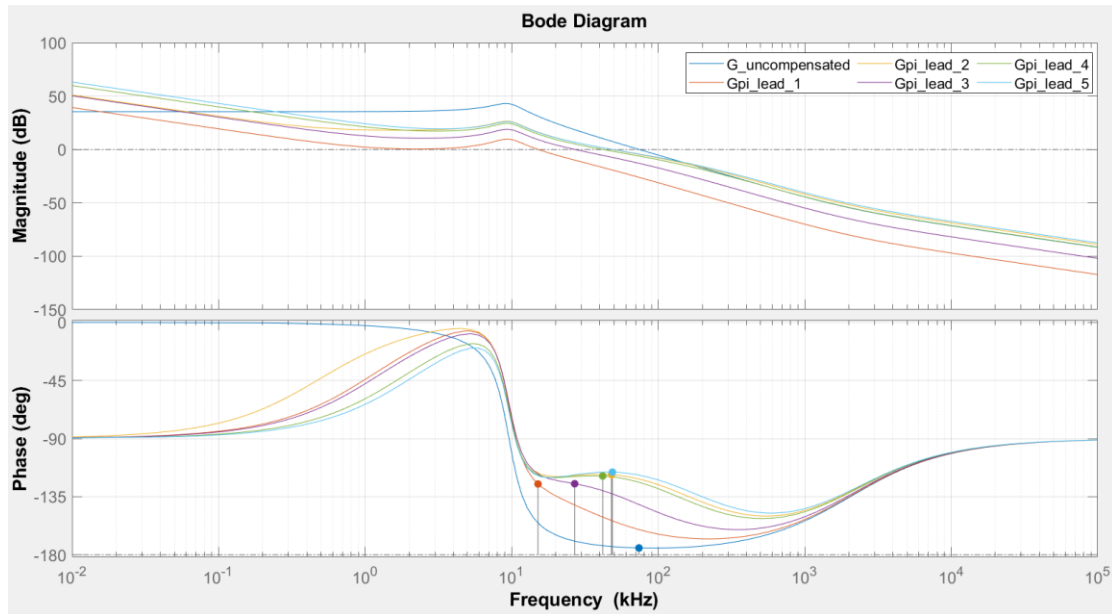


Figure 9. Compensated DC-DC buck converter with SA optimization frequency domain outputs.

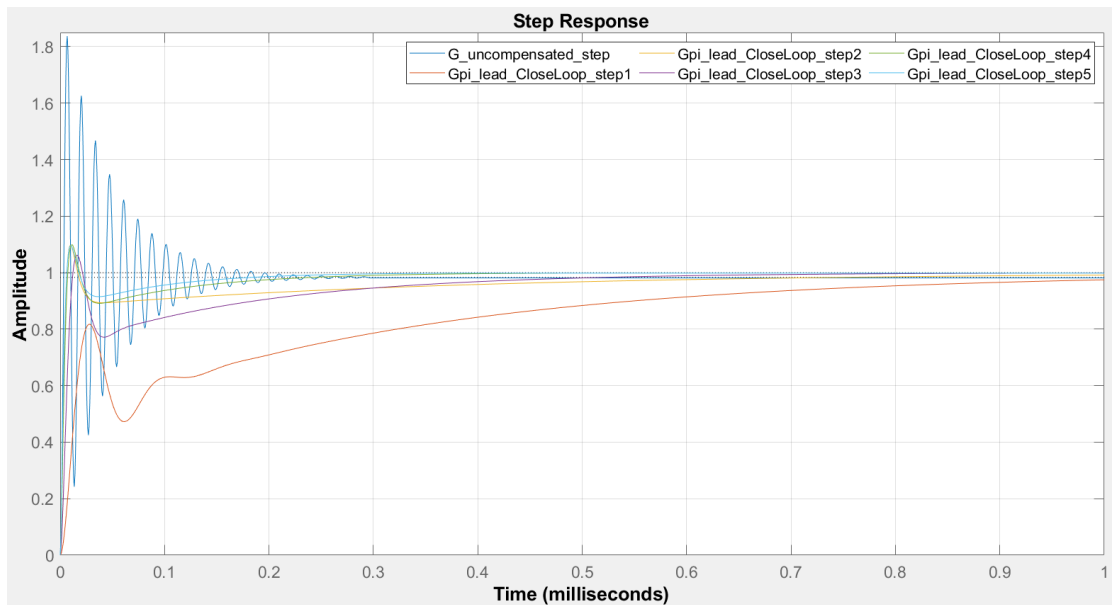


Figure 10. Compensated DC-DC buck converter with SA optimization time domain output.

3. Results and Discussion

As seen in table 4, the probability of approaching the optimal values for each parameter increases as the number of iterations increases. Each step generates the SA outcome in this procedure by starting from an independently random point. Since steps are executed

independently, it cannot be guaranteed that the results will improve at every step. When computing the best solution, the value with the lowest cost among all steps is considered the optimal solution. This operation aims to minimize the probability of encountering poor results due to the risk of SA getting trapped in local minima.

Therefore, the larger the maximum number of iterations, the higher the probability of identifying the global optimum value as the best solution.

In this paper, the transfer function from the duty cycle to the output voltage of a non-ideal DC-DC Buck Converter has been derived using the state-space averaging technique. Subsequently, a PI-Lead Compensator controller has been utilized for voltage mode PWM control, regulating the DC-DC output voltage. The parameters of this cascaded structure have been optimized using the Simulated Annealing algorithm, resulting in the improvement of the DC-DC Buck Converter system's Phase Margin, Gain Crossover Frequency (GCF), and low-frequency gain parameters, thereby enhancing its output performance.

The use of the Simulated Annealing algorithm has expedited the determination of PI-Lead Compensator parameters. This algorithm efficiently provides the most suitable value within the specified lower and upper limits, eliminating trial and error and minimizing the possibility of prediction errors. Furthermore, through multiple simulated iterations, the SA algorithm has demonstrated its effectiveness in finding optimal solutions in complex and broad search spaces for optimizing PI-Lead Compensator parameters. An essential advantage of this process is the adjustability of the iteration count, allowing fine-tuning for optimal results. As a result, the challenges encountered in controller design have been significantly reduced.

Table 4. Dc-Dc Buck Converter System Pi-Lead Compensator Outputs of Sa Algorithm Iterations

Number of Restart	Output of Cost Function	Overshoot (%)	Rise Time (s)	Settling Time (Transient Response) (s)	Steady State Error	Low Frequency Region Gain (dB)
-	Uncomp	86.8	2.31e-06	183e-06	0.983	35.4 (Constant)
1	173,0030	< 1(Unstable)	545e-06	1080e-06	1	20 (Slope)
2	0,1774	9.69	4.37e-06	680e-06	1	19.6 (Slope)
3	0,2618	6.2	8.22e-06	488e-06	1	19.8 (Slope)
4	0,1243	9.88	4.99e-06	222e-06	1	19.9 (Slope)
5	0,0955	9.55	4.35e-06	168e-06	1	20 (Slope)

However, it is essential to note that the Simulated Annealing algorithm may encounter the possibility of getting trapped in local minima. As a result, the probability of finding the global minimum value with the Simulated Annealing algorithm is maximized by starting from random points for a few iterations, as determined by the maximum iteration count. Therefore, the algorithm's efficiency is subject to its implementation and parameter settings.

The results obtained in this study provide evidence that optimizing controller parameters significantly improves the performance of the Buck Converter. Moreover, this optimization method is not limited to determining PI-Lead Compensator parameters designed explicitly for the DC-DC Buck Converter; it can also be adapted for optimizing parameters of similar compensator systems designed for other types of DC-DC converters.

This study demonstrates the potential for using heuristic algorithms in electronic circuit design for broader applications. As future work, it may be suggested to investigate the efficacy of other heuristic algorithms (for example, Genetic Algorithm, Particle Swarm Optimization, etc.) in the design of the PI-Lead compensator controller.

Author Contributions

The percentage of the author(s) contributions is presented below. All authors reviewed and approved the final version of the manuscript.

	K.D.	B.D.
C	50	50
D	50	50
S	50	50
DCP	50	50
DAI	50	50
L	50	50
W	50	50
CR	50	50
SR	50	50
PM	50	50
FA	50	50

C=Concept, D= design, S= supervision, DCP= data collection and/or processing, DAI= data analysis and/or interpretation, L= literature search, W= writing, CR= critical review, SR= submission and revision, PM= project management, FA= funding acquisition.

Conflict of Interest

The authors declared that there is no conflict of interest.

Ethical Consideration

Ethics committee approval was not required for this study because of there was no study on animals or humans.

Acknowledgements

This study has emerged as a part of my master's thesis, and I would like to express my deep gratitude to my advisor for his unwavering support throughout this process. I would like to thank ASELSAN A.Ş., who financed a part of my research and furthered my research by providing technical information and approval. Kübra DOĞAN, as the author, expresses her gratitude to this valuable institution for her contributions at every stage of the collection of outputs, data analysis and article writing. I would like to thank all the people and institutions who contributed, especially ASELSAN, for making this research happen.

References

Amaral AMR, António JMC. 2022a. Simulation tool to evaluate fault diagnosis techniques for DC-DC converters. *Symmetry* 14(9): 1886. DOI: 10.3390/sym14091886.

Amaral AMR, António JMC. 2022b. Using python for the simulation of closed-loop pi controller for a buck converter. *Signals*, 3(2): 313-325. DOI: 10.3390/signals3020020.

Basso CP. 2014. *Switch-Mode power supplies*. McGraw Hill, New York, USA, 2nd ed., pp: 117.

Bishop RC, Dorf RH. 2011. *Modern control systems*. Pearson, New York, USA, pp: 1104.

Bose BK. 2002. *Modern power electronics & AC drives*. Prentice Hall, London, UK, pp: 736.

Bose BK. 2020. *Power electronics and motor drives: advances and trends*. Academic Press, London, UK, pp: 934.

Buck-Converter-PI-Lead-Compensator-SA. 2022. URL: <https://github.com/kd94/Buck-Converter-PI-Lead-Compensator-SA> (Accessed date: March, 15, 2022).

Chibante R, 2010. *Simulated annealing: theory with applications*. Intechopen, London, UK, pp: 302.

Corradini L. 2015. *Digital control of high-frequency switched-mode power converters*. John Wiley & Sons-IEEE Press, London, UK, pp: 368.

de Azpeitia MAP. 2021. *Design and control of power converters 2019*. MDPI, Basel, Switzerland, pp: 402.

Duan W, Zhang H, Wang C. 2018. Deformation estimation for time series InSAR using simulated annealing algorithm. *Sensors*, 19(1): 115. DOI: 10.3390/s19010115.

Eiben AE, James ES. 2015. *Introduction to evolutionary computing*. Springer-Verlag, Berlin, Heidelberg, Germany, pp: 287.

Ekinci S, Baran H. 2019. Improved kidney-inspired algorithm approach for tuning of PID controller in AVR system. *IEEE Access*, 7: 39935-39947. DOI: 10.1109/ACCESS.2019.2906980.

Erickson RW, Maksimović D. 2020. *Fundamentals of power electronic*. Springer, Cham, New York, USA, 3rd ed., pp: 1103.

Feng T, Yu D, Wu B, Wang H. 2023. A micro-hotplate-based oven-controlled system used to improve the frequency stability of mems resonators. *Micromachines*, 14(6): 1222. DOI: 10.3390/mi14061222.

Fraga-Gonzalez LF, Fuentes-Aguilar RQ, Garcia-Gonzalez A, Sanchez-Ante G. 2017. Adaptive simulated annealing for tuning PID controllers. *AI Commun*, 30(5): 347-362. DOI: 10.3233/AIC-170741.

Franklin GF. 2002. *Feedback control of dynamic systems*. Upper Saddle River: Prentice hall, London, UK, pp: 928.

Gaing Z-L. 2004. A Particle swarm optimization approach for optimum design of PID controller in AVR system. *IEEE*, 19(2):

384-391. DOI: 10.1109/TEC.2003.821821.

Garg, Man M, Yogesh VH, Mukesh KP. 2015. Design and performance analysis of a Pwm Dc–Dc buck converter using PI-Lead compensator. *Arab J Sci Engin*, 40: 3607-3626. DOI: 10.1007/s13369-015-1838-z.

Glover FW, Gary AK. 2006. *Handbook of metaheuristics*. Springer Science & Business Media, London, UK, pp: 570.

Hekimoğlu B, Serdar E. 2020. Optimally designed PID controller for a DC-DC buck converter via a hybrid whale optimization algorithm with simulated annealing. *Electrica*, 20(1): 19-27. DOI: 10.5152/electrica.2020.19034.

Kazimierczuk MK. 2015. *Pulse-width modulated DC-DC power converters*. John Wiley & Sons, London, UK, pp: 960.

Li H, Hui YB, Wang Q, Wang HX, Wang LJ. 2022. Design of anti-swing pid controller for bridge crane based on PSO and SA algorithm. *Electronics*, 11.19: 3143. DOI: 10.3390/electronics11193143.

Magzoub MA, Thamer A. 2022. Optimal design of automatic generation control based on simulated annealing in interconnected two-area power system using hybrid PID—fuzzy control. *Energies*, 15.4: 1540. DOI: 10.3390/en15041540.

Middlebrook RD, Slobodan C. 1976. A general unified approach to modelling switching-converter power stages. *IEEE Power Electronics Specialists Conference*, June 8-10, Cleveland, OH, USA, pp: 18-34. DOI: 10.1080/00207217708900678.

Mohan N, Tore M. 2003. *Power electronics: converters, applications, and design*. John Wiley & Sons, London, UK, pp: 832.

Moorthi VR. 2005. *Power electronics: devices, circuits and industrial applications*. Oxford University Press, London, UK, pp: 1028.

Nalepa R, Karol N, Błażej S. 2020. Hybrid tuning of a boost converter pi voltage compensator by means of the genetic algorithm and the d-decomposition. *Energies*, 14.1: 173. DOI: 10.3390/en14010173.

Nise NS. 2020. *Control systems engineering*. John Wiley & Sons, London, UK, pp: 800.

Ogata K. 2010. *Modern control engineering*. Upper Saddle River, Prentice Hal, New Jersey, USA, pp: 904.

Pressman AI. 2009. *Switching power supply design*. McGraw-Hill Education, New York, USA, pp: 550.

Qu J, Zhang Z, Li H, Li M, Xi X. 2023. Design and experiments of a two-stage fuzzy controller for the off-center steer-by-wire system of an agricultural mobile robot. *Machines*, 11.2: 314. DOI: 10.3390/machines11020314.

Rashid MH. 2010. *Power electronics: circuits, devices, and applications*. Pearson, New York, USA, pp: 1031.

Rashid MH. 2017. *Power electronics handbook*. Butterworth-Heinemann, Berlin Germany, pp: 254.

Simulated Annealing Options-MATLAB. 2022. URL: <https://www.mathworks.com/help/gads/simulated-annealing-options.html#bq26j8s-4> (Accessed date: March, 15, 2022).

Suntio T, Messo T. 2019. *Power electronics in renewable energy systems*. MDPI AG, Basel, Switzerland, pp:604.

Surya S, Mohan KS, Sheldon W. 2021. Modeling of average current in non-ideal buck and synchronous buck converters for low power application. *Electronics*, 10(21): 2672. DOI: 10.3390/electronics10212672.

Surya S, Sheldon W. 2021. Generalized circuit averaging technique for two-switch PWM DC-DC converters in CCM. *Electronics*, 10(4): 392. DOI: 10.3390/electronics10040392.

Surya S, Sheldon W. 2021. Modeling of average current in ideal and non-ideal boost and synchronous boost converters.

- Energies, 14(16): 5158. DOI: 10.3390/en14165158.
- Umanand L. 2009. Power Electronics: essentials & applications. Wiley India Pvt. Limited, London, UK, pp: 944.
- Volkov T. 2015. Fundamentals of power electronics. Scitus Academics LLC, London, UK, pp: 306.
- Wang X, Bingwen Q, Hongdong W. 2021. Comparisons of Modeling Methods for Fractional-Order Cuk Converter. Electronics, 10.06: 710. DOI: 10.3390/electronics10060710.
- Yang C, Xie F, Chen Y, Xiao W, Zhang B. 2020. Modeling and analysis of the fractional-order flyback converter in continuous conduction mode by caputo fractional calculus. Electronics, 9(9): 1544. DOI: 10.3390/electronics9091544.
- Yang XS. 2020. Nature-inspired optimization algorithms. Academic Press, London, UK, pp: 160.
- Zeb K, Nazir MS, Ahmad I, Uddin W. 2021. Control of transformerless inverter-based two-stage grid-connected photovoltaic system using adaptive-pi and adaptive sliding mode controllers. Energies, 14(9): 2546. DOI: 10.3390/en14092546.



PI-PD CONTROLLER DESIGN BASED ON WEIGHTED GEOMETRIC CENTER METHOD FOR TIME DELAY ACTIVE SUSPENSION SYSTEMS

Abdullah TURAN¹, Hüseyin AGGUMUS¹, Mahmut DASKIN^{2,3*}

¹Sirnak University, Department of Mechanical and Metal Technologies, 7300, Sirnak, Türkiye

²İnönü University, Faculty of Engineering, Department of Mechanical Engineering, 44280, 10 Malatya, Türkiye


³Cranfield University, Energy and Sustainability Theme, MK43 0AL, Cranfield, United Kingdom


Abstract: In this study, a PI-PD controller was designed via weighted geometric center method (WGC) for a quarter vehicle model to suppress the vertical vibrations. The proposed design is based on finding the weighted geometric center of the area formed by the control parameters that make the system stable. The WGC method has two main stages. First, an area formed by the parameters of the PD controller (k_p , k_d) in the inner loop is obtained and the weighted geometric center of this area is calculated. Then, using these obtained parameters, the inner loop is reduced to a single block, and the parameters of the PI controller in the external loop (k_p , k_i) are calculated using the stability boundary curve as in the first step, and the weighted geometric center is calculated. The simulation results show that the PI-PD controller designed with the weighted geometric center method offers successful responses for the time delay quarter vehicle system.

Keywords: Quarter vehicle model, PI-PD controller, Weighted geometrical center method, Stability

*Corresponding author: İnönü University, Faculty of Engineering, Department of Mechanical Engineering, 44280, 10 Malatya, Türkiye

E mail: mahmut.daskin@inonu.edu.tr (M. DASKIN)

Abdullah TURAN  <https://orcid.org/0000-0002-0174-2490>

Hüseyin AGGUMUS  <https://orcid.org/0000-0002-7158-677X>

Mahmut DASKIN  <https://orcid.org/0000-0001-7777-1821>

Received: October 10, 2023

Accepted: December 25, 2023

Published: January 15, 2024

Cite as: Turan A, Aggumus H, Daskin M. 2024. PI-PD controller design based on weighted geometric center method for time delay active suspension systems. *BSJ Eng Sci*, 7(1): 89-95.

1. Introduction

The aim of the studies on suspension systems, which is one of the most important parts of vehicle dynamics, is to suppress the vibrations that occur in the vehicle due to road defect/roughness and to increase the vehicle's handling. To achieve this, basically three different control applications are used, namely active (Kararsiz et al., 2021) semi-active (Paksoy and Metin, 2019), and passive (Paksoy and Metin, 2020). Although active control applications show high performance, they require high cost. Semi-active control applications have higher performance, and they require less cost compared to passive control applications. Passive control applications exhibit lower performance compared to the other two control applications, while also being more affordable.

Adaptive, classical PID and robust control types, applications of quarter vehicle model on vibration control are available in the literature. Uncertainties in the system model, different operating conditions and high-performance requirements require more efficient control systems such as adaptive ones.

However, the intricate nature of adaptive control design poses challenges, rendering the process arduous. Therefore, researchers tend to use robust control methodologies to avoid poor performance output due to system and modeling uncertainties.

Adaptive and robust controllers either require very complex control and/or adaptive architectures, or the desired performance is achieved with high-order controllers.

In recent years, low-order PID controllers, which are simply used to control higher-order operations, are preferred. PID controller is widely used in industrial applications due to the simplicity of the control structures, easy to understand, easy to maintain and low cost (A Turan et al., 2019). In addition, many methods such as Ziegler-Nichols step response, Ziegler-Nichols final cycle, Cohen-Coon internal model control, error-integral criterion adjustment formulas, gain and phase margin are available in the literature to determine the optimum parameters (Åström et al., 1993; Åström and Hägglund, 1995; Ho et al., 1995; Ziegler and Nichols, 1942). However, in some cases, the closed-loop responses of the mentioned controllers may not be at the desired level (Åström et al., 1993). In the studies on the development of these methods, the desired answers are not always obtained (Zhuang and Atherton, 1993). Therefore, the studies carried out to determine the optimum controller parameters are still up to date.

The design studies for tuning the PID control parameters can be classified into three categories as optimization (Ho et al., 1998; Pai et al., 2010; A Turan and Aggumus,



2021; Turan, 2021; Yeroglu et al., 2009), tuning formulas for a particular class (Chidambaram and Sree, 2003; Luyben, 2003), and studies for determining the controller parameters region (Atic et al., 2018; Onat, 2013; Ozyetkin et al., 2018). In the literature, stability boundary location method in the calculation of PID parameters seems to have attracted more attention of researchers recently. PID controllers tuned with the proposed methods have performed successfully for certain classes of systems. However, PID controllers have inherent limitations in controlling time-delayed unstable processes (Kaya, 2003; Kaya, 2016).

Compared to traditional PID controllers, PI-PD controller structure has advantages. While PID controllers may not always show the desired performance in the control of unstable and resonant systems, PI-PD controllers show effective performance for the aforementioned systems (Kaya, 2016; Park et al., 1998; Tan, 2009). In addition, the number of PI-PD control parameters is one more than the number of PID control parameters.

Some of the important studies presented in the literature on PI-PD controller design can be found in (Nema and Padhy, 2015; Özbek and Eker, 2016; Ozyetkin et al., 2020; Padhy and Majhi, 2006). However, studies on PI-PD are not sufficient and the parameters of the controllers are adjusted after complex processes.

The proposed method in this study is based on drawing the stability boundary location, which is dependent on the controller and frequency parameters, in the parameter plane. The weighted geometric center method, which was first proposed for the PI control of time-delayed systems, is based on the stable area calculation timeline of the mentioned control parameters (Onat, 2013). The mentioned WGC method has been used in successful applications in PI/PI-PD/PID design so far (Onat et al., 2021; Onat, 2018; Onat et al., 2017; Onat et al., 2012; Ozyetkin et al., 2018; Ozyetkin et al., 2019; Ozyetkin et al., 2020; Turan et al., 2019). The advantage of the WGC method over other methods (genetic algorithm (Ahmad et al., 2014), LQR (Kumar and Jerome, 2013), Jaya algorithm (Sain et al., 2018), Ziegler-Nichols tuning (Ho et al., 1996), Astrom-Hagglund autotune (Ho et al., 1997)) is that the control parameters are calculated numerically without any optimization process.

This study consists of five sections. In Section 2, the quarter vehicle model is presented. The design procedure of the PI-PD controller is then given in Section 3. The simulation results are presented in Sections 4. The conclusions are drawn in Section 5.

2. Materials and Methods

2.1. Quarter Vehicle Model

The quarter vehicle model, which is widely preferred in studies due to its simple structure, is defined with two degrees of freedom, z_1 and z_2 , as seen in Figure 1. In the model, there are two masses named m_1 and m_2 , one suspended and the other one unsuspended, respectively (Paksoy and Metin, 2020). The connection between these

masses is the suspension system. Suspension spring coefficient is k_1 and suspension damping coefficient is c_1 . The spring coefficient of the wheel is k_2 and since the damping value is very small, it has been neglected. h is the path input applied to the model. The equations of motion of the quarter vehicle model seen in Figure 1 are given in equation 1 and 2.

$$m_1 \ddot{z}_1 + c_1(\dot{z}_1 - \dot{z}_2) + k_1(z_1 - z_2) + f_u = 0 \quad (1)$$

$$m_2 \ddot{z}_2 - k_1(z_1 - z_2) + k_2(z_2 - h) - f_u = 0 \quad (2)$$

The f_u expressed in the equations represents the force produced by the controller. Mass values for vehicle parameters are $m_1=338.8$ kg, $m_2=59$ kg. Spring coefficients are $k_1=15000$ N/m, $k_2=15000$ N/m. The damping value of the suspension is $c_1=600$ N.s/m (Paksoy and Metin, 2020). $G_p(s)$ is the transfer function of the system and it is given in equation 3.

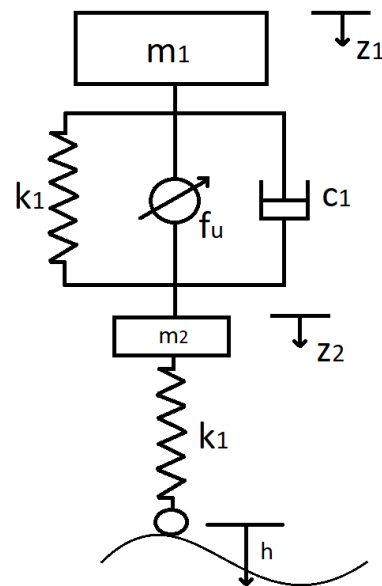


Figure 1. Quarter vehicle model.

$$G_p(s) = \frac{-0.019908s^2 + 1.7927 \cdot 10^{-8}s - 9.5276}{s^4 + 11.9446s^3 + 3518.955s^2 + 5716.5781s + 142914.4519} \quad (3)$$

PI-PD Controller Design Procedure

The diagram of the PI-PD control system is shown in Figure 2. Through the inner loop with the PD controller shown in the figure, the transfer function of the system is reduced and its response is improved. In other words, it can transform the unstable process in the open loop into the stable process in the open loop. Thus, the poles of the obtained system are better positioned. Then, the performance of the system is tried to be increased with the PI controller in the second loop.

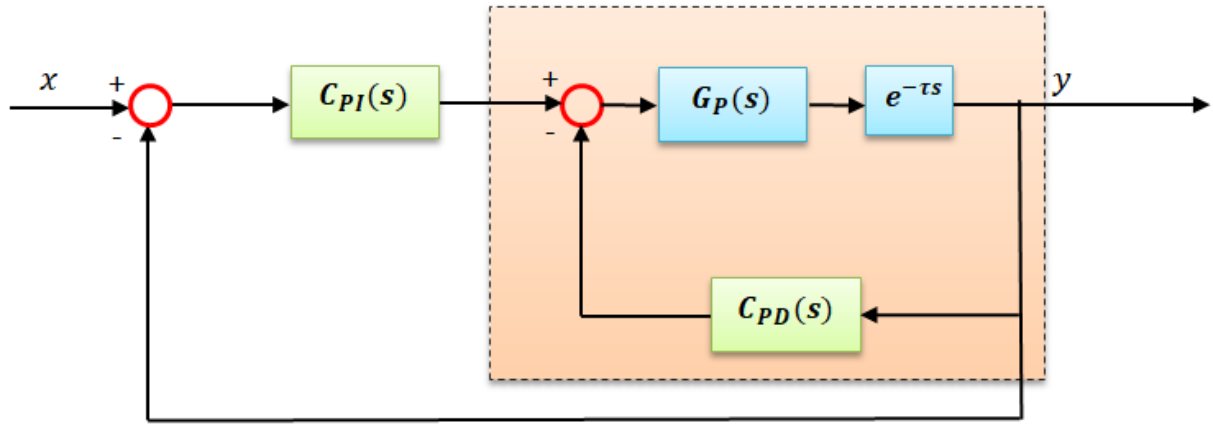


Figure 2. PI-PD Control System with time delay.

The transfer function of the system can be described as in equation 4.

$$G_P(s) = \frac{N_P(s)}{D_P(s)} \quad (4)$$

Here, τ represents delay time of the system. C_{PD} and C_{PI} are models of PD and PI controller, respectively (equations 5 and 6).

$$C_{PD}(s) = \frac{N_{PD}}{D_{PD}} = \frac{(k_f + 100k_d)s + 100k_f}{s + 100} \quad (5)$$

$$C_{PI}(s) = \frac{N_{PI}}{D_{PI}} = \frac{k_p s + k_i}{s} \quad (6)$$

Here, k_d and k_f are the derivative and proportional gains of the PD controller. k_p and k_i symbolize the proportional and integral gains of the PI controller, respectively. The closed loop characteristic equation with PD controller is given in equation 7.

$$\Delta_{PD}(s) = D_P(s)D_{PD}(s) + N_P(s)N_{PD}(s)e^{-\tau s} = 0 \quad (7)$$

The proposed design procedure consists of three steps; **Step1.** By calculating the stable area parameters of the C_{PD} , the stability region in the k_d - k_f plane is obtained. For this, if $s = j\omega$ and $e^{-\tau j\omega} = \cos(\tau\omega) - j\sin(\tau\omega)$ changes are applied in equation 8.

$$\Delta_{PD}(\tau\omega) = D_P(\tau\omega)D_{PD}(\tau\omega) + N_P(\tau\omega)N_{PD}(\tau\omega) (\cos(\tau\omega) - j\sin(\tau\omega)) = 0 \quad (8)$$

Here, if Δ_{PD} is separated to its real and imaginary part equation 9 is obtained.

$$\Delta_{PD} = R_{\Delta,PD} + jI_{PD} = 0 \quad (9)$$

Here $R_{\Delta,PD}$ and $I_{\Delta,PD}$ are functions of k_d , k_f and ω . By equating the real and imaginary parts of Δ_{PD} to zero, two equations with two unknowns with parameters (k_d , k_f) are obtained. The system of equality is given in equation 10.

$$R_{\Delta,PD}(k_f, k_d, \omega) = 0, I_{\Delta,PD}(k_f, k_d, \omega) = 0 \quad (10)$$

The equation (linear) system based on frequency (ω) is solved and then a curve is drawn with the k_d - k_f parameters obtained in the k_d - k_f plane. Finally, the stable region of this area and the WGC is determined.

2.2. Calculation of WGC Point

The WGC method is based on two principles. First, it is the computation of the region of stabilizing controller parameters. For this, the stability boundary curve method is used. The second basis of the method is to determine the WGC point of the stability area by means of the parameters forming the boundary curve of the stability region. To understand the WGC method better, the design of the PD controller in the inner loop is detailed. In this context, if two equations with two unknowns (k_d , k_f) in Eq. (7) are solved depending on the frequency (ω) (rad/s), the stability boundary locus and stability region of the PD controller is obtained as in Figure 3. Time delay of the system is considered as 0.1 s.

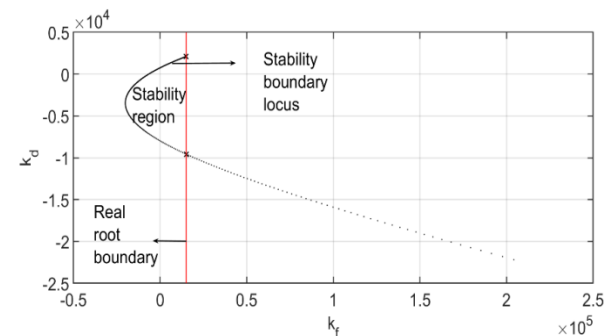


Figure 3. The stability boundary curve and stability region of PD controller.

The real root boundary line, which is formed by the change of system parameters, is the line shows the location of the closed-loop roots in the s -plane. In Figure 3, The stability region is obtained by choosing random points from different areas seen in the graph and using the Hurwitz stability test method.

In the figure, the stability boundary curve is obtained with $\omega \in [0, 15.8]$. The stability boundary curve is represented as pairs (k_f , k_d) corresponding to each value of ω . As can be seen in Figure 2, the points are located at different intervals for each ω value. The line $k_f = 15000$ indicates the boundary of the stability boundary curve. Closed stability region consists of m boundary position

points expressed as $(k_{f1}, k_{d1}), (k_{f2}, k_{d2}), \dots, (k_{fm}, k_{dm})$ coordinates and their reflections on the true root line. m reflection points can be expressed as $(15000, k_{d1}), (15000, k_{d2}), \dots, (15000, k_{dm})$ coordinates. In other words, the stability region is surrounded by $2 \cdot m$ points. $k_f=15000$ can be considered independent of ω because the stability boundary curve is limited to the true root line $k_f=15000$ (Cem Onat, 2013). As a result, using the coordinate values of the stability boundary curve points and their reflection points, the WGC points of the stability region can be obtained by equations 11 and 12, in Figure 4.

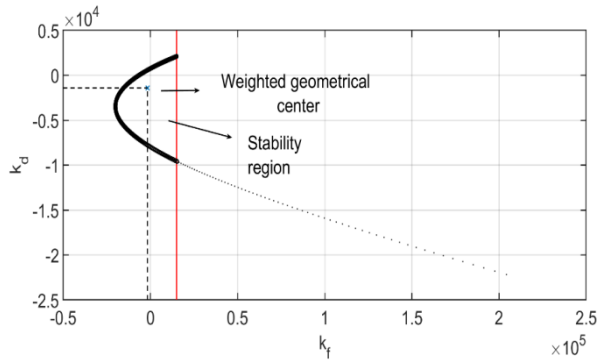


Figure 4. (k_f, k_d) pairs corresponding to each value of ω for stability boundary locus and the weighted geometrical center point.

$$k_{d\text{wgc}} = \frac{1}{m} \sum_{i=1}^m k_{d_i} \quad (11)$$

$$k_{f\text{wgc}} = \frac{1}{2m} [\sum_{i=1}^m k_{f_{ij}} + (15000 \cdot m)] \quad (12)$$

It is a fact that choosing ω with a smaller step size (e.g., 0.05 also results in larger m values) will allow us to get more accurate results than with a larger step size. Results may be affected by step size changes but have no significant effect on stability (Munevver Mine Ozyetkin et al., 2020). Thus, the WGC point of the PD controller is obtained as $(k_f, k_d) = (-1703, -1421)$.

Step 2. The inner loop is reduced using the selected PD control parameters ($k_f = -1703, k_d = -1421$). Reduced inner loop transfer function is given in equation 13.

$$G(s) = \frac{N(s)}{D(s)} = \frac{G_p(s)}{1 + G_{PD}(s)G_p(s)} = \frac{N_P(s)D_{PD}(s)e^{-\tau s}}{D_P(s)D_{PD}(s) + N_P(s)N_D(s)e^{-\tau s}} \quad (13)$$

Step 3. The purpose of the inner loop PD controller is only to achieve stability, but the purpose of the outer loop controller is to both ensure stability and meet the performance requirements of the closed loop system. Accordingly, at this stage of the controller design, the control block diagram is as shown in Figure 5.

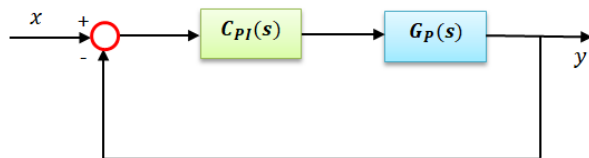


Figure 5. Reduced block diagram.

The stability region is obtained for the PI controller by means of the reduced transfer function in the k_p-k_i plane. PI controller parameters can also be calculated using the given procedure for calculating the C_{PD} parameters. The application of $s = j\omega$ change to the characteristic equation of the outer loop is given in equation 14 (Maslen and Schweitzer, 2009).

$$\Delta_{PI}(j\omega) = D(j\omega)D_{PI}(j\omega) + N(j\omega)N_{PI}(j\omega)e^{-j\tau\omega} = 0 \quad (14)$$

If Δ_{PI} is decomposed into its virtual and real parts (equation 15);

$$\Delta_{PI} = R_{\Delta_{PI}} + I_{\Delta_{PI}} = 0 \quad (15)$$

If the procedure described above to obtain the PD controller parameters is also used to obtain the PI parameters, the following equations are obtained. By solving the set of (linear) equations depending on the frequency (ω), the stability region as in Figure 6 and WGC are determined by plotting the obtained k_p and k_i parameters in the $k_p - k_i$ plane in Figure 7. It is a fact that choosing ω with a smaller step size (eg 0.01 also results in larger m values) will allow us to get more accurate results than with a larger step size. Thus, the WGC point of the PI controller is obtained as $(k_p, k_i) = (-5185, -20870)$.

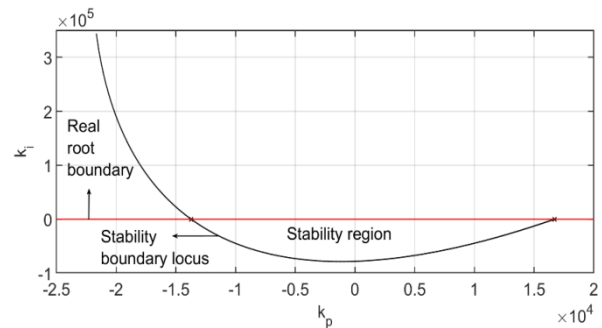


Figure 6. The stability boundary curve and stability region of PD controller

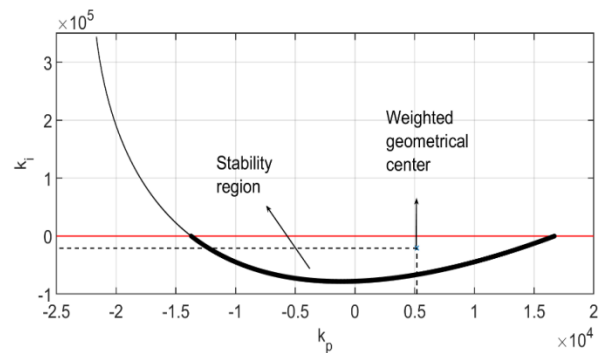


Figure 7. (k_p, k_i) pairs corresponding to each value of ω for stability boundary locus and the weighted geometrical center point.

3. Results and Discussion

Simulations were performed with MATLAB-Simulink software to examine the effectiveness of the proposed control method on the system. In the quarter vehicle

model, the displacement and acceleration responses of the vehicle body were evaluated. In addition, the PSD (Power Spectral Density) response of the system was examined for performance analysis in the frequency domain. ISO 8606 Norm is used for road surface profile classification (Agostinacchio et al., 2014). This standard, in which road pressure is classified according to different categories, is often preferred to test control performances in vehicle vibrations (Paksoy & Metin, 2020). An ISO 8608 standard C class road entrance seen in Figure 8 has been applied to the system. Vehicle speed is accepted as 30 m/s.

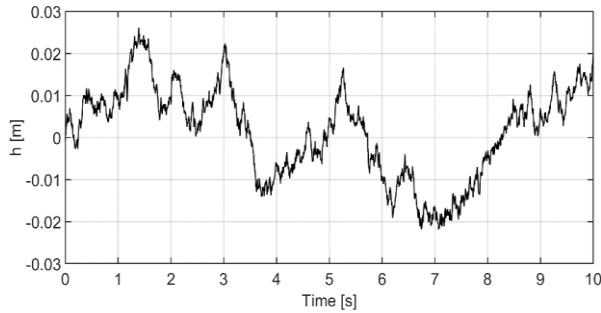


Figure 8. ISO C class road entrance.

In the simulations, the passive situation where there is no control application in the system and the situation with the PI-PD controller designed with the WGC method are compared. The most important data in terms of comfort in vehicles are acceleration responses. Another important data is the displacement responses. Displacement responses are given in Figure 9 and simulation results of acceleration responses are given in Figure 10. It is clearly seen that the controlled state is more effective than the passive state in suppressing both displacement and acceleration responses.

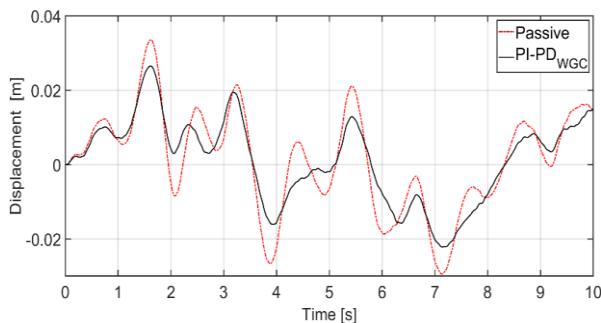


Figure 9. Suspension displacement

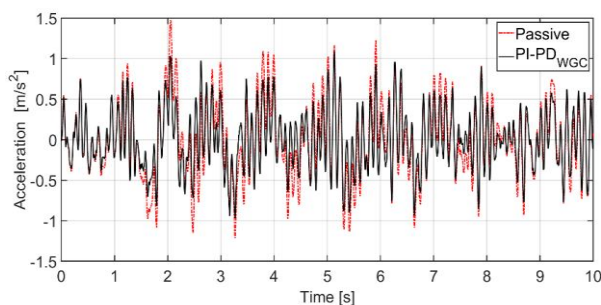


Figure 10. The acceleration of the vehicle body.

In order to analyze the system responses in the frequency domain, the PSD values of the system were examined. Figure 11 shows the acceleration PSD values of the vehicle body. It has been observed that the state in which the controller acts suppress the resonance peaks more effectively than the passive state.

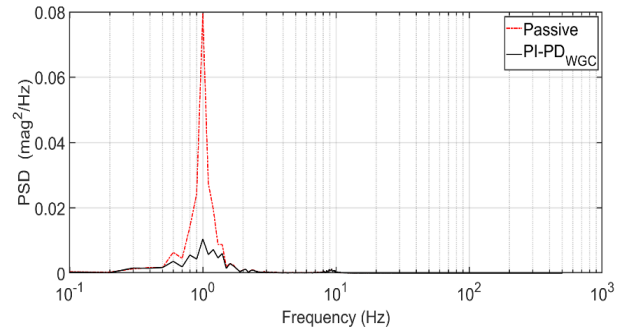


Figure 11. PSD response of vehicle body acceleration.

In order to see the results more clearly, RMS (Root Mean Square) values are given in Table 1 for the numerical evaluation of the system responses. The amount of improvement in displacement RMS value of the body is 16.6%, and in acceleration values it is 21%.

Table 1. RMS values

Control cases	z_1	\ddot{z}_1
Passive	0.0141	0.4767
PI – PD _{WGC}	0.0117	0.3765

While evaluating control performance, suspension displacement (z_1-z_2), whose limits are set according to the passive control situation, also needs to be considered. In Figure 12, PI – PD_{WGC} control condition also reduced suspension displacements.

4. Conclusion

In this study, PI-PD was designed with the WGC method, which is an effective and simple tuning method for a time-delayed quarter vehicle model. The method is based on calculating stabilizing PD and PI controller parameter regions plotted using the stability boundary locus in the (k_r, k_d) -plane and the (k_p, k_i) -plane and computing the weighted geometrical centres of these regions. The proposed method does not use any circular optimization algorithm. The fact that the method allows to calculate the controller parameters numerically on the model offers a good numerical solution to control engineers, especially for practical applications. The simulation results clearly show that the PI PD controller designed with the proposed method for the quarter-car model with the targeted delay time is successful in suppressing the system responses.

Designed using the WGC method, the PI-PD controller can be easily applied to any system class to improve the

performance of processes. In future studies, controller parameters can be optimized with meta-heuristic algorithms using artificial intelligence techniques.

Author Contributions

The percentage of the author contributions is presented below. The author reviewed and approved the final version of the manuscript.

%	A.T.	H.G	M.D.
C	40	30	30
D	50		50
S		100	
DCP	100		50
DAI		50	50
L	50	50	
W	30	40	30
CR	20	20	60
SR			100
PM	20	20	20
FA	20	20	20

C=Concept, D= design, S= supervision, DCP= data collection and/or processing, DAI= data analysis and/or interpretation, L= literature search, W= writing, CR= critical review, SR= submission and revision, PM= project management, FA= funding acquisition.

Conflict of Interest

The authors declared that there is no conflict of interest.

Ethical Consideration

Ethics committee approval was not required for this study because of there was no study on animals or humans.

References

Ahmad I, Shahzad M, Palensky P. 2014. Optimal PID control of magnetic levitation system using genetic algorithm. *IEEE International Energy Conference and Exhibition (EnergyCon)*, May 13-16, Dubrovnik, Croatia, pp: 1-5.

Åström KJ, Hägglund T. 1995. *Pid controllers: theory, design, and tuning*. The international society of measurement and control. URL: <https://aicp.files.wordpress.com/2012/07/1-0-1-k-j-astrom-pid-controllers-theory-design-and-tuning-2ed.pdf> (accessed date: March 21, 2023).

Åström KJ, Hägglund T, Hang CC, Ho WK. 1993. Automatic tuning and adaptation for PID controllers-a survey. *Control Eng Pract*, 1(4): 699-714.

Atic S, Cokmez E, Peker F, Kaya I. 2018. PID controller design for controlling integrating processes with dead time using generalized stability boundary locus. *IFAC*, 51: 924-929.

Chidambaram M, Sree RP. 2003. A simple method of tuning PID controllers for integrator/dead-time processes. *Comp Chem Engin*, 27(2): 211-215.

Ho MT, Datta A, Bhattacharyya SP. 1996. A new approach to feedback stabilization. *Proceedings of 35th IEEE Conference on Decision and Control*, December 15-17, Kobe, Japan, pp: 4643-4648.

Ho MT, Datta A, Bhattacharyya, SP. 1997. A linear programming

characterization of all stabilizing PID controllers. *Proceedings of the American Control Conference*, June 15-17, New Mexico, Mexico, 6: 3922-3928.

Ho WK, Hang CC, Cao, LS. 1995. Tuning of PID controllers based on gain and phase margin specifications. *Automatica*, 31(3): 497-502.

Ho WK, Lim KW, Xu W. 1998. Optimal gain and phase margin tuning for PID controllers. *Automatica*, 34(8): 1009-1014.

Kararsiz G, Paksoy M, Metin M, Basturk, HI. 2021. An adaptive control approach for semi-active suspension systems under unknown road disturbance input using hardware-in-the-loop simulation. *Tran Inst Meas Control*, 43(5): 995-1008.

Kaya I. 2003. A PI-PD controller design for control of unstable and integrating processes. *ISA Trans*, 42(1): 111-121.

Kaya I. 2016. PI-PD controllers for controlling stable processes with inverse response and dead time. *Electr Eng*, 98(1): 55-65.

Kumar EV, Jerome J. 2013. LQR based optimal tuning of PID controller for trajectory tracking of magnetic levitation system. *Prodecia Eng*, 64: 254-264.

Luyben WL. 2003. Identification and tuning of integrating processes with deadtime and inverse response. *Ind Eng Chem Res*, 42(13): 3030-3035.

Maslen EH, Schweitzer G. 2009. *Magnetic bearings: theory, design, and application to rotating machinery*. In *Magnetic Bearings*. Springer, New York, USA, pp: 521.

Nema S, Padhy PK. 2015. Identification and cuckoo PI-PD controller design for stable and unstable processes. *Trans Inst Meas Control*, 37(6): 708-720.

Onat C, Daskin M, Turan A, Özgüven ÖF. 2021. Manyetik levitasyon sistemleri için ağırlıklı geometrik merkez yöntemi ile PI-PD kontrolcü tasarımı. *Müh Makina*, 62: 556-579.

Onat C. 2018. A new design method for PI-PD control of unstable processes with dead time. *ISA Trans*, 84: 69-81.

Onat C, Sahin M, Yaman Y. 2013. Optimal control of a smart beam by using a luenberger observer. *3rd International Conference of Engineering Against Failure (ICEAF III)*, 26-28 June, Kos, Greece, pp: 804-811.

Onat C, Turan A, Daskin, M. 2017. WGC based PID tuning method for integrating processes with dead-time and inverse response. *International Conference on Mathematics and Engineering*, 10 - 12 May, İstanbul, Türkiye, pp: 274-279.

Onat C. 2013. A new concept on PI design for time delay systems: weighted geometrical center. *Int Innov Comp Inf Control*, 9(4): 1539-1556.

Onat C, Hamamci SE, Obuz S. 2012. A practical PI tuning approach for time delay systems. *IFAC Proceed*, 45(14): 102-107.

Özbek NS, Eker I. 2016. Gain-scheduled PI-PD based modified Smith predictor for control of air heating system: experimental application. *International Mediterranean Science and Engineering Congress*, 26-28 October, Adana, Türkiye, pp: 706-715.

Ozyetkin MM, Onat C, Tan N. 2018. PID tuning method for integrating processes having time delay and inverse response. *IFAC-PapersOnLine*, 51(4): 274-279.

Ozyetkin MM, Onat C, Tan, N. 2019. PI-PD controller design for time delay systems via the weighted geometrical center method. *Asian J Control*, 22(5): 1811-1826.

Ozyetkin MM, Onat C, Tan, N. 2020. PI-PD controller design for time delay systems via the weighted geometrical center method. *Asian J Control*, 22(5): 1811-1826.

Padhy PK, Majhi S. 2006. Relay based PI-PD design for stable and unstable FOPDT processes. *Comp Chem Eng*, 30(5): 790-796.

- Pai NS, Chang SC, Huang CT. 2010. Tuning PI/PID controllers for integrating processes with deadtime and inverse response by simple calculations. *J Process Control*, 6: 726-733.
- Paksoy M, Metin M. 2019. Nonlinear semi-active adaptive vibration control of a half vehicle model under unmeasured road input. *J Vib Control*, 25(18): 2453-2472.
- Paksoy M, Metin M. 2020. Nonlinear adaptive semiactive control of a half-vehicle model via hardware in the loop simulation. *Turk J Electr Eng Comput Sci*, 28(3): 1612-1630.
- Park JH, Sung SW, Lee IB. 1998. An enhanced PID control strategy for unstable processes. *Automatica*, 34(6): 751-756.
- Sain D, Swain SK, Mishra SK. 2018. Real Time Implementation of Optimized I-PD Controller for the Magnetic Levitation System using Jaya Algorithm. *IFAC-PapersOnLine*, 51(1): 106-111.
- Tan N. 2009. Computation of stabilizing PI-PD controllers. *Int J Control Autom Syst*, 7(2): 175-184.
- Turan A, Aggumus A. 2021. Implementation of Advanced PID Control Algorithm for SDOF System. *J Soft Comp Artif Intell*, 2(2): 43-52.
- Turan A, Onat C, Şahin M. 2019. Active vibration suppression of a smart beam via PID controller designed through weighted geometric center method. 10th Ankara International Aerospace Conference, AJAC-2019, 13-15 September, Ankara, Türkiye, pp: 79.
- Turan A. 2021. Improved optimum PID controller tuning by minimizing settling time and overshoot. in *advances in machinery and digitization*. URL: https://assets.researchsquare.com/files/rs-844641/v1_covered.pdf?c=1631877580 (accessed date: March 15, 2022).
- Yeroglu C, Onat C, Tan N. 2009. A new tuning method for PID controller. *International Conference on Electrical and Electronics Engineering-ELECO 2009*, 5-8 November, Bursa, Türkiye, pp: 12-316.
- Zhuang M, Atherton DP. 1993. Automatic tuning of optimum PID controllers. *IET Control Theory Appl*, 140(3): 216-224.
- Ziegler JG, Nichols NB. 1942. Optimum settings for automatic controllers. *Transact Amer Soc Mechan Engin*, 69(8): 759-765.



AN INTEGRATED OVERVIEW OF BLASTING DAMAGE CRITERIA FOR ENGINEERING STRUCTURES

Davut YILMAZ^{1*}

¹Ankara Yıldırım Beyazıt University, Department of Civil Engineering, 06010, Ankara, Türkiye

Abstract: Blasting applications are frequently used during the construction of engineering structures. In our country, damage assessment criteria created by reference to the Report of Investigations RI 8507 prepared by the United States Bureau of Mines (USBM) are used to control the impact of blast vibrations on existing structures or structures under construction. In this study, the structures in the database of that report of investigation and the points on which the damage criteria are based are examined. Moreover, in the light of the other studies carried out by different researchers about the blast damage criteria in engineering structures, the requirement of reevaluation of USBM damage criteria for reinforced concrete buildings, tunnels, pipelines and other engineering structures has been revealed.

Keywords: Blasting, Damage criteria, Peak particle, Velocity

*Corresponding author: Ankara Yıldırım Beyazıt University, Department of Civil Engineering, 06010, Ankara, Türkiye

E mail: yilmazdavut1967@gmail.com (D. YILMAZ)

Davut YILMAZ <https://orcid.org/0000-0002-9981-7875>

Received: December 05, 2023

Accepted: December 27, 2023

Published: January 15, 2024

Cite as: Yılmaz D. 2024. An integrated overview of blasting damage criteria for engineering structures. BŞJ Eng Sci, 7(1): 96-108.

1. Introduction

The effects of blast-induced vibrations on existing or structures being built in our country are controlled by the Environmental Noise Management and Evaluation Regulation, which has been created with reference to the Research Report RI 8507 prepared by the United States Bureau of Mining Affairs (USBM).

However, USBM Research Report RI 8507 is based on data from the effects of blasting vibrations, particularly from coal mine operations, on wood-framed, plaster or gypsum-clad 1-2 stories buildings. Therefore, the research report in question loses its validity for reinforced concrete buildings, tunnels, pipelines and similar engineering structures.

Considering the criteria in the USBM Research Report RI 8507, the limit values selected for blast-induced vibrations are even below the vibration values that may be generated by construction machinery in some cases.

The researcher (Wiss, 1981) has given the vibrations of a 0.46 kg explosive depending on the distance in Figure 1 for reference with various construction machines, trucks, rock breakers. As can be seen in Figure 1, it is possible for a truck to pass at approximately 1 meter from a structure, to create a particle velocity of 25 mm/s in the structure.

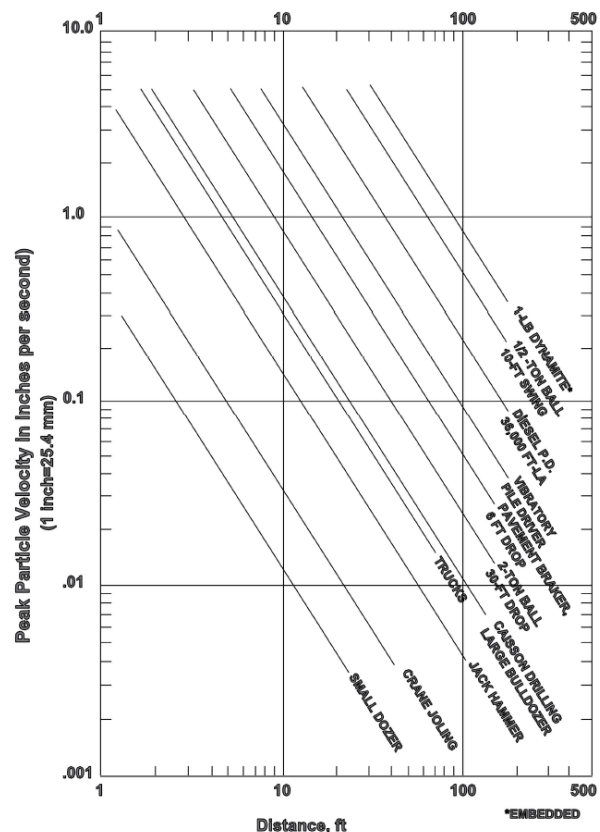


Figure 1. Relative magnitude of vibrations from construction machinery (Wiss, 1981).

These peak particle velocities are further increased by the effect of vibrations, especially in bridges built in the past with high oscillations. In addition, hydraulic



breakers used right next to the buildings in excavations in the city can create particle velocities of about 100 mm/s. Similar effects apply to roller compacted concrete dams (RCD). In such dams, the concrete layer, which is usually 30-40 cm thick, is transported by large trucks (trucks), laid with dozers and compacted with rollers.

Considering that the trucks are as close as the layer thickness to the concrete, which has just gained a part of its strength, it is possible for the peak particle velocities to reach 50 mm/s. In addition to these, regardless of whether the concrete that is getting its setting is mass or structural concrete, or the concrete that has reached a certain age and is gaining its strength, the permissible vibration values may be chosen unnecessarily low, and the construction speed could be unnecessarily reduced, and accordingly, the construction costs increase. These considerations reveal the necessity of reviewing the USBM damage criteria for engineering structures.

The aim of this study is to reevaluate the damage criteria for reinforced concrete buildings, tunnels, pipelines, and similar engineering structures by examining the data on which the USBM Research Report RI 8507 damage criteria are based.

2. Damage Criteria of USBM RI 8507

The USBM damage criteria developed for the protection of wood-framed, gypsum or gypsum-clad 1-2-story buildings from blast-induced vibrations of open coal mines were adopted by the Open Mining Operations (OSM) Bureau in 1983 with little change. Later, the USBM damage criteria was made a part of Open Coal Mine legislation and entered into force throughout the USA in 2001.

In the USBM Research Report RI 8507, vibration limits are given for the most typical and common 1-2 stories buildings with wood frame, plaster or plasterboard cladding in the USA. Peak particle velocity (PPV) or displacement limits measured in the foundation soil close to the structure, which depend on the prevailing vibration frequency, are used to evaluate the possible crack formation in these structures (Siskind et al., 1980).

In the USBM Research Report RI 8507, blast points in an open coal mine operation; High amplitude low frequency cascading waves were considered surface waves when their closest distance to structures in the database was over 75 meters (or even 100 meters). The reason for this is probably 1.5-3 m thick soil covers (Siskind et al., 1980). In other measurements included in the USBM Research Report RI 8507, the thickness of the cover is 0-1.5 m in construction excavations, the distance to the measurement point is 10-50 m, and the thickness of the cover in the quarries is less than 3 m. The frequency distribution of the explosions is given in Figure 2.

At 15-75 m distances from the blasting point, the strongest waves are surface waves (Siskind, 2005). Rayleigh surface waves are created by the interaction of pressure (P) and shear waves (S) with geological structures, and by the ground-air interface effect. One of

the characteristics of surface waves is that the amplitude of motion decreases rapidly with depth from the surface. The thickness of the surface layers and the propagation speed determine the frequencies of Rayleigh surface waves.

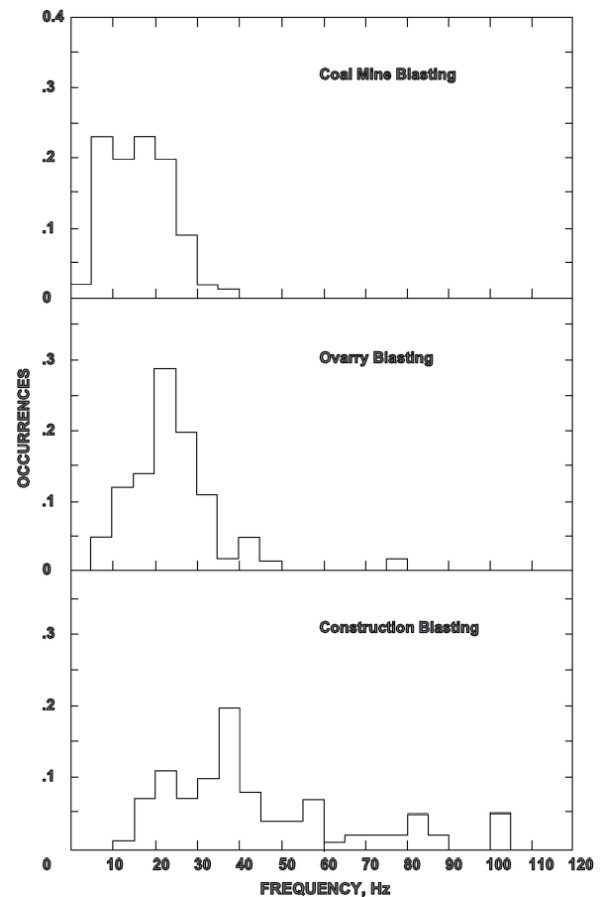


Figure 2. Frequencies of vibrations from coal mine, quarry, and construction blasting (Siskind et al., 1980).

The USBM Research Report RI 8507 does not evaluate the impact of vibrations on structures using structural vibration measurements. The main purpose of the USBM damage criteria is to prevent the formation of resonant horizontal frequencies since the frequencies created by the blasts in open coal mines may coincide with the natural frequencies of the structures in the database, and thus to prevent damage to these structures. Peak particle velocities in the USBM damage criteria are given as 12.7 mm/s and 19.0 mm/s, respectively, in the resonance region with a frequency band of 4 to 12 Hz for the structures in question. These limits, which were determined to prevent the formation of cosmetic cracks in buildings, were obtained from the division of ground vibrations with a maximum building amplification coefficient of 4.5.

In the USBM Research Report RI 8507, structural damage is classified based on the structure's response to ground vibrations. According to the definition of structural damage, damages are divided into 3 classes and are shown in Figure 3. These three types of damage identified are classified as follows: (1) Threshold: paint

removal, small cracks in wall coverings at the corners of the building, growth of old cracks, (2) Slight damage: loosening and removal of wall coverings, openings in stone walls cracks close to partitions in places, cracks up to 3 mm, spillage of loose mortar materials, (3) Major

damage: formation of many cracks larger than 3 mm, ruptures in arched structures, conditions causing structural weakness, spills in masonry walls, reduction in structural load carrying capacity.

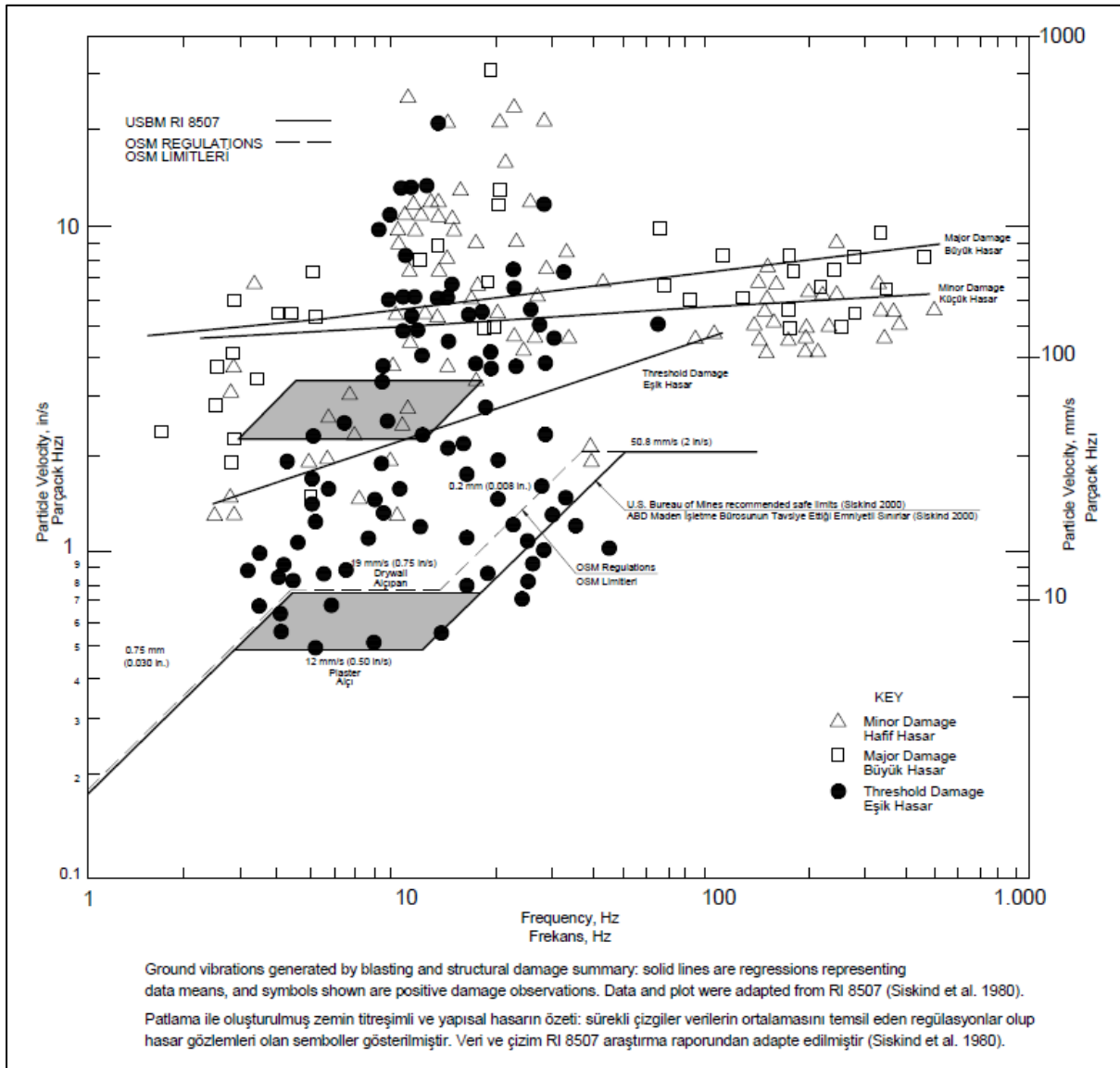


Figure 3. Damage Criteria of USBM and OSM (Siskind et al., 1980; Svinkin, 2015)

Siskind (2005) created the damage graph in Figure 3 by reporting 233 boundary, minor and major damage from blast-induced vibrations belonging to a total of 718 opencast mines and quarries. The maximum allowable particle velocity is over 51 mm/s and the data without any damage were not included in the study. When the data are examined, it is seen that the damage depends on the dominant frequency of the blast and the peak particle velocity. In the study in question, the frequency of vibrations and the frequencies of structures do not overlap in regions where the frequency is between 2-5 Hz and 60-450 Hz. In these regions, the response of the structure to blast-induced vibrations is determined by the soil-structure interaction. Peak particle velocities that can damage the structure are between 33-191 mm/s in

the region where the frequencies are between 2 and 5 Hz, and between 102-254 mm/s in the region where the frequencies are between 60-450 Hz, which is considerably higher than the USBM damage limit values (Svinkin, 2007). In this case, for cases where the natural frequency of the structure and the frequency of blasting vibrations do not coincide, the USBM limits are set on the very safe side, and it unnecessarily limits the applications in practical life.

The amplitude, frequency and significant vibration duration of the blast-induced vibration waves recorded on the ground vary depending on the location of the blasting application. Among the most important reasons for this change are the encountering of vibration waves with different geological structures as they progress, the

spread of vibration waves over a larger area, and the absorption of motion, especially at high frequencies. The blast design and excavation geometry, the delay interval, the amount of explosive used in each delay interval, the direction of the blasting, the thickness of the blasted unit and the distance between the blast holes determine the characteristic of vibration waves in the regions close to the blast source. The impact of the blast design on the characteristics of vibration waves decreases in regions far from the blasting source whereas the effect of the transmitting ground rock and the soil cover layer on this rock increases (Siskind et al., 1980).

The damage criteria created by the Ministry of Environment and Urbanization with reference to the USBM Research Report RI 8507 are given in the Environmental Vibration Principles and Criteria section of the Environmental Noise Management and Evaluation Regulation. In this section, blasting in mines and quarries and areas where similar activities are carried out should not damage the surrounding structures. It is stated that the vibration level to be measured on the ground next to the closest building to blasting cannot exceed the values given in Table 1. It is seen that the values given in Table-1 are the values determined by the USBM damage criteria.

Table 1. The highest allowable values of the vibrations that will occur due to blasting in mines and quarries and similar areas, the closest very sensitive (Annex: RG-27/4 / 2011-27917) and ground vibrations that will be created outside the sensitive area of use)

Vibration Frequency (Hz)	Maximum Allowable Peak Particle Velocity (mm/s)
1	5
4-10	19
30-100	50

3. Damage Criteria

3.1. Crandell Damage Criteria

The first studies on the establishment of damage criteria were made by Crandell. Energy Ratio (E.R.) defined by Crandell (1949). The relationship between particle velocity and energy ratio is presented in Equation 1.

$$\text{Crandell Energy Ratio} = E.R. = \frac{a^2}{f^2} \quad (1)$$

Where, a= acceleration (ft/s²), f= frequency (Hertz).

Since the relationship between displacement (D) and particle velocity (V) in a harmonic wave motion is given as $D=V/(2\pi f)$ depending on the frequency (f), the displacement also changes depending on the change in frequency. Thick soil cover and long distances on the rock cause low frequency and long duration wave movements. As a result, this change in motion increases the building response and the potential for damage to nearby structures (Siskind et al., 1980). It is possible to calculate the Energy Ratio for sinusoidal motion with the help of Equation 2.

$$E.R. = \frac{a^2}{f^2} = \frac{4\pi^2 f^2 v^2}{f^2} = 4\pi^2 v^2 \quad (2)$$

As can be seen from Equation 2, the Energy Ratio is proportional to the square of the peak particle velocity and is independent of the frequency, unlike the USBM criterion. Crandell Energy Ratio suggested the E.R.= 3 limit as the safe limit, which corresponds to a peak particle velocity of approximately 83.8 mm/s (3.3 inch/s) (Figure 4). However, the more commonly used Energy Ratio value is E.R.=1, and according to this value, the peak particle velocity becomes 48.3 mm/s (Bollinger, 2018).

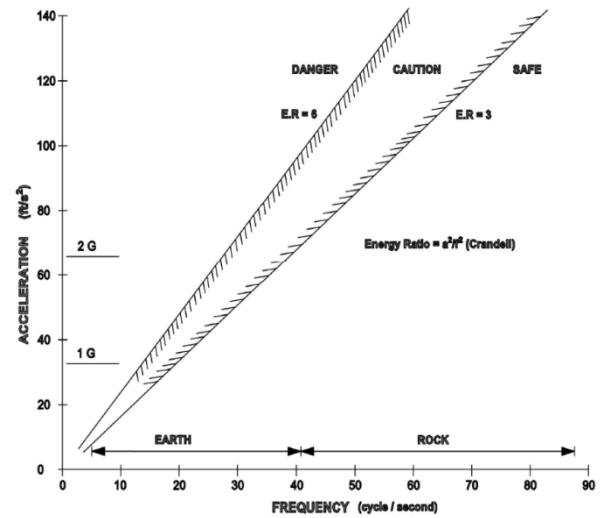


Figure 4. Damage prevention limits of Crandell

3.2. Approach of Edwards VE Northwood's Particle Velocity

Edwards and Northwood conducted experimental studies on brick structures with masonry basements resting on sandy-clay and glacial deposits in Canada. Based on the findings of these studies, it was determined that the best damage criterion for all soil types was the peak particle velocity (PPV), and the damage occurred between 101.6 mm/s (4 inch/s) and 127 mm/s (5 inch/s). As a result of the study, they recommended that the safe limit value be taken as 50.8 mm/s (2 inches/s) [8]. Damage criteria based on their results are given in Table 2.

Table 2. Damage criteria according to Edwards and Northwood's particle velocity approach (Edwards and Northwood, 1960)

Particle particle velocity (mm/s)	Damage
<50.8	None
50.8-101.6	Minor
>101.6	Major

3.3 Approach of Bauer and Calder

Bauer and Calder have given the possible damages that may occur in solid rock depending on the peak particle velocity in Table 3, and the particle velocity-related

damage estimates for various equipment and various types of structures are given in Table 4 (Calder, 1977).

3.4. Swedish Standard

Standardization methods for guide levels for vibrations in buildings from blasting are done in two ways. The more common practice is to regulate the guide peak particle velocities by frequency, as buildings are more likely to be damaged by resonance with low-frequency vibrations. The second type, much less used, is the determination of peak particle velocity guide levels based on the distance and the type of ground beneath the building. The Swedish Standard is one of three countries in the world that sets guide levels taking into account distance and ground type (Jansson, 2018). In the Swedish Standard, vertical particle velocity is used because it generally gives the higher value. It is recommended to measure particle velocity vibrations at the foundation of the building (Jansson, 2018).

Table 3. Damages that may occur in solid rock depending on the peak particle velocity (Calder, 1977)

Peak particle velocity (mm/s)	Effects on hard rock masses
>2500	Complete break-up of rock masses
635-2500	Strong tensile and some radial cracking of rock
250-635	Minor tensile slabbing in rock
<250	No fracturing of intact rock

Table 4. Damage criteria depending on the type of structure (Calder, 1977)

Type of structure	Type of damage	Peak particle velocity at which damage starts (mm/s)
Houses	Plaster cracking	51
Concrete block as in a new house	Cracks in blocks	200
Cased drill holes	Horizontal offset	380
Mechanical equipment pumps, compressors	Shafts misaligned	1000
Prefabricated metal building on concrete pads	Cracked pads, building twisted and distorted	1500

According to the Swedish Standard, the following equation is used to calculate the guide levels for vibrations caused by blasting (SS 4604866, 2011).

$$v = v_0 \times F_b \times F_m \times F_d \times F_t \tag{3}$$

Where, v_0 is the uncorrected velocity under the building depending on the ground type, F_b is the building coefficient showing the vibration sensitivity, F_m is a coefficient depending on the weakest material forming the structure, F_d is the distance between the building and the blasting source, and F_t is a factor depending on the duration of the blasting job.

The uncorrected peak particle velocity v_0 can be obtained from Tables 5, 6 and 7 and Figure 5 depending on the soil type, or it can also be obtained as mm/s by dividing the P wave velocity in m/s by 65 (Jansson, 2018).

Table 5. Guideline limits for vertical PPV in different substrata (Jonson, 2012)

Substrata of foundation	Substratum	Vertical PPV, v_0 mm/s
Loosely layered moraine, sand gravel, clay	Clay	18
Compactly layered moraine, schist, limestone	Moraine	35
Granite, gneiss, hard limestone, quartzitic sandstone, diabase	rock	70

Table 6. Vibration sensitivity factors for different structures, F_b (Jonson, 2012)

Class	Building	Building Factor, F_b
1	Heavy constructions such as bridges, quays, defense installations, etc.	1.7
2	Industrial and office buildings, consisting mainly of prefabricated elements	1.2
3	Normal residential buildings	1.0
4	Especially sensitive buildings and buildings with high vaults or constructions with large spans	0.65
5	Guideline values for especially sensitive heritage buildings, installations or environments identified in the investigation shall be determined separately. (Per special investigation.)	≤0.5

Table 7. Vibration sensitivity factors for different materials. F_m (Jonson, 2012)

Class	Material	Material factor, F_m
1	Reinforced concrete, steel, wood	1.20
2	Plain concrete, brick, concrete hollow blocks, lightweight-aggregate concrete	1.0
3	Autoclaved aerated concrete, plaster, lath-and-plaster stucco, rene dr, etc.	0.75
4	Sand-lime brick, tiled oven with sensitive joints	0.65

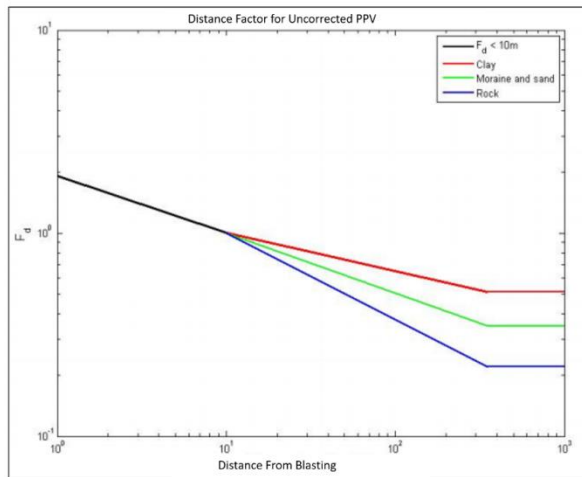


Figure 5. Change of distance factor (F_d) depending on ground type according to Swedish Standard (SS 4604866, 2011).

The F_t time factor used to consider the duration of the blasting work is taken between 1 for construction operations such as tunnels and highways, and 0.75-1 for quarry and mining operations.

3.5. DIN 4150 German Standard

In DIN 4150 German Norm, the peak particle velocity values are determined depending on the frequency. Permissible values according to the structure type are given in Table 8. While the allowable velocity is lowest in unsound structures such as old and worn historical monuments, it reaches its highest value in reinforced concrete and steel structures (Schillinger, 1996; Karadoğ an, 2008).

3.6. British Standard

The values given in Table 9 of the British Standard BS 7385 give the maximum allowable levels to avoid cosmetic damage under temporary vibrations that do not cause resonance in low-rise buildings. If the vibration is continuous and occurs at small frequencies that may cause resonance, it is recommended to use low limits and reduce the values given in Table 9 by 50% (BS7385, 1993).

Table 8. Particle velocity limits according to structure type and frequency in German Standard DIN 4150 (Schillinger, 1996)

Frequency (Hz)	Peak particle velocity (mm/s)	Type of building
0-10	3	Historical building
0-10	5	Durable building, Masonry brick
0-10	20	Reinforced concrete, Steel construction
10-50	3-8	Historical building
10-50	5-15	Durable building, Masonry brick
10-50	20-40	Reinforced concrete, Steel construction
50-100	8-10	Historical building
50-100	15-20	Durable building, Masonry brick
50-100	40-50	Reinforced concrete, Steel construction

Table 9. Temporary vibration guide levels for cosmetic damage (BS7385, 1993)

Type of building	Peak component particle velocity in frequency range of predominant pulse
Reinforced or framed structures	4 Hz to 15 Hz 15 Hz and above
Industrial and heavy commercial buildings	50 mm/s at 4 Hz and above
Unreinforced or light framed structures	15 mm/s at 4 Hz increasing to 20 mm/s at 15 Hz
Residential or light commercial type buildings	20 mm/s at 15 Hz increasing to 50mm/s at 40 Hz and above

Note 1: Values referred to are at the base of the building.
 Note 2: For unreinforced or light framed structures at frequencies below 4 Hz, a maximum displacement of 0.6mm (zero to peak) should not be exceeded.

3.7. Indian Standard

The Indian Standard has been regulated by DGMS (Tech) (S&T) (1997) Circular No. 7, published on August 29, 1997, regarding vibrations caused by blasting. It is

desirable that measurements be made adjacent to the structure. Permissible peak particle velocities are determined according to the dominant frequency of blast-induced vibrations and the types of structures (Table 10).

Table 10. Maximum allowable particle velocities in mining areas (DGMS, 1997)

Type of structure	Dominant excitation frequency, Hz		
	<8 Hz	8-25 Hz	>25 Hz
A) Buildings/structures not belong to the owner			
(i) Domestic houses/structures (kuchha brick and cement)	5	10	15
(ii) Industrial buildings (RCC and framed structures)	10	20	25
(iii) Objects of historical importance and sensitive structures	2	5	10
B) Buildings belonging to owner with limited span of life			
(i) Domestic houses/structures (kuchha, brick and cement)	10	15	25
(ii) Industrial buildings (RCC and framed structures)	15	25	50

3.8. France Standard

In the French Standard, allowable peak particle velocity is determined according to the structure type and frequency (Karadoğan, 2008).

Table 11. Highest peak particle velocity according to French Standard (Karadoğan, 2008)

Type of structure	Peak particle velocity (mm/s)		
	4-8 Hz	8-30 Hz	30-100 Hz
House	8	12	15
Sensitive	6	9	12
Very sensitive	4	6	9

4. Damage Criteria for Different Engineering Structures in Literature

In studies based on the USBM Research Report RI 8507, the maximum allowable particle velocity is given as 50

mm/s, taking into account the structures in the database. The damage criteria given for different engineering structures in the literature are summarized below.

In AASTHO Designation R 8-96, it is stated that it is common to apply the USBM damage criteria to other types of structures from the database on which they are based, but it is not the right approach to apply the USBM damage criteria to foundations, buried pipelines and underground structures (AASTHO Designation, 2004). Svinkin (2015) points out that the USBM criteria are valid for 1-2-storey buildings with wood skeletons, plaster or gypsum boards, but do not cover structures such as concrete, electricity poles, pipelines, bridges. Hendron, (1977) and Langefors and Kihlstrom (1978) give the damage criterion as 10-12 in/s (250-300 mm/s) for tunnels and pipelines.

Olofsson (1990) suggests the permissible peak particle velocity of 150 mm/s for reinforced concrete structures resting on rock. Wiss (1981), on the other hand, states that concrete that has taken full strength can resist up to 125 mm/s particle velocity levels without being damaged. According to the measurements he made, it has been determined that high pressure pipelines can withstand particle velocities of 250-500 mm/s without being damaged.

Francini and Baltz, (2008) suggest values between 125-250 mm/s as permissible peak particle velocity for pressure pipelines constructed of steel. The vibration limit for the second line built parallel to the 1368 km long high-pressure gas pipeline currently in operation was chosen as 305 mm/s and the blasting process was successfully applied without damaging the existing pipeline (ISEE, 2011).

Crawford and Ward (1965) state that the peak particle velocity does not cause any damage up to 250 mm/s in concrete structures and up to 75 mm/s in mortar masonry structures. Moreover, the unit displacement values corresponding to these particle velocities are given as 100 μ and 30 μ, respectively. Persson et al. (1981) gives the allowable peak particle velocity for pulses with a vibration duration of less than 0.5 s, as 200 mm/s for reinforced concrete tanks resting on rock, 100 mm/s for modern steel or reinforced concrete tall structures, 70-100 mm/s for 15-18 m span underground galleries, 70 mm/s for brick or masonry buildings, and 25 mm/s for Swedish National Museum buildings. These values have been chosen low enough so as not to cause damage to the structures. However, even the lowest value is large enough to be felt by the people around.

(Siskind, 2005) stated that the peak particle velocity can be taken as 300 mm/s for underground structures, including the interaction of tunnels opened close to each other, and 125 mm/s for pressure pipes in multiple blasting. However, referring to the studies of (Oriard, 1994), he states that a peak particle velocity of 300 mm/s is appropriate in case of blasting one hole at a time, provided that the hole diameter does not exceed 63.5 mm for blasts to be made at distances closer than 6

meters.

In the Tennessee Valley Authority (TVA) specification, allowable peak particle velocities depending on the age of the concrete are given in Table 12 (Oriard and Coulson, 1980). The biggest difference that distinguishes this study from similar studies is that the concrete strength is determined depending on the frequency by using the Distance Factor. As the distance increases, the geometric spread and the damping frequency in the rock decrease. The falling frequency also increases the particle velocity and hence the unit displacement. By using the values in Table 12, the permissible particle velocity is found to be 300 mm/s if MF=0.6 is used for long distances of concrete aged 10 days and older, which has largely gained its strength. This is in line with the values given in the studies (Hendron, 1977; Langefors and Kihlstrom, 1978). TVA has been using the values given in Table 12 for many years without any problems (Oriard, 2002).

It should also be taken into account that the TVA specification includes 3 types of ground conditions, and these ground conditions impose some limitations. In the first case, blasting is carried out in the rock at higher elevations than the concrete. In this case, there is no question of any damage to the concrete and the data in Table 12 can be used exactly. In the second and third cases, blasting is done at lower levels than the concrete. In this case, if there is a slope flatter than 1 Vertical to 2 Horizontal slope between the lower level of the concrete and the lowest level where the explosive is placed, the data in Table 12 can be used exactly without the need for any operation. However, if the slope in question is steeper or if the blasting is done adjacent to the concrete, then blasting can be done, but subject to the approval of the authorities. Also, tall structures built above ground can amplify movement on the ground floor. In this case, half of the values given in Table 12 are used (ISEE, 2011). Hulshizer and Desai (1984), Kwan and Lee (2002) and Ahmed (2016) found similar results with Oriard and Coulson (1980) in their studies on fresh concrete. For 0-3day old concrete, China limits the vibration rate to 15-20 mm/s for frequencies below 10 Hz, while it gives 25 mm/s for 50 Hz. On the other hand, Finland allows peak particle velocities of 45-90 mm/s, Norway 5-50 mm/s, and Sweden 30mm/s without limiting frequency (Ahmed, 2016). Ahmed (2016), after reviewing all the studies, emphasizes that 60 mm/s peak particle velocity is suitable for 0-0.5day old concrete, and a particle velocity of 140 mm/s for 0.5-3day concrete do not harm the concrete.

It is necessary to be very careful when using the values in the standards of some countries. Because while determining the limits, damage limits can be kept lower than necessary in order to manage social perceptions and complaints about blasting rather than technique. This also applies to the preparation of the DIN 4150 Standard. The limits in this standard are not damage limits (Siskind, 2005).

Table 12. Blast damage criteria for mass concrete (Oriard and Coulson, 1980)

Age of concrete (from batching time)	Allowable particle velocities from blast induced vibrations, mm/s
0- 4 hours	100 x DF
4 hours- 1 day	150 x DF
1 to 3 days	225 x DF
3 to 7 days	300 x DF
7 to 10 days	375 x DF
10 days or more	500 x DF

DF= distance factor.

Distance factor as defined below;

Distance factor	Distance from blast to concrete, Meters
1	0-15
0,8	15-50
0,7	50-75
0,6	Greater than 75

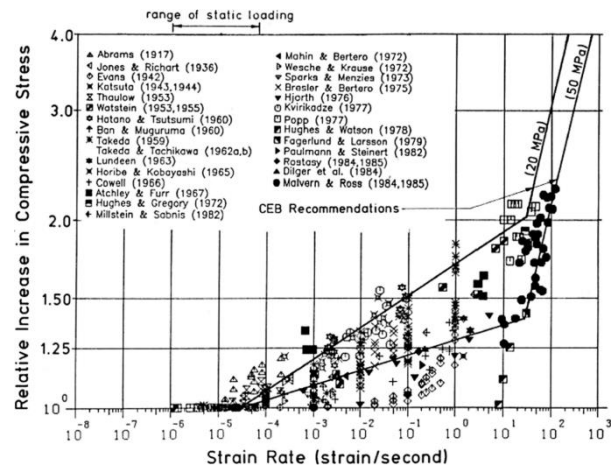


Figure 6. Effect of loading speed on concrete strength (Bischoff and Perry, 1991).

Along with the curing time, the loading speed is among the factors that determine the concrete strength. As the frequency of vibration increases, the concrete strength increases as the loading speed increases. While the strain rate is 10⁻⁵ per second in static loads, this rate is between 100 and 1000 per second in blast-induced loads (Bischoff and Perry, 1991). This increase in loading rate leads to a 1.5-to-3.5-fold increase in the compressive strength of concrete, called the Dynamic Increase Factor (DAF), as shown in Figure 6 (Bischoff and Perry, 1991).

The increase in the loading speed leads to an increase in the tensile strength of concrete about 2 times more than the increase in the compressive strength of the concrete (Ahmed, 2016). These increases in compressive and tensile strengths of concrete under loading speeds under the influence of blast-induced vibrations are one of the main reasons why buried concrete tunnel linings or structures resting on bedrock perform well without being damaged under high peak particle velocities.

Therefore, shotcrete for several hours withstands vibration rates of 500-1000 mm/s without cracking (Ahmed, 2016).

Isaac and Bubb (1981), based on their own experience and the findings of researchers in Scandinavian countries, determined that the allowable peak particle velocity increases in parallel with the strength of concrete. They showed that concrete with a strength of 40 MPa could withstand a peak particle velocity of 187mm/s, depending on the ductility of the concrete and the surrounding rock conditions.

In some nuclear power plant constructions in Spain, the allowable peak particle velocity has been determined depending on the concrete strength in the constructions carried out simultaneously with the concrete pouring (Jimeno Carcedo et al., 1995). Mass concretes are subjected to vibrations after 8 hours passed from the time of pouring. The peak particle velocity is increased in parallel to strength gained. Allowable peak particle velocity reaches 100 mm/s when the strength of concrete becomes 15 MPa. Similarly, in structural concretes, when the strength exceeds 25 MPa, the permissible peak particle velocity is risen to 60 mm/s but it cannot go beyond 100 mm/s.

(Karadoğan, 2008) found the accepted values of the Environmental Noise Evaluation and Management Regulation published by the Ministry of Environment and Urbanization to be high for Türkiye. The referred values have been adapted from USBM Norm of the United States. The reasons for these high values are that the field constants, frequency values and response levels of the residents in Türkiye and the natural frequency values of the building stock in the country are different from the data on which the USBM Norm of the United States is based. Although the residences in the USA are generally one or two floors and have high frequencies, the residences in our country are generally five floors and above and their natural frequencies are low. In the measurements made in the field, the frequency of blast-induced vibrations was measured close to the frequencies of the building stock. Based on these findings, Karadoğan et al. (2014) [35] developed the damage criteria for Türkiye depending on the building type as in Figure 7.

5. Identification of Damage Criteria Using Response Spectrum

The ratio of the structure size to the wavelength of the blast-induced vibration determines which of the displacement, velocity and acceleration vibration limits will cause damage first. If the dimensions of the structure are very small compared to the wavelength of the vibration, the criterion that determines the damage will be the displacement, while if the size of the structure is too large compared to the wavelength of the vibration, the criterion that determines the damage will be acceleration. In the region between these two, the speed

determines the damage. Damage criteria for buildings resting on solid rock can also be expressed in terms of frequency. In this case, at frequencies lower than 20-50 Hz, the damage determining criterion is displacement, while when the frequencies exceed 200 Hz, the damage determining criterion is acceleration. Between these two, peak particle velocity damage is the determining criterion (Figure 8).

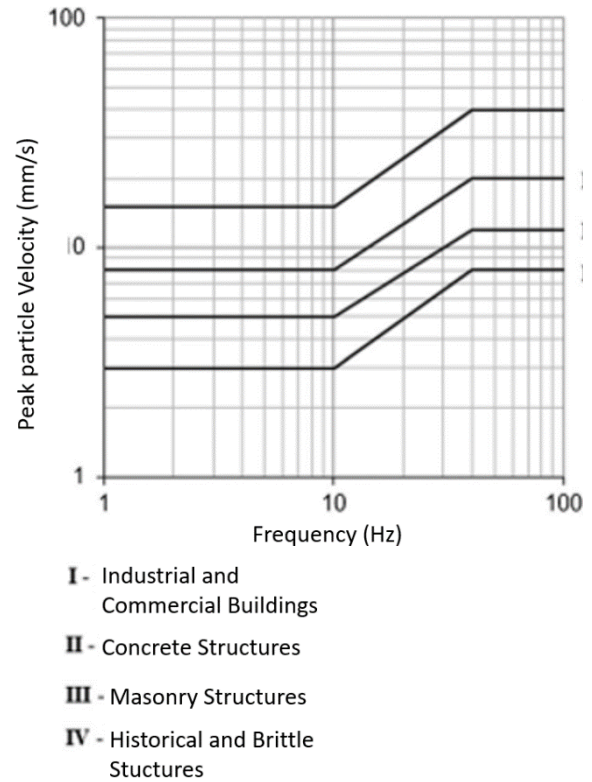


Figure 7. Damage criteria for Türkiye (Karadoğan et al. 2014)

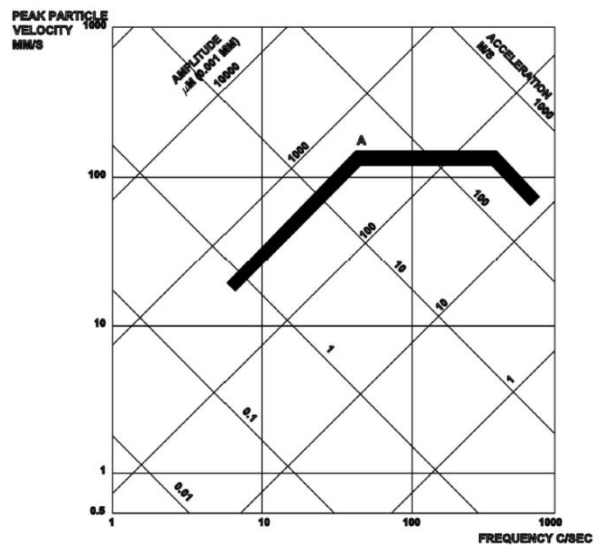


Figure 8. Frequency-dependent variation of displacement, velocity and acceleration limits of damage criteria for structures on rock (Persson et al., 1981).

In reinforced concrete structures, permissible damage criteria can be determined with the help of response spectrum based on the damage values given by TVA for mass concretes. In this case, the allowable particle velocity given for mass concrete can be divided by the building's response coefficient to determine the allowable peak particle velocity to be measured outside the building. For the same purpose, measurements can be

made at critical openings and points inside buildings. Measurements made inside the buildings emerge as a safer approach, as they will include the response of the foundation ground sitting on different types of soils other than the rock, as well as the response of the building to blast-induced vibrations. However, this process may not always be possible in practice as it will require structural analysis and measurement in the right places.

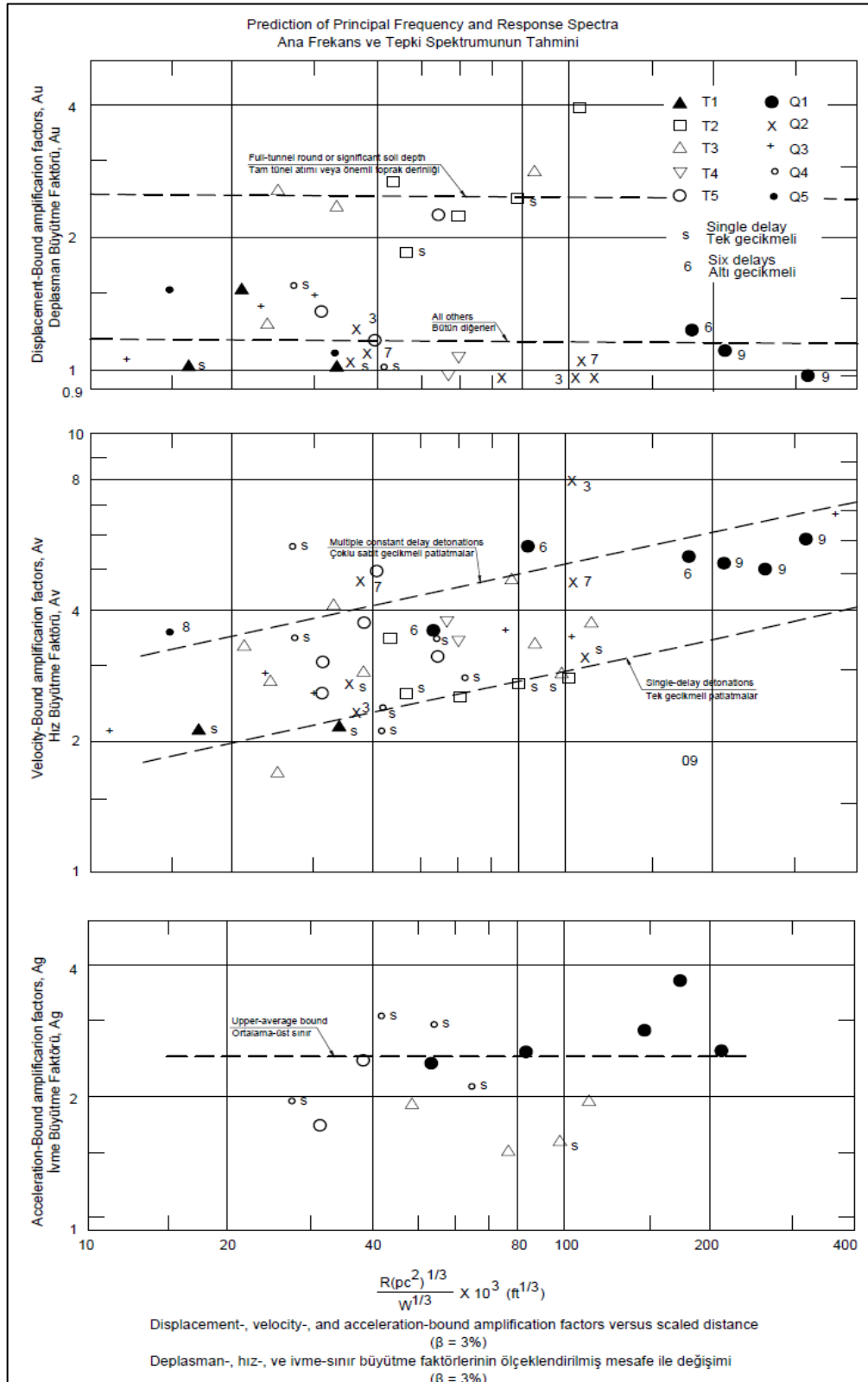


Figure 9. Variation of magnification coefficients with scaled distance (Dowding, 1985).

By using the peak particle velocities measured in the ground together with the response spectrum amplification factors, allowable peak particle velocity limits can be determined depending on the type of building. (Dowding, 1985) gives the building magnification factor approximately 3-4 for multiple blasts with scaled distance around 30-50 and damping rate of 3%. (Medearis, 1978) showed that 5% damping ratio would be more appropriate in his studies. The amplification factor corresponding to 5% damping rate for reinforced concrete buildings is calculated between 2-3, using the coefficients determined by (Dowding, 1985) and given in Table 13. (Medearis, 1978) gives the magnification factor between 2-3 for the mean +1 standard deviation for frequencies between 10 to 50 Hz; this value is very close to the values calculated by (Dowding, 1985) method.

Taking the Distance Factor (MF) into account, if the allowable particle velocity of 300 mm/s for the concrete (Oriard and Coulson, 1980) is divided by the amplification coefficient between 2-3 for buildings, the permissible value for the peak particle velocities measured on the ground is 100-150 mm/s will be calculated between If blasting is done very close to the building, allowable particle velocities can be taken between 150-250 mm/s for relatively high frequencies. It is seen that these calculated limits are compatible with the values given by Hendron (1977), Olofsson (1990) and Persson et al. (1981).

Table 13. If the damping ratio of the response spectrum is desired for values other than 3%, the coefficients that must be multiplied by the factors obtained from Figure 9

β %	A_u	A_v	A_g
2	1.05	1.10	1.20
3	1	1	1
5	0.83	0.76	0.72
10	0.65	0.52	0.42

β % damping ratio; A_u , A_v , A_g are amplification factors for displacement, velocity, and acceleration, respectively.

6. Results and Discussion

In studies based on the USBM Research Report RI 8507, the maximum allowable particle velocity is given as 50 mm/s, taking into account the structures in the database of the mentioned research report. However, the damage criteria determined in the aforementioned report lose its validity for reinforced concrete buildings, tunnels, pipelines, mass concretes and similar engineering structures. Among the reasons for this are that the soil and structure amplifications are different from the structures in the database of the USBM Research Report RI 8507, the loading speed increases as the frequencies increase, and the material strength increases with the increase in loading speed. In addition to these, it should also be taken into account that the acceptance that fresh

concrete is affected by vibrations too much and that the permissible peak particle velocities should be kept very low does not correspond to the real situation.

Deep foundations, buried pipelines, and underground structures do not amplify movement from the ground. Surface waves lose their effect rapidly as the depth increases, and that is, ground deamplification rather than ground amplification with depth occurs. For this reason, the application of USBM damage criteria to structures that do not have such amplifications will cause excessive design and will lead to an unnecessary reduction of construction speeds, since the building amplifications that are effective in determining the damage criteria of the USBM Research Report RI 8507.

The load-bearing system in reinforced concrete framed structures is less flexible than wood-frame structures on which the USBM damage criteria are based. In addition, stress concentrations observed in gypsum boards located at the corner points or junction points of wood-framed structures will be less in reinforced concrete-framed structures. Similarly, displacement differences caused by materials with different stiffnesses, such as wood and drywall react differently to vibration waves, but this type of differences are not expected to occur in reinforced concrete structures. For this reason, much less damage will be observed in reinforced concrete structures that are exposed to the same vibration as wood-framed structures.

On the other hand, studies initiated especially by TVA and later confirmed by many researchers have shown that fresh concrete and mass concretes can withstand peak particle velocities well above the values in the specifications. Strength increases depending on the loading speed also reveal that higher peak particle velocities can be allowed, especially at high frequencies.

For all these reasons explained, it is considered that USBM damage criteria should not be applied to reinforced concrete buildings, tunnels, pipelines, mass concretes and similar engineering structures, and cost increases should not be created by unnecessarily reducing construction speeds.

Allowable peak particle velocities for these structures are given below. TVA has been applying the allowable particle velocity of 300 mm/s for mass concretes that have gained 28-day strength without any problems for many years. This value is a value that can be used safely for mass concretes resting on the bedrock, buried structures and tunnel linings. In pressure pipes, the permissible particle velocity can be taken as 250-300 mm/s for single blasting, and a value between 125-150 mm/s, which is approximately half of this value, for multiple blasting.

The loading rate of concrete is 10-100 million times higher than static loading in vibrations caused by high frequency blasting (Bischoff and Perry, 1991). This situation increases the compressive strength of concrete 1.5-3.5 times, and the tensile strength about 2 times more than the increase in compressive strength. Thus, at

high frequencies, concrete can withstand particle velocities up to 1000 mm/s without being damaged (Oriard, 2002).

By using the peak particle velocities measured in the ground together with the response spectrum amplification factors, allowable damage limits can be determined depending on the type of building. Considering the studies of Dowding (1985) and Medearis (1978), the magnification factor can be taken between 2-3 for 5% damping rate and frequencies between 10-50 Hz.

Considering the response of reinforced concrete structures, that is, amplification of movement from the foundation level, allowable particle velocities for reinforced concrete structures can be taken between 100-150 mm/s. Permissible particle velocities for single blasts can be increased to between 150-250 mm/s if blasting is done very close to the building.

7. Conclusions

The USBM Research Report RI 8507 is based on data from the effects of blasting vibrations, particularly from coal mine operation, on wood-framed, plaster or gypsum-clad 1-2 story buildings. The damage criteria were determined in such a way that structure would not be damaged by the effect of the resonance occurring as a result of the overlapping of the frequencies of the blast-induced surface waves and the frequencies of the structures in the database of the mentioned research report.

In studies conducted by different researchers in the literature for different types of engineering structures, it has been revealed that 50 mm/s particle velocity, which is the upper limit of the USBM damage criteria, can be selected higher.

Although it is common to apply the USBM damage criteria to structures other than those in the database on which the study is based, it is not the right approach. Therefore, it is necessary to re-evaluate the USBM damage criteria for engineering structures.

Oriard and Coulson (1980) showed that USBM PPV criteria may be conservative even for fresh concrete because it was not as much affected by vibrations as thought.

Author Contributions

The percentage of the author contributions is presented below. The author reviewed and approved the final version of the manuscript.

	D.Y.
C	100
D	100
S	100
DCP	100
DAI	100
L	100
W	100
CR	100
SR	100

C=Concept, D= design, S= supervision, DCP= data collection and/or processing, DAI= data analysis and/or interpretation, L= literature search, W= writing, CR= critical review, SR= submission and revision.

Conflict of Interest

The author declared that there is no conflict of interest.

Ethical Consideration

Ethics committee approval was not required for this study because of there was no study on animals or humans.

References

- AASHTO Designation. 2004. R 8-96. Standard Recommended Practice for Evaluation of Transportation-Related Earthborne Vibrations, AASHTO, New York, USA, pp: 1-13.
- Ahmed L. 2016. Impact-type vibration effects on young concrete for tunnelling. BeFo Rep (Stiftelsen Bergteknisk Forskning/Rock Engineering Research Foundation), 147: 48.
- Bischoff PH, Perry SH. 1991. Compressive behaviour of concrete at high strain rates. Mater Struct, 24: 425-450.
- Bollinger GA. 2018. Blast vibration analysis. Courier Dover Publications, New York, USA, pp: 160.
- Calder P. 1977. Pit slope manual. Chapter 7, Perimeter blasting. CANMET, Energy, Mines and Resources, Ottawa, Canada, pp: 22-76.
- Crandell FJ. 1949. Ground vibration due to blasting and its effect upon structures. Boston Society of Civil Engineers, Boston, USA, pp: 110.
- Crawford R, Ward HS. 1965. Dynamic strains in concrete and masonry walls. Division of Building Research, National Research Council of Canada, Ottawa, Canada, pp: 1-16.
- DGMS (Tech) (S&T). 1997. Circular No.7. Directorate General of Mines Safety, Dhanbad, India, pp: 9-14.
- Dowding CH. 1985. Blast vibration monitoring and control. Prentice Hall Inc, New York, USA, pp: 45.
- Edwards AT, Northwood TD. 1960. Experimental studies of the effects of blasting on structures. Washington: Division of Building Research, National Research Council, Washington, USA, pp: 26.
- Francini RB, Baltz WN. 2008. Blasting and construction vibrations near existing pipelines: what are appropriate levels? In International Pipeline Conference, September 29–October 3, Calgary, Alberta, Canada, pp: 519-531.

- Hendron, AJ. 1977. Engineering of rock blasting on civil projects: Structural and geotechnical mechanics. Englewood Cliffs, NJ: Prentice-Hall, New York, USA, pp: 242-277.
- Hulshizer AJ, Desai AJ. 1984. Shock vibration effects on freshly placed concrete. *J Construct Engin Manage*, 110(2): 266-285.
- Isaac ID, Bubba C. 1981. Engineering aspects of underground cavern excavation at Dinorwic, part 2 drilling and blasting. *Tunnels & Tunnelling Inter*, 13(5).
- ISEE. 2011. Blasters' handbook. International Society of Explosives Engineers, Cleveland, Ohio, USA, pp: 741.
- Jansson A, Eriksson M. 2018. Assessment of the Swedish Standard for blasting induced vibrations. URL: <https://publications.lib.chalmers.se/records/fulltext/255554/255554.pdf> (accessed date: March 13, 2022)
- Jimeno CL, Jimeno EL, Carcedo FJA. 1995. Drilling and blasting of rocks. Geo-Mining Technological Institute of Spain, Zaragoza, Spain, pp: 389.
- Jonson D. 2012. Controlling shock waves and vibrations during large and intensive blasting operations under Stockholm City. *Tunnel Rock Drill Blast*, 2012: 49-58.
- Karadogan A, Kahriman A, Ozer U. 2014. A new damage criteria norm for blast-induced ground vibrations in Turkey. *Arabian J Geosci*, 7(4):1617-26,
- Karadoğan A. 2008. Investigation of the Feasibility of Establishing National Building Damage Criteria for Vibrations Caused by Blasting. PhD thesis, Institute of Sciences, İstanbul University, İstanbul, Türkiye, pp: 248.
- Kwan AKH, Lee PKK. 2002. Testing the shock vibration resistance of concrete for setting vibration control limits against blasting damage. *Proceedings of the 27th Conference on Our World in Concrete and Structures*, 29-30 August, Singapore, pp: 32-37.
- Langefors U, Kihlstrom B. 1978. The modern techniques of rock blasting. John Wiley and Sons Inc, New York, USA, pp: 438.
- Medearis K. 1978. Rational damage criteria for low rise structures subjected to blasting vibrations. *Proceed Instt Civil Engin*, 65(3): 611-621.
- Olofsson SO. 1990. Applied explosives technology for construction and mining. Second edition. APPEX Applied Explosives Technology, Stockholm, Sweden, pp: 253.
- Oriard LL, Coulson JH. 1980. TVA blast vibration criteria for mass concrete. *Minimizing Detriment Construct Vibrat*, 80(175): 101-123.
- Oriard LL. 1994. Vibration and ground rupture criteria for buried pipelines (No. CONF-940144-). International Society of Explosives Engineers, Cleveland, USA, pp: 645.
- Oriard LL. 2002. Explosives engineering, construction vibrations and geotechnology. International Society of Explosives Engineers, Cleveland, USA, pp: 680.
- Persson A, Holmberg R, Lande G, Larsson B. 1981. Underground blasting in a city. Pergamon, Subsurface Space, Stockholm, Sweden, pp: 199-206.
- Schillinger RR. 1996. Environmental effects of blast induced immissions (No. CONF-960262-). International Society of Explosives Engineers, Cleveland, USA, pp: 653.
- Siskind DE, Strachura VJ, Stagg MS, Kopp JW. 1980. Structure response and damage produced by airblast from surface mining. US Department of the Interior, Bureau of Mines, New York, USA, pp: 243.
- Siskind DE. 2005. Vibrations from blasting. International Society of Explosives Engineers, Cleveland, USA, pp: 245.
- Standard B. 1993. Evaluation and measurement for vibration in buildings. BS7385 Part 2. Stockholm, Sweden, pp: 11.
- Svinkin, M. R. 2007. Forensic engineering of intolerable structural vibrations and damage for construction and industrial dynamic sources. *Forensic Engineering*, New York, USA, pp: 384-398.
- Svinkin, M. R. 2015. Tolerable limits of construction vibrations. *Practice Period Struct Design Construc*, 20(2): 04014028.
- Swedish Standard SS 4604866. 2011. Institute S. S. Vibration and shock - Guidance levels for blasting-induced vibration in buildings. Stockholm, Sweden, pp: 23
- Wiss JF. 1981. Construction vibrations: state-of-the-art. *J Geotech Engin Div*, 107(2): 167-181.



VALORISATION OF THE EFFECT OF WASTE ALUMINUM SAWDUST ON CONCRETE: DURABILITY CHARACTERISTICS AND ENVIRONMENTAL IMPACTS

Tuba DEMİR^{1*}, Bahar DEMİREL¹, Melek ÖZTÜRK¹

¹Firat University, Faculty of Technology, Department of Civil Engineering, 23119, Elazığ, Türkiye

Abstract: The aim of this study is to examine the effect of replacing waste aluminum sawdust (AS) with fine aggregate on the strength and durability properties of concrete. For this, concrete mixtures with a cement dosage of 400 kg/m³, water/cement (W/C) ratio of 0.40-0.50-0.60 were prepared. Aluminum sawdust obtained from Elazığ industrial site was added to the concrete mixtures by replacing 0%, 0.5% and 1% fine aggregate by volume. After curing in the curing pool for 28 days, the produced concrete samples were placed in the carbonation tank and exposed to the accelerated carbonation test in three different time periods as the 1st, 3rd and 7th days. Tests of compressive strength, splitting tensile strength, ultrasound transmission velocity, porosity and carbonation depth were performed on concrete samples before and after carbonation. The samples that were exposed to carbonation were compared with the samples that did not undergo carbonation. In addition, the microstructure of AS concrete was investigated using scanning electron microscopic images (SEM). In the microscopic images, larger cracks, openings and interfacial voids were observed in the concrete matrix with the addition of AS. However, due to the formation of ettringite in these gaps and cracks after carbonation, the cavities became smaller. As a result of the experiments, it was observed that the optimum W/C ratio was 40% and the AS amount was 0.5% in the use of AS in concrete. In addition, it was found that the carbonation effect improves the compressive and splitting tensile strength and increases the ultrasound transmission rate. Finally, life cycle assessment (LCA) was conducted to evaluate the environmental impacts of the prepared concrete samples. Considering the large amount of natural aggregate consumption, it is thought that the use of waste materials in concrete will provide environmental and economic benefits.


Keywords: Aluminium sawdust, Carbonation, Hardened properties, Microscopic image, Life cycle assessment

*Corresponding author: Firat University, Faculty of Technology, Department of Civil Engineering, 23119, Elazığ, Türkiye

E mail: t.demir@firat.edu.tr (T. DEMİR)

Tuba DEMİR  <https://orcid.org/0000-0003-2092-1029>

Bahar DEMİREL  <https://orcid.org/0000-0001-7483-2668>

Melek ÖZTÜRK  <https://orcid.org/0000-0003-4439-7508>

Received: August 21, 2023

Accepted: December 27, 2023

Published: January 15, 2024

Cite as: Demir T, Demirel B, Öztürk M. 2024. Valorisation of the effect of waste aluminum sawdust on concrete: Durability characteristics and environmental impacts. BSEng Sci, 7(1): 109-120.

1. Introduction

With the continuity of continuity of the construction sector and the emergence of new needs in the field of construction, there is a great increase in concrete production (Ramachandran and Beaudoin, 2001). This rising increase in the construction sector also increases the production of concrete and increases the use of aggregate, one of the main components of concrete. This leads to rapid depletion of natural resources (Osei and Jackson, 2016). For the protection of the ecosystem and sustainable development, it becomes necessary to reduce the use and accumulation of waste products. Many studies on the use of waste materials silica fume, fly ash, blast furnace slag, waste foundry sand, wood ash, etc. as partial substitutes for natural materials in concrete production have facilitated to reduction of dependence on natural materials (Siddique et al., 2020).

The expansion of construction has an important role in the increase in environmental problems. Buildings produce harmful emissions and wastes by consuming natural resources and energy during their lifetime. As a

result, they create environmental pollution (Golewski, 2021). It is estimated that around 11 billion tons of aggregate is consumed every year worldwide. Approximately 8 billion tons of this aggregate amount is used in concrete production (Golewski, 2021). This situation poses a great threat to the environment. In addition, the transportation process of these aggregates also brings great cost (Babu et al., 2015). Therefore, the use of industrial by-products in concrete production has become a necessity in order to protect the environment and contribute to the economy (Cheng, et al., 2013). The use of recyclable materials in buildings requires many processes such as disassembling these materials for recycling, collecting, grouping and obtaining a new product. However, it will provide significant environmental benefits in terms of raw material savings, resource efficiency, energy efficiency and reduction of environmental pollution (Miličević et al., 2011; Martínez-Lage et al., 2020). For this purpose, scientific researches continue to be carried out on the recycling of industrial wastes that pose an environmental threat and their use in concrete, in the construction sector as well as in many



other sectors. In these studies, materials such as metal powder and sawdust, steel and wood chips, aluminum powder and sawdust are used in the production of concrete (Alwaeli and Nadziakiewicz, 2012; Zhong et al., 2018). Among these materials, aluminum sawdust is one of the newest waste materials (Öztürk, 2020).

Aluminum sawdust (AS) is a waste material produced by the industrial industry. In the aluminum industry, which is one of the most advanced recycling industries today, approximately 50% of the aluminum used in the world is recovered. Aluminum production from scrap is 95% more efficient than primary aluminum production (Binici et al., 2013). The application of AS can not only reduce environmental damage but also can save concrete materials. Substituting cement in concrete contributes to more economical and environmentally friendly concrete production by reducing the amount of cement usage. It also has many advantages over traditional concrete, such as low bulk density, better heat preservation and less pollution to our environment (Cheng et al., 2013).

Considering the type and severity of external effects that they will be exposed to during their service life while the structures are being designed ensures that the structures can maintain their functionality throughout their lifetime. A concrete designed according to the environmental conditions, produced in high quality, well placed and cared for can fulfill its duty for many years without any repair. However, the performance of concrete may decrease in the face of some internal and external factors. A durable concrete; It is concrete that resists these effects (Demir et al., 2022). Exposed and unprotected reinforced concrete structures cause corrosion damage. In Türkiye; it was observed that corrosion damage occurred in many of the structures damaged in the earthquake. There is also the danger of corrosion in our existing structures. The most important factor causing corrosion is carbonation. Carbonation also causes deterioration of the durability of the structures (Balapour et al., 2018; Flores et al., 2015).

In previous literature studies, the mechanical properties of wastes such as wood shavings, glass dust, and marble powder on concrete were generally investigated. However, there are hardly any studies on the use of AS in concrete production. The aim of this study is to examine the effect of the use of waste aluminum sawdust (AS) by replacing it with fine aggregate on the strength and durability properties of concrete, to contribute to the improvement of concrete, to prevent environmental pollution by evaluating waste materials, and to determine the replacement rate of AS with fine aggregate and to contribute to the literature to present relevant data. After literature research, many trial mixtures were poured to determine material mixing ratios. After these trial mixtures, reference mixtures were determined. For this, concrete mixtures with a cement dosage of 400 kg/m³, W/C ratio of 0.40, 0.50% and 0.60% were prepared. Aluminum sawdust obtained from Elazığ industrial site was added to the concrete mixtures by

replacing 0%, 0.5% and 1% fine aggregate by volume. After curing in the curing pool for 28 days, the produced concrete samples were placed in the carbonation tank and exposed to the accelerated carbonation test in three different time periods as the 1st, 3rd and 7th days. Tests of compressive strength, splitting tensile strength, ultrasound transmission velocity, and porosity and carbonation depth were performed on concrete samples before and after carbonation. The samples that were exposed to carbonation were compared with the samples that did not undergo carbonation. In addition, the microstructure of AS concrete was investigated using scanning electron microscopic images. In the microscopic images, larger cracks, openings and interfacial voids were observed in the concrete matrix with the addition of AS. However, due to the formation of ettringite in these gaps and cracks after carbonation, the cavities became smaller. As a result of the experiments and cost comparison, it was found that the optimum W/C ratio was 40% and the amount of AS was 0.5%. In addition, it was found that the carbonation effect improves the compressive and splitting tensile strength, and increases the ultrasound transmission rate.

2. Constituent Materials and Mix Details

2.1. Materials

In this study, CEM I 42.5 R Portland cement obtained from Elazığ Çimentoş cement factory was used (TS EN 197-1, 2012). In the experiments, river aggregate with the largest grain diameter (D_{max}) of 8 mm, obtained from Palu District of Elazığ Province, was used. Aggregate; It was used in three classes: 0-2 mm, 2-4 mm and 4-8 mm. Aluminum Sawdust (AS) was used as waste material. AS was supplied from Elazığ industrial zone. The chemical properties of these materials are given in Table 1.

Aluminum is one of the newest members of the metal world. Aluminum, which is in the light metal class, is widely used due to its advantages in technical properties (Zhang et al., 2023). When various alloys are added, their mechanical properties reach levels comparable to steel. It is widely used in various industrial fields such as medicine, food, aerospace, automotive and construction (Geçkinli, 2002). The appearance of the AS used in the study is shown in Figure 1.

2.2. Mix Design and Sample Preparation

In this study, 9 concrete mixtures with cement dosage of 400 kg/m³, W/C ratio of 0.40-0.50-0.60, respectively, were prepared in order to examine the variation range of strength properties of AS-reinforced concretes at fixed cement dosage at different ratios. In these mixtures, 0.5% and 1.0% AS was used by replacing the fine aggregate by volume. 3 different concrete series were prepared for the control series without AS (free carbonation) and 6 different concrete series were prepared at the rates of 0.5% and 1.0% for the series with AS. Details of mixing ratios are summarized in Table 2.

Table 1. Chemical properties of materials used in the study

Chemical properties	Cement (C)	Chemical properties	Aluminium Sawdust (AS)
CaO	63.33	Al	89.96
SiO ₂	19.07	Zn	4.97
Fe ₂ O ₃	3.72	Mg	2.11
Al ₂ O ₃	4.82	Cu	0.26
SiO ₃	2.83	Mn	0.25
Na ₂ O	0.39	Fe	0.24
K ₂ O	0.65	Si	0.15
MgO	1.10	Cr	0.025
Cl	0.009	Ti	0.012
Insoluble residue	0.20	Pb	0.005
Loss of ignition	2.70	Sn	0.003



Figure 1. Aluminium sawdust sample used in the study.

Table 2. Proportions of the concrete mixtures (kg/m³)

Mixture Code	Cement	Water	AS	Fine aggregate (0-2) mm	Fine aggregate (2-4) mm	Coarse aggregate (4-8) mm
0.4AS0	400	186.59	0.00	562	544	659
0.4AS5	400	186.59	3.11	559	544	659
0.4AS10	400	186.59	6.21	556	544	659
0.5AS0	400	225.02	0.00	528	512	620
0.5AS5	400	225.02	2.92	526	512	620
0.5AS10	400	225.02	5.85	523	512	620
0.6AS0	400	263.44	0.00	495	480	581
0.6AS5	400	263.44	2.74	493	480	581
0.6AS10	400	263.44	5.48	490	480	581

2.3. Production of Samples and Testing Program

Within the scope of the study, 9 series with and without AS were prepared to investigate the effect of AS on pre- and post-carbonation compressive strength, splitting tensile strength, ultrasound transmission rate, porosity test and carbonation depth measurement. For the implementation of all tests, a total of 216 concrete samples, 24 in each concrete series, were produced. Flow chart of the study is shown in Figure 2.

2.4. Experimental Methods and Procedures

2.4.1. Compressive strength

Compressive strength test of concrete samples was determined according to TS EN 12390-3 standard (TS EN 12390-3, 2019). The 100x100x100 mm specimens were

placed in the compression testing machine and were loaded at 3 kN/sec. The average compressive strength of three cube specimens of each concrete mixture was termed as the compressive strength of that concrete mixture.

2.4.2. Split Tensile Strength

Splitting tensile strength test is determined according to TS EN 12390-6 standard (TS EN 12390-6, 2010). The cube specimens (100x100x100 mm) were placed in the compression testing machine and were loaded at 0.47 kN/sec. 100 mm long iron pieces were placed on the upper and lower parts of the samples in order to prevent the samples from disintegrating and fragmenting and to ensure fracture in a uniform section.

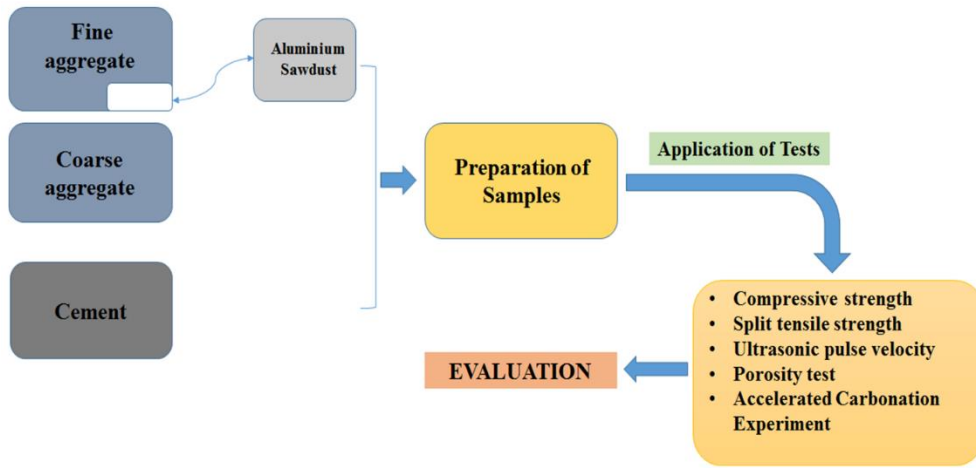


Figure 2. Flow chart of the study.

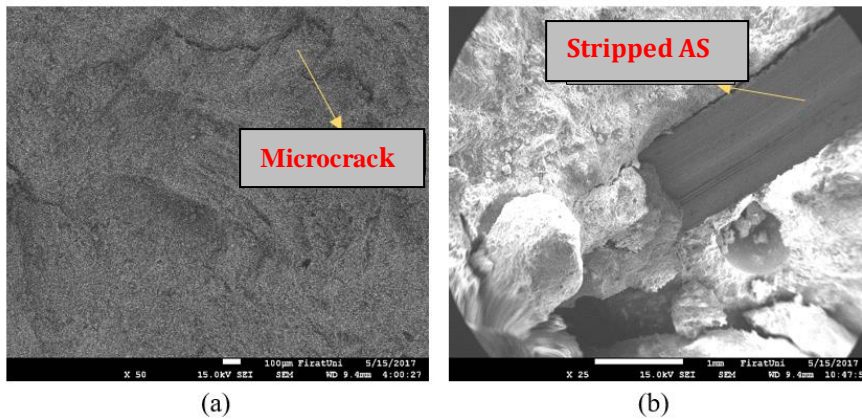


Figure 3. SEM image of the sample (a) without AS (b) with AS.

The average compressive strength of three cube specimens of each concrete mixture was termed as the compressive strength of that concrete mixture. Splitting tensile strength of concrete specimens was calculated as given in the Equation 1.

$$f_{ct} = \frac{2P}{\pi DL} \quad (1)$$

where;

f_{ct} : Split-tensile strength of concrete in MPa

P : Maximum load N

D : Diameter of the cube-specimen in 'mm'

L : Length of the cube-specimen in 'mm'.

2.4.3. Ultrasonic pulse velocity (UPV)

The UPV test was determined according to the TS EN 12504-4 standard (TS EN 12504-4, 2004). Ultrasound velocity measurement was made with an ultrasound measuring instrument with a digital display. Before starting the measurements, the device was calibrated each time. Vaseline was applied to the sample surface to prevent any gaps between the probes and the concrete sample. The transmission time of the sound through the concrete sample was determined by placing an ultrasound transmitter on one end of the concrete sample and a receiver receiving the sound waves passing through the material at the other end. From here, the propagation speed of sound was found (Saint-Pierre et

al., 2016). Ultrasound test was applied to 3 samples from each of 9 different concrete series, including samples subjected to carbonation before carbonation, 1 day, 3 days and 7 days carbonation. Two readings were taken from the 4 side surfaces of the samples prepared for the experiment. The averages of the measured data of each series were recorded as the sound waves transmission time of that series.

2.4.4. Porosity test

The porosity test was determined according to the TS EN 772-4 standard (TS EN 772-4, 2000). The porosity determination test was applied to 3 samples from each of 9 different concrete series, which were cured in lime-saturated water for 28 days, using a porosity measuring scale. The porosity value was obtained by using the formula given in Equation 2 (Safiuddin and Hearn, 2005). The averages of the data obtained as a result of this experiment were recorded as the porosity value of that series.

$$p = \frac{W_{ssd} - W_{dry}}{W_{ssd} - W_{water}} * 100 \quad (2)$$

P : Porosity (%)

W_{ssd} : Saturated surface dry weight of samples (kg)

W_{dry} : Oven-dry weight of samples (kg)

W_{water} : Weight of samples under water (kg) (TS EN 772-4, 2000).

2.4.5. SEM observations

In the study, the microstructure of AS concrete was investigated using scanning electron microscopy (SEM). In the SEM images, the formation of wider cracks, openings and interfacial voids in the concrete matrix was observed with the addition of AS (Figure 3).

When Figure 3 (a) is examined, despite the x50 magnification, no obvious cracks were observed in the micro image without AS. When Figure 3 (b) is examined, it is understood from the micro-image of the sample that the adherence due to the use of sawdust is not complete, and from the trace left by the AS peeling off. In addition, microcracks are clearly visible.

2.4.6. Accelerated carbonation experiment

The carbonation depth was measured in accordance with the BS EN 13293-2004 standard (Safiuddin and Hearn, 2005). For carbonation to take place, sodium dichromate was chosen for 55% humidity at 20 °C (Figure 4) (Gönen and Yazıcıoğlu, 2005). The saturated solution of sodium dichromate was placed in the water container inside the tank and the temperature of the water was kept at 20 °C throughout the experiment. The samples were placed in the tank at regular intervals and with no surfaces touching each other, and the lid of the tank was tightly closed so that there would be no gas leakage. 40% CO₂ was given into the tank from the CO₂ filled tube via a one-way valve. In 9 different concrete series, the samples

were exposed to carbonation according to different time periods as 1 day, 3 days and 7 days.

Compressive strength, splitting tensile strength, ultrasound and porosity tests were performed on the samples removed from the carbonation tank. The samples, which were divided into two after the split tensile test, were cleaned from the dust and particles on the surface, and then 1% phenolphthalein (C₂OH₁₄O₄) - 70% ethyl alcohol solution was sprayed. It reacted with phenolphthalein and its hydration product, Ca(OH)₂ and dyed that area pink, and no color change was observed in the carbonation parts of the samples. Depths of parts that do not change color on concrete samples As seen in Figure 5, it was measured from 8 different places and carbonation depth was determined using Equation 3.

$$D = \frac{A_1 + A_2 + B_1 + B_2 + C_1 + C_2 + D_1 + D_2}{8} \quad (3)$$

D : Average carbonation depth (mm)

A,B,C : Carbonation depth of each surface.

The results of pre-carbonation (free carbonation) and post-carbonation compressive strength, splitting tensile strength, ultrasound transmission velocity and porosity tests are summarized in Table 3.

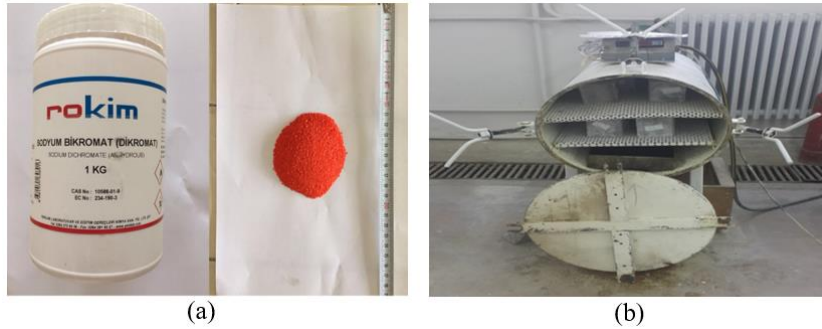


Figure 4. (a) Sodium bichromate salt (b) Gas-leakproof tank used for carbonation test.

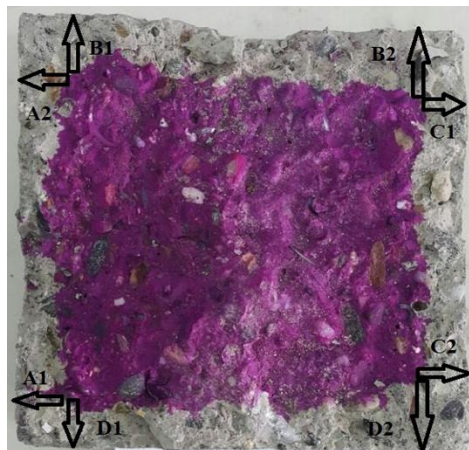


Figure 5. Carbonation depth measured at the sample surface.

Table 3. Test results of concrete series containing various percentages of AS

Mixture Code		0.4AS0	0.4AS5	0.4AS10	0.5AS0	0.5AS5	0.5AS10	0.6AS0	0.6AS5	0.6AS10	
Compressive strength (MPa)	Free Carbonation	67.78	49.15	39.03	53.34	40.09	36.58	37.19	36.1	34.91	
	Carbonation days	1	68.65	50.92	40.36	56.06	41.02	36.97	41	38	36.37
		3	69.14	51.03	41	56.1	42.56	39.21	41.84	39	37.56
		7	69.8	57.23	46.08	57.84	45.99	40.76	43.55	42	39.7
Split tensile strength (MPa)	Free Carbonation	3.8	2.65	2.43	3.38	2.57	2.41	3	2.5	2.25	
	Carbonation days	1	3.93	2.96	2.58	3.43	2.94	2.84	3.08	2.5	2.38
		3	4.35	3.19	2.75	3.55	3.12	2.85	3.14	2.67	2.4
		7	4.75	3.58	2.99	4.12	3.3	2.91	3.2	2.9	2.87
Ultrasonic pulse velocity (km/sec)	Free Carbonation	4.85	4.66	4.55	4.44	4.37	3.91	4.42	4.28	3.89	
	Carbonation days	1	4.82	4.77	4.55	4.32	4.2	4.16	4.38	4.3	4.09
		3	4.98	4.73	4.54	4.38	4.25	4.13	4.44	4.3	4.07
		7	5	4.8	4.65	4.66	4.36	4.33	4.5	4.35	4.16
Porosity test (%)	Free Carbonation	6.03	6.9	7.19	11.53	14.96	14.99	12.46	17.55	18.14	
	Carbonation days	1	7.4	12.16	11.49	11.75	14.49	14.17	14.15	16.28	17.27
		3	8.34	11.35	12.48	11.25	14.39	14.11	13.8	15.1	16.51
		7	7.35	10.48	11.3	11.26	14.34	14.09	14.5	15.3	15.95

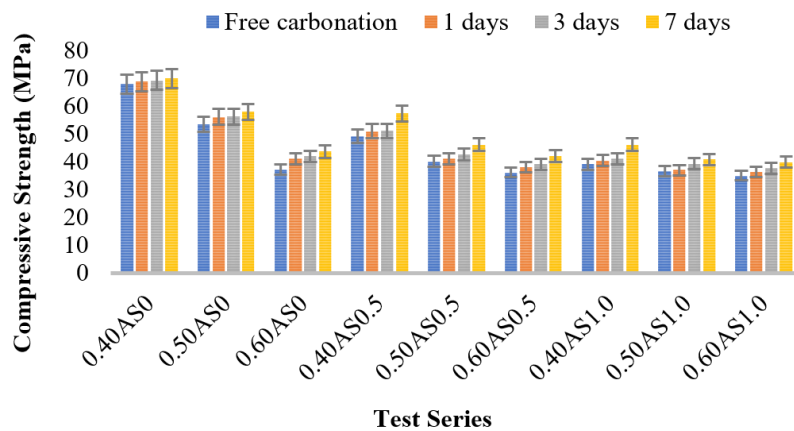


Figure 6. Relationship between compressive strength-carbonation curing ages.

3. Results and Discussion

3.1. Compressive Strength

The compressive strength values of the prepared series, with and without AS were determined according to the different curing times before and after the carbonation test (Figure 6). In accordance with the literature, the time-dependent compressive strength value increased as expected. However, with the increase of AS amount, the compressive strength value decreased. Due to AS particle sizes, it could not fully settle in the mortar and created voids, and at the same time, it negatively affected the workability of the concrete. Therefore, it was concluded that the compressive strength of concrete also decreased. Seyed; In his study with steel fiber, he mentioned that the steel fiber additive affects the workability of concrete negatively and reduces the compressive strength (Gupta et al., 2016). The changes in the compressive strength values of the series without AS and with 0.5% AS, with a W/C ratio of 0.40-0.50-0.60 before carbonation, are 27.37%, 24.84% and 2.93%, respectively. On the other

hand, the compressive strength value of the series exposed to carbonation for 7 days increased by 2.89% compared to pre-carbonation. This shows that carbonation has a positive effect on the compressive strength of concrete.

With the emergence of CaCO₃, which is the product of the carbonation reaction in concrete, an increase in density occurred in the carbonated parts and this density increase on the surface showed itself with a slight increase in strength. This situation is also compatible with the literature. Erdogan (2003) stated that the water released as a result of the carbonation event may cause some increase in strength by helping the hydration of the cement.

3.2. Split Tensile Strength

The comparison of the splitting tensile strength values of the prepared test series was determined according to the different curing times before and after the carbonation test, with and without AS (Figure 7).

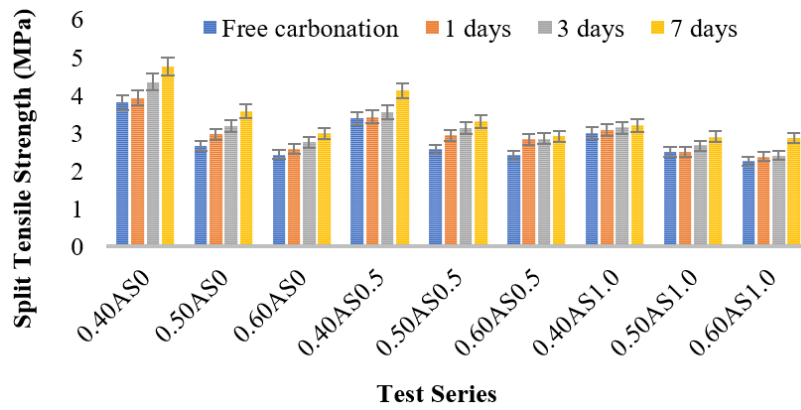


Figure 7. Relationship between split tensile strength-carbonation curing ages.

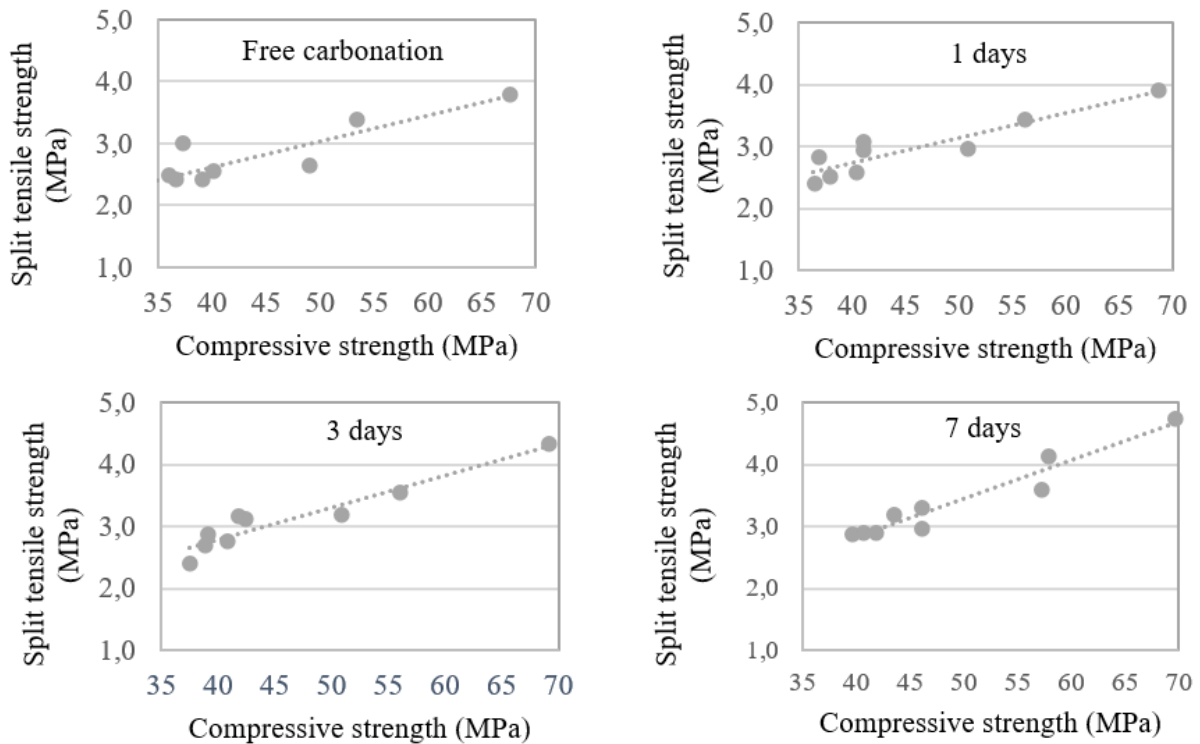


Figure 8. Relationship between compressive strength and split tensile strength of all test series.

In Figure 7, when the concrete samples exposed to carbonation for 7 days were examined, the split tensile strength values increased between 6.65% and 34.68% compared to the control samples. Among the samples exposed to carbonation for 7 days, the highest splitting tensile strength is seen in 0.4AS0 concrete samples, and the lowest splitting tensile strength is seen in 0.6AS10 concrete samples. It is seen that the most suitable ratio for the concrete series containing AS, which has been exposed to carbonation for 7 days, is the 0.4AS5 concrete series. In summary, it is seen that the splitting tensile strength of the concrete mixtures containing AS is lower than the concrete mixtures without AS at all curing ages, and the splitting tensile strength decreases due to the voids formed as the amount of AS increases.

When the comparison of compressive strength and splitting tensile strength values is examined in Figure 8, split tensile strength values increase in parallel with the compressive strength in accordance with the literature.

3.3. Ultrasonic Pulse Velocity (UPV)

When Figure 9 is examined, the highest ultrasound transmission rate in the control series is seen in the 0.4AS0 series, and the lowest ultrasound transmission rate in the 0.6AS10 series. It was determined that the most suitable ratio for the concrete series containing AS that was not exposed to carbonation was the 0.4AS5 series.

In Figure 9, there was an increase of approximately 3% between the control series and the 7-day ultrasound transmission rate values. It was determined that carbonation increased the ultrasound transmission rate. CaCO_3 , which is formed as a result of carbonation, reduces the permeability and creates a structure with less voids in the concrete. Thus, as the ultrasound waves propagate faster in the concrete, the ultrasonic transmission velocity values increased due to carbonation.

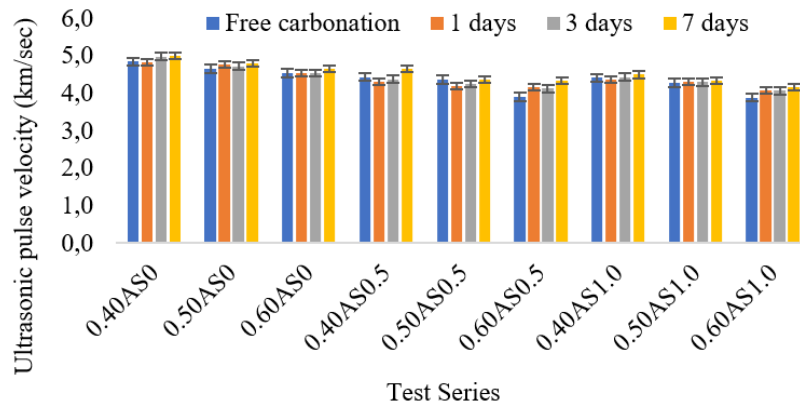


Figure 9. Relationship between ultrasonic pulse velocity-carbonation curing ages.

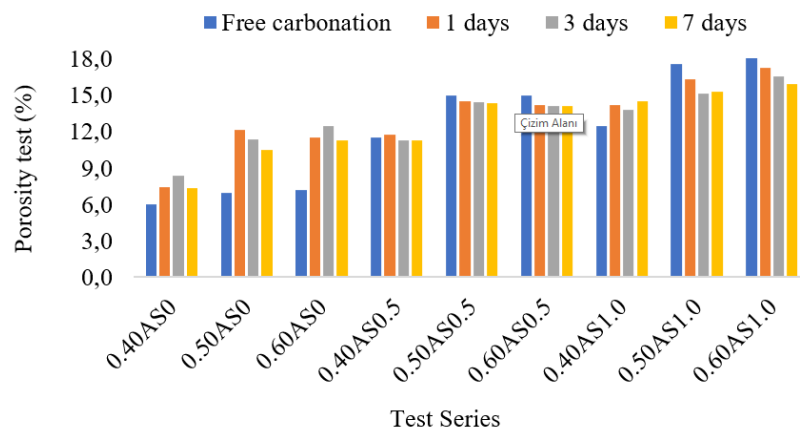


Figure 10. Relationship between porosity-carbonation curing ages.

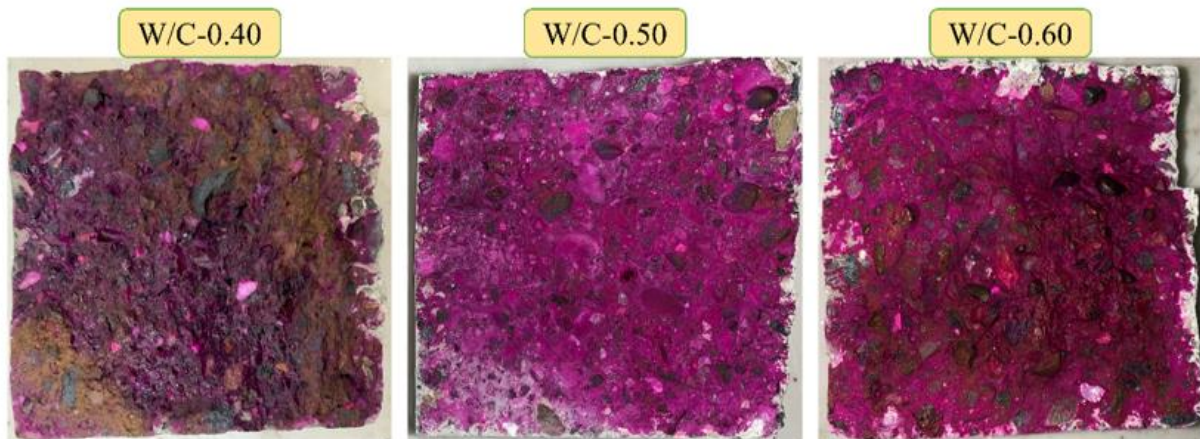


Figure 11. Carbonation depths of series with different W/C ratios after 7 days of carbonation (mm).

3.4. Porosity Test

Porosity test results of control series and 1, 3, 7-day series presented at Figure 10. Among the control series, the highest porosity rate was observed in the 0.6AS10 series, and the lowest porosity rate was observed in the 0.4AS0 series. It is seen that the porosity increases as the AS ratio and W/C ratio increase. Calcium carbonate, which emerges as a product of carbonation, occupies more space than calcium hydroxide, thus reducing the porosity of carbonated concrete (Cauger et al., 2010; Tafraoui, et al., 2016). The CO₂ penetrating into the concrete and the Ca(OH)₂

that comes out with the hydration of the calcium silicate components in the cement react to form CaCO₃ (calcium carbonate), which is larger in volume. Increasing the amount of voids in the concrete means more CO₂ entering the concrete. This causes the formation of more CaCO₃ (calcium carbonate) and increases the depth of carbonation. When Figure 11 is examined, it is seen that the carbonation depth increases as the W/C ratio increases. The reason for this is that excess water creates a hollow structure in the concrete and facilitates the entry of CO₂ into the concrete, causing more CaCO₃ (calcium carbonate) to form (Brandt, 2005).

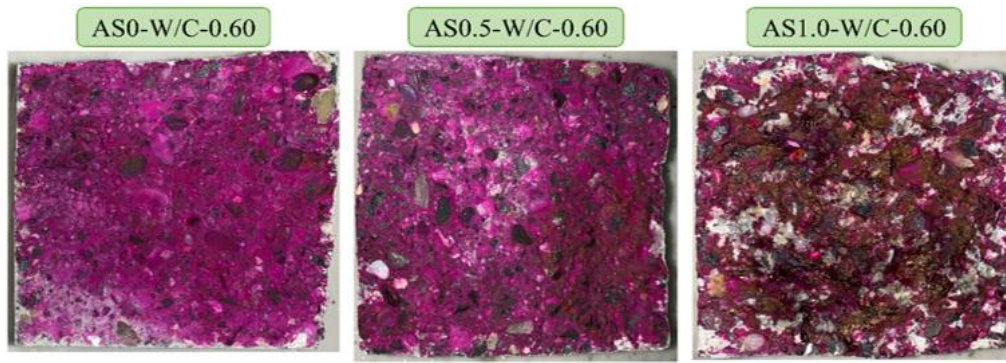


Figure 12. Carbonation depths of series with different sawdust ratios after 7 days of carbonation (mm).

As can be seen in Figure 12, the increase in sawdust rate causes an uneven distribution in carbonation. Since the increase in the amount of sawdust makes it difficult for the concrete to settle, gaps have occurred in the parts where the sawdust is concentrated. These gaps facilitated the progression of CO₂ into the interior of the concrete. For this reason, the carbonation event not only occurred on the outer surface of the concrete, but also affected the inner parts of the concrete.

The relationship between compressive strength and carbonation depth is shown in Figure 13. When Figure 13 is examined, it is observed that the compressive strength value decreases with increasing carbonation depth. As the compressive strength increases, the permeability of concrete decreases. As a result, the CO₂ required for carbonation cannot easily penetrate the concrete and the amount of carbonation decreases (Erdogan, 2003). When the comparison is made according to the amount of AS, the compressive strength values of the series containing AS were higher.

3.5. Environmental Impacts with Life Cycle Assessment (LCA)

In this section, it is aimed to determine the environmental and economic effects of the concrete samples produced. According to the International Standard ISO 14044, one of the techniques for analyzing the environmental impact of manufactured products is the life cycle assessment (LCA) (Wang et al., 2017; Dong, 2018; Jain et al., 2020). With the LCA, it is possible to estimate the magnitude of environmental impacts. In this context, Energy Consumption (EC), Global Warming Potential (GWP) and Waste Generation (WG) were taken into account (Table 4). The flow chart of the life cycle prepared for this purpose is given in Figure 14.

When the feasibility of using waste materials in concrete is investigated, many advantages are provided in terms of sustainability, efficient use of natural resources, and reduction of the number of transportation required for the transportation of aggregates, by reducing the use of natural aggregate and replacing it with waste material. However, when the use of AS as a waste material in concrete is evaluated in terms of EC, GWP and WG, higher energy consumption has emerged in concretes with AS added. Parallel to this, the GWP and WG values also showed the same trend (Figure 15).

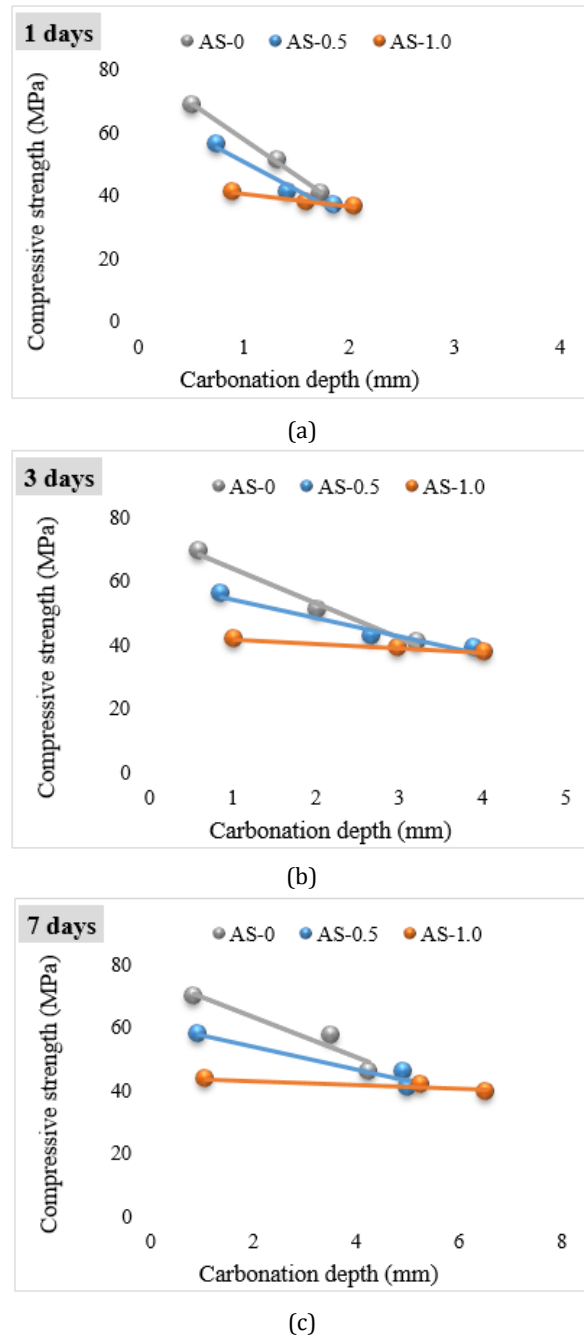


Figure 13. Relationship between compressive strength-carbonation depth (a) 1 days (b) 3 days (c) 7 days.

Table 4. Environmental impacts for process

Process	Energy Consumption (MJ)	Global Warming Potential (g CO ₂ eq)	Waste Generation (kg)
Cement production (per kg)	3.9854	881.987	
Cement transport (per km.kg)	1.5409	114.286	
FA production (per kg)	0.0219	2.108	-1
FA transport (per km.kg)	1.5409	114.286	
NA production (per kg)	0.0219	2.108	-1
NA transport (per km.kg)	1.5409	114.286	
Concrete production (per m ³)	20.0689	6529.676	

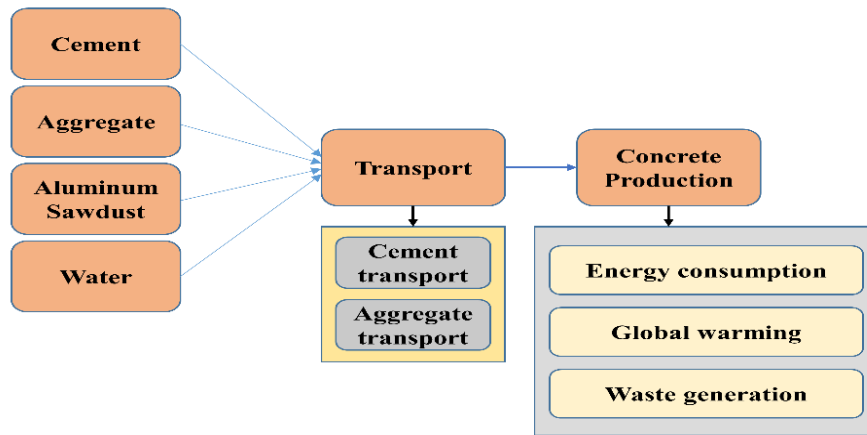


Figure 14. Environmental assessment of the concrete production process by LCA.

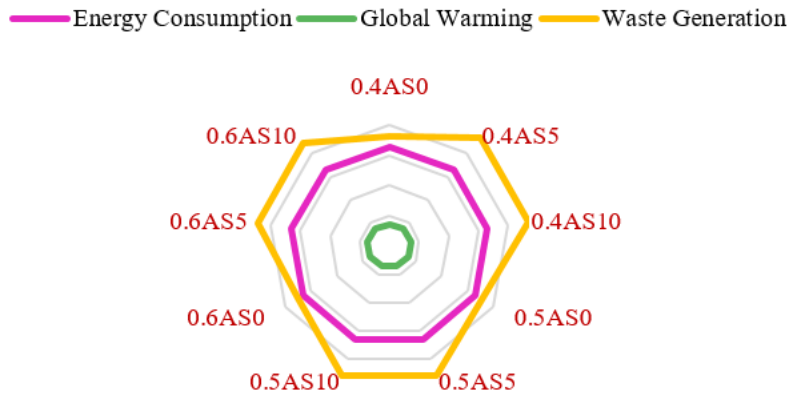


Figure 15. Life cycle results.

4. Conclusion

In this study, the changes in the mechanical properties of the concrete mixtures produced using different AS ratios in 3 different carbonation time periods and the environmental evaluation of these concretes were investigated. The findings obtained as a result of the study are given below in substances.

1. The highest increase in the compressive strength value after carbonation is observed in the 0.4AS5 series, and this increase is approximately 16%.
2. Since the homogeneous distribution of AS in the concrete mixture cannot be achieved, the workability of the concrete series with AS has decreased. As a result, the compressive strength of concrete was adversely affected. On the other hand, splitting tensile strength of AS added concrete series increased despite the negative

workability. The reason for this is that AS acts as reinforcement in the mortar and prevents the formation of cracks. Therefore, the use of AS in concrete up to a certain rate has a positive effect.

3. After a certain amount of AS, there was a decrease in compressive strength, splitting tensile strength and ultrasound transmission rate, while an increase in porosity and carbonation depth was observed. As with all other waste materials, the use of waste material above a certain rate adversely affects the mechanical properties of concrete.
4. In all series, as the number of days exposed to carbonation increased (from 0 to 7 days), the compressive strength, splitting tensile strength and ultrasound transmission velocity values increased in parallel with the carbonation depth.

The most significant increase was observed in the 0.4AS5 series. This situation shows the suitability of the use of AS in concrete, its usability in terms of economy and sustainability. On the other hand, when the evaluation was made within the scope of LCA, there was an increase in EC, GWP and WG values in the use of AS.

- Further research will be conducted to determine the effect of waste materials on carbonation and mechanical properties of concrete. Mechanical properties and structural behavior after cracking will be evaluated. In addition, the environmental impact of the use of waste materials in concrete will be evaluated, the positive and negative contribution of waste materials will be determined and comprehensive studies will be carried out on their use in concrete.

Author Contributions

The percentage of the author(s) contributions is presented below. All authors reviewed and approved the final version of the manuscript.

	T.D.	B.D.	M.Ö.
C	40	50	10
D	40	50	10
S	50	40	10
DCP	40	40	20
DAI	40	40	20
L	30	30	40
W	60	30	10
CR	40	50	10
SR	60	30	10

C=Concept, D= design, S= supervision, DCP= data collection and/or processing, DAI= data analysis and/or interpretation, L= literature search, W= writing, CR= critical review, SR= submission and revision.

Conflict of Interest

The authors declared that there is no conflict of interest.

Ethical Consideration

Ethics committee approval was not required for this study because of there was no study on animals or humans.

References

Alwaeli M, Nadziakiewicz J. 2012. Recycling of scale and steel chips waste as a partial replacement of sand in concrete. *Construct Build Mater*, 28(1): 157-163.

Babu VS, Mullick AK, Jain KK, Singh PK. 2015. Strength and durability characteristics of high-strength concrete with recycled aggregate-influence of processing. *J Sustain Cement-Based Mater*, 4(1): 54-71.

Balapour M, Joshaghani A, Althoey F. 2018. Nano-SiO₂ contribution to mechanical, durability, fresh and microstructural characteristics of concrete: A review. *Construct Build Mater*, 181: 27-41. <https://doi.org/10.1016/j.conbuildmat.2018.05.266>.

Binici H, Temiz H, Sevinç AH, Mustafa E, Mehmet K, Şayir Z.

2013. Investigation of high temperature effect of concretes containing aluminum sawdust, pumice and aerated concrete powder. *Construct Technol E-J*, 9(1): 1-15.

Brandt AM. 2005. Cement-based composites: materials, mechanical properties and performance. CRC Press, New York, US, pp: 544.

Cauberg N, Remy O, Pivard, J. 2010. Evaluation of durability and cracking tendency of ultra high performance concrete. *Taylor Francis, Creep, Shrinkage and Durability Mechanics of Concrete and Concrete Structures*, 2010: 695-700.

Cheng Y, You W, Zhang C, Li H, Hu J. 2013. The implementation of waste sawdust in concrete. *Engineering*, 5(12): 943.

Demir T, Ulucan M, Alyamac KE. 2022. Determination of the early age strength of high-strength concrete using RSM method. *Fırat Univ J Eng Sci*, 34(1): 105-114. <https://doi.org/10.35234/fumbd.972829>.

Öztürk M. 2020. The effect of waste aluminum sawdust reinforcement on the carbonation of concrete. MSc thesis, Graduate School of Natural and Applied Sciences, Fırat University, Elazığ, Türkiye, pp: 73.

Dong Y. 2018. Performance assessment and design of ultra-high performance concrete (UHPC) structures incorporating life-cycle cost and environmental impacts. *Construct Build Mater*, 167:414-425. <https://doi.org/10.1016/j.conbuildmat.2018.02.037>.

Erdogan T. 2003. Concrete. METU Press, Ankara, Türkiye, pp: 259.

Flores Medina N, Barluenga G, Hernández-Olivares F. 2015. Combined effect of Polypropylene fibers and Silica Fume to improve the durability of concrete with natural Pozzolans blended cement. *Construct Build Mater*, 96: 556-566. <https://doi.org/10.1016/j.conbuildmat.2015.08.050>.

Geçkinli E. 2002. Heat treatment of aluminum alloys. 2nd Heat Treatment Symposium, 2 - 3 June, İstanbul, Turkey, pp: 7-8,

Golewski GL. 2021. Green concrete based on quaternary binders with significant reduced of CO₂ emissions. *Energies*, 14(15): 4558.

Gönen T, Yazıcıoğlu S. 2005. Accelerated carbonation experiment and apparatus in concrete. *Polytechnic J*, 8(2): 233-237.

Gupta T, Chaudhary S, Sharma RK. 2016. Mechanical and durability properties of waste rubber fiber concrete with and without silica fume. *J Cleaner Prod*, 112: 702-711.

Jain S, Singhal S, Pandey S. 2020. Environmental life cycle assessment of construction and demolition waste recycling: A case of urban India. *Resour Conservat Recycl*, 155: 104642.

Martínez-Lage I, Vázquez-Burgo P, Velay-Lizancos M. 2020. Sustainability evaluation of concretes with mixed recycled aggregate based on holistic approach: Technical, economic and environmental analysis. *Waste Manag*, 104: 9-19.

Miličević I, Štirmer N, Bjegović D. 2011. Optimizing the concrete mixture made with recycled aggregate using experiment design. *Recent Advances in Fluid Mechanics and Heat & Mass Transfer*, August 23-25, Florence, Italy, pp: 110-115.

Osei DY, Jackson EN. 2016. Compressive strength of concrete using sawdust as aggregate. *Int J Sci Eng Res*, 7(4): 1349-1353.

Ramachandran VS, Beaudoin JJ. 2001. Handbook of analytical techniques in concrete. William Andrew Inc., London, UK, pp: 964.

Safiuddin M, Hearn N. 2005. Comparison of ASTM saturation techniques for measuring the permeable porosity of concrete. *Cement Concrete Res*, 35(5): 1008-1013.

Saint-Pierre F, Philibert A, Giroux B, Rivard P. 2016. Concrete quality designation based on ultrasonic pulse velocity.

- Construct Build Mater, 125: 1022-1027.
- Siddique R, Singh M, Mehta S, Belarbi R. 2020. Utilization of treated saw dust in concrete as partial replacement of natural sand. *J Cleaner Prod*, 261: 121226.
- Tafraoui A, Escadeillas G, Vidal T. 2016. Durability of the Ultra High Performances Concrete containing metakaolin. *Construct Build Mater*, 112: 980-987. <https://doi.org/10.1016/j.conbuildmat.2016.02.169>.
- TS EN 12390-3. 2019. Concrete-Hardened Concrete Tests-Part 3: Determination of Compressive Strength of Test Samples. Turkish Standards Institute, Ankara, Türkiye.
- TS EN 12390-6. 2010. Testing Hardened Concrete Part 6: Splitting Tensile Strength of Test Specimens. Turkish Standards Institute, Ankara, Türkiye.
- TS EN 12504-4. 2004. Testing concrete-Part 4: Determination of Ultrasonic Pulse Velocity. Ankara, Türkiye,
- TS EN 197-1. 2012. Cement - Part 1: General Cements, Composition, P. and C. C. Ankara, Türkiye.
- TS EN 772-4. 2000. Methods of test for masonry units-Part 4: Determination of real and bulk density. Turkish Standards Institute, Ankara, Türkiye.
- Wang J, Wang Y, Sun Y, Tingley DD, Zhang Y. 2017. Life cycle sustainability assessment of fly ash concrete structures. *Renew Sustain Energy Rev*, 80: 1162-1174.
- Zhang S, Zhang N, Zhang Y, Ding C, Zhang Y. 2023. Modification of granite sawdust with aluminum ester coupling agent and its novel application in high-density polyethylene composite plate. *J Build Eng*, 76: 107364.
- Zhong R, Wille K, Viegas R. 2018. Material efficiency in the design of UHPC paste from a life cycle point of view. *Construct Build Mater*, 160: 505-513. <https://doi.org/10.1016/j.conbuildmat.2017.11.049>.



EFFECT OF DIFFERENT STEP-LAP JOINTS ON THE NATURAL FREQUENCIES OF DIFFERENT ADHESIVELY BONDED METALLIC MATERIALS: A NUMERICAL STUDY

Ali İhsan KAYA^{1*}


¹Adiyaman University, Engineering Faculty, Mechanical Engineering Department, Adiyaman, 02040, Türkiye

Abstract: Due to their many applications' benefits, adhesively bonded joints are widely utilized in nearly every industry, including space, marine, automotive, and aeronautics. Since unpredicted loadings may cause resonance in the structures, an accurate prediction of the bonded joints' dynamic characteristics is crucial. Therefore, in this study, modal analysis was performed on the two-, three-, four- and double-step adhesively bonded lap joints of Aluminum (Al), Copper (Cu), and Mild steel (Ms) materials with Epoxy Araldite adhesive. Ansys commercial program was utilized to analyze it numerically. The results showed that modeling the bonding region of single lap joints as two-, three-, and four-step adhesively bonded lap joints has no significant effect on the natural frequencies. This modeling has a minor incremental effect on the natural frequencies. However, Double-step lap joints were found to cause a considerable reduction in natural frequencies compared to not only single lap joints but also two-, three-, and four-step adhesively bonded lap joints. Double-step bonding caused a decrease of 8.82%, 8.57%, and 8.73% for Al-Al, Cu-Cu, and Ms-Ms. In general, in all models, the best increase or decrease in terms of natural frequencies was found to be Cu-Cu adhesively lap joints.

Keywords: Adhesively bonded joints, Step-lap joints, Modal analysis, Finite element method

*Corresponding author: Adiyaman University, Engineering Faculty, Mechanical Engineering Department, Adiyaman, 02040, Türkiye

E mail: alikaya@adiyaman.edu.tr (A. İ. KAYA)

Ali İhsan KAYA  <https://orcid.org/0000-0002-3040-5389>

Received: December 04, 2023

Accepted: December 27, 2023

Published: January 15, 2024

Cite as: Kaya Aİ. 2024. Effect of different step-lap joints on the natural frequencies of different adhesively bonded metallic materials: A numerical study. BSJ Eng Sci, 7(1): 121-128.

1. Introduction

An adhesive is positioned between the adherend surfaces during the process of adhesive bonding, which creates an adhesive bond. Because adhesive joints combine many types of materials and have good damping qualities, high corrosion and fatigue resistance, fracture retardation, and labor, time, and cost savings, they are widely utilized in load-bearing structures across a wide range of industries. In addition to these better qualities, adhesive joints are the subject of some research that is being conducted in the literature because of their lightweight and simplicity of application (da Silva and Marques, 2008; Shang et al., 2019). As a result, simple fixes, including adhesive joints to link materials have been proposed and are still being proposed.

Single- and double- acting adhesive types are the most commonly utilized in bonded connections. A study (Apalak and Engin, 1997) used bonding models in single and double-reinforced lap joints. Four distinct single-lap joints of hybrid AA2024-T3 aluminum alloy and carbon/epoxy composites were explored by Gültekin et al. (2017). The impact of functionalized boron carbide and boron nitride nanoparticles on the bonded joints of aluminum alloy (AA2024-T3) was examined by Gültekin and Yazici (2022). The impact of surface preparation on the strength and performance of single-lap aluminum-

copper alloy joints for automotive applications was investigated by Boutar et al. (2016). They discovered that there was an inverse relationship between surface roughness and the shear strength of single lap joints, with rougher surfaces having lower wettability. The aluminum and carbon-epoxy components of hybrid adhesively-bonded single lap joints were examined by Ribeiro et al. (2016). The bonding strength of hybrid metal-fiber reinforced polymer single-lap joints was examined by Thomas et al. (2021).

Thakare and Dhumne (2015), simulated the different joint techniques of welding, riveting and adhesive bonding of Mild Steel (MS) by using the Finite Element Method (FEM) and stated that, with good fatigue and force resistance, these adhesives can offer substantial cost and weight reduction benefits. Erbayrak et al. (2017), used the FEM to investigate the impact of different adhesive types on the free transverse vibration of a single lap joint and concluded that varying the type of adhesive has a substantial impact on the natural frequency of lap joints. Hussain and Ingole (2022), surveyed the significant advancements in the field of dynamic characteristics of mechanical and structural joints, as well as the frequency domain dynamic analysis approach for nonlinear system parametric identification in structural dynamics. Aabid et al. (2021), studied a



beam plate structure's adhesive joints. Aluminum 2024-T3 and Araldite 2014 were taken into consideration for the beam and adhesive bond. They concluded that the adhesive layer used in the lap joint needs to be lengthy and thick to improve the structural performance of vehicle scale models. Dhilipkumar et al. (2022), have made an effort to provide a succinct overview of the vibrational properties, such as natural frequency, damping factor, and modal strain energies, which influence the strength of joints that are adherently linked. Ramalho et al. (2022), reviewed the most current studies that focus on the numerical examination of adhesive joints' dynamic behavior. Three distinct fields were identified under dynamic behavior: modal analysis, fatigue, and variable strain rate and impact. Sindi et al. (2021), used a functionally graded adhesive with a comparison of steel and aluminum adherents in their FEM model, and it was found that it produced natural frequency predictions that were consistent with the analytical model. Using a FEM, the first 20 natural frequencies of Single Lap Joints (SLJs) were predicted by He (2012). He and Oyadiji (2001), used a FEM to investigate the effects on the adhesive mechanical characteristics' natural frequencies. They found that, in general, changes to the Poisson's ratio do not significantly affect the natural frequencies. Van Belle et al. (2018), investigated a number of joining techniques for SLJ both numerically and experimentally. It was discovered that the natural frequencies predicted by the numerical technique for the adhesive joints were comparable to those seen in the experiments. Yaman and Sansveren (2021), examined composite SLJ, SSJ, and DSJ with various geometric modifications both experimentally and numerically. For the various joint configurations, there was a good correlation between the FEA and the experiments. Additionally, it was demonstrated that the natural frequencies are significantly affected by the fiber orientation angle and adherent thickness, increasing with the latter. Conversely, as overlap duration grows and adherent thickness drops, the damping ratio gets better. Du and Shi (2014), considered how vibration fatigue affects the modal characteristics of single-lap joints and tried to determine how the modal characteristics of the jointed structure and the fatigue damage in the adhesive layer are related. Different step-lap joint's fatigue performances subjected to tensile loading were studied by Demiral and Mamedov (2023). They studied how the step-lap joint's failure characteristics change under cyclic tensile loading because these loadings can cause adhesively bonded joints to fail, even at low percentages of their static strengths.

Although studies on the modal analysis of adhesively bonded joints have started to increase in recent decades, new studies in this field are important in terms of understanding the nonlinear dynamics and the effect of different adherents and adhesives on the dynamic characteristics of adhesively bonded joints. Therefore, in

this study, modal analysis was performed on the two-, three-, four- and double-step lap joints of Al, Cu, and Ms plate materials with Epoxy Araldite adhesive. Ansys commercial program was utilized in order to analyze it numerically. To the best of the author's knowledge, although there are studies on the modal analysis of adhesively bonded joints, there is no such comprehensive study on the change in dynamic properties of different metallic materials for the structural state of two-, three-, four- and double-step adhesively bonded lap joints in different configurations. Therefore, this study aims to fill this gap in the literature and contribute to the literature on the change of dynamic parameters of adhesively bonded joints.

2. Materials and Methods

2.1. Modal Analysis

The process of creating a mathematical model for a system's dynamic behavior by ascertaining its innate dynamic properties, such as natural frequencies, damping factors, and mode shapes, is known as modal analysis. The effectiveness of many structural dynamics applications depends only on having a precise mathematical model for a dynamic structure. Finite element modeling, which takes the form of mass and stiffness matrices, can be used to create such a model. Because of the robustness of this technique, the resulting FE model may be crucial for further applications such as prediction (He and Fu, 2001).

Numerous variables, including the type of joint, geometrical specifications, adherend materials, and adhesive properties, affect the strength and dynamic properties of bonded joints. Since unpredicted loadings may cause resonance in the structures, an accurate prediction of the bonded joints' dynamic characteristics is crucial for the appropriate characterization of their service life.

Ramalho et al. (2022), stated that numerical models currently used in the literature are becoming the benchmark for evaluating various analytic techniques. Furthermore, the studies that conducted experimental and numerical data demonstrated how accurate these models were in predicting the natural frequencies. Therefore, the modal analysis of the lap joints is performed using one of the FE programs in this study. Ansys 2023, a commercial program, was used to simulate the modal analysis of different step-lap composite joints. A thorough analysis was conducted to determine how the various step-lap arrangements, as per the geometric configurations in Demiral and Mamedov (2023), affected the metallic joints' service life.

2.2. Validation of the Method

For validation, the study of Patil and Barjibhe (2013), was taken into consideration. Al-Al, Cu-Cu, and Ms-Ms plates with epoxy adhesives, as in the considered study, were modeled in Design Modeler. The dimensions of all plates were 140 mm x 38 mm x 5 mm, and the overlap length was 15 mm. Since the adhesive thickness is not

specified in the relevant study and the thickness of adhesive material is more a determinant of the damping coefficient than the natural frequencies of bonded material, a 0.15 mm thickness was chosen as such by Du and Shi (2014). The properties of materials used for analysis are given in Table 1. "Bonded" contacts were identified on the model. "Multi-Point Constraint (MPC)", generally the ideal contact formulation option for contacts with no separations and bonded contacts, was chosen for formulation, and "Nodal-Normal to Target" was used for detection method (Giannetti, 2020). Mesh numbers were reduced until no significant change was seen in the analysis results, as stated by Moaveni (2015). After the change in the analysis results reaches very low levels, the mesh parameters for the element are decided upon. Therefore, the default element size was utilized. The Contact sizing method was used to have more elements on the bonded areas, as could be seen in Figure 1. Then the geometry was meshed. The mesh geometry was consisted of 42842 nodes and 7814 elements. The obtained results were compared with the aforementioned study, as seen in Table 2. As can be seen from the results, the analysis results of this study are quite compatible with the results of Patil and Barjibhe (2013).

2.3. Numeric Analysis of Step-Lap joints

After the validation process, by using the same formulation, detection method and other properties, modal analysis of step-lap joints with different geometric configurations as such in the study of Demiral and Mamedov (2023), was carried out. The different geometric configurations in the study of Demiral and

Mamedov (2023), were adapted into the current study accordingly. Hence, materials and thickness were altered proportionally. Because the thickness in the relevant study was different from the thickness in the current study, step-lap configurations were adapted proportionally according to the measurements given in the reference study.

The Same procedure was followed in the process of analyzing step-lap joints. "Bonded" type contact region were determined. The behavior in the analysis was chosen as "Symmetric". Since "Symmetric" behavior is more complex and refers to both Contact and Target surfaces (URL1). Multi-Point Constraint (MPC), generally the ideal contact formulation option for contacts with no separations and bonded contacts, was chosen for formulation, and "Nodal-Normal to Target" was used for the detection method (Zhu, 2017). "Nonlinear Mechanics" was favored under the mesh module for the physics reference because of the nonlinear structure of adhesive lap joints. A Fixed boundary condition was applied for having a cantilever beam as shown in Figure 2. A mesh convergence was conducted as in the validation section. To have more mesh geometry in the contact region, contact sizing was added to the bonded areas. After meshing, the skewness of the mesh geometry was obtained as 0.625 which was reported as a good ratio (Çitil et al., 2019). After the solution, the participation factor summary was examined to comment on in-plane and out-of-plane modes. Besides, the "Ratio of Effective Mass to Total Mass" under the solution module was always checked to have a ratio of 90 % for the plane axes.

Table 1. Properties materials used for validation

Bonded Materials	Aluminum	Copper	Mild Steel	Araldite
Young Modulus (GPa)	70.3	129.8	200	0.93
Density (kg/m ³)	2700	8960	7850	1070
Poisson ratio	0.35	0.34	0.303	0.32

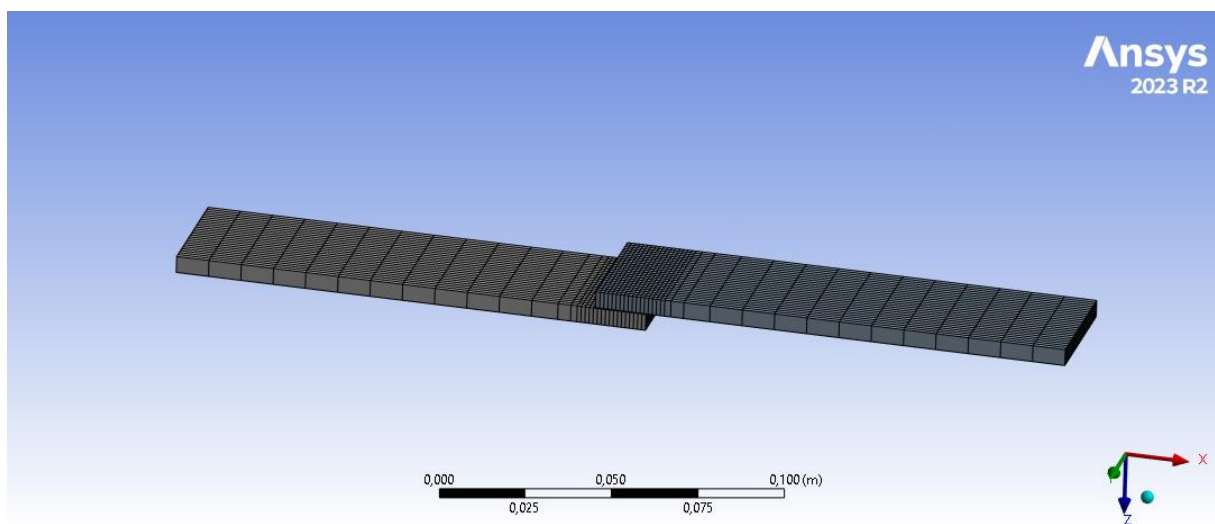


Figure 1. Mesh configuration of the single lap model.

Table 2. Natural frequencies of the analysis

Bonded Materials	Mode I ^a	Mode I*	Difference (%)
Al-Al	59.476	59.002	0.8
Cu-Cu	42.563	42.062	1.12
Ms-Ms	58.975	58.203	1.33

^a This study, *Patil and Barjibhe (2013).

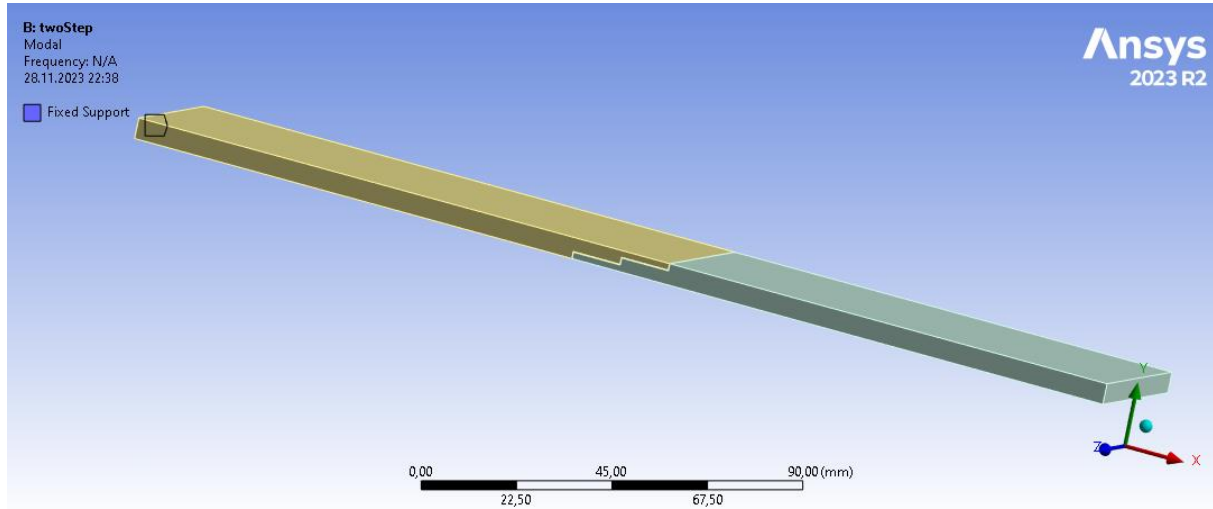


Figure 2. An example of boundary conditions for stepped lap joint.

3. Results and Discussion

Since most adhesives are viscoelastic, they have an advantage over alternative joining techniques in terms of mitigating vibration issues (Ramalho et al., 2022). In this instance, the modal loss factor tends to rise with increasing adhesive thickness and overlap length. To find the ideal adhesive thickness for a certain application, one must constantly analyze these two parameters because raising the adhesive thickness also causes a drop in natural frequencies. In the validation method section, the single-lap overlap length was 15 mm (Patil and Barjibhe, 2013). To adapt this thickness value to the reference study, a re-analysis was carried out with an overlap length of 25 mm for the single-lap joints by using the same analysis steps. The first three natural frequency analysis results are given in Table 3. By comparing Tables 2 and 3, it is possible to comment that the joint's natural frequencies increase with the overlap length. However, it was reported that its impact on joint strength becomes negligible beyond a certain length (Akpınar et al., 2022). Wani (2015), stated that as the joint's overlap length increases, so does the system's inherent frequency. Given that the joint system has a tendency to stiffen as overlap length increases, this pattern makes sense. However, for overlap lengths of 30 mm and more, it is almost constant. In terms of natural frequencies, the same outcomes were reported in other studies (Wang et al., 2019, Ingole and Chatterjee, 2011). Therefore, it could be stated that the increase in natural frequencies is compatible with the literature.

The first ten extracted natural frequency results after re-modeling the bonded area into two-step lap joints are

given in Table 4. When the frequencies in the relevant table are examined, it is seen that the fundamental natural frequencies for all metallic two-step lap joints are increased. When the current analysis result is compared to single-lap joints results in Table 3, the following consequences could be deduced based on fundamental natural frequencies: While the increase for Al-Al two-step lap joints is around 0.34%, this rate is around 0.61% for Cu-Cu and 0.42% for Mild steel two-step lap joints. Therefore, it was observed that there is a minor increase, although not a significant improvement, in the natural frequencies of all metallic two-step lap joints. The improvement in fundamental natural frequencies was the best in Cu-Cu two-step lap joints; this was followed by Ms and Al two-step lap joint structures, respectively.

Table 3. The first three natural frequencies of single-lap joints for 25 mm overlap length

Bonded Materials	Mode I	Mode II	Mode II
Al-Al	63.785	402.15	456.25
Cu-Cu	47.422	300.74	340.63
Ms-Ms	62.838	397.75	451.82

The results of the first ten extracted natural frequencies of the three-step lap joints are given in Table 5. When this table is reviewed, it is seen that the natural frequencies in all metallic three-step lap joints are close to the results of two-step lap joints, and there is no substantial change in terms of fundamental natural frequencies but rather a slight increase in the case of three-step lap joints.

Table 4. Natural frequencies of two-step cantilever lap joints

Natural Frequencies of Extracted Modes (Hz)			
Modes	Al-Araldite-Al	Cu-Araldite-Cu	Ms-Araldite-Ms
1 st mode	64.001	47.71	63.102
2 nd mode	400.52	298.8	395.2
3 rd mode	473.41	353.15	468.15
4 th mode	789.68	591.31	794.39
5 th mode	1122.2	836.42	1106.3
6 th mode	2214.5	1651.6	2183.4
7 th mode	2396.5	1794.4	2409.6
8 th mode	2704.5	2019.6	2681.4
9 th mode	3701.4	2758.4	3645.3
10 th mode	4084.3	3056.9	4101.4

Table 5. Natural frequencies of three-step cantilever lap joints

Natural Frequencies of Extracted Modes (Hz)			
Modes	Al-Araldite-Al	Cu-Araldite-Cu	Ms-Araldite-Ms
1 st mode	63.982	47.693	63.069
2 nd mode	400.48	298.73	395.06
3 rd mode	472.99	352.83	467.73
4 th mode	789.19	590.93	793.86
5 th mode	1122.6	836.7	1106.5
6 th mode	2214.6	1651.5	2183
7 th mode	2395.3	1793.6	2408.3
8 th mode	2702.9	2018.3	2679.5
9 th mode	3697.3	2755.2	3640.7
10 th mode	4081.4	3054.7	4098.3

Table 6. Natural frequencies of four-step cantilever lap joints

Natural Frequencies of Extracted Modes (Hz)			
Modes	Al-Araldite-Al	Cu-Araldite-Cu	Ms-Araldite-Ms
1 st mode	63.894	47.63	62.997
2 nd mode	399.84	298.26	394.51
3 rd mode	472.7	352.62	467.45
4 th mode	788.73	590.59	793.41
5 th mode	1121.1	835.6	1105.2
6 th mode	2214.1	1651.3	2183
7 th mode	2393.7	1792.4	2406.7
8 th mode	2701.7	2017.4	2678.4
9 th mode	3704.5	2760.7	3648.4
10 th mode	4079.7	3053.5	4096.7

When the analysis results of three-step lap joints are compared to single-lap joints' results in Table 3, the following deductions could be extracted based on fundamental natural frequencies: in the case of Al-Al three-step lap joints, the increase is found to be 0.31% while it is obtained as 0.57% for the Cu-Cu three-step lap joints and 0.37% for Mild steel three-step lap joints. Consequently, it was found that all metallic three-step lap joints have somewhat higher natural frequencies, albeit not noticeably better. Cu-Cu three-step lap joints showed the most improvement amongst fundamental natural frequencies of all metallic materials; mild steel and aluminum three-step lap joint structures came in a row, respectively. It should be emphasized that these results are compatible with the two-step lap joints.

The results of the first ten extracted natural frequencies of the four-step lap joints are given in Table 6. When this table is examined, it is seen that the natural frequencies in all metallic lap joints are almost the same in the three-step lap joints. Therefore, it could be stated that among the all fundamental natural frequencies of all metallic materials, Cu-Cu three-step lap joints demonstrated the biggest improvement; mild steel and aluminum four-step lap joint followed, respectively. It is important to note that these outcomes are consistent with the results of two- and three-step lap joints.

The natural frequency results of the first ten extracted natural frequencies of the double-step joints are given in Table 7. When this table is reviewed, unlike the analysis results of the two-, three-, and four-step lap joints, all

metallic joints showed a substantial decrease in terms of natural frequency. When single-lap joints are taken into consideration for comparison to the double-step lap joint results, the following conclusion may be drawn based on the fundamental natural frequencies: Al-Al, Cu-Cu and Ms-Ms double-step lap joints showed a decrease of 8.82%, 8.57% and 8.73% respectively. Hence, it was observed that all metallic adhesively bonded structures were affected at approximately the same reduction rate in the case of the geometric configuration of double-step lap joints. Besides, it was found that the results of double-step lap joints are the geometric configuration that has the most adverse effect among the geometric lap joints considered.

When Tables 4, 5, 6 and 7 are compared, one can observe that the geometrical configurations of two-, three-, and four-step lap joints have no significant effect on the natural frequencies as per a single-lap joint. Therefore, it is possible to say that there is no point in modeling the bonding zone in a two-, three-, and four-step geometric configuration, which is more difficult in terms of production and application than single-lap, when the natural frequencies are considered. However, double-step geometric modeling is found to have a significant negative effect on the natural frequencies compared to the other geometric configurations. Although Demiral and Mamedov (2023) stated that the double-step-lap joint had a 21.8% longer lifetime comparing fatigue cycles with other models, the analysis results in this study showed that the double-step geometric model is the weakest lap joint in terms of dynamic parameters. Therefore, it is beneficial to avoid the use of this geometric model in applications where dynamic parameters are deterministic.

Utilizing a Finite Element Analysis (FEA), He (2012) and He and Oyadiji (2001) investigated the impacts on the adhesive mechanical characteristics' natural frequencies. They demonstrated that, in general, modifications to the Poisson's ratio do not significantly affect the natural

frequencies. The same was noted for realistic variations in Young's modulus; however, the natural frequencies underwent a dramatic alteration when a very low Young's modulus, less than 1 GPa, was used. Therefore, these reported findings support the finding that the natural frequency results of the metallic materials analysed in this study are close to each other.

It is reported that the overlap length only slightly affects frequency by Guo and Wang (2020). Furthermore, there is a very little tendency for the natural frequency to decrease as adhesive thickness increases. The impact of bonding length and adhesive thickness on shifting resonance frequencies is still limited because of its small mass. He (2012) found comparable results regarding adhesive thickness, while Gunes et al. (2010), stated similar tendencies regarding bonding length. While it has no effect on the resonance frequency when combining materials with a high density. This finding is in line with the initial parameters of this study.

Du and Shi (2014), stated that the modal frequency changes seen in their studies require drastic decreases in modulus and contact area values, which may not always be feasible, according to their simulation data. Besides, changes in the adhesive mechanical properties—Young's modulus, density, and Poisson's ratio—did not significantly affect the natural frequencies, according to Apalak et al. (2006). Therefore, the natural frequency results for different step lap joints in Al and Ms are very close to each other, and the significant decrease in natural frequencies caused by the sudden geometric change in the bonding zone is in line with the findings of this study.

4. Conclusion

In this study, the effect of different stepped configurations of the bonding area on the natural frequencies of adhesively bonded joints of metallic materials is investigated. The conclusions drawn from this study can be summarized as follows:

Table 7. Natural frequencies of double-step cantilever lap joints

Natural Frequencies of Extracted Modes (Hz)			
Modes	Al-Araldite-Al	Cu-Araldite-Cu	Ms-Araldite-Ms
1 st mode	58.161	43.358	57.351
2 nd mode	363.94	271.48	359.11
3 rd mode	431.06	321.55	426.26
4 th mode	751	562.34	755.51
5 th mode	1020.1	760.29	1005.7
6 th mode	2013.4	1501.7	1985.3
7 th mode	2276.9	1704.8	2289.5
8 th mode	2481.7	1853	2459.9
9 th mode	3370.5	2511.6	3319.6
10 th mode	3784.2	2899.7	3891.1

- It was seen that commercial FEM programs could be successfully used to model the dynamic parameters of adhesively bonded joints because the compatibility was approximately 98%.
- Modeling the bonding region of single lap joints as two-, three-, and four-step adhesively bonded lap joints has no significant effect on the natural frequencies. This modeling has a minor incremental effect on the natural frequencies.
- Although the increase in natural frequency is minor among two-, three-, and four-step adhesively bonded lap joints, it is observed that there is a relatively bigger improvement in the natural frequency of Cu-Cu lap joints compared to other metallic materials.
- Double-step lap joints were found to cause a considerable reduction in natural frequencies compared to not only single-lap joints but also two-, three-, and four-step adhesively bonded lap joints.

Author Contributions

The percentage of the author(s) contributions is presented below. All authors reviewed and approved the final version of the manuscript.

	A.İ.K.
C	100
D	100
S	100
DCP	100
DAI	100
L	100
W	100
CR	100
SR	100
PM	100
FA	100

C=Concept, D= design, S= supervision, DCP= data collection and/or processing, DAI= data analysis and/or interpretation, L= literature search, W= writing, CR= critical review, SR= submission and revision, PM= project management, FA= funding acquisition.

Conflict of Interest

The author declared that there is no conflict of interest.

Ethical Consideration

Ethics committee approval was not required for this study because of there was no study on animals or humans.

References

Aabid A, Khan SA, Al-Khalifah T, Parveez B, Anjum A. 2021. Parametric Analysis of Adhesively Bonded Single Lap Joint Using Finite Element Method. In: *Intelligent Manufacturing and Energy Sustainability*, 2020, Springer, Singapore, pp: 675-686. https://doi.org/10.1007/978-981-33-4443-3_65.

Akpınar S, Hacısalihoğlu I, Çalık A. 2022. The effect of geometry on joint strength in adhesively bonded joints with the same

adhesive area. *Mech Adv Mat Struct*, 2022: 1-13. <https://doi.org/10.1080/15376494.2022.2162641>.

ANSYS. 2023. The general purpose finite element software (Version 23.R2), Swanson Analysis Systems, Inc., Houston, TX, US.

Apalak MK, Ekici R, Yildirim M. 2006. Optimal design of an adhesively-bonded corner joint with single support based on the free vibration analysis. *J Adhes Sci Technol*, 20(13): 1507-1528. <https://doi.org/10.1163/156856106778666426>.

Apalak MK, Engin A. 1997. Geometrically non-linear analysis of adhesively bonded double containment cantilever joint. *J Adhes Sci Technol*, 11(9): 1153-1195. <https://doi.org/10.1163/156856197X00570>.

Boutar Y, Naimi S, Mezlini S. 2016. Effect of surface treatment on the shear strength of aluminium adhesive single-lap joints for automotive applications. *Int J Adhes Adhes*, 67: 38-43. <https://doi.org/10.1016/j.ijadhadh.2015.12.023>.

Çitil Ş, Bozkurt I, Aydın MD. 2019. Experimental and 3D non-linear stress analysis of adhesively bonded pipes with curved-surface lap joints. *J Adhes*, 95(5-7): 515-528. <https://doi.org/10.1080/00218464.2018.1562922>.

da Silva LFM, Marques EAS. 2008. Joint strength optimization of adhesively bonded patches. *J Adhes*, 84: 915-934. <https://doi.org/10.1080/00218460802505275>.

Demiral M, Mamedov A. 2023. Fatigue performance of a step-lap joint under tensile load: A numerical study. *Polymers*, 15(8): 1949. <https://doi.org/10.3390/polym15081949>.

Dhilipkumar T, Rajesh M, Soundhar A. 2022. Dynamic behaviour of adhesively bonded structures in aerospace applications: An overview. In: Sultan MTH., Rajesh M, Jayakrishna K, edit. *Repair of Advanced Composites for Aerospace Applications*, CRC Press, Boca Raton, US, pp: 47-53.

Du Y, Shi L. 2014. Effect of vibration fatigue on modal properties of single lap adhesive joints. *Int J Adhes Adhes*, 53: 72-79. <https://doi.org/10.1016/j.ijadhadh.2014.01.007>.

Erbayrak E, Ozer H, Erbayrak S, Çeper K, Ağirkol B, Güner E. 2017. Effect of adhesive type on Free Transverse Vibration of single lap joint. URL: <https://www.researchgate.net/> (accessed date: November 01, 2023).

Giannetti, FA. 2020. Finite Element modelling to predict wear in joint replacements. PhD thesis, University of Bologna, Department of Electrical, Electronic and Information Engineering, Cesena, Italy, pp: 46.

Gültekin K, Akpınar S, Özel A. 2017. Effects of unbalance on the adhesively bonded composites-aluminium joints. *J Adhes*, 93(9): 674-687. <https://doi.org/10.1080/00218464.2015.1136998>.

Gültekin K, Yazici ME. 2022. Mechanical properties of aluminum bonded joints reinforced with functionalized boron nitride and boron carbide nanoparticles. *P I Mech Eng L-J Mat*, 236(1): 37-49. <https://doi.org/10.1177/14644207211056020>.

Gunes R, Kemal Apalak M, Yildirim M, Ozkes I. 2010. Free vibration analysis of adhesively bonded single lap joints with wide and narrow functionally graded plates. *Compos Struct*, 92(1): 1-17. <https://doi.org/10.1016/j.compstruct.2009.06.003>.

Guo Q, Wang S. 2020. Free vibration analysis and optimal design of adhesively bonded double-strap joints by using artificial neural networks. *Latin Am J Solids Struct*, 17(4): e271. <https://doi.org/10.1590/1679-78255878>.

He J, Fu ZF. 2001. *Modal Analysis*, Butterworth-Heinemann, 2nd ed., Oxford, UK, pp: 1-11.

He X, Oyadiji SO. 2001. Influence of adhesive characteristics on the transverse free vibration of single lap-jointed

- cantilevered beams. *J Mater Process Technol*, 119(1-3): 366-373. [https://doi.org/10.1016/S0924-0136\(01\)00936-0](https://doi.org/10.1016/S0924-0136(01)00936-0).
- He X. 2012. Numerical and experimental investigations of the dynamic response of bonded beams with a single-lap joint. *Int J Adhes Adhes*, 37: 79-85. <https://doi.org/10.1016/j.ijadhadh.2012.01.008>.
- Hussain F, Ingole S. 2022. A review on frequency domain analysis approach for parametric identification of nonlinear joints. *Recent Advances in Machines and Mechanisms: Select 9-11 December, Jabalpur, India*, pp: 79-96. https://doi.org/10.1007/978-981-19-3716-3_7.
- Ingole SB, Chatterjee A. 2011. Vibration analysis of single lap adhesive joint: experimental and analytical investigation. *J Vib Control*, 17(10): 1547-1556. <https://doi.org/10.1177/1077546310380429>.
- Moaveni S. 2015. *Theory and Application with ANSYS*, 4th ed. Pearson Education Limited, Essex, UK, pp: 435-438.
- Patil YB, Barjibhe RB. 2013. Modal analysis of adhesively bonded joints of different materials. *Int J Mod Eng Res*, 3(2): 633-636.
- Ramvalho LDC, Sánchez-Arce IJ, Gonçalves DC, Belinha J, Campilho RDSG. 2022. Numerical analysis of the dynamic behaviour of adhesive joints: A review. *Int J Adhes Adhes*, 118: 103219. <https://doi.org/10.1016/j.ijadhadh.2022.103219>.
- Ribeiro TEA, Campilho RDSG, da Silva LFM. 2016. Damage analysis of composite-aluminium adhesively-bonded single-lap joints. *Compos Struct*, 136: 25-33. <https://doi.org/10.1016/j.compstruct.2015.09.054>.
- Shang X, Marques EAS, Machado JJM, Carbas RJC, Jiang D, da Silva LFM. 2019. Review on techniques to improve the strength of adhesive joints with composite adherends. *Compos B Eng*, 177: 107363. <https://doi.org/10.1016/j.compositesb.2019.107363>.
- Sindi SA, Othman R, Almitani KH. 2021. Theoretical solution for the axial vibration of functionally graded double-lap adhesive joints. *Math Mech Solids*, 26(6): 823-842. <https://doi.org/10.1177/1081286520967709>.
- Thakare NB, Dhumne AB. 2015. A review on design and analysis of adhesive bonded joint by finite element analysis. *SSRG Int J Mech Eng*, 2(4): 6.
- Thomas R, Fischer F and Gude M. 2021. Adhesives for increasing the bonding strength of in situ manufactured metal-composite joints. *P I Mech Eng D-J Aut*, 235(13): 3256-3269. <https://doi.org/10.1177/0954407020965759>.
- URL1: ANSYS Mechanical APDL Contact Technology Guide 18.2, page 266. https://www.academia.edu/38866112/ANSYS_Mechanical_A_PDL_Contact_Technology_Guide (accessed date: October 02, 2023).
- Van Belle L, Brandolisio D, Deckers E, Jonckheere S, Claeys C, Pluyers B, Desmet W. 2018. Experimental validation of numerical structural dynamic models for metal plate joining techniques. *J Vib Control*, 24(15): 3348-3369. <https://doi.org/10.1177/1077546317704794>.
- Wang S, Li Y, Xie Z. 2019. Free vibration analysis of adhesively bonded lap joints through layerwise finite element. *Compos Struct*, 223: 110943. <https://doi.org/10.1016/j.compstruct.2019.110943>.
- Wani SS. 2015. Vibration analysis of adhesively bonded single lap joint. *Int Res J Eng Technol*, 2(2): 290-297.
- Yaman M, Sansverren MF. 2021. Numerical and experimental vibration analysis of different types of adhesively bonded joints. *Struct*, 34: 368-380. <https://doi.org/10.1016/j.istruc.2021.07.071>.
- Zhu Y. 2017. Best Practices for Contact Modeling using ANSYS. URL: <https://pic.huodongjia.com/ganhuodocs/2017-09-15/1505456086.9.pdf> (accessed date: September 04, 2023).



FALSE POSITIVES IN LUMINAL TESTING

Yakup GULEKCI^{1*}, Fatma CAVUS YONAR²

¹Kutahya Health Sciences University, Faculty of Engineering and Natural Sciences, Department of Forensic Sciences, 43100 Kutahya, Türkiye


²Istanbul University-Cerrahpasa, Institute of Forensic Sciences and Legal Medicine, 34500, Istanbul, Türkiye


Abstract: The blood sample is one of the most essential pieces of evidence that helps criminal experts in the elucidation of the crime. However, cleaning the blood found at the crime scene after the crime is committed makes it difficult to detect the crime. Therefore, experts have attached great importance to research on blood samples left at the crime scene. Although many test kits are used, especially in detecting erased blood, the luminol kit is widely used at crime scenes. In the luminol kit, the reaction takes place with the addition of hydrogen peroxide (H₂O₂). Since it is known that hydrogen peroxide can react with other substances containing Fe (II) ions that may be present in the environment during the reaction, it was aimed to carry out research to determine which substances luminol interferes with, especially those that may be found in a domestic crime scene in this study. In domestic crime scenes, there are limited substances that can replicate the distinct, enduring luminescence characteristic of a reaction between luminol and genuine bloodstains, while the uncharacteristic glow produced from many other surfaces is likely to be recognised with the naked eye by a good expert, experienced and knowledgeable in the field. In this regard, the prepared samples were treated with luminol in a dark environment, and the reactions occurring in the first seconds were recorded. The results obtained with this reagent are recommended to be supported by other blood test reagents or confirmatory tests, as there are substances that give false positive results with luminol reagents in the present study.

Keywords: Luminol, Blood, Chemiluminescence, False positivity, Crime Scene investigation

*Corresponding author: Kutahya Health Sciences University, Faculty of Engineering and Natural Sciences, Department of Forensic Sciences, 43100 Kutahya, Türkiye

E mail: yakup.gulekci@ksbu.edu.tr (Y. GULEKCI)

Yakup GULEKCI  <https://orcid.org/0000-0001-9643-6850>

Fatma CAVUS YONAR  <https://orcid.org/0000-0001-5941-8434>

Received: November 15, 2023

Accepted: January 01, 2024

Published: January 15, 2024

Cite as: Gulekci Y, Cavus Yonar F. 2024. False positives in luminal testing. BSJ Eng Sci, 7(1): 129-138.

1. Introduction

Forensic biology primarily examines evidential objects found at crime scenes regarding biological fluids (Virkler et al., 2009; An et al., 2012). At a crime scene, an investigator often comes across various types of evidence, among which bodily fluids hold significant evidentiary value. Blood, semen, and saliva are the fluids most frequently encountered, in addition to vaginal secretions and urine. Accurate detection and identification of these fluids at the crime scene can lead to early detection of the offence. For example, while the presence of blood at a crime scene indicates some physical fight or violent assault, the presence of semen makes it possible to focus on the possibility of sexual assault (An et al., 2012). While these definitions assist in guiding the investigation's course, the fundamental objective of identifying bodily fluids lies in pinpointing the exact nature of the fluid and ascertaining the identity of the individual who deposited the biological material at the crime scene, achieved through DNA analysis. In other words, identification can be made by determining the genotypic or phenotypic characteristics of the person to whom the fluid belongs. The main methods used to detect body fluids are screening and confirmation tests. Screening tests are designed to assess the likelihood of

the presence of bodily fluids on the evidence. In instances where the result of the screening test is affirmative, a confirmatory test is then employed to ascertain the exact type of fluid with greater certainty (Li, 2015). The diverse screening and confirmatory tests used in identifying body fluids aim to identify one or more components within the body fluid.

Blood is the most commonly found biological fluid at crime scenes and is arguably the most important source for genetic analyses (DNA and RNA analyses) (James et al., 2005). Methods such as visual examination, analyses that determine the presence or absence of blood through the catalytic action of haemoglobin, and confirmatory tests involving antigen-antibody reactions are employed for blood detection. The main problems encountered when applying the methods used to detect blood are the observation of false positive or false negative results. The studies documented in the literature highlight instances of false positives and negatives associated with catalytic colour tests, chemiluminescent substances, and immunoassays. These studies point out various interfering agents that can disrupt accurate blood identification, potentially causing erroneous positive or negative outcomes (Cox, 1991; Tobe et al., 2007; Li, 2015).



Synthesised in 1902 in Germany, the chemical name of luminol, according to IUPAC, is 5-Amino-2,3-dihydro-1,4-phthalazindione, 5 - Amino - 1, 2, 3, 4 - tetrahydrophthalazine - 1, 4 - dione, 3 - aminophthalhydrazide (Barni et al., 2007). Its molecular formula is $C_8H_7O_3N_3$. Luminol is a green-yellow crystalline powder and is odourless. It is dangerous for luminol, which is flammable, to coexist with strong oxidising agents. It emits light in reaction with oxidisers and is sensitive to light (Tajani, 2014). In case of poisoning, it may cause damage to mucous membranes, skin, eyes, and gastrointestinal system (Barni et al., 2007). Since it can maintain its stability for 8-12 hours, it is recommended to prepare it shortly before use (Thorpe, 1987).

Luminol is often used to identify blood that is difficult to see at crime scenes or where attempts have been made to remove it, but trace amounts are still present (Barni et al., 2007; Rogiski et al., 2012). Luminol helps to visualise

bloodstain patterns that can be integral to understanding the sequence of events that occur during an attack. In the luminol kit, which is available in commercial formulations for ease of use, the reaction takes place with the addition of hydrogen peroxide (H_2O_2). During the reaction, hydrogen peroxide reacts with other substances containing metal ions, such as Fe (II), that may be present in the environment and glow. When an oxidizing molecule like hydrogen peroxide is present alongside a catalyst, luminol emits a bluish-coloured light. This luminescence reaction takes place as follows: metal ions in the medium catalyse the oxidation reaction of luminol with H_2O_2 and oxidise it to aminophthalate (Figure 1). Aminophthalate forms a high-energy structure and emits light from the excess energy (Wells et al., 1996). Hydrogen peroxide interacting with blood causes bubbles to form at the edges of the stain (Finnis et al., 2013).

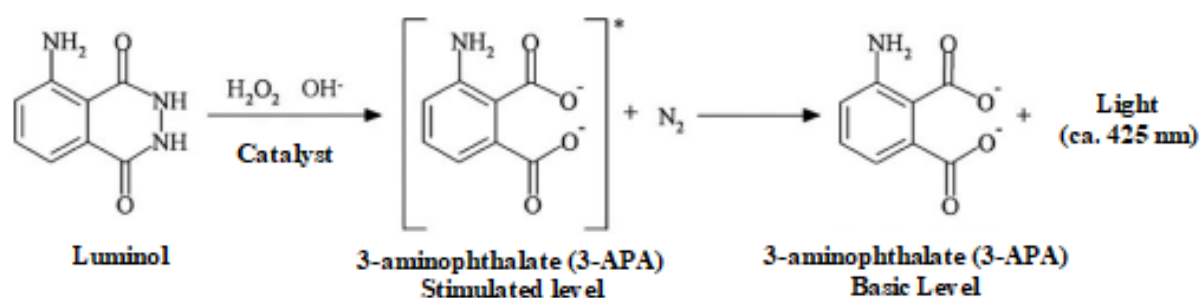


Figure 1. Reaction of luminol during blood detection (Stoica et al., 2016).

Iron in haemoglobin (Li, 2015), the protein responsible for carrying oxygen within the cell, which is found in the red cells of the blood called erythrocytes and constitutes by 44% of the blood volume, acts as a metal catalyst and enables this reaction to take place. Haemoglobin, a tetrameric molecule, is composed of four polypeptide chains, comprising two alpha (α) and two beta (β) chains. Embedded in each polypeptide chain is a "haem" molecule, also known as ferroprotoporphyrin, which is a dark red-coloured blood pigment. Central to each haem molecule is an iron ion (Fe^{2+}), which has the capacity to bind with oxygen molecules (Marengo-Rowe, 2006; Molnar et al., 2019). The haem molecule of erythrocytes is the most crucial blood component that attracts the attention of forensic sciences in detecting and identifying blood.

The light produced in this reaction, called chemiluminescence, appears bluish in the dark environment (Barni et al., 2007). Therefore, the presence of blood in wiped environments, which is not possible to see with the naked eye, is proved as a result of the reaction. To evaluate the blood stains detected with the help of luminol applied by spraying at crime scenes as evidence, it is essential to photograph the radiation that occurs quickly. A completely dark environment is required during photography (Laux, 2005).

Studies have shown that fresh blood samples show a weaker and shorter chemiluminescence reaction than old, dry and deconstructed blood samples (Klein et al., 2007). The same is true for the comparison of diluted and undiluted blood.

Luminol, an alkaline chemical, includes an oxidizing agent that facilitates the conversion of Fe^{2+} to Fe^{3+} . As a result, the transformation of hemin into haematin in bloodstains is amplified when luminol is used. This process involves haematin acting as a catalyst in the breakdown of peroxide and in the oxidation of luminol by peroxide, forming a catalytic cycle (Barni et al., 2007).

Bloodstains that have aged tend to have a higher concentration of haematin compared to recent ones, which explains why luminol exhibits a stronger glow in older bloodstains. The interaction between luminol and haematin in a catalytic cycle is an example of a redox reaction, a type of chemical reaction that involves changes in the oxidation states of certain atoms or molecules. Such reactions encompass both oxidation and reduction processes (Cheyne, 2011).

Initially, in an alkaline environment, haematin's breakdown of hydrogen peroxide results in the formation of hydroxyl radicals (OH^{\cdot}) and hydroxyl anions (OH^-). These by-products then oxidize Haematin ($Fe^{III}P$) in a two-electron oxidation step, leading to the creation of the

hydroxyl-ferryl porphyrin radical ($\text{Fe}^{\text{IV}}\text{P}^{+\cdot}$), a potent oxidizing agent. Subsequently, $\text{Fe}^{\text{IV}}\text{P}^{+\cdot}$ catalyzes the oxidation of deprotonated luminol (LH^-) to the luminol radical ($\text{L}^{\cdot-}$) through a one-electron oxidation reaction. This radical is then reduced back to hydroxyl-ferryl porphyrin ($\text{Fe}^{\text{IV}}\text{P}$). In turn, $\text{Fe}^{\text{IV}}\text{P}$ undergoes a one-electron reduction back to haematin, a process that occurs concurrently with the oxidation of another luminol molecule that has had a proton removed, forming

another luminol radical. This establishes a catalytic cycle that replenishes haematin, enabling it to continue cycling as long as there is a supply of hydrogen peroxide and luminol (as shown in Figure 2). Consequently, repeated applications of luminol can be carried out with minimal reduction in the reaction's intensity. The only significant reduction in intensity arises from the dilution of the bloodstain with the water present in the luminol solution (Barni et al., 2007).

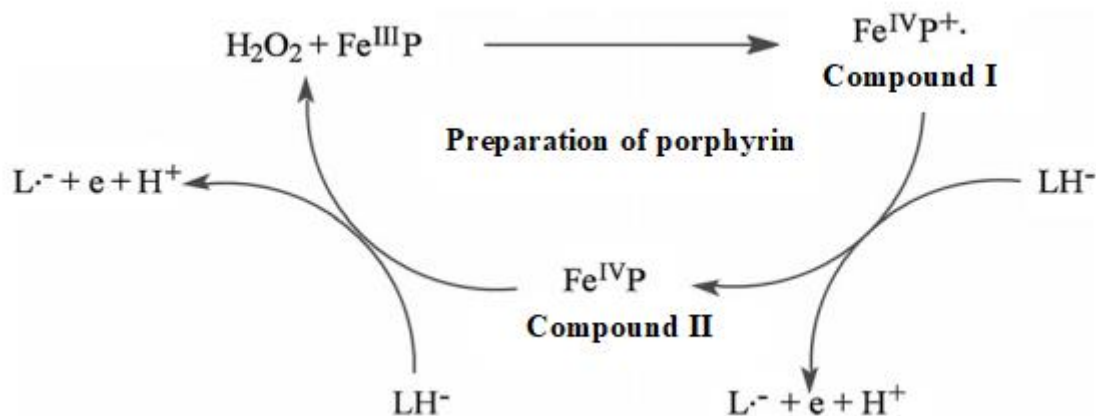


Figure 2. The redox cycle involving the iron ion of methemoglobin in the luminol reaction leads to the generation of luminol radicals (Cheyne, 2011).

When blood dries and ages, different chemical and biological changes occur in the blood. These changes cause the formation of methaemoglobin from haemoglobin by oxidation of iron in haem prosthetic groups from Fe (II) to Fe (III) (Patzelt, 2004). This effect affects the catalytic properties of blood in reactions in which luminol is produced. Old blood stains give a more intense and longer glow than fresh ones (Della et al., 2000; James et al., 2005).

Experienced crime scene investigators can often distinguish the luminescence caused by a substance other than blood from the reaction given by blood by paying attention to the luminescence's colour, the luminescence's brightness, and the luminescence's duration.

The main advantages of using luminol are that it can detect dilute blood spots down to $1:10^{10}$, it does not severely damage genetic material, and it can be applied multiple times at different times to visualise a spot (Barni et al., 2007; Rogiski et al., 2012; Chourasiya et al., 2017; Shivangi et al., 2021). One drawback of this technique is that with each subsequent application, the chemiluminescence diminishes due to the decreasing availability of haemoglobin for interaction with the luminol-hydrogen peroxide mixture. This reduction in intensity can pose challenges in photographing and documenting the stain as it is found at the crime scene or in its original location. Furthermore, a significant limitation of luminol is its lack of specificity to human haemoglobin. This is because luminol reacts with various substances including certain metals, animal haemoglobin, plant peroxidases found in fruits and vegetables, and

cleaning agents that contain hypochlorite, like chlorine bleach (Barni et al., 2007; Rogiski et al., 2012). Luminol cannot distinguish between human and animal blood as it also catalyses the reaction with haemoglobins belonging to species other than human haemoglobin. If a blood stain found at the crime scene belongs to an animal, no result will be obtained in the DNA analysis stages. In order to prevent this, other tests that can distinguish between human and animal blood are required (Creamer et al., 2003; Quickenden et al., 2004). Oxidants and plant peroxidases constitute a significant threat in screening tests (Li, 2015). Oxidants can catalyse the chemical reaction even in the absence of haemoglobin, leading to false positive results. Examples include metals such as copper, nickel, cobalt, chromium, manganese, and bleaches and detergents containing hypochlorite ions. Plant peroxidases also catalyse the oxidation reaction, i.e. they can react with reagents similarly to haemoglobin (Seitz et al., 1972; Cox, 1991; Quickenden et al., 2001a; Quickenden et al., 2001b; Ming et al., 2001; Creamer et al., 2003; Creamer et al., 2005; Tobe et al., 2007).

Some studies in the literature have attempted to determine the metals with which luminol reacts. Luminol can make coordination bonds with some metals due to the functional groups in its chemical structure. This allows metals to be detected in samples. Mn (III) containing micro peroxidase 8 ($\text{Mn}(\text{IIIMP}8)$) plays a catalysing role in the oxidation of luminol with hydrogen peroxide at high pH, making it possible to see the chemiluminescence reaction (Yeh et al., 2003). When these and similar studies are taken into consideration, it

is seen that the studies have focused on the chemiluminescence property of luminol.

Increased knowledge by crime scene investigators about potential false positives/negatives in identifying blood helps ensure that evidential evidence is appropriately collected from the scene and thoroughly analysed. False positives and positive hypothetical results, where stains are identified as blood, can lead experts to waste resources and unnecessary labour by collecting non-evidential evidence from the crime scene or from the person (Petersen et al., 2014). In addition, false negative results that may occur in screening tests may cause evidence that may help the course of the investigation to be left behind. In order to prevent these and similar results, in our study, we tried to identify the substances that give false positive results with luminol, which is one of the frequently used screening tests at the crime scene. No representative experiment has been conducted in Türkiye regarding the substances that give false positive responses with luminol. An experiment was conducted to address which substrates, other than blood, produced or grown in Türkiye can react positively with luminol. There are only a handful of substances capable of replicating the strong, enduring, uniform glow that is characteristic of the reaction between luminol and an authentic bloodstain. Moreover, the atypical glow that luminol produces on various other surfaces is often discernible to the naked eye. Furthermore, the interpretation of patterns at a crime scene contaminated with substances that react positively with luminol requires considerable experience on the part of the forensic scientist.

2. Materials and Methods

2.1. Preparation of Luminol

Since inhalation or absorption of luminol solution by the skin may cause irritation, personal protective equipment was worn during the preparation of the luminol solution, and the working area was ventilated.

This study used solution B in a bottle labelled LUMINOL16B, powder A in a bottle labelled LUMINOL16A, and SIRCHIE brand luminol (North Carolina, USA) sold as a spray nozzle (Figure 3). Firstly, the cap of solution bottle B was opened and prepared for the procedure. Then, the cap of the bottle containing powder A was opened, and all the powder in the bottle was transferred to bottle B. The spray nozzle supplied with the solutions was attached to bottle B and shaken until all the solids were dissolved. Thus, luminol was ready for use (Sirchie, 2011).

2.2. Preparation of Samples

In order to prevent possible contamination, the surface and consumables used were cleaned with Zefirol IM Liquido (Molteni, Switzerland) before the experimental work, and the consumables used were autoclaved and kept under UV for 30 min.

In this study, apple, dried apricot, pineapple, mulberry, grape, celery, parsley, carrot, spinach, curly, bay leaf, purple cabbage, potato, tomato, garlic, onion,

horseradish, turnip were used as fruit and vegetable group, detergent powder and bleach cleaning agents, milk, eggs and buttermilk of animal origin, inorganic substances such as naphthalene, iodine tincture, copper powder, tile dust, iron rust, mud and soil samples were preferred. Fruit and vegetable samples were pre-cleaned by washing and drying with distilled water and then crushed in a mortar and pestle. The detergent powder was dissolved in distilled water and naphthalene in methanol (Merck, Germany). Copper powder, tile powder, iron rust and soil were mixed with distilled water. Other selected materials were used directly without any pretreatment.



Figure 3. SIRCHIE brand luminol reagents

The 4x5 cm² calico fabrics, which were sterilised and checked to see whether they reacted with luminol before the application of the samples (blind sample), were used as ground and absorbent surfaces. Stains from the fruit-vegetable and animal foods groups were applied to the calico fabrics in an area of 2x2 cm². Dissolved detergent powder and mothballs, bleach, iodine tincture, copper powder, tile powder, iron rust, soil and mud samples were applied to the calico with the help of an automatic pipette (Eppendorf, Germany) in 500 µl volume (Figure 4). The prepared samples were allowed to dry for 24 hours at room temperature in a biosafety cabinet (Thermo Heraeus Herasafe KS 15 Class II Type A2 Biological Safety by Thermo Fisher, USA).

2.3. Application of Luminol to Prepared Samples

Since the possible irritation of the luminol solution on the skin or respiratory tract cannot be ruled out, a face mask and disposable gloves were worn during the application, and the working area was ventilated. All stages of the study were carried out under a fume cupboard using personal protective equipment.

The luminol prepared as described above was applied in a thin, single coat from a distance of 5-10 cm to cover the target surfaces completely (King et al., 2005). The chemical-resistant liquid with a maximum speed of 1.3 mL/sec was sprayed using a spray pump nozzle

(Divortex, Türkiye) and allowed to dry in a fume hood (Figure 5), (Divortex, 2023).



Figure 4. Images of some prepared samples

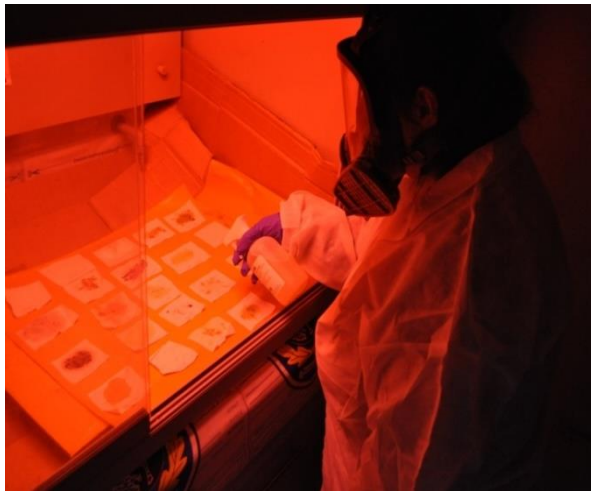


Figure 5. Application of luminol to the samples by spraying

2.2. Chemiluminescence Evaluation

Chemiluminescence formation after luminol application was visually observed and photographed. The results obtained during the application were evaluated and recorded by an experienced crime scene investigator. A Nikon D7200 camera with a shutter/exposure time of 16 seconds and a light sensitivity of ISO 400 was used for photographic documentation. Visual assessment was performed partly using the sandwich method (superimposing photographs taken in the light and the dark from the same recording position in an image processing program) and partly using the after-flash/backlighting method (a flashlight is thrown onto the ceiling behind the camera, or the ceiling is continuously illuminated with a weak light source while recording brightness in the dark).

It is challenging to visualise differences in the intensity of

luminescence reactions, that is, the intensity of the luminescence, with the naked eye or in photographs. During the waiting period of a few minutes during which the reaction takes place, false positive reactions occur at least as spontaneously as true positive reactions but decay much more rapidly (Klein et al., 2007).

Experienced crime scene investigators can distinguish the chemiluminescence produced by real blood from that produced by other substances by evaluating parameters that can be observed with the naked eye, such as emission intensity, duration, and spatial distribution. However, since this approach is subjective, unofficial and without quantitative evaluation, it may lead to misinterpretations. Since the chemiluminescence of some false positive samples may be weaker than that of blood, these samples may be confused with diluted bloodstains (Barni et al., 2007). In such cases, using probabilistic and descriptive reagents for bloodstains helps to select samples that will give reliable results for subsequent DNA analyses (Lytle et al., 1978).

The interpretation of luminol chemiluminescence properties applied at the crime scene should consider the physical structure of the object on which the bloodstains are found, the object's chemical composition containing the stains and other substances present on the substrate. Metals, some paints and varnishes have a distinct and identifiable emission pattern from blood, with the spatial distribution of luminescence and emission intensity (Barni et al., 2007). It is not easy to apply luminol reagent and to obtain high chemiluminescence quality since processes such as wiping and painting to prevent blood from being visible can be applied more easily on non-absorbent surfaces than on absorbent ones (Lytle et al., 1978).

3. Results and Discussion

Identification within the scope of forensic biology includes the identification of the available biological fluid and the process of making DNA-based identifications that can reveal the relationships between the event/crime scene/suspect and victim with advanced analysis techniques. While screening and confirmation tests for biological fluid identification are highly beneficial in forensic contexts, it's crucial for scientists and crime scene investigators to consider potential interfering substances that could lead to false positives or negatives. These inaccuracies can stem from the presence of similar identifying elements in other body fluids or tissues, materials from plants or animals, common household products, or due to incorrect storage methods.

While the appearance of bright blue glow (Figure 6) resulting from the reaction was expected to be a blood stain, the brightness of the glow was higher in some substances (strongly positive in apple, dried apricot, pineapple, turnip, detergent powder, bleach, iodine tincture, copper powder, purple cabbage, iron rust and soil) and lower in some substances (positive in onion, horseradish, potato, tomato, tile powder, mud and garlic)

as shown in Table 1. No radiation (negative) was observed in mulberry, grape, celery, milk, parsley, egg, carrot, buttermilk, spinach, mothballs, lettuce, and bay leaf, especially in animal foods. The difference in the degree of positivity in soil and mud samples with similar structures is thought to be due to their heterogeneous nature. Other findings are consistent with the literature (Castello et al., 2002; Adair et al., 2008). The chemical background of the false positive reaction is still unclear. Therefore, not all substances that can trigger the reaction are known. False positive results have been observed in the presence of some metals such as copper or iron ions, dyes (potassium permanganate), cleaning agents/bleaching agents (sodium hypochlorite), plant components (chlorophyll) or vegetables (root vegetables containing peroxidase), photosynthetic microorganisms (Arnhold et al., 1991; Quickenden et al., 2001b). After a detailed examination of the ingredients of the cleaning products, this can be explained by the use of percarbonate or, peroxide or sodium hypochlorite as bleaching agents. A strong positive reaction was observed for the product containing sodium

hypochlorite. The same was true for the root vegetable species tested. According to the studies of Quickenden (Creamer et al., 2003) and Creamer (Quickenden et al., 2001b), a positive reaction was observed in parsnip and potato, whereas in the study, a positive reaction was observed in potato and freshly cut horseradish. Possibly very different peroxidase content in fruits and vegetables due to season; fertilisation can explain this (Klein et al., 2007). In addition, these differences may also be due to the different preparation protocols of the luminol kit. In some studies, luminol is prepared as a solution containing only sodium carbonate and sodium perborate (Grodsky's approach), while in some serological or criminal studies, it is usually prepared as a three-component solution of sodium hydroxide and hydrogen peroxide (Weber's approach). This solution should be kept in a cold environment away from direct sunlight (Grodsky et al., 1951; Weber, 1966). Various chemical additives have been used to increase the selectivity of these formulations, but none have found widespread use (Arnhold et al., 1993).

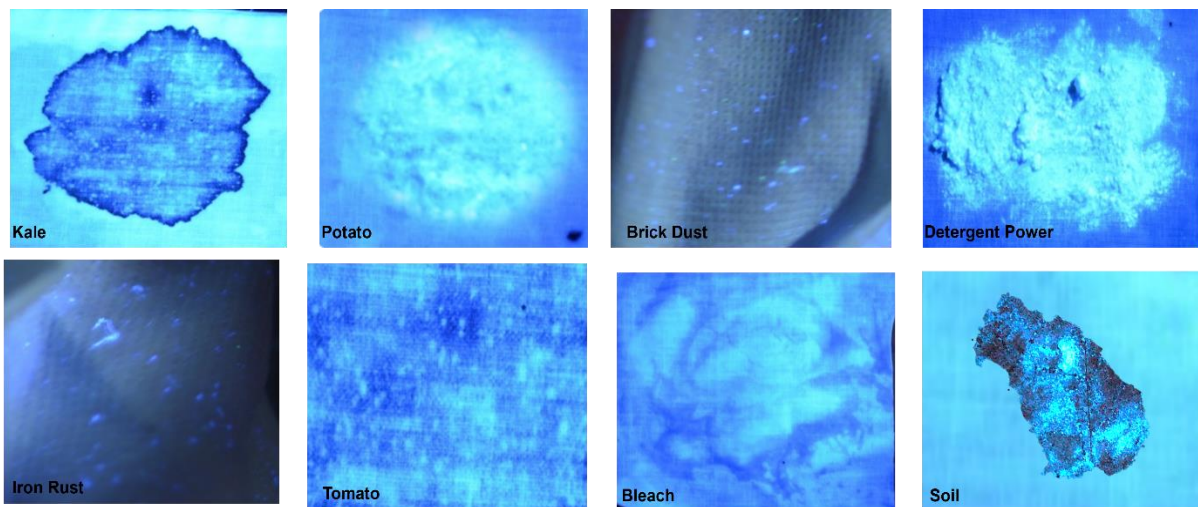


Figure 6. Some substances giving positive results with Luminol.

Table 1. Chemiluminescence observed after luminol administration

Samples	Chemiluminescence Occurrence	Samples	Chemiluminescence Occurrence
Apple	++	Onion	+
Dried apricots	++	Horseradish	+
Pineapple	++	Turnip	++
Mulberry	-	Detergent powder	++
Grape	-	Bleach	++
Celery	-	Milk	-
Parsley	-	Egg	-
Carrot	-	Buttermilk drink	-
Spinach	-	Naphthalene	-
Lettuce	-	Iodised tincture	++
Bay leaf	-	Copper powder	++
Purple cabbage	++	Tile dust	+
Potato	+	Iron rust	++
Tomato	+	Mud	+
Garlic	+	Soil	++

"-" indicates negative result; "+" indicates positive result; "++" indicates strong positive result.

In catalytic colour tests, potent oxidizing agents like copper, nickel, and chlorine bleach are capable of catalyzing the oxidation-reduction reaction even without the presence of haemoglobin, falsely indicating the presence of blood. Similarly, plant peroxidases can impact these tests due to their structural resemblance to haemoglobin, which enables them to catalyze the reaction (Novelli, 2020). To effectively deal with potential false positives, it is necessary to be aware of the environment in which the finding is found, to understand what substances may be near or on the suspect stain, and to be aware of appropriate collection and analysis methods. Oxidants can typically be detected by sequentially applying catalytic reagents and observing for any discolouration before introducing hydrogen peroxide. Hydrogen peroxide added to a blood stain will cause bubbles to be produced at the edges of the stain. However, no bubbles were observed for any substance in the experiment, resulting in false positives. Peroxidases found in plants like horseradish, potato, tomato, and onion can be neutralized through the application of high heat before conducting tests. However, this approach is seldom utilized in analyses due to the likelihood of high heat causing damage to genetic material.

BlueStar® Forensic is another screening test based on the principle of chemiluminescence (Dilbeck, 2006; Virkler et al., 2009; Novelli, 2020). This product includes a luminol-based substance in tablet form, which readily dissolves. When mixed with distilled water, this solution is sprayed onto the suspected stain area. The reagent reacts with haemoglobin, producing a blue luminescence that can be both seen and captured in photographs. In a comparative analysis performed by the Scottsdale and Saint Louis police departments, BlueStar® demonstrated superior qualities compared to traditional luminol. These advantages include the ability to detect more dilute bloodstains, better performance on bleach-treated stains, no need for total darkness for visualisation, brighter, longer-lasting chemiluminescence intensity, and no attenuation of the glow with repeated applications. Luminol does not react with other biological fluids except blood (Barni et al., 2007; Adair et al., 2008). Since it contains urea peroxide, a stable oxidant, it can be used days after preparation. It is an easy-to-prepare test that does not damage DNA (Dilbeck, 2006). Nevertheless, researchers recommend confirmation of the luminol reaction with other specific serological tests.

Studies of screening tests that investigate the sensitivity and specificity of blood have reported that the Kastle-Meyer (KM) test, also called phenolphthalein, is the most sensitive method to detect blood diluted to 1:10⁻⁹ (Cox, 1991; Tobe et al., 2007; Chourasiya et al., 2017). The reduced form of phenolphthalein is retained on Kastle-Meyer zinc granules and oxidised back to phenolphthalein by haemoglobin catalysis. It emits pink with positive results (James et al., 2005). However, some studies have contradictory results on leukomalachite green (LMG), one of the screening tests. In one of these

studies, positive results were reported up to 1:10.000 blood dilution, while in another one, it was reported that LMG could only be positive up to 1:5000 blood dilution. In addition, interfering agents causing false positives and negatives for KM, LMG, Ortho-tolidine (O-tol) and Tetramethylbenzidine (TMB) tests were also studied. Quebracho extract (a typical skin tannin), sodium percarbonate (the main component of detergents containing active oxygen) and beverages containing vitamin C (ascorbic acid) have been reported to produce varying degrees of false-negative results in catalytic colour tests, chemiluminescent reagents, and immunoassays for the detection of blood (Novelli, 2020). Immunochromatographic-based tests that are widely used in blood screening are HemaTrace® from Abacus Diagnostics, Seratec® HemDirect, Hexagon OBTI® from Human GmbH and RSID™- Blood from Independent Forensics (Johnston et al., 2003; Misencik et al., 2007). HemaTrace®, Hexagon OBTI® and HemDirect are based on human haemoglobin. The major disadvantages of these tests are their cross-reactivity with ferret or upper primate blood, that is, the possibility of false positive results and the possibility of false negative results if the test input volume is large.

However, due to the possibility that luminol and similar screening tests may disrupt the structure of the genetic materials of blood samples found at the crime scene after misapplication, it is imperative to develop and use new compounds as an alternative possibility in forensic sciences in order to completely eliminate this negativity and disadvantages related to the use of luminol. Studies on the development of luminol analogues with higher specificity and sensitivity, which can get faster results at crime scenes, meet the common denominator of nanotechnology and forensic sciences (Karabchevsky et al., 2016; Fereja et al., 2019; Fatoki, 2020).

In this study, various substances that have the potential to cause false positive results using luminol, one of the preferred forensic screening tests for the detection of blood, were discussed. The importance of examining any substance that causes false positive or negative results in forensic analyses, especially regarding screening tests, cannot be underestimated. This is the best way to ensure that any findings that may be encountered at a crime scene are accurately analysed most efficiently. The more that is known about a potential problem, the more cautious the expert will be about an uncertain test result in the field or the laboratory.

5. Conclusion

If a hypothetical test result for a body fluid is negative, the suspected stain is considered to be of no forensic significance, and no further testing is performed. However, if the stain is blood and there is a condition that prevents the analysis of blood in screening tests, the investigation will be deprived of an important piece of evidence, as confirmatory analyses for the detection of blood cannot be performed. In addition, the presence of

interfering agents at the crime scene, which causes false positive results, will cause the stain to be misidentified, increasing the workload and cost in criminal laboratories in terms of confirmatory analyses. In this case, it causes delays in justice services. In order to prevent the interaction of luminol with the substances that cause false positives identified in this study, it is recommended that the content of the kit components be updated, luminol analogues be identified, or alternative screening tests be considered. Although luminol is frequently used at crime scenes for reasons such as ease of use, it may cause illusions as a result of a false positive result. Accordingly, the stain thought to be blood as a result of luminol application at the crime scene must be confirmed to be blood by a second test such as Kastle-Meyer in the laboratory.

False negative or positive results obtained by screening tests used in the detection of blood, one of the biological fluids frequently encountered at crime scenes, is a subject that has attracted the attention of the forensic sciences community and has recently gained momentum in detailed research. Much more research is still needed to understand better how interfering agents affect screening tests. In particular, the literature has limited information on agents that cause false negativity.

Future studies should be motivated by situations that reflect "real world" conditions commonly found at active crime scenes, as opposed to controlled laboratory settings. In this study, the screening tests were performed on actual items like readily available detergents with active oxygen found in stores, common food products typically present in an average person's refrigerator, and various substrates that one might typically encounter at a crime scene. Future studies could also examine whether genotypic or phenotypic profiling can be developed from stains containing blood contaminated with these interfering agents and on which screening tests have been performed. Such an approach would be beneficial in deciding whether stains yielding positive or negative results for blood warrant further genetic analysis.

Author Contributions

The percentage of the author(s) contributions is presented below. The author reviewed and approved the final version of the manuscript.

%	Y.G	F.Ç.Y
C	50	50
D	50	50
S	60	40
DCP	40	60
DAI	60	40
L	40	60
W	40	60
CR	50	50
SR	50	50
PM	50	50
FA	50	50

C=Concept, D= design, S= supervision, DCP= data collection and/or processing, DAI= data analysis and/or interpretation, L= literature search, W= writing, CR= critical review, SR= submission and revision, PM= project management, FA= funding acquisition.

Conflict of Interest

The authors declare no conflict of interest. The funders had no role in the design of the study, in the collection, analyses, or interpretation of data, in the writing of the manuscript, or in the decision to publish the results.

Ethical Consideration

Ethics committee approval was not required for this study because of there was no study on animals or humans.

Acknowledgements

The authors would like to thank Istanbul University-Cerrahpasa Institute of Forensic Sciences and Legal Medicine, Forensic Sciences Laboratory and Kutahya Health Sciences University, Application and Research Centre Laboratory for providing laboratory facilities and a convenient working environment for this study.

References

- Adair TW, Gabel R, Shimamoto S, Tewes R. 2008. A comparison of the luminol and blue star blood reagents in detecting blood in soil nearly four years after deposition. *IABPA News*, 24(4): 5-8.
- An JH, Shin KJ, Yang WI, Lee HY. 2012. Body fluid identification in forensics. *BMB Rep*, 45(10): 545-53. <https://doi.org/10.5483/BMBRep.2012.45.10.206>.
- Arnhold J, Mueller S, Arnold K, Grimm E. 1991. Chemiluminescence intensities and spectra of luminol oxidation by sodium hypochlorite in the presence of hydrogen peroxide. *J Biolumin Chemilumin*, 6(3): 189-192.
- Arnhold J, Mueller S, Arnold K, Sonntag K. 1993. Mechanisms of inhibition of chemiluminescence in the oxidation of luminol by sodium hypochlorite. *J Biolumin Chemilumin*, 8(6): 307-313. <https://doi.org/10.1002/bio.1170080604>.

- Barni F, Lewis SW, Berti A, Miskelly GM, Lago G. 2007. Forensic application of the luminol reaction as a presumptive test for latent blood detection. *Talanta*, 72(3): 896-913. <https://doi.org/10.1016/j.talanta.2006.12.045>.
- Castello A, Alvarez M, Verdu F. 2002. Accuracy, reliability, and safety of luminol in bloodstain investigation. *Canadian Soc Foren Sci J*, 35(3): 113-121.
- Cheyne M. 2011. Illuminating latent blood. Application methods, fixatives, alternatives and new formulas for luminol. MSc thesis, The University of Auckland, Forensic Science, Auckland, New Zealand, pp: 222.
- Chourasiya L, Mahakalkar A. 2017. To compare and study differential detection of human and animal blood using phenolphthalein, tetramethylbenzidine and luminol assays. *Int J Recent Trends Eng Res*, 3(11): 82-102.
- Cox M. 1991. A study of the sensitivity and specificity of four presumptive tests for blood. *J Foren Sci*, 36(5): 1503-1511. <https://doi.org/10.1520/JFS13170J>.
- Creamer JI, Quickenden TI, Apanah MV, Kerr KA, Robertson P. 2003. A comprehensive experimental study of industrial domestic and environmental interferences with the forensic Luminol test for blood. *Lumin*, 18: 193-198.
- Creamer JI, Quickenden TI, Leah BC. 2005. At tempted cleaning of bloodstains and its effect on the forensic luminol test. *Lumin*, 20: 411- 413.
- Da Silva RR, Agustini BC, da Silva ALL, Frigeri HR. 2012. Luminol in the forensic science. *J Biotech Biodiv*, 3(4):172-177.
- Dilbeck L. 2006. Use of BlueStar forensic in lieu of luminol at crime scenes. *J Forensic Identif*, 56(5): 706-20.
- Divortex, 2023. Kimyasal dayanıklı sıvı püskürtme (Sprey) şişesi 1 Lt. URL: <https://www.divortex.com.tr/aksesuarlar/kimyasal-dayanikli-sivi-puskurtme-sprey-sisesi-1-lt>. (accessed date: Sep 23, 2023).
- Fatoki TH. 2020. In-Silico investigation of luminol, its analogues and improved mechanism of chemiluminescence for blood identification beyond forensics. *bioRxiv*, 01.
- Fereja TH, Kitte SA, Gao W, Yuan F, Snizhko D, Qi L, Xu G. 2019. Artesunate-luminol chemiluminescence system for the detection of hemin. *Talanta*, 204: 379-385.
- Finnis J, Lewis J, Davidson A. 2013. Comparison of methods for visualizing blood on dark surfaces. *Sci Justice*, 53(2): 178-186.
- Grodsky M, Wright K, Kirk PL. 1951. Simplified preliminary blood testing--An improved technique and a comparative study of methods. *J Crim L Criminol Police Sci*, 42: 95.
- James SH, Kish PE, Sutton TP. 2005. Principles of bloodstain pattern analysis: theory and practice, CRC Press, Boca Raton, 1st ed., New York, USA, pp: 533.
- James SH, Nordby JJ, Forensic Science: An introduction to scientific and investigative techniques, CRC Press, New York, USA, 2nd ed., pp: 667.
- Johnston S, Newman J, Frappier R. 2003. Validation study of the Abacus Diagnostics ABACard® HemaTrace® membrane test for the forensic identification of human blood. *Can Soc Forensic Sci J*, 36(3): 173-83. <https://doi.org/10.1080/00085030.2003.10757560>.
- Karabchevsky A, Mosayyebi A, Kavokin AV. 2016. Tuning the chemiluminescence of a luminol flow using plasmonic nanoparticles. *Light Sci Applicat*, 5(11): 16164-16164.
- King R, Miskelly G. 2005. The inhibition by amines and amino acids of bleach-induced luminol chemiluminescence during forensic screening for blood. *Talanta*, 67(2):345-353. <https://doi.org/10.1016/j.talanta.2005.01.034>.
- Klein A, Feudel E, Türk E, Püschel K, Gehl A. 2007. Luminescence after the use of luminol: Positive or false positive? *Rechtsmedizin*, 17: 146-152.
- Laux L. 2005. The detection of Blood Using Luminol. in: James SH, Kish PE, Sutton TP. (Eds.), Principles of bloodstain pattern analysis: theory and practice. CRC Press, Boca Raton, 1st ed., New York, USA, pp: 369-389.
- Li R. 2015. Forensic Biology. CRC Press, New York, USA, 2nd ed., pp: 533.
- Lytle LT, Hedgecock DG. 1978. Chemiluminescence in the visualization of forensic bloodstains. *J Foren Sci*, 23(3): 550-562.
- Manna AD, Montpetit S. 2000. A novel approach to obtaining reliable PCR results from luminol treated bloodstains. *J Foren Sci*, 45(4): 886-890.
- Marengo-Rowe AJ. 2006. Structure-function relations of human hemoglobins. *Proc Bayl Univ Med Cent*, 19(3): 239-245.
- Ming Lin J, Shan X, Hanaoka S, Yamada M. 2001. Luminol chemiluminescence in unbuffered solutions with a cobalt(II) - ethanolamine complex immobilized on resin as catalyst and its application to analysis. *Anal Chem*, 73: 5043-5051. <https://doi.org/10.1021/ac010573+>.
- Misencik A, Laux DL. 2007. Validation study of the Seratec HemDirect hemoglobin assay for the forensic identification of Human Blood. *MAFS Newsl*. URL: <https://pdfs.semanticscholar.org/2c56/c17d14e06a7472f6246596d10f76164844bb.pdf>. (accessed date: Sep 25, 2023).
- Novelli BC. 2020. A review of substances reported to cause false positives and negatives in forensic blood identification tests. MSc thesis, Boston University, School of Medicine, Boston, USA, pp: 66.
- Patzelt D, 2004. History of forensic serology and molecular genetics in the sphere of activity of the German Society for Forensic Medicine. *Forensic Sci Int*, 144: 185-191.
- Petersen D, Kovacs F. 2014. Phenolphthalein false-positive reactions from legume root nodules. *J Forensic Sci*, 59(2): 481-484. <https://doi.org/10.1111/1556-4029.12352>.
- Quickenden TI, Cooper PD. 2001a. Increasing the specificity of the forensic luminol test for blood. *Lumin*, 16: 251-253.
- Quickenden TI, Creamer JI. 2001b. A study of common interferences with the forensic luminol test for blood. *Lumin* 16: 295-298. <https://doi.org/10.1002/bio.657>
- Quickenden TI, Ennis CP, Creamer JI. 2004. The forensic use of Luminol chemiluminescence to detect traces of blood inside motor vehicles. *Lumin*, 19: 271-277.
- Rogiski da Silva R, Agustini B, Lopes da Silva AL, Frigeri HR. 2012. Luminol in the forensic science. *J Biotech Biodiv*, 3(4): 172-177.
- Seitz WR, Hercules DM. 1972. Determination of trace amounts of iron(II) using chemiluminescence analysis. *Anal Chem*, 44: 2143-2149. <https://doi.org/10.1021/AC60321A020>.
- Shivangi G, Apoorva G, Suresh B, Yadav DS, Mahanta P. 2021. Comparative study of presumptive and confirmatory tests for detection of blood on serial dilutions and washed stains. *Int J Health Res Medico Leg Prae*, 7(1): 59-64.
- Sirchie. 2011. Luminol. URL: https://www.sirchie.com/media/resourcecenter/item/l/u/luminol_ti02-48eng-rev10e.pdf. (accessed date: Sep 23, 2023).
- Stoica BA, Bunescu S, Neamtu A, Bulgaru-Iliescu D, Foia L, Botnariu EG. 2016. Improving luminol blood detection in forensics. *J Foren Sci*, 61(5): 1331-1336.
- Stott RAW, Kricka LJ. 1987. Biolumin chemilumin symp. John Wiley & Sons Ltd., Chichester, New York, USA, pp: 237-240.
- Tajani, A. 2014. Photonics for forensic applications. *Photon*

- Safet Secur, 1987: 368-397.
- Thorpe GHG, Kricka L J. 1987. Chemilumin: New Perspectives. Scholmerich JR, Andreesen R, Kapp A, Ernst M, Woods W, editors. Biolumin. Wiley, Chichester, UK, pp: 199–208.
- Tobe SS, Watson N, Daéid NN. 2007. Evaluation of six presumptive tests for blood, their specificity, sensitivity, and effect on high molecular-weight DNA. J Forensic Sci, 52(1): 102–109. <https://doi.org/10.1111/j.1556-4029.2006.00324.x>.
- Virkler K, Lednev IK. 2009. Analysis of body fluids for forensic purposes: from laboratory testing to non-destructive rapid confirmatory identification at a crime scene. Foren Sci Inter, 188(1-3): 1-17.
- Weber K. 1966. Die Anwendung der Chemilumineszenz des Luminols in der gerichtlichen Medizin und Toxikologie. Dtsch Z ges gerichtl Med, 57: 410–423.
- Wells PG, Winn LÇM. 1996. Biochemical toxicology of chemical teratogenesis. Critical Review in Biochem. Mol. Biol. 31 (1): 1-40.
- Yeh HC, Lin WY. 2003. Enhancement of chemiluminescence from the oxidation of luminol with hydrogen peroxide catalyzed by Mn (III)-Microperoxidase 8. J Chinese Chem Soc, 50(1): 81-88.



DOĞAL OLARAK BULUNAN KIRMIZI PİGMENT LİKOPEN VE SAĞLIĞA FAYDALI ETKİLERİ ÜZERİNE SİSTEMATİK BİR YOLCULUK

Güney AKINOĞLU^{1*}, Arzu ERDAL²

¹Ondokuz Mayıs University, Faculty of Agriculture, Department of Soil Science and Plant Nutrition, 55139, Samsun, Türkiye

²Ondokuz Mayıs University, Faculty of Medicine, Department of Medical Pharmacology, 55139, Samsun, Türkiye

Özet: Likopen, başta domates ve domates türevi gıdalar olmak üzere bazı sebze ve meyvelerde doğal olarak bulunan, karotenoidler grubuna ait kırmızı renkli bir pigmenttir. Likopen pigmenti, güçlü bir antioksidan ve pro-vitamin A aktivitesi göstermeyen bir karotenoid olarak kabul edilir. Likopen, spesifik biyolojik özelliklere katkıda bulunabilecek benzersiz yapısal ve kimyasal özelliklere sahiptir. Diyabet, kardiyovasküler hastalıklar, kanserler, cilt ve kemik rahatsızlıkları, nörolojik bozukluklar gibi çeşitli hastalıkların önlenmesi ve tedavisinde likopenin çok çeşitli yararlı etkilere sahip olduğu bildirilmiştir. Deney hayvanlarında ve insanlarda likopenin biyoyararlanımı, dokularda dağılımı, metabolizması, atılımı ve biyolojik etkileri ile ilgili bilgiler literatürde birikmeye başlasa da bu konuda daha fazla araştırma yapılması gerekmektedir. Bu derleme, likopenin özellikleri, likopen kaynakları, alınımı ve biyoyararlanımı ile birlikte insan sağlığındaki olası rolü hakkındaki mevcut bilgi durumunu özetlemektedir.

Anahtar kelimeler: Likopen, Karotenoid, Domates, Antioksidan, İnsan sağlığı


A Systematic Journey on the Naturally-Occurring Red Pigment Lycopene and Its Beneficial Effects on Health


Abstract: Lycopene is a red pigment that belongs to the carotenoid group and occurs naturally in some vegetables and fruits, especially tomatoes and tomato-derived foods. The lycopene pigment is considered a powerful antioxidant and a carotenoid that has no pro-vitamin A activity. Lycopene has unique structural and chemical properties that can contribute to specific biological properties. Lycopene is thought to have a variety of beneficial effects in the prevention and treatment of various diseases such as diabetes, cardiovascular disease, cancer, skin and bone disorders, and neurological disorders. Although information is gradually accumulating in the literature on the bioavailability, tissue distribution, metabolism, excretion, and biological effects of lycopene in experimental animals and humans, further research is needed. This review summarizes the current state of knowledge on the properties, sources, absorption and bioavailability of lycopene and its potential role in human health.

Keywords: Lycopene, Carotenoid, Tomato, Antioxidant, Human health

*Sorumlu yazar (Corresponding author): Ondokuz Mayıs University, Faculty of Agriculture, Department of Soil Science and Plant Nutrition, 55139, Samsun, Türkiye

E mail: guney_akinoglu@gmail.com (G. AKINOĞLU)

Güney AKINOĞLU  <https://orcid.org/0000-0003-4624-2876>

Arzu ERDAL  <https://orcid.org/0000-0002-4845-6504>

Gönderi: 18 Temmuz 2023

Kabul: 24 Kasım 2023

Yayınlanma: 15 Ocak 2024

Received: July 18, 2023

Accepted: November 24, 2023

Published: January 15, 2024

Cite as: Akinoğlu G, Erdal A. 2024. A systematic journey on the naturally-occurring red pigment lycopene and its beneficial effects on health. BSJ Eng Sci, 7(1): 139-154.

1. Giriş

Gıda pigmentleri, gıdanın rengini belirleyen veya gıdayı renklendirmek için kullanılabilen maddelerdir (Awolu ve Oladeji, 2021). Gıdanın rengi ve aroması, tüketicinin belirli bir gıdayı kabul etmesini etkilemektedir (Akinoğlu ve Korkmaz, 2016). İlk renklendiriciler, pancar kökünden elde edilen pigmentler gibi doğal maddelerden yapılmıştır (Petropoulos ve ark., 2019), ancak daha sonra yüksek üretim maliyetleri ve elde edilen renkteki farklılıklar nedeniyle bundan vazgeçilmiştir (Awolu ve Oladeji, 2021). Öte yandan, sentetik renklendirici maddelerin kullanımından kaynaklanan çeşitli sağlık sorunları nedeniyle günümüzde doğal kaynaklı renk katkı maddelerine olan ilgi yeniden artış göstermektedir (Dey ve Nagababu, 2022). Gıda yan ürünlerinden elde edilen aktif bileşenlere ilişkin geniş araştırma ve

geliştirmeler, sürdürülebilir bir çevre doğrultusunda döngüsel ekonomi paradigması altında gerçekleştirilmektedir (Faria-Silva ve ark., 2020). Doğal kaynaklı pigmentlerin doza bağlı ve bileşiğe özgü bir şekilde genel antioksidan kapasiteye katkıda bulunduğu bildirilmiştir (McGill, 2009; Agcam ve ark., 2017; Petropoulos ve ark., 2019). Doğal pigmentlerdeki önemli bileşikler bazı polifenoller, karotenoidler, klorofiller ve betalainlerdir (Shoji, 2007; Aberoumand, 2011; Pan ve ark., 2018; Hossain ve ark., 2019; Orgeron ve ark., 2019). Karotenoidler; karotenler ve ksantofiller olmak üzere iki başlıca gruba ayrılır. α -karoten, β -karoten, β , ψ karoten (γ karoten) ve likopen gibi karotenler hidrokarbonlardır. Öte yandan, ksantofiller (β -kriptoksantin, lutein, zeaksantin, astaksantin, fukoksantin ve peridin) ise hidroksi, karbonil, aldehit, karboksilik, epoksit ve furanoksit grupları gibi oksijen atomları içeren



karotenoidlerdir (Jaswir ve ark., 2011).

Likopen; domates, papaya, pembe greyfurt, pembe guava ve karpuz gibi kırmızı renkli meyve ve sebzelerde bol miktarda bulunan bir pigmenttir. Bu kırmızı renkli pigment ilk olarak 1876 yılında Fransız kimyager Millardet tarafından domateste keşfedilmiştir. Daha sonra Schunck (1903), domatesten izole edilen kırmızı renk maddesinin görünüş, kristal form, çözünürlük ve absorpsiyon spektrumu bakımından karotenden ayırt edilebilirliğini bildirmiş ve likopeni, domatesin (*Solanum lycopersicum*) bilimsel adından gelen "lycopin" olarak adlandırmıştır.

Likopen bir karotenoid hidrokarbondur (karoten olarak da adlandırılır). Bu bileşiklerin uzatılmış konjuge çift bağ sistemi, karotenoidlerin cezbedici renklerinden sorumlu önemli bir özelliktir, çünkü ışık emici kromoforu oluşturur (Rodriguez-Amaya ve Kimura, 2004). Bu bileşiklerde görünür rengin varlığı, en az yedi konjuge çift bağ gerektirir. Konjuge çift bağların sayısı arttıkça, maksimum absorpsiyon için daha yüksek dalga boyu değeri gözlenir (Rodriguez-Amaya, 2001; Kong ve ark., 2010).

Likopen, gıda endüstrisi tarafından bir gıda katkı maddesi olarak ve aynı zamanda sağlığa yararlı etkileri bakımından oldukça rağbet gören pigmentlerden biridir (Rao ve Argawal, 1999). Daha önce yürütülmüş olan in vitro ve in vivo çalışmalarda, likopenin kardiyovasküler hastalık, ateroskleroz, kanser ve nörodejeneratif bozukluklar gibi kronik hastalıkları önlemede yararlı bir rol üstlendiği rapor edilmiştir (Kong ve ark., 2010).

Bu derleme, likopenin özelliklerine genel bir bakış sunmakla birlikte likopen alımı, biyoyararlanımı, dağılımı ve insan sağlığına etkileri hakkında bilgiler de içermektedir.

2. Likopenin Fiziksel ve Biyokimyasal Özellikleri

Karotenoidler, meyve ve sebzelerde yaygın olarak bulunur. İnsanlar tarafından tüketilen bitkisel ürünlerde, başta cis-trans izomerleri olmak üzere 600'den fazla karotenoid karakterize edilmiştir (Crupi ve ark., 2023). Kimyasal olarak, karotenoidler iki ana sınıfa ayrılabilir (Maoka, 2020). Birinci sınıftaki karotenoid türleri; likopen, α -karoten, β -karoten, γ -karoten ve ξ -karoten gibi büyük ölçüde doymamış hidrokarbon karotenoidlerdir. Bunlar oksijen içermez ve genellikle turuncu ve kırmızı renktedirler. İkinci sınıftaki karotenoid türleri ise oksijenli türevler olan ve uç halkalar üzerinde belirli yerlerde bir veya daha fazla oksijenli grup ikame edicisi içeren ksantofillerdir (örneğin, β -kriptoksantin, lutein ve zeaksantin). İki karotenoid sınıfı, poliizoprenoid yapı ve bir dizi merkezi olarak yerleşmiş konjuge çift bağ gibi ortak yapısal özellikleri paylaşmaktadır. Domates meyvesinde karotenoid sınıfına ait olan 21'den fazla pigment tanımlanmış ve nicelleştirilmiştir (Shi ve Le Maguer, 2010). Likopen, domates meyvesindeki başlıca hidrokarbon karotenoiddir. Bununla birlikte, domates

meyvesi az miktarda α -karoten, β -karoten, γ -karoten, ξ -karoten, fitoen, fitofluen, nörosporen ve lutein de içerir (Gould, 1992). Domates meyvesindeki ana karotenoid türlerinin dağılımı Tablo 1'de verilmiştir.

Tablo 1. Karotenoid türlerinin domates meyvesine katkıları (Gross, 1987)

Başlıca karotenoidler	Bileşim, %	Konjuge çift bağ sayısı
Likopen	80-90	11
α -karoten	0,03	9
β -karoten	3-5	9
γ -karoten	1-1,3	7
ξ -karoten	1-2	7
Fitoen	5,6-10	3
Fitofluen	2,5-3,0	5
Neurosporen	7-9	9
Lutein	0,011-1,1	10

2.1. Likopenin Fiziksel Özellikleri

Likopenin fiziksel özellikleri Tablo 2'de özetlenmiştir. Likopen, olgun domates meyvelerinin tipik parlak kırmızı renginden sorumlu olan uzun, iğne benzeri kristaller şeklinde bir yapıdır. Kloroform, benzen ve diğer organik çözücülerde likopenin çözünürlüğü sudan daha fazladır (Shi ve Le Maguer, 2010).

Tablo 2. Likopenin fiziksel özellikleri (Shi ve ark., 2002)

Moleküler formülü	C ₄₀ H ₅₆
Moleküler ağırlığı	536,85 Dalton (Da)
Erime noktası	172-175°C
Kristal form	Uzun, kırmızı, iğne yapılı
Toz formu	Koyu kırmızısı- kahverengi
Çözünürlüğü	Kloroform, heksan, benzen, karbon disülfid, aseton, petrol eteri içinde çözünür
Duyarlılık	Işık, oksijen, yüksek sıcaklık, asitler

2.2. Likopenin Biyokimyasal Özellikleri

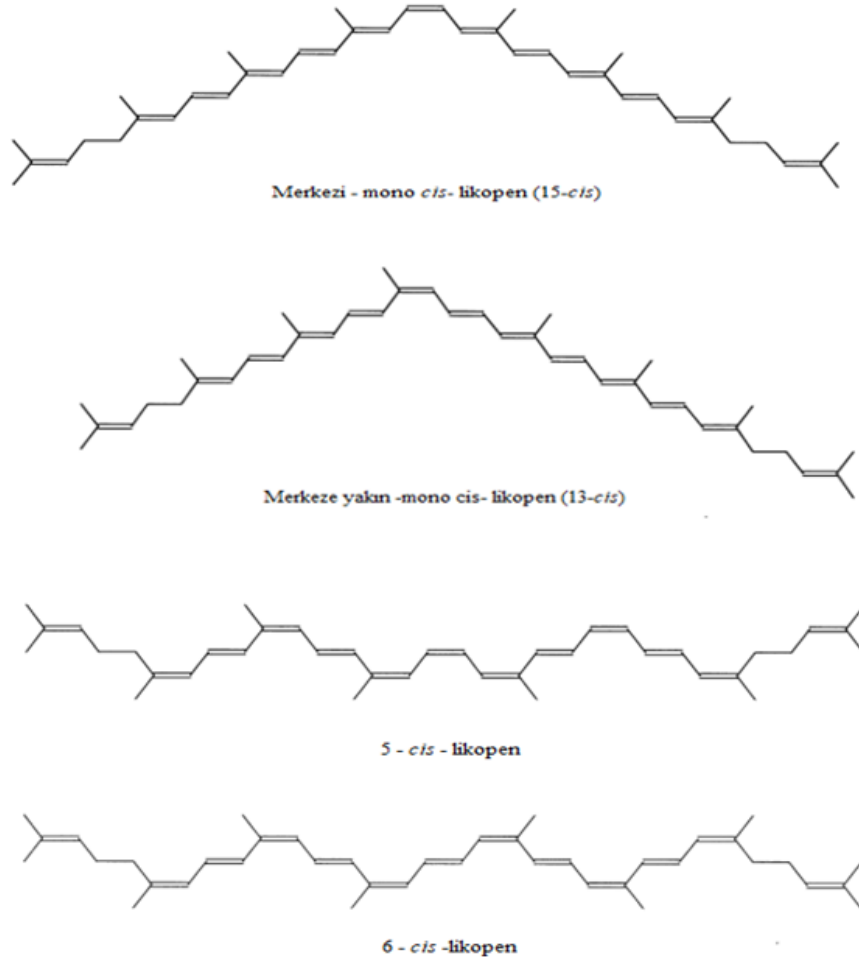
Asiklik yapısı, geniş konjuge çift bağ dizisi ve aşırı hidrofobikliği ile likopen, antioksidan da dâhil olmak üzere birçok benzersiz ve değişik biyolojik özellik sergiler. Likopen, en etkili singlet oksijen söndürücüler arasındadır (Di Mascio ve ark., 1989; Conn ve ark., 1991). Çeşitli karotenoid türleri için söndürme hızı sabitelerinde (K_q) önemli farklılıklar söz konusudur (Tablo 3). Likopen ve diğer karotenoidlerin antioksidan aktiviteleri, singlet oksijen söndürme özellikleri ve peroksil radikallerini yakalama yetenekleri ile ön plana çıkar (Foote ve Denny, 1968; Burton ve Ingold, 1984).

Tablo 3. Karotenoidlerin antioksidan aktivitelerinin karşılaştırılması (Di Mascio ve ark., 1991; Conn ve ark., 1992; Miller ve ark., 1996).

Likopen	
Singlet oksijen söndürme, $10^9 \times Kq (m^{-1} s^{-1})$	31
Radikal temizleme (Trolox eşdeğerleri)	2,9
Karotenoid radikal anyonlarının O_2 ile reaksiyonu, $10^8 \times k (m^{-1} s^{-1})$	2
Diğer karotenoidlerin singlet oksijen söndürmesi ($10^9 \times Kq (m^{-1} sn^{-1})$)	
γ -karoten	25
α -karoten	19
β -karoten	14
Lutein	8
Astaksantin	24
Biksin	14
Kantaksantin	21
Zeaksantin	10

Karotenoid türlerinin söndürme aktivitesi, konjuge çift bağların sayısına bağlı olup, karotenoid uç gruplarından veya siklik uç grupları içeren karotenoidlerdeki süstitüentlerin doğasından daha az etkilenirler (Foote

ve Denny, 1968; Stahl ve ark., 1993). Likopenin all-trans, mono-cis ve poly-cis formları dâhil olmak üzere çeşitli geometrik izomerlerde var olduğu bilinmektedir. Likopenin all-trans izomeri, taze domateslerde en baskın geometrik izomerdir ve termodinamik olarak en kararlı formdur. Yine de, likopen, domates işleme ve depolama sırasında trans-cis izomerizasyona uğrayabilir. Domates türevli çeşitli gıdalarda all-trans izomer, toplam likopenin %35 ila %96'sını oluşturur (Schierle ve ark., 1996). Likopenin 5-cis, 9-cis ve 15-cis izomerleri, domates türevi gıdalarda ve insan dokularında Nükleer Manyetik Rezonans (NMR) spektroskopisi ile tanımlanmıştır (Zumbrunn ve ark., 1985). Domates bazı gıdalarda 5-cis-izomer oranı, % 4 ila %27 arasında olmakla birlikte, diğer izomerlerden de oldukça daha düşük düzeydedir (Schierle ve ark., 1996). Likopenin cis-izomerleri, insan serumu ve dokusundaki toplam likopenin %50'den fazlasına katkıda bulunur (Krinsky ve ark., 1990). Likopenin bazı cis-izomerlerinin yapıları Şekil 1'de gösterilmiştir. Genel olarak, cis-izomerler, all-trans muadillerinden daha polardır ve kıvrımlı formları nedeniyle kristalleşmeye daha az eğilimlidir. Cis-izomerler ayrıca yağ ve hidrokarbon çözücülerde all-trans izomerlerden daha fazla çözünür. Cis-izomerlerin biyoaktivite potansiyeli, değişen yapısal formlar nedeniyle, tüm trans-izomere kıyasla değişkenlik gösterir (Shi ve Le Maguer, 2010).

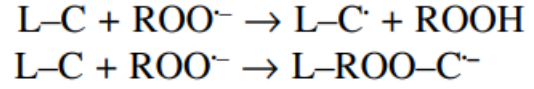


Şekil 1. Likopenin *cis*-izomerlerinin kimyasal yapıları.

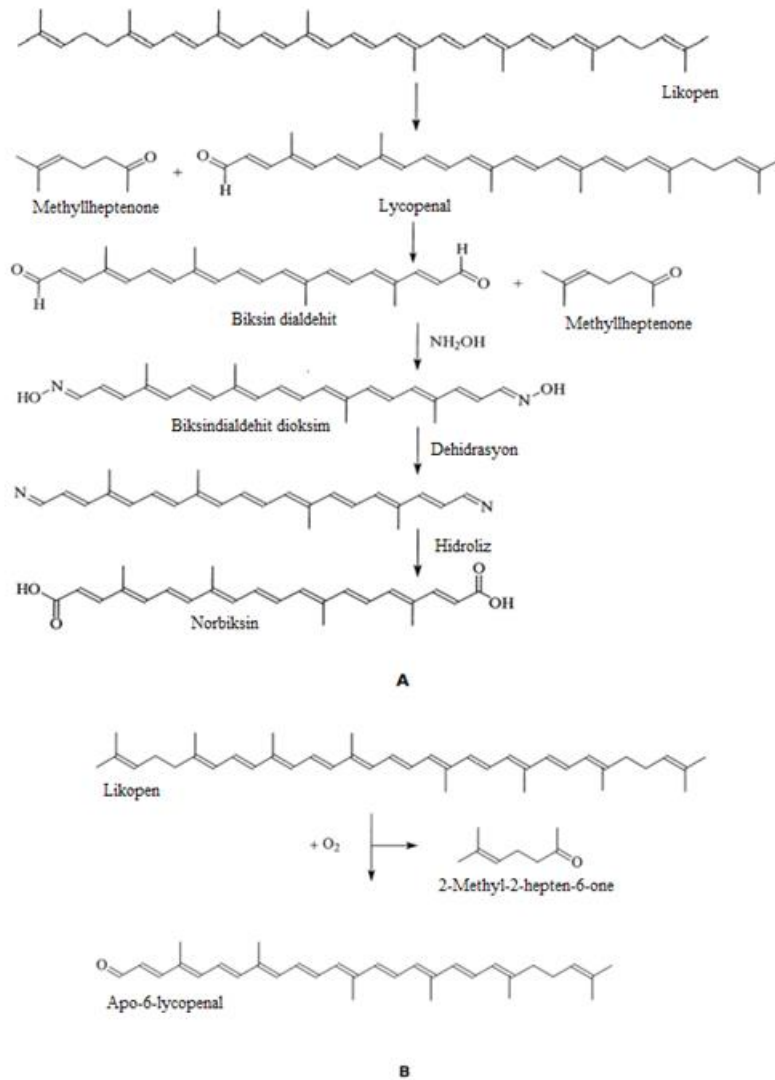
Gıda sistemlerinde likopen ile ilgili stabilite çalışmalarının çoğu bozunma ile ilgilidir. Likopen, işlenmiş domates ürünlerinde metalik iyonlar (Cu^{+2} , Fe^{+3} , vb.) veya oksijen varlığında ısıtılarak kısmen yok edilebilir. Konjuge bir polien olarak likopenin, domates işleme, izomerizasyon ve oksidasyon sırasında en az iki değişikliğe uğraması beklenebilir. Likopen izomerizasyonunun domates ürünlerinde olduğu kadar saf likopen formlarında da olduğu bildirilmiştir. Likopen izomerizasyonu, işlem görme aşamasında da meydana gelebilir. Öte yandan, cis-izomerin trans-forma dönüştürülmesi, ürünün depolanması sırasında meydana gelebilecek başka bir reaksiyondur. Cis-izomerler kararsız durumdayken; trans-izomerler kararlı temel durumdadır (Shi ve Le Maguer, 2010).

Etkili bir antioksidan olarak likopen, oldukça reaktif tekli

oksijeni (O_2^-) söndürür ve peroksil radikallerini ($\text{ROO}\cdot$) yakalar. Likopen-oksijen radikali etkileşimleri, ikinci dereceden hızlı reaksiyonlar olarak kabul edilebilir. Bu etkileşimde likopen daha az etkili olmakla birlikte, her iki yönde de elektron transferi gözlenir (Conn ve ark., 1992). Potansiyel indirgeme, süperoksit radikali bir iyon olan (O_2^-)'nin oluşumu ile ilgilidir (Palozza, 1998).



Bir prooksidan olarak hareket edebilen ve otooksidasyona uğrayan peroksil radikali oluşturmak da mümkündür. Önerilen likopen bozunma yolu Şekil 2A, B'de gösterilmiştir.



Şekil 2. Likopen bozunması için önerilen reaksiyon yollarının şematik görünümü.

(A) Önerilen likopen bozunma yolları (Karrer ve Jucker, 1950'den uyarlanmıştır), (B) Işığa duyarlılık sırasında likopenden apo 6-likopenal ve 2-metil-2-hepten-6-one oluşumu için önerilen yol (Ukai ve ark, 1994'den uyarlanmıştır)

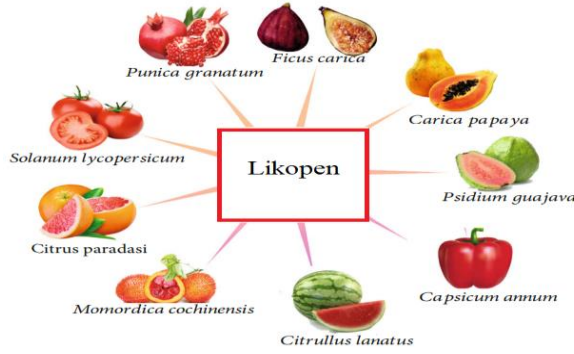
Oksijen fonksiyonları, (1) bir metil veya metilen

grubunun ikamesi, (2) bir karbon-karbon çift bağına ilavesi şeklinde iki ana tip reaksiyonla ortaya çıkıyor gibi görünmektedir. Açıkçası, oksidatif bozunma normal C40-karbon iskeletinin her iki ucunda da meydana gelebilir. Yaygın olarak kabul edilen terminoloji kurallarına göre, orijinal C40 yapısının C20 ve C20' metil gruplarını

tutmayan bozulmuş bir ürün artık bir karotenoid değildir. Likopen bozunması meydana gelirken, elde edilen nihai ürünler, moleküllerin çift bağ bölgelerindeki doğrudan oksidatif parçalanmanın sonuçlarıdır (Shi ve Le Maguer, 2010).

3. Besinlerde Likopen

Likopen, 11 doğrusal konjuge ve iki konjuge olmayan çift bağa sahip doymamış asiklik bir karotenoiddir. A vitamininin temel yapısında bulunan terminal β -iyonik halkadan yoksun olduğu için A vitamininin öncüsü değildir (Kong ve ark., 2010). Domates, pembe greylift, kırmızı üzüm, karpuz ve kırmızı guava gibi bazı meyve ve sebzelerin kırmızı rengi, likopenin varlığından kaynaklanmaktadır (Şekil 3).



Şekil 3. Likopen içeren bazı besinler (Arain ve ark., 2018; Khan ve ark., 2021).

Diyetle alınan likopenin en az % 85'i domates ve domates ürünü kaynaklıdır (Sabbağ ve Sürücüoğlu, 2011; Kurt, 2003). Bazı meyve ve sebzelerdeki likopen miktarları Tablo 4'te verilmiştir. Meyve ve sebze türlerine bağlı olarak likopen miktarında önemli değişiklikler görülebilmektedir (Zengin ve Kurt, 2018).

Tablo 4. Meyve ve sebzelerdeki likopen miktarları (Kurzeja ve ark., 2009; Yılmaz, 2011; İzgi, 2012; Zengin ve Kurt, 2018)

Likopen içeren besinler	Likopen içeriği (ppm)
Karpuz	23,0 - 42,0
Guava	52,3 - 55,0
Greyfurt	3,5 - 33,6
Papaya	1,1 - 53,0
Kuşburnu	6,8 - 7,1
Kabak	3,8 - 4,6
Tatlı patates	0,2 - 1,1
Elma pulpu	1,1 - 1,8
Taze kayısı	0,05
Konserve kayısı	0,65
Kurutulmuş kayısı	8,6
İşlenmiş kırmızı biber	10,8 - 26,2

Likopen, karotenoidler grubundaki en etkili singlet oksijen söndürücü olarak rapor edilmiştir. Söndürme

yeteneği esas olarak konjuge çift bağ sayısına bağlıdır ve sıklık veya asiklik uç grupların varlığından daha az etkilenir (Stah ve Sies, 1996). Ek olarak, geniş ölçüde konjuge bir polien sistemine sahip zincir yapısı, oksidatif bozunmaya duyarlılık gibi biyolojik özellikleri açısından önemlidir (Shi ve ark., 2002).

3.1. Domates Meyvesinde Likopen

Likopen, olgun domateslerde en çok bulunan karotenoid olmakla birlikte, mevcut pigmentlerin yaklaşık %80-90'ını oluşturur. Taze domates meyvelerindeki likopen içeriği; domates çeşidine, olgunluğuna ve meyvenin yetiştiği çevre koşullarına göre değişiklik gösterebilmektedir. Genel olarak, domates meyvesi 100 g taze ağırlık başına yaklaşık 3-5 mg arasında likopen içerir (Hart ve Scott, 1995). Bazı domates çeşitleri ise daha yüksek miktarlarda likopen içermektedir. Tonucci ve ark. (1995), domates meyvesinin 100 gramında 9,27 mg değerinin üzerinde likopen içerdiğini bildirmiştir. Bazı koyu kırmızı renge sahip domates çeşitlerinde yapılan araştırmada 100 gram meyvenin 15 mg'dan fazla likopen içerirken; sarı çeşitleri 100 gramında sadece 0,5 mg likopen içerdiği rapor edilmiştir (Hart ve Scott, 1995). Domates olgunlaştıkça likopen kapsamı artış gösterir (Shi ve Le Maguer, 2010). Heinonen ve ark. (1989), domateslerdeki likopen konsantrasyonunun haziran ayından-ağustos ayına kadar daha yüksek; ekim ayından-mart ayına kadar ise daha düşük olduğunu bildirmiştir. Diğer yandan, Lurie ve ark. (1996), nispeten yüksek sıcaklıkların (38°C) likopen üretimini engellediğini; düşük sıcaklıkların ise hem meyve olgunlaşmasını hem de likopen üretimini engellediğini bildirmişlerdir.

Domates meyveleri etilen ile muamele edildiğinde, meyvedeki likopen oluşumunun yaklaşık 2 gün daha erken meydana geldiği belirtilmiştir (Jeffery ve ark., 1984). Rin mutantındaki likopen sentezinin, 10 mg·kg⁻¹ etilen varlığında yüksek O₂ seviyesi koşullarında arttığı bildirilmiştir (Frenkel ve Garrison, 1976). Öte yandan, etanolün domateste olgunlaşmayı ve likopen sentezini engellediği bildirilmiştir (Saltveit ve Mencarelli, 1988). Ek olarak, Sheehy ve ark. (1988), poligalakturonazdaki bir azalmanın likopen sentezini etkilemediğini tespit etmişlerdir.

Domates meyvelerindeki likopen içeriğinin; gübre, hasat zamanı ve çeşit seçiminde geliştirilmiş tekniklerle artırılacağı rapor edilmiştir (Lampe ve Watada, 1971; Mohr, 1979). Al-Wandawi ve ark. (1985), yaş ağırlık bazında 100 g domates kabuğunun 12 mg likopen içerdiğini; buna karşın, 100 g olgun bir domatesin yalnızca 3,4 mg likopen içerdiğini bildirmişlerdir. Bu nedenle, domates kabuğundaki likopen konsantrasyonu, bütün olgun domateslerdekinden yaklaşık üç kat daha fazladır (Shi ve Le Maguer, 2010). Bununla birlikte, D'Souza ve ark. (1992) domates meyvelerinin kabuğunun ve perikarpının likopen açısından zengin olduğunu bildirmişlerdir. Sharma ve Le Maguer (1996), domatesin kabuk kısmının likopen içeriğinin (53,9 mg/100 g), meyve etinin likopen içeriğinden (11 mg /100 g) yaklaşık beş kat daha fazla likopen içerdiğini tespit etmişlerdir.

Böylece, domates kabuklarının zengin bir likopen kaynağı olduğunu sonucuna varılabilir.

4. Bitki Hücrelerinde Likopen Biosentezi

Hücresel düzeyde, likopen domates meyvelerinin kloroplastlarında lokalizedir ve fotosentetik pigment-protein kompleksindeki thylakoid membranlar arasında bulunabilir (Bouvier ve ark., 1998; Akhtar ve ark., 1999). Domates bitkisinde meyve olgunlaşmasının erken aşamalarında, kloroplastlardaki baskın pigment yeşil renkli klorofildir. Klorofil bozunmaya uğradıkça renk yeşilden beyaza dönüşür. Kloroplastlardaki klorofil azaldığında, likopen biosentezlenir ve meyvenin yapısındaki eş zamanlı değişikliklerle beyazdan kırmızıya doğru renk değişimi meydana gelir (Harris, 1970; Khudairi, 1972; Matienzo ve Yedaly, 1973). Kromoplast gelişiminin son aşaması, kromoplastın büyük bir bölümünü kaplayan likopen kristallerinin oluşumudur ve kromoplastlarda hacimli kırmızı katmanlar olarak görünür (Laval-Martin, 1974). En fazla likopen konsantrasyonları perikarpta bulunur (Simpson ve ark., 1977). Domateslerdeki likopen ve diğer karotenoidlerin biosentezi, 14C izleyicileri kullanılarak kapsamlı bir şekilde incelenmiştir (Porter ve Anderson, 1967; Buggy ve ark., 1969). Bir öncü olduğuna inanılan mevalonik asit, likopen üretimi için her basamakta hidrojen kaybıyla peyderpey dönüştürülür. Dehidrojenasyon büyük olasılıkla her basamakta yer alır. Böylece, likopen, küçük kürecikler halinde domates pulpunda asılı duran kromoplastlarda bulunur. Likopen katı mikro kristaller olarak görünür ve bu nedenle onlardan yansıyan ışık domatese tipik parlak kırmızı rengini vermektedir (Shi ve Le Maguer, 2010).

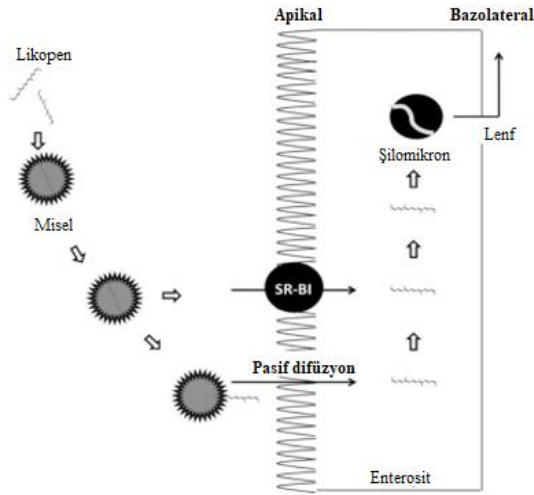
5. Likopenin Alınımı, Biyoyararlanımı ve Dağılımı

ABD'deki diyet likopen alımının %80'inden fazlası ketçap, domates suyu, spaghetti sosu ve pizza sosu gibi işlenmiş domates ürünlerinden elde edilmektedir (Clinton, 1998). Gıdaların işlem görmesi, genellikle su kaybı yoluyla konsantrasyon artışına sebebiyet verir. Dolayısıyla, işlenmiş gıdalarda bulunan likopen miktarı, taze gıdalarda bulunanlardan genellikle çok daha yüksek değerlerdedir. Örneğin, ketçap 100 gram ağırlık başına 9,9-13,44 mg likopen içerirken; taze domates 100 gram yaş ağırlık başına 0,88-7,74 mg likopen içerir (Rao ve ark., 1998, Nguyen ve Schwartz, 1998). Diyetle likopen alımı, çalışılan popülasyona bağlı olarak büyük ölçüde değişir. Ortalama bir İtalyan birey, günde 14,3 mg toplam karotenoid tüketir (Lucarini ve ark., 2006). Likopen, günde ortalama 7,4 mg'lık bir alım ile İtalyan diyetindeki karotenoidlerin en büyük oranını oluşturur (Lucarini ve ark., 2006). Amerika Birleşik Devletleri'nde ortalama günlük likopen alımı erkekler için 6,6-10,5 mg arasında belirlenirken; kadınlar için bu değer, 5,7-10,4 mg arasında değişmektedir (Porrini ve Riso, 2005). Diğer ülkeler için bildirilen ortalama likopen alımı Birleşik

Krallık'ta 1,1 mg/gün, İspanya'da 1,6 mg/gün, Avustralya'da 3,8 mg/gün, Fransa'da 4,8 mg/gün ve Hollanda'da 4,9 mg/gün'dür (Porrini ve Riso, 2005).

Likopen biyoyararlanımı, gıda işleme ve diyet bileşimi gibi bir dizi faktörden etkilenebilir. Likopen, taze bitkisel mahsullerin kloroplastlardaki karotenoid-protein komplekslerine bağlı bir şekilde veya kromoplastların içinde kristal bir formda bulunabilir (Parada ve Aguilera, 2007). İşleme ve depolamanın likopen yapısı üzerindeki etkileri ve stabilitesi birkaç nedenden dolayı ilgi çekici bir vaziyet almıştır. Uygun olmayan işleme ve depolama (yani, ışığa ve oksijene maruz kalma), likopen izomerlerinin oranını değiştirebilir veya likopeni tamamen bozabilir. Bu da, bu gıda ürünlerini tüketici için daha az arzu edilir bir hale getirir (Xianquan ve ark., 2005). Geleneksel ticari işleme yöntemlerinin, likopen seviyeleri veya cis/trans izomerizasyonu üzerinde önemli bir etkisi yoktur (Nguyen ve Schwartz, 1998). Aslında, ısıl işlem, likopenin doku matrisinden salınmasına izin veren hücresel zarları bozarak likopen biyoyararlanımını genel olarak geliştirir (Nguyen ve ark., 2001). Birçok çalışma, ısıl işlem görmüş domates ürünlerinden elde edilen likopenin, taze domateslerden elde edilen likopenin daha fazla biyoyararlı olduğunu göstermiştir (Stahl ve Sies, 1992; Gärnter ve ark., 1997; Allen ve ark., 2002). Absorbe edilen mutlak likopen miktarı dozla önemli ölçüde değişmez. Erkekler üzerinde likopen emilimine yönelik yapılan bir araştırmada, bireylerin bir porsiyon domates suyu tükettikten sonra likopen emilimi araştırılmıştır (Diwadkar-Navsariwala ve ark., 2003). Bu araştırmada bireylere 10 mg ila 120 mg likopen vermek için sabit bir yağ yüzdesi ile farklı hacimlerde domates suyunu tüketmeleri sağlanmıştır. Araştırma bulgularında absorbe edilen mutlak likopen miktarının dozla büyük ölçüde değiştiği görülmüştür. Dozdan bağımsız olarak emilen likopen aralığı 1,8 mg ile 14,3 mg arasında olup, ortalama 4,7 mg olarak belirlenmiştir. 120 mg likopen içeren domates suyunu tüketen erkeklerin absorbe ettiği likopen miktarı, 10 mg likopen içeren domates suyunu tüketen erkeklerin absorbe ettiği miktardan önemli ölçüde farklılık göstermediği rapor edilmiştir. Araştırmacılar, emilen likopen miktarı üzerindeki en büyük etkinin dozdan ziyade, bireyler arası farklılıklardan kaynaklandığını öne sürmüşlerdir (Diwadkar-Navsariwala ve ark., 2003). Likopen biyoyararlanımı, diyet bileşiminden büyük ölçüde etkilenir (Xianquan ve ark., 2005). Likopen yağda çözünen bir bileşik olduğu için yağ ile birlikte tüketilmesi biyoyararlanımını artırır (Bacanli ve ark., 2017). Örneğin, tam yağlı soslu salataları tüketmenin, az yağlı soslu salataları yemekten daha yüksek kan karotenoid seviyelerine yol açtığı bildirilmiştir. Aynı çalışmada, salatalar yağsız tüketildiğinde ölçülebilir bir likopen alımının olmadığı da belirtilmiştir (Brown ve ark., 2004). Unlu ve ark. (2005) ise benzer bir sonucu yaptıkları çalışma ile bildirmişlerdir. Bu çalışmada, avokadolu (bir lipid kaynağı olarak) domates sosu tüketiminin, avokadosuz sos tüketimine kıyasla likopen emiliminde

4,4 kat artışa neden olmuştur. Likopen sindirimi ve emiliminin bir şeması Şekil 4'te gösterilmiştir.



Şekil 4. İnce bağırsakta likopenin sindirimi ve emilimi (During ve Harrison, 2004; During ve ark., 2005).

Likopen, yutulduktan sonra karışık misellere dâhil edilmeden önce gıda matrisinden salınmalıdır. Miseller öğünden gelen safra tuzları, kolesterol ve yağ asitlerini içerir. Misel yapısının amfililik doğası, sulu sindirimde çözünür lipofilik besinlerin tutulmasına yardımcı olur. Miseller, bağırsak hücrelerinin (enterositler) apikal tarafındaki karıştırılmamış su tabakasına yaklaşır ve likopen pasif olarak apikal membran boyunca yayılır (During ve Harrison 2004). Tarihsel olarak, araştırmacılar likopenin diyet lipitleriyle aynı yolla, yani pasif difüzyonla emildiğini düşünüyorlardı (Furr ve Clark, 1997). Bunun ise kısmen doğru olduğu hâlâ düşünülmektedir. Bununla birlikte, araştırmacılar, likopen emiliminin, temizleyici reseptör sınıf B tip I (SR-BI) olarak bilinen bir kolesterol membran taşıyıcısı tarafından kolaylaştırılabileceğini keşfettiler (During ve ark., 2005; Moussa ve ark., 2008). Araştırma ayrıca likopen emiliminin diğer taşıyıcılar tarafından kolaylaştırılabileceğini ileri sürmüştür, ancak bu henüz doğrulanmamıştır (During ve ark., 2005, Moussa ve ark., 2008). Likopen enterosit içine girdikten sonra diğer diyet lipitleriyle birlikte şilomikronlara paketlenir (During ve Harrison, 2004). Şilomikronlar daha sonra bazolateral zarı boyunca taşınır ve sonunda şilomikronları kana salan lenfatik sisteme girerler.

Diğer karotenoidler veya kolesterol ile rekabet de likopen emilimini etkileyebilir. İnsanlar üzerinde tokluk sonrası yapılan bir araştırmada, domates püresi + ıspanak luteini (30 mg) veya kapsüllü luteini (30 mg) birlikte tüketmenin, tek başına domates püresi (30 mg) tüketiminden sonra gözlemlenen likopen seviyelerine kıyasla şilomikron likopen düzeylerini sırasıyla %70 ve %61 azalttığını göstermiştir (Tyssandier ve ark., 2002). Bununla birlikte, deneklerin bu gıdaları üç hafta boyunca her gün bir önceki dozun (15 mg likopen + 15 mg lutein) yarısında tükettiğinde, likopenin kararlı durum plazma

seviyelerinde herhangi bir fark gözlenmediği de bildirilmiştir (Tyssandier ve ark., 2002). Johnson ve ark. (1997) tarafından insanlar üzerinde yapılan bir araştırmada, yağdaki β -karoten kristallerinin (60 mg) yağdaki likopen kristalleri (60 mg) ile birlikte uygulanmasının, tek başına likopen uygulamasına kıyasla 24 saatlik postprandial serum likopen eğrisinin altındaki alanını (EAA) dört kat arttırdığı gözlemlenmiştir. Bir gıda ürününün parçası olarak likopen emiliminin, β -karoten içeren gıda ürünleri ile birlikte tüketilmesi durumunda artıp artmayacağı açık değildir. Likopenin kolesterol taşıyıcı SR-BI tarafından taşındığını gösteren son araştırmalar göz önüne alındığında, SR-BI ifadesindeki genetik farklılıkların da likopen emilimini etkilemesi muhtemeldir (Story ve ark., 2010). Ek olarak, likopen emilimi, probiyotikler ve tek nükleotid polimorfizmleri (SNP'ler) gibi diğer faktörlerden etkilenbilir (Story ve ark., 2010). Yapılan bir çalışmada, probiyotik içeren yoğurdu toplam 4 hafta boyunca tüketen 17 kadından oluşan bir grubun kanlarındaki likopen düzeyleri, normal yoğurt tüketenlerinkine kıyasla düşük bulunmuştur (Fabian ve Emaldfa, 2007). Bu çalışma sonuçları, probiyotiklerin likopen biyoyararlanımını veya metabolizmasını etkileyebileceğini düşündürmektedir (Fabian ve Emaldfa, 2007). Öte yandan, Borel ve ark. (2007), insan kanındaki karotenoid düzeylerinin, lipid taşınmasıyla ilişkili apolipoprotein A-IV ve B'deki SNP'lerden etkilendiğini bildirmiştir.

İşlenmiş domates ürünlerinde bulunan likopenin %90'dan fazlası all-trans yapısındadır (Nguyen ve Schwartz, 1998, Nguyen ve ark., 2001; Boileau ve ark., 2002). İn vivo çalışmalar, likopenin cis-izomerlerinin, all-trans izomerinden daha fazla biyoyararlı görüldüğünü göstermektedir (Stahl ve Sies, 1992; Unlu ve ark., 2007). Diğer yandan, in vitro deneyler ise likopen cis-izomerlerinin biyoyararlanımının artmasının, en azından kısmen, all-trans likopen ile karşılaştırıldığında artan miselizasyon ve enterosit tarafından artan alıma bağlı olduğu sonucunu desteklemektedir (Failla ve ark., 2008). Likopenin dokular arasındaki dağılımı oldukça seçicidir (Kaur ve ark., 2017). Absorbe edilen likopen, dolaşım sistemi yoluyla vücutta dağılır (Kaur ve ark., 2017). Likopen, yaklaşık 2-3 günlük yarı ömrü ile insan plazmasındaki en baskın karotenoiddir (Stahl ve Sies, 1996). Likopen konsantrasyonu 0,2–21,4 nmol/g doku aralığında değişmektedir (Clinton ve ark., 1996). Plazma lipoproteinleri, insan vücudunda karotenoidlerin ve likopenin başlıca dağıtım araçlarıdır (Dias ve ark., 2014). Bu nedenle, likopen doku seviyelerindeki farklılıkların, lipoprotein reseptörlerinin ve kolesterol taşıyıcılarının doku ekspresyonundaki varyasyonla ilişkili olması kuvvetle muhtemeldir (Kaur ve ark., 2017). İnsan organları likopeni değişen seviyelerde biriktirir (Tablo 5). Likopen; testisler, adrenal bezler ve karaciğerde en yüksek konsantrasyonlarda bulunurken; böbrek, yumurtalık ve akciğerde ise daha düşük konsantrasyonlarda bulunur (Kun ve ark., 2006). Dışkı ve idrar yoluyla likopen atılımı da rapor edilmiştir (Kaur ve

ark., 2017). İnsanda, toplam serum karotenoidleri yaklaşık 1-2 μM seviyelerindedir ve likopen insan serumunda bulunan başlıca karotenoidlerden biridir (Su ve ark., 2002). Plazma likopen seviyesi, farklı ülkelerde yaşayan insanlar arasında değişkenlik gösterebilmektedir (Kaur ve ark., 2017).

Tablo 5. İnsan organlarındaki likopen seviyeleri (Clinton ve ark., 1996)

Organ/Doku	Likopen (nmol / g yaş ağırlık)
Adipoz doku	0,2-1,3
Deri	0,4
Beyin sapı	Tespit edilemedi
Karaciğer	1,3-5,7
Akciğer	0,2-0,6
Adrenal bezler	1,9-21,6
Mide	0,2
Kalın bağırsak	0,3
Göğüs	0,8
Testis	4,3-21,4
Yumurta	0,3
Prostat	0,8

6. Hastalık Bağlamında Likopenin Etkisi

Artan kanıtlar, likopen açısından zengin bir diyetin kardiyovasküler hastalık (CVD) ve bazı kanser riskini önleyebileceğini veya azaltabileceğini göstermektedir (Selgas ve ark., 2009; Zuorro ve ark., 2012). Bazı bilim insanları günlük 5-7 mg likopen alımının bu besin maddesinin faydalarını elde etmek için yeterli olabileceğini öne sürmektedir (Campos ve ark., 2017). Kanser veya kardiyovasküler hastalıkların varlığında, daha yüksek konsantrasyonlarda likopen alımı (35-75 mg/gün) önerilebilir (Elvira-Torales ve ark., 2019; Grabowska ve ark., 2019).

6.1. Kanser

Prostat, mesane, özofagus, pankreas, kolon (veya sindirim sistemi), akciğer, meme kanseri, servikal kanser, lösemi, oral ve rektal kanserler gibi bazı kanserleri önlemede ve ayrıca tümörlerin büyümesini geciktirmede ve tümörogenezi inhibe etmede likopen etkilidir (Şahin ve ark., 2019). Buna ek olarak, bazı araştırmalar likopenin yararlı etkisinin belirli organlara özgü olabileceğine değinmektedir (Kong ve ark., 2010). Epidemiyolojik çalışmalar, diyetle alınan likopen ile belirli kanser türlerinin riski arasında ters bir ilişki olduğunu ortaya koymaktadır (Kelkel ve ark., 2011). Prostat kanseri hastalarında likopen açısından zengin bir diyet ile beslenmenin, oksidatif stresi azalttığı ve sonuç olarak plazma lipoproteinlerine, serum proteinlerine ve lenfosit DNA'sına verilen hasarı hafiflettiği rapor edilmiştir. Bu sayede, likopen kanser gelişimini engellemekte ve prostat tümörlerinin saldırganlığını azaltmaktadır (Kelkel ve ark., 2011). Buna karşılık, bazı çalışmalar likopen alımının olumlu etkilerini göstermemiştir; ancak bu çalışmaların bir kısmı sadece

gıda alım sıklığı anketine dayanan zayıf bir çalışma tasarımıyla yürütülmüş olan çalışmalardır (Kong ve ark., 2010). Bazı araştırmacılar, likopen ile bazı ilerlemiş hastalık riski arasında ters bir ilişki olduğunu öne sürmektedir (Kong ve ark., 2010). Tablo 6, likopenin çeşitli kanser türleri üzerindeki etkisine ilişkin farklı çalışmaları özetlemektedir.

6.2. İnflamatuar Hastalıklar

Likopen, antioksidan genlerin ekspresyonunu aktive etme ve inflamatuvar mediatörlerin indüklenmesinden sorumlu sinyal yollarını düzenleme kapasitesi nedeniyle inflamasyon ve redoks dengesizliği üzerinde olumlu etkilere sahiptir. Böylece likopen, Nrf2'nin nükleer translokasyonundan sorumlu olan antioksidan genlerin ekspresyonunu aktive eder (Campos ve ark., 2017). Likopen ayrıca tümör nekroz faktörü (TNF)- α salınımını inhibe eder ve interlökin (IL)-10 üretimini uyarır (Ascenso, 2012). Likopenin çeşitli anti-inflamatuar etkileri: a) siklooksijenaz ve lipooksijenaz ekspresyonunun modülasyonu; b) indüklenebilir nitrik oksit sentazın düzenlenmesi; c) NF-kB'nin yanı sıra aktivatör protein-1 (AP-1) ve MAPK sinyali ile etkileşim şeklinde özetlenebilir (Kelkel ve ark., 2011). Erkek fareler üzerinde yapılan bir araştırmada, likopenin, intraperitoneal lipopolisakarit enjeksiyonundan sonra plazma interlökin (IL)-6 ve TNF- α 'nın yukarı regülasyonunu önemli ölçüde azaltabileceği ve 6 saat sonunda beyin dokusunda inflamatuvar hasarı önleyebileceği sonucuna varılmıştır (Zhang ve ark., 2016).

İnsülin direnci ve tip 2 diyabetin patogenezinin, interlökin (IL)-1 β , TNF- α ve C-reaktif protein düzeylerindeki artışla ilişkili olduğu gösterildiğinden, bu hastalıkların inflamasyonla yakından bağlantılı olduğu düşünülmektedir (Zeng ve ark., 2017). Yüksek yağlı bir diyetle beslenen farelerle yapılan bir araştırmada, likopenin IL -1 β , TNF- α ve C-reaktif proteindeki artışları önleyerek inflamasyonu iyileştirdiği rapor edilmiştir (Zeng ve ark., 2017). Bu sonuçlar doğrultusunda likopenin insülin direncini, inflamasyonu ve lipid birikimini önlediği söylenebilir (Zeng ve ark., 2017).

6.3. Cilt Hastalıkları

Likopen, hücre zarlarının prostaglandin ve fosfolipid bileşenlerinin sentezi nedeniyle cilt koruma mekanizmalarını arttırabilmektedir (Ascenso, 2012). Bu nedenle, likopenin topikal uygulaması inflamatuvar infiltratı azaltabilir (Ascenso, 2012). Deney hayvanlarıyla yürütülmüş olan bir araştırmada, farelerin kulaklarındaki antralin kaynaklı ödem ve eritemin giderilmesinde, %0,05 likopenin epikütan uygulamasının 1 mg/g betametazon solüsyonu ile yapılan tedaviye benzer şekilde etki gösterdiği kanıtlanmıştır (Ascenso ve ark., 2013).

Bazı yazarlar, bireyin yaşam koşullarının insan derisindeki karotenoid konsantrasyonunu etkilediğini öne sürmektedir (Lademann ve ark., 2011). Nitelikli kutanöz likopen konsantrasyonu sigara içenlerde daha

düşükken, vejeteryanlarda daha yüksektir (Lademann ve ark., 2011).

Likopen, epidermal ornitin dekarboksilazı inhibe ederek, enflamatuvar tepkileri azaltarak, normal hücre proliferasyonunu koruyarak ve DNA hasarını önleyerek akut ultraviyole (UV) B kaynaklı fotohasara karşı koruyucu ve önleyici etki oluşturur (Lopes ve Reed, 2009; Ascenso, 2012). Gerçekten de, nontümörijenik insan immortalize keratinositleri (HaCaT) hücre dizisi kullanılarak yapılan bir çalışma, likopenin ışık hasarının derecesine bağlı olarak ışınlanmış hücrelerde düzeltici bir işleve sahip olabileceğini göstermiştir (Ascenso ve

ark., 2016). Başka bir çalışmada ise, likopenin plazma izomerlerindeki bir artışın, nükleer hormon reseptörü sinyal yollarının aktivasyonunu değiştirebileceğini, dolayısıyla da atopik dermatit (AD) fenotipinden nispeten sorumlu olduğu öne sürülmüştür (Lucas ve ark., 2018). Ayrıca, HR-1 tüsüz farelerle yapılan bir çalışmada, likopenin oral uygulanmasından sonra görsel görünüm, cildin nem seviyeleri, dermisteki enflamatuvar hücreler ve cilt kalınlığı gibi AD semptomlarını iyileştirebileceğini ortaya konulmuştur (Hiragun ve ark., 2016).

Tablo 6. Likopenin bazı kanser türlerinde bildirilen etkileri (Caserio ve ark., 2020)

Kanser tipi	Çalışma tipi	Likopenin etkisi	Referans
Kolonorektal kanser	Prospektif kohort çalışması	Serum likopen seviyelerinden sorumlu olan yeşil-sarı renkli sebzelerin fazla miktarda tüketimi, kırsal kesimde yaşayan Japon bireylerin kolorektal kanser ölüm riskini azaltabilir.	(Ito ve ark., 2005; Story ve ark., 2010)
	Vaka-kontrol çalışması	Likopen ile kolorektal kanser riski arasında bir ilişki yoktur.	(Kune ve Watson, 2006; Story ve ark., 2010)
Akciğer kanseri	Kohort çalışması	Likopenin içeren gıdaların fazla tüketimi ile akciğer kanserine yakanma riski azalır.	(Holick ve ark., 2002; Sahin ve ark., 2019)
Yumurtalık kanseri	Vaka kontrol çalışması	Özellikle premenopozal kadınlarda yumurtalık kanseri riski ile likopen tüketimi arasında ters orantılı bir ilişki vardır.	(Cramer ve ark., 2001; Sahin ve ark., 2018)
Pankreas kanseri	Vaka kontrol çalışması	Likopen içeriği yüksek olan domates ve domates bazlı ürünlerin tüketimi pankreas kanserinin azalmasına yardımcı olabilir.	(Nkondjock ve ark., 2005; Sahin ve ark., 2019)
	Meta analiz	Likopen veya likopen içeren gıdaların tüketimi prostat kanserine yakalanma riskini azaltır.	(Aydemir ve ark., 2013; Etminan ve ark., 2004)
Prostat kanseri	Prospektif gözlemsel çalışma	Likopen alımı prostat kanseri riskinde azalma ile ilişkilidir.	(Giovannucci ve ark., 2002; Kong ve ark., 2010)
	Prospektif kohort çalışması	Yiyecek veya takviye olarak daha yüksek likopen alımı, erkeklerde iyi huylu prostat hiperplazisi riskini (%18) azaltır.	(Kristal ve ark., 2008; Story ve ark., 2010)

Ciltte doğal olarak bulunan potansiyel antioksidanların çeşitliliğine bakılmaksızın, aşırı reaktif oksijen türleri (ROS) üretimi genellikle cildin antioksidan yeteneğini aşar (Ascenso ve ark., 2016). Bu nedenle, fotoproteksiyon karotenoidlerin topikal veya sistemik olarak uygulanmasıyla artırılabilir (Alda ve ark., 2009). Antioksidan mikro besinler ile oral fotokoruma kavramı giderek daha önemli hale gelmektedir (Groten ve ark., 2019). Aslında, likopen içeren antioksidan mikrobesein takviyesinden sonra cilt pürüzlülüğünün (Lademann ve ark., 2011), cilt yaşlanmasının ve çizgi ve kırışıklık oluşumunun azaldığı gösterilmiştir (B. Lopes ve ark., 2010). Bununla birlikte, besin takviyesi sonucu plazma likopen seviyelerinde bir artış, her zaman önemli bir fotokoruma ile ilişkili değildir (Groten ve ark., 2019). Güneş kremi formülasyonlarının kullanımıyla

karşılaştırılmayacak olsa da, diyetle alınan likopen ultraviyole (UV) radyasyona karşı bazal bir koruma sağlayabilir (Narciso Tomé, 2014). Diğer yandan, bazı yazarlar likopenin foto-koruyucu özellikler sergilemediğini, hatta aksine likopenin güneşe maruz kalma altındaki kararsızlığının pro-oksidan etkiler yaratması nedeniyle UV radyasyonunun neden olduğu daha kötü DNA hasarını teşvik ettiğini öne sürmektedir (Narciso Tomé, 2014). Yapılan bir çalışmada, daha öncesinde UV radyasyonuna maruz kalmış farelere likopen ve/veya deksametazon içeren topikal formülasyonlar uygulanmıştır (Shah ve Mahajan, 2014). Morfolojik ve biyokimyasal değerlendirmeler dikkate alındığında, likopen jeli fotoyaşlanmaya karşı daha yüksek koruma sağlarken, deksametazon jeli muhtemelen oksidatif stres oluşturma kapasitesi

nedeniyle başarısız bulunmuştur (Shah ve Mahajan, 2014). Ne yazık ki likopen diğer karotenoidlere göre UV radyasyonuna daha duyarlıdır (Moran ve ark., 2013). Deride, likopenin tüketildiği UV maruziyeti sırasında radikal söndürme gerçekleşir (Kong ve ark., 2010). Aslında, likopen seviyeleri ışınlanmadan sonraki ilk 30 dakika içinde çok hızlı bir şekilde azalır (Lademann ve ark., 2011). Likopenin fotodegradasyonu, çözünmüş oksijen tüketimini önlemek için sistemin oksijensizleştirilmesiyle önlenebilir (Nishino ve ark., 2011).

6.4. Diğer Hastalıklar

Likopenin kolesterolü düşürdüğü (Jaswir ve ark., 2011) ve aterosklerotik plakları azaltarak kardiyovasküler hastalığı iyileştirmeye yardımcı olduğu çeşitli çalışmalarda öne sürülmüştür (Durairajanayagam ve ark., 2014).

7-ketokolesterol (7-KC) aterosklerozda önemli bir role sahip gibi görünmektedir (Palozza ve ark., 2010). Bazı yazarlar likopenin insan makrofajlarında hem oksidatif stresi hem de apoptozu azaltarak 7-KC'nin zararlı etkilerini önleyebileceğini öne sürmektedir (Palozza ve ark., 2010). Görünen odur ki, iskemik hastalıklarda nakledilen ve likopen ile ön işleme tabi tutulmuş mezenkimal kök hücreler, belirli doku yaralanmalarının tedavisinde kullanılabilir, çünkü likopen, apoptozla ilişkili sinyal yolunu baskılayarak ve antioksidan proteini güçlendirerek iskemik hasarı önleyebilmektedir (Kim ve ark., 2015).

Yüksek serum likopen seviyeleri, yaşa bağlı makula dejenerasyonu riskinin daha düşük olmasıyla da ilişkilendirilebilir. Bunun nedeni, likopenin gözde bulunan singlet oksijeni söndürme yeteneğinin yanı sıra makulayı dolaylı olarak etkileyen aterojenik süreçler üzerindeki etkisidir (Mares-Perlman ve ark., 1995; Kelkel ve ark., 2011; Martínez ve Melendez-Martínez, 2016).

Likopen, mikroorganizmalara karşı yeterli bir savunma sağlayarak adaptif bağışıklık tepkisini aktive edebilir (Campos ve ark., 2017). Böylece bakteriyel enfeksiyon ve radyasyona karşı koruma sağlar (Ascenso, 2012).

Ayrıca, serum likopeni; plazma glikozu ve açlık insülin konsantrasyonları ile ters ilişkilidir (Kong ve ark., 2010). Kesitsel bir çalışma, diyetle alınan likopenin, açlık kan şekerindeki düşüğe bağlı olarak gestasyonel diabetes mellitus riskini azaltabileceğini desteklemektedir (Gao ve ark., 2019). Aslında, likopen tüketiminde 1 mg'lık bir artışın, açlık kan şekerini 0,005 mmol/L düşürerek gestasyonel diyabet riskini %5 azalttığı bildirilmiştir (Gao ve ark., 2019).

Oksidatif stres sperm canlılığını, hareketliliğini ve DNA hasarını etkileyebilir, bu da esas olarak idiyopatik erkek faktörüne bağlı infertilitenin önemli bir nedenidir (Durairajanayagam ve ark., 2014). Likopen; katalaz ve glutatyon peroksidaz gibi antioksidanları artırarak bağışıklığı güçlendirmenin yanı sıra spermatozoanın lipid peroksidasyonunu ve DNA hasarını azaltabilmektedir (Durairajanayagam ve ark., 2014). Nitekim, bir çalışmada likopenin Beltsville sulandırıcılarında horoz sperminin

kriyoprezervasyonu üzerindeki etkisi incelenmiş ve dondurucu sulandırıcının likopen veya likopen nanolipozomları ile desteklenmesinin, muhtemelen redoks dengesinin, hücresel enerji metabolizmasının ve membran korumasının iyileştirilmesi nedeniyle sperm kalitesini, özellikle de hareketliliği ve mitokondriyal aktiviteyi iyileştirdiği tespit edilmiştir (Najafi ve ark., 2018).

Kolşisin ile tedavi edilen sıçanlarla yapılan bir çalışma, likopenin beyin antioksidan savunma mekanizmalarının hızlanması ve nitrik oksit yollarının aşağı regülasyonu nedeniyle nörolojik defisitleri tersine çevirebileceğini ve bilişi geliştirebileceğini öne sürmektedir (Prakash ve Kumar, 2013).

Alzheimer hastalığı, başta β -Amyloid₁₋₄₂ ($A\beta_{1-42}$) olmak üzere beyinde β -amiloid birikimi ile kendini gösterir (Sachdeva ve Chopra, 2015). $A\beta_{1-42}$ peptitleri enjekte edilen sıçanlarda yapılan bir çalışma, likopen tedavisinin $A\beta_{1-42}$ ile indüklenen mitokondriyal disfonksiyonu, NF- κ B, IL-1 β , TNF- α ve dönüştürücü büyüme faktörü (TGF)- β gibi enflamatuar sitokin araçlarını ve beyindeki kaspaz-3 aktivitesini önemli ölçüde azaltabileceğini göstermektedir (Sachdeva ve Chopra, 2015).

Oksidatif stres, Parkinson hastalığının patogeneğinde önemli bir role sahip olabilir (Kaur ve ark., 2011). Rotenonla tedavi edilen sıçanlarda yapılan bir çalışma, likopenin sadece antioksidanlarda rotenona bağlı değişiklikleri değil, aynı zamanda indüklenen oksidatif stresi ve nörodavranışsal eksiklikleri de önleyebileceğini göstermiştir (Kaur ve ark., 2011). Bu nedenle, likopen takviyesi, oksidatif stresin arttığı nörodejeneratif hastalıklarda uygulanabilir (Kaur ve ark., 2011).

7. Likopenin Önerilen Dozu

Günlük likopen tüketimi için ideal bir doz olmadığı unutulmamalıdır. Önceki çalışmalar sadece farklı seviyelerde likopen alımı hakkında fikir vermesi bakımından yararlı olacaktır. Örneğin, bir in vivo çalışma likopenin (6,5 mg/gün) erkeklerde kansere karşı etkili olduğunu ortaya koymuştur (Giovannucci ve ark., 1995). Ancak, ilerlemiş PCa durumunda likopen dozu 10,0 mg/gün'e kadar arttırılmalıdır. Başka bir çalışmada, yaşlı bir popülasyonda likopen takviyesi (15 mg/gün, 12 hafta boyunca) doğal öldürücü hücre aktivitesini %28 oranında arttırarak bağışıklık fonksiyonunu iyileştirmiştir (Corridan ve ark., 1998). Bu nedenle, çeşitli sağlık amaçları için farklı likopen dozları ve takviye sürelerinin önerilebileceği görülmektedir. Son olarak, farklı epidemiyolojik çalışmalara göre, günlük likopen alımının günde 2 ila 20 mg olması önerilebilir (Saini ve ark., 2020).

8. Likopenin Güvenilirlik ve Toksikite Seviyesi

Tıbbi bitkiler ve bitki türevi fitokimyasallar konusunda güvenlik takibi önemli bir konu olarak ele alınmalıdır (Khiveh ve ark., 2017; Shakeri ve ark., 2018). Likopenin

olası toksisitesine ilişkin çeşitli in vitro ve in vivo çalışmalar bulunmaktadır. Örneğin, likopenin (10,0 µM'a kadar) sıçanın serebellar granül nöron hücre kültürlerinde, hücre canlılığı üzerinde toksisitesi olmadığı bildirilmiştir (Qu ve ark., 2013). Sıçan hipokampal nöron hücre kültürleri üzerinde yapılan bir başka çalışmada ise bu hücrelere uygulandığında likopenin önemli bir toksik etkisi olmadığını göstermiştir (Qu ve ark., 2011). Ancak karotenoidlerin yüksek doku konsantrasyonlarında bazı özel durumlarda pro-oksidan etki gösterebileceği görülmektedir (Wang, 2004). Sıçanlar üzerinde yapılan bir toksikolojik çalışma, incelenen en yüksek dozda (diyet %1,0 seviyesinde) hiçbir yan etkinin gözlemlenmediğini göstermiştir (Jonker ve ark., 2003). Farklı likopen formlarının (yani domatesten elde edilen likopen, sentetik likopen ve kristalize özütü) değişik gıda ürünlerinde kullanıldığında genellikle güvenli olarak kabul edildiği unutulmamalıdır (Trumbo, 2005). Normal ve sıradan dozlarda likopen kullanımından kaynaklanan herhangi bir yan etki bildirimi yoktur (Krinsky ve ark., 2000). İnsanlar üzerinde yapılan çalışmalar, likopen için gözlemlenmeyen yan etki düzeyinin günde 3,0 g/kg vücut ağırlığı olduğunu ileri sürmüştür. Günlük likopen alımının bu seviyenin önemli ölçüde altında olduğu tahmin edilmektedir. Alımı için 99. persentil bile günde 123 mg düzeyindedir (Trumbo ve ark., 2001). Sitokrom P450 2E1 ekspresyonunun yüksek dozlarda likopen ve alkol tarafından indüklenebileceği görülmektedir. Bu nedenle, yüksek dozda eş zamanlı kullanımlarından kaçınılmalıdır (Veeramachaneni ve ark., 2008). Ayrıca, likopenin güçlü antioksidan etkisi nedeniyle, kemoterapi ve radyoterapi alan hastalarda önlemler alınmalıdır (Cassileth, 2010). Bir vaka raporunda, birkaç yıl boyunca her gün yaklaşık 2 litre domates suyu içen bir kadın bireyde likopenemi tanımlanmıştır. Likopenemiye bağlı olarak bireyin karaciğerinde likopen birikintileri (hepatik disfonksiyon kanıtı olmaksızın) ve ciltte koyu turuncu renk değişikliği gözlemlenmiştir. Aynı birey domates suyu tüketimini bıraktıktan 3 hafta sonra likopenodermi gözden kaybolmuştur (Reich ve ark., 1960).

9. Likopen Düzeyini Belirleme Yöntemleri

Gıda ve biyolojik numunelerdeki likopen içeriğini ölçmek ve analiz etmek için çeşitli analitik yöntemler geliştirilmiştir. Bunlar arasında ultraviyole-görünür (UV-VIS) spektrofotometri (Davis ve ark., 2003), sıvı kromatografisi (LC), ince tabaka kromatografisi (TLC) ve yüksek performanslı sıvı kromatografisi (HPLC) bulunmaktadır (Lee ve Chen, 2002; Ishida ve Chapman, 2004; Xu ve ark., 2006). Diğer birçok yüksek hızlı karşı akım kromatografisi (Baldermann ve ark., 2008), fiber optik görünür yansıma spektroskopisi (Choudhary ve ark., 2009) ve kızılötesi spektroskopisi (De Nardo ve ark., 2009) de geliştirilmiştir. Bununla birlikte, all-E-likopenin Z izomerleri ile ayrılmasını sağlamak için çok fazla zaman (genellikle >20 dakika) ve çözücü tüketirler. UV-VIS spektrofotometresi HPLC analizinden daha kullanışlı,

daha hızlı ve daha ucuzdur ve çok sayıda numune nispeten kısa sürede işlenebilir. Bununla birlikte, UV-VIS spektrofotometresi çok küçük miktarlardaki likopeni (1,0 µg'dan az) tespit edemezken, HPLC 1,0 ng kadar küçük miktarları tespit edebilir (Hyman ve ark., 2004).

10. Sonuçlar

Meyve ve sebzeler, hayati fitokimyasallar ve biyoaktif moleküllerin varlığı nedeniyle beslenme alanında büyük önem kazanmaktadır. Besinlerin içerisindeki bu bileşikler vücut metabolizmasını tetikleyip, değiştirmenin yanı sıra detoksifikasyon mekanizmasını da modüle eder.

Likopen, başta domates olmak üzere bazı meyve ve sebzelerde doğal olarak bulunan bir kırmızı renkli bir pigmenttir. Likopen güçlü antikanser, antioksidan, antiinflamatuvar ve antidiyabetik potansiyele sahiptir. Aynı zamanda, bu pigment insanları kalp, karaciğer, kemik, deri, sinir ve üreme sistemi hastalıklarına karşı koruyan bir nutrasötiktir. Bununla birlikte, gen ekspresyonu çalışmalarına özel bir vurgu yaparak, alta yatan etki mekanizmalarını ortaya çıkarmak için daha fazla araştırma yapılması gerekmektedir. Ek olarak, bu fonksiyonel gıdanın önerilen ve etkili dozlarının daha fazla araştırılması gerekmektedir. Genotoksitesisi, maternal toksisitesi ve teratojenik etkileri ile ilgili güvenlik endişeleri de sorgulanmalıdır.

Sonuç olarak, doğal olarak oluşan karotenoid bakımından zengin meyve ve sebzelerin yanı sıra likopen içeren işlenmiş domates ürünlerinin insan sağlığı ve hastalıkları üzerinde olumlu etkileri sebebiyle tüketilmelerinin teşvik edilmesi sağlanmalıdır.

Katkı Oranı Beyanı

Yazar(lar)ın katkı yüzdesi aşağıda verilmiştir. Tüm yazarlar makaleyi incelemiş ve onaylamıştır.

	G.A.	A.E.
K	50	50
T	60	40
Y	50	50
KT	60	40
YZ	100	
KI	50	50
GR	100	

K= kavram, T= tasarım, Y= yönetim, KT= kaynak tarama, YZ= Yazım, KI= kritik inceleme, GR= gönderim ve revizyon.

Çalışma Beyanı

Yazarlar bu çalışmada hiçbir çıkar ilişkisi olmadığını beyan etmektedirler.

Kaynaklar

- Aberoumand A. 2011. A review article on edible pigments properties and sources as natural biocolourants in foodstuff and food industry. World J Dairy Food Sci, 6: 71-78.
- Agcam E, Akyıldız A, Balasubramaniam VM. 2017. Optimization of anthocyanins extraction from black carrot pomace with thermosonication. Food Chem, 237: 461-470.

- Akhtar MS, Goldschmidt EE, John I, Rodoni S, Matile P, Grieson D. 1999. Altered patterns of senescence and ripening in gf, a stay-green mutant of tomato (*Lycopersicon esculentum* Mill.). J Exp Bot, 50: 1115-1122.
- Akinoğlu G, Korkmaz A. 2016. Topraksız tarımda farklı substrat miktarı ve besin çözeltisi uygulamalarının domateste beslenme ve verim kriterlerine etkisi. Toprak Bilimi ve Bitki Besleme Dergisi, 4: 49-56.
- Alda LM, Gogoşaş L, Bordean D-M, Gergen I, Alda S, Moldovan C, Niță L. 2009. Lycopene content of tomatoes and tomato products. J Agroalimnt Process Technol, 15: 540-2.
- Allen CM, Smith AM, Clinton SK, Schwartz SJ. 2002. Tomato consumption increases lycopene isomer concentrations in breast milk and plasma of lactating women. J Am Diet Assoc, 102: 1257-62.
- Al-Wandawi H, Abdul-Rahman M, AlShaikhly K. 1985. Tomato processing waste as essential raw materials source. J Agric Food Chem, 33: 804-807.
- Araın MA, Mei Z, Hassan FU, Saeed M, Alagawany M, Shar AH, Rajput IR. 2018. Lycopene: a natural antioxidant for prevention of heat-induced oxidative stress in poultry. Worlds Poult Sci J, 74: 89-100.
- Ascenso A, Pedrosa T, Pinho S, Pinho F, de Oliveira JM, Cabral Marques H, Oliveira H, Simões S, Santos C. 2016. The effect of lycopene preexposure on UV-B-irradiated human keratinocytes. Oxid Med Cell Longev, 2016: 8214631.
- Ascenso A, Pinho S, Eleutério C, Praça F, Lopes Badra Bentley MV, Oliveira H, Santos C, Simões S. 2013. Lycopene from tomatoes: Vesicular nanocarrier formulations for dermal delivery. J Agric Food Chem, 61: 7284-7293.
- Ascenso A. 2012. Carrier-mediated dermal delivery for prevention or treatment of skin disorders.
- Awolu OO, Oladeji OA. 2021. Natural plant pigments and derivatives in functional foods developments. EJFST, 5: 25-40.
- Aydemir G, Kasiri Y, Birta E, Béke G, Garcia AL, Bartók EM, Rühl R. 2013. Lycopene-derived bioactive retinoic acid receptors/retinoid-X receptors-activating metabolites may be relevant for lycopene's anti-cancer potential. Mol Nutr Food Res, 57: 739-747.
- Bacanli M, Başaran N, Başaran AA. 2017. Lycopene: Is it beneficial to human health as an antioxidant? Turk J Pharm Sci, 14: 311-318
- Baldermann S, Ropeter K, Kohler N, Fleischmann P. 2008. Isolation of all-trans lycopene by high-speed counter-current chromatography using a temperature-controlled solvent system. J Chromatogr A, 1192: 191-193.
- Boileau TWM, Boileau AC, Erdman JW Jr. 2002. Bioavailability of all-trans and cis-isomers of lycopene. Exp Biol Med (Maywood), 227: 914-19.
- Borel P, Moussa M, Reboul E, Lyan B, Defoort C, Vincent-Baudry S, Maillot M, Gastaldi M, Darmon M, Portugal H, Planells R, Lairon D. 2007. Human plasma levels of vitamin E and carotenoids are associated with genetic polymorphisms in genes involved in lipid metabolism. J Nutr, 137: 2653-2659.
- Bouvier F, Backhaus RA, Camara B. 1998. Induction and control of chromoplastspecific carotenoid genes by oxidative stress. J Biol Chem, 273: 30651-30659.
- Brown MJ, Ferruzzi MG, Nguyen ML, Cooper DA, Eldridge AL, Schwartz SJ, White WS. 2004. Carotenoid bioavailability is higher from salads ingested with full-fat than with fat-reduced salad dressing as measured with electrochemical detection. Am J Clin Nutr, 80: 396-403.
- Buggy MJ, Britton G, Goodwin TW. 1969. Stereo-chemistry of phytoene biosynthesis by isolated chloroplasts. Biochem J, 114: 641-643.
- Burton GW, Ingold KU. 1984. β -carotene: an unusual type of lipid antioxidant. Science, 224: 569-573.
- Campos KKD, Araújo GR, Martins TL, Bandeira ACB, Costa GP, Talvani A, Garcia CCM, Oliveira LAM, Costa DC, Bezerra FS. 2017. The antioxidant and anti-inflammatory properties of lycopene in mice lungs exposed to cigarette smoke. J Nutr Biochem, 48: 9-20.
- Caseiro M, Ascenso A, Costa A, Creagh-Flynn J, Johnson M, Simões S. 2020. Lycopene and Human Health. LWT - Food Sci Technol, 127: 109323
- Cassileth B. 2010. Lycopene. Oncology, 24: 296.
- Choudhary R, Bowser TJ, Weckler P, Maness NO, McGlynn W. 2009. Rapid estimation of lycopene concentration in watermelon and tomato puree by fiber optic visible reflectance spectroscopy. Postharvest Biol Technol, 52: 103-109.
- Clinton SK, Emenhiser C, Schwartz SJ, Bostwick DG, Williams AW, Moore BJ, Erdman JW Jr. 1996. Cis-trans lycopene isomers, carotenoids, and retinol in the human prostate. Cancer Epidemiol Biomarkers Prev, 5: 823-833.
- Clinton SK. 1998. Lycopene: chemistry, biology, and implications for human health and disease. Nutr Rev, 56: 35-51.
- Conn PF, Lambert C, Land EJ, Schalch W, Truscott TG. 1992. Carotene-oxygen radical interactions. Free Radic Res Commun, 16: 401-408.
- Conn PF, Schalch W, Truscott TG. 1991. The singlet oxygen and carotenoid interaction. J Photochem Photobiol B Biol, 11: 41-47.
- Corridan B, O'Donohue M, Morrissey P. 1998. Proceedings of Proceedings-Nutrition Society of London. Cambridge University Press; Cambridge, UK: Carotenoids and immune response in elderly people; p. 4A.
- Cramer DW, Kuper H, Harlow BL, Titus-Ernstoff L. 2001. Carotenoids, antioxidants and ovarian cancer risk in pre- and postmenopausal women. Int J Cancer, 94: 128-134.
- Crupi P, Faienza MF, Naeem MY, Corbo F, Clodoveo ML, Muraglia M. 2023. Overview of the potential beneficial effects of carotenoids on consumer health and well-being. Antioxidants, 12: 1069.
- D'Souza MC, Singha S, Ingle M. 1992. Lycopene concentration of tomato fruit can be estimated from chromaticity values. HortScience, 27: 465-466.
- Davis AR, Fish WW, Perkins-Veazie P. 2003. A rapid spectrophotometric method for analyzing lycopene content in tomato and tomato products. Postharvest Biol Technol, 28: 425-430.
- De Nardo T, Shiroma-Kian C, Halim Y, Francis D, Rodrigues-Saona LE. 2009. Rapid and simultaneous determination of lycopene and β -carotene contents in tomato juice by infrared spectroscopy. J Agric Food Chem, 57: 1105-1112.
- Dey S, Bommu Hema Nagababu BH. 2022. Applications of food color and bio-preservatives in the food and its effect on the human health. Food Chem Adv, 1: 100019.
- Di Mascio P, Kaiser S, Sies H. 1989. Lycopene as the most efficient biological carotenoid singlet oxygen quencher. Arch Biochem Biophys, 274: 532-538.
- Di Mascio P, Murphy ME, Sies H. 1991. Antioxidant defense systems: the role of carotenoids, tocopherols, and thiols. Am J Clin Nutr 53: 194S-200S.
- Dias IHK, Polidori MC, Lietai L. 2014. Plasma levels of HDL and carotenoids are lower in dementia patients with vascular comorbidities. J Alzheimer's Dis, 40: 399-408.
- Diwadkar-Navsariwala V, Novotny J, Gustin DM, Sosman JA, Rodvold KA, Crowell JA, Stacewicz-Sapuntzakis M, Bowen PE. 2003. A physiological pharmacokinetic model describing the

- disposition of lycopene in healthy men. *J Lipid Res*, 44: 1927-39
- Durairajanayagam D, Agarwal A, Ong C, Prashast P. 2014. Lycopene and male infertility. *Asian J Androl*, 16: 420-425.
- During A, Dawson HD, Harrison EH. 2005. Carotenoid transport is decreased and expression of the lipid transporters SR-BI, NPC1L1, and ABCA1 is downregulated in caco-2 cells treated with ezetimibe. *J Nutr*, 135: 2305-12.
- During A, Harrison EH. 2004. Intestinal absorption and metabolism of carotenoids: insights from cell culture. *Arch Biochem Biophys*, 430: 77-88.
- Elvira-Torales LI, Garcia-Alonso J, Periago-Castón MJ. 2019. Nutritional importance of carotenoids and their effect on liver health: A review. *Antioxidants (Basel)*, 8, 229
- Etmiman M, Takkouche B, Caamaño-Isorna F. 2004. The role of tomato products and lycopene in the prevention of prostate cancer: A meta-analysis of observational studies. *Cancer Epidemiol Biomarkers Prev*, 13: 340-345.
- Fabian E, Elmadfa I. 2007. The effect of daily consumption of probiotic and conventional yoghurt on oxidant and antioxidant parameters in plasma of young healthy women. *Int J Vitam Nutr Res*, 77: 79-88.
- Failla ML, Chitchumroonchokchai C, Ishida BK. 2008. In vitro micellarization and intestinal cell uptake of cis isomers of lycopene exceed those of all-trans lycopene. *J Nutr*, 138: 482-86.
- Faria-Silva C, Ascenso A, Costa AM, Marto J, Carvalheiro M, Ribeiro HM, Simões S. 2020. Feeding the skin: A new trend in food and cosmetics convergence. *Trends Food Sci Technol*, 95: 21-32.
- Foote CS, Denny RW. 1968. Chemistry of singlet oxygen. VII. Quenching by β -caotene. *J Am Chem Soc*, 90: 6233-6235.
- Frenkel C, Garrison SA. 1976. Initiation of lycopene synthesis in the tomato mutant rin influenced by oxygen and ethylene interaction. *HortScience*, 11: 20-21.
- Furr HC, Clark RM. 1997. Intestinal absorption and tissue distribution of carotenoids. *J Nutr Biochem*, 8: 364-77.
- Gao Q, Zhong C, Zhou X, Chen R, Xiong T, Hong M, Li Q, Kong M, Han W, Sun G, Yang X, Yang N, Hao L. 2019. The association between intake of dietary lycopene and other carotenoids and gestational diabetes mellitus risk during mid-trimester: A cross-sectional study. *Br J Nutr*, 121: 1405-1412.
- Gärtner C, Stahl W, Sies H. 1997. Lycopene is more bioavailable from tomato paste than from fresh tomatoes. *Am J Clin Nutr*, 66: 116-22.
- Giovannucci E, Ascherio A, Rimm EB, Stampfer MJ, Colditz GA, Willett WC. 1995. Intake of carotenoids and retinol in relation to risk of prostate cancer. *J Natl Cancer Inst*, 87: 1767-1776.
- Giovannucci E, Rimm EB, Liu Y, Stampfer MJ, Willett WC. 2002. A prospective study of tomato products, lycopene, and prostate cancer risk. *J Natl Cancer Inst*, 94: 391-398.
- Gould WV. 1992. *Tomato Production, Processing, and Technology*, CTI Publications, Baltimore, USA.
- Grabowska M, Wawrzyniak D, Rolle K, Chomczyński P, Oziewicz S, Jurga S, Barciszewski J. 2019. Let food be your medicine: Nutraceutical properties of lycopene. *Food Funct*, 10: 3090-3102.
- Gross J. 1987. *Pigments in Fruits*, Academic Press, Orlando.
- Groten K, Marini A, Grether-Beck S, Jaenicke T, Ibbotson SH, Moseley H, Ferguson J, Krutmann J. 2019. Tomato phytonutrients balance UV response: Results from a double-blind, randomized, placebo-controlled study. *Skin Pharmacol Physiol*, 32: 101-108.
- Harris WM. 1970. Chromoplasts of tomato fruits. III. The high-delta tomato. *Bot Gaz*, 131: 163-166.
- Hart DJ, Scott KJ. 1995. Development and evaluation of an HPLC method for the analysis of carotenoids in foods, and the measurement of the carotenoid content of vegetables and fruits commonly consumed in the UK. *Food Chem*, 54: 101-111.
- Heinonen MI, Ollilainen V, Linkola EK, Varo PT, Koivisto PE. 1989. Carotenoids in Finnish foods, vegetables, fruits, and berries. *J Agric Food Chem*, 37: 655-659.
- Hiragun M, Hiragun T, Oseto I, Uchida K, Yanase Y, Tanaka A, Okame T, Ishikawa S, Mihara S, Hide M. 2016. Oral administration of β -carotene or lycopene prevents atopic dermatitis-like dermatitis in HR-1 mice. *J Dermatol*, 43: 1188-1192.
- Holick CN, Michaud DS, Stolzenberg-Solomon R, Mayne ST, Pietinen P, Taylor PR, Virtamo J, Albanes D. 2002. Dietary carotenoids, serum β -carotene, and retinol and risk of lung cancer in the alpha-tocopherol, beta-carotene cohort study. *Am J Epidemiol*, 156: 536-547.
- Hossain B, Kamrul N, Biswas B. 2019. Studies of the compositional characteristics of commercial roasted beet root chips snacks. *J Eng Res Rep*, 4: 1-8.
- Hyman JR, Gaus J, Foolad MR. 2004. A rapid and accurate method for estimating tomato lycopene content by measuring chromaticity values of fruit puree. *J Am Soc Hortic Sci*, 129: 717-723.
- Ishida BK, Chapman MH. 2009. Carotenoid extraction from plants using a novel, environmentally friendly solvent. *J Agric Food Chem*, 57: 1051-1059.
- Ito Y, Kurata M, Hioki R, Suzuki K, Ochiai J, Aoki K. 2005. Cancer mortality and serum levels of carotenoids, retinol, and tocopherol: A population-based followup study of inhabitants of a rural area of Japan. *APJCP*, 6: 10-15.
- İzgi C. 2012. Farklı Kurutma Metotlarının Domatesteki Likopen Miktarına Etkisi. Yüksek Lisans Tezi, Namık Kemal Üniversitesi, Fen Bilimleri Enstitüsü, Tekirdağ, pp: 59.
- Jaswir I, Noviendri D, Hasrini RF, Octavianti F. 2011. Carotenoids: Sources, medicinal properties and their application in food and nutraceutical industry. *J Med Plant Res*, 5: 7119-7131.
- Jeffery D, Smith C, Goodenough P, Prosser I, Grierson D. 1984. Ethyleneindependent and ethylene-dependent biochemical changes in ripening tomatoes. *Plant. Physiol*, 74: 32-38.
- Johnson EJ, Qin J, Krinsky NI, Russell RM. 1997. Ingestion by men of a combined dose of beta-carotene and lycopene does not affect the absorption of beta-carotene but improves that of lycopene. *J Nutr*, 127: 1833-37.
- Jonker D, Kuper CF, Fraile N, Estrella A, Rodríguez Otero C. 2003. Ninety-day oral toxicity study of lycopene from *Blakeslea trispora* in rats. *Regul Toxicol Pharmacol*, 37: 396-406.
- Karrer P, Jucker E. 1950. *Carotenoids*. Elsevier, New York, USA, pp: 1950.
- Kaur G, Sandal A, Dhillon NS. 2017. Lycopene and human health-A review. *Agricultural Reviews*, 38: 282-289.
- Kaur H, Chauhan S, Sandhir R. 2011. Protective effect of lycopene on oxidative stress and cognitive decline in rotenone induced model of Parkinson's disease. *Neurochem Res*, 36: 1435-1443.
- Kelkel M, Schumacher M, Dicato M, Diederich M. 2011. Antioxidant and antiproliferative properties of lycopene. *Free Radic Res*, 45: 925-940.
- Khan U.M, Sevindik M, Zarrabi A, Nami M, Ozdemir B, Kaplan DN, Selamoglu Z, Hasan M, Kumar M, Alshehri MM, Sharifi-Rad J. 2021. Lycopene: Food Sources, Biological Activities, and Human Health Benefits. *Oxid Med Cell Longev*, 2021: 2713511.
- Khiveh A, Hashempur MH, Shakiba M, Lotfi MH, Shakeri A, Kazemeini S, Mousavi Z, Jabbari M, Kamalinejad M, Emtiazy M.

2017. Effects of rhubarb (*Rheum ribes* L.) syrup on dysenteric diarrhea in children: A randomized, double-blind, placebo-controlled trial. *J Integr Med*, 15: 365-372.
- Khudairi AK. 1972. The ripening of tomatoes. *Am Sci*, 60: 696-707.
- Kim JY, Lee JS, Han YS, Lee JH, Bae I, Yoon YM, Kwon SM, Lee SH. 2015. Pretreatment with lycopene attenuates oxidative stress-induced apoptosis in human mesenchymal stem cells. *Biomol Ther (Seoul)*, 23: 517-524.
- Kong KW, Khoo HE, Prasad KN, Ismail A, Tan CP, Rajab NF. 2010. Revealing the power of the natural red pigment lycopene. *Molecules*, 15: 959-987.
- Krinsky NI, Beecher G, Burk R, Chan A, Erdman JJ, Jacob R, Jialal I, Kolonel L, Marshall J, Taylor Mayne PR. 2000. Dietary reference intakes for vitamin C, vitamin E, selenium, and carotenoids. Washington, DC: The National Academies Press, doi: 10.17226/9810.
- Krinsky NI, Russett MD, Handeman GJ, Snodderly DM. 1990. Structural and geometrical isomers of carotenoids in human plasma. *J Nutr*, 120: 1654-1662.
- Kristal AR, Arnold KB, Schenk JM, Neuhaus ML, Goodman P, Penson DF, Thompson IM. 2008. Dietary patterns, supplement use, and the risk of symptomatic benign prostatic hyperplasia: Results from the prostate cancer prevention trial. *Am J Epidemiol*, 167: 925-934.
- Kun Y, Lule US, Xiao-Lin D. 2006. Lycopene: its properties and relationship to human health. *Food Rev Intr*, 22: 309-33
- Kune G, Watson L. 2006. Colorectal cancer protective effects and the dietary micronutrients folate, methionine, vitamins B6, B12, C, E, selenium, and lycopene. *Nutr Cancer*, 56: 11-21.
- Kurt H. 2003. Siçanlarda Karbon Tetraklorit'in (CCl₄) Oluşturduğu Oksidatif Stresin Katesin ve Likopen İle Önlenmesi, Doktora Tezi, Eskişehir Osmangazi Üniversitesi, Sağlık Bilimleri Enstitüsü, Eskişehir.
- Kurzeja E, Stec M, Kościółek A, Wardas M, Pawłowska-Góral K. 2009. Biological activity of lycopene, *Farm PrzegNauk*, 10: 17-19.
- Lademann J, Meinke MC, Sterry W, Darvin ME. 2011. Carotenoids in human skin. *Exp Dermatol*, 20: 377-382.
- Lampe C, Watada AE. 1971. Postharvest quality of high pigment and crimson tomato fruit. *J. Am Soc Hort Sci*, 96: 534-535.
- Laval-Martin D. 1974. La maturation du fruit de tomate cerise: Mise en évidence, par cryodécapage, de l'évolution des chloroplastes en deux types de chromoplastes. *Protoplasma*, 82: 33-59.
- Lee MT, Chen BH. 2002. Stability of lycopene during heating and illumination in a model system. *Food Chem*, 78: 425-432.
- Lopes LB, Reed R. 2009. A simple and rapid method to assess lycopene in multiple layers of skin samples. *Biomed Chromatogr*, 24: 154-159.
- Lopes LB, VanDewall H, Li HT, Venugopal V, Li HK, Naydin S, Hosmer J, Levendusky M, Zheng H, Bentley MV, Levin R, Hass MA. 2010. Topical delivery of lycopene using microemulsions: Enhanced skin penetration and tissue antioxidant activity. *J Pharm Sci*, 99: 1346-1357.
- Lucarini M, Lanzi S, D'Evoli L, Aguzzi A, Lombardi-Boccia G. 2006. Intake of vitamin A and carotenoids from the Italian population—results of an Italian total diet study. *Int J Vitam Nutr Res*, 76: 103-9.
- Lucas R, Mihály J, Lowe GM, Graham DL, Szklenar M, Szegedi A, Töröcsik D, Rühl R. 2018. Reduced carotenoid and retinoid concentrations and altered lycopene isomer ratio in plasma of atopic dermatitis patients. *Nutrients*, 10: 1390.
- Lurie S, Handros A, Fallik E, Shapira. 1996. Reversible inhibition of tomato fruit gene expression at high temperature. *Plant Physiol*, 110: 1207-1214.
- Maoka T. 2020. Carotenoids as natural functional pigments. *J Nat Med*, 74: 1-16.
- Mares-Perlman JA, Brady WE, Klein R, Klein BEK, Bowen P, Stacewicz-Sapuntzakis M, Palta M. 1995. Serum antioxidants and age-related macular degeneration in a population-based case-control study. *Arch of Ophthalmol*, 113: 1518-1523.
- Martínez A, Melendez-Martínez AJ. 2016. Lycopene, oxidative cleavage derivatives and antiradical activity. *Comput Theor Chem*, 1077: 92-98.
- Matienco BT, Yedaly EM. 1973. Ultrastructure of Carotenoidoplasts, Academic Press, New York, NY, USA
- McGill AEJ. 2009. The potential effects of demands for natural and safe foods on global food security. *Trends Food Sci Technol*, 20: 402-406.
- Miller NJ, Sampson J, Candeias LP, Bramley PM, Rice-Evans CA. 1996. Antioxidant activities of carotenes and xanthophylls. *FEBS Lett*, 384: 240-242.
- Mohr WP. 1979. Pigment bodies in fruits of crimson and high pigment lines of tomatoes. *Ann Bot*, 44: 427-434.
- Moran NE, Erdman JW, Clinton SK. 2013. Complex interactions between dietary and genetic factors impact lycopene metabolism and distribution. *Arch Biochem Biophys*, 539: 171-80.
- Moussa M, Landrier J, Reboul E, Ghiringhelli O, Comera C, Collet X, Fröhlich K, Böhm V, Borel P. 2008. Lycopene absorption in human intestinal cells and in mice involves scavenger receptor class B type I but not Niemann-Pick C1-like 1. *J Nutr*, 138: 1432-36.
- Najafi A, Taheri RA, Mehdipour M, Farnoosh G, Martínez-Pastor F. 2018. Lycopene-loaded nanoliposomes improve the performance of a modified Beltsville extender broiler breeder roosters. *Anim Reprod Sci*, 195: 168-175.
- Narciso Tomé AM. 2014. O Licopeno na prevenção do envelhecimento cutâneo - Ficção ou realidade. Faculdade de Farmácia da Universidade de Lisboa.
- Nguyen ML, Francis D, Schwartz SJ. 2001. Thermal isomerisation susceptibility of carotenoids in different tomato varieties. *J Sci Food Agric*, 81: 910-17.
- Nguyen ML, Schwartz SJ. 1998. Lycopene stability during food processing. *Proc Soc Exp Biol Med*, 218: 101-5.
- Nishino M, Miuchi T, Sakata M, Nishida A, Murata Y, Nakamura Y. 2011. Photostability of lycopene dispersed in an aqueous solution. *Biosci Biotechnol Biochem*, 75: 1389-1391.
- Nkondjock A, Ghadirian P, Johnson KC, Krewski D. 2005. Dietary intake of lycopene is associated with reduced pancreatic cancer risk. *J Nutr*, 135: 592-597.
- Orgeron R II, Pope J, Green V, Erickson D. 2019. Phytonutrient intake and body composition: Considering colors. *FFHD*, 9: 108-122.
- Palozza P, Parrone N, Catalano A, Simone R. 2010. Tomato lycopene and inflammatory cascade: Basic interactions and clinical implications. *Curr Med Chem*, 17: 2547-2563.
- Palozza P. 1998. Prooxidant actions of carotenoids in biologic systems. *Nutr Rev*, 56: 257-265.
- Pan WH, Yeh NH, Yang RY, Lin WH, Wu WC, Yeh WT, Sung MK, Lee HS, Chang SJ, Huang CJ, Lin BF, Chiang MT. 2018. Vegetable, fruit, and phytonutrient consumption patterns in Taiwan. *J Food Drug Anal*, 2: 145-153.
- Parada J, Aguilera JM 2007. Food microstructure affects the bioavailability of several nutrients. *J Food Sci*, 72: R21-32.
- Petropoulos SA, Sampaio SL, Gioia FD, Tzortzakis N, Roupheal Y, Kyriacou MC, Ferreira I. 2019. Grown to be blue- Antioxidants properties and health effects of coloured vegetables. Part I: Root vegetables. *Antioxidants*, 8: 617.

- Porrini M, Riso P. 2005. What are typical lycopene intakes? *J Nutr*, 135: 2042S-45S.
- Porter JW, Anderson DG. 1967. Biosynthesis of carotenoids. *Ann Rev Plant Physiol*, 18: 197-228.
- Prakash A, Kumar A. 2013. Lycopene protects against memory impairment and mito-oxidative damage induced by colchicine in rats: An evidence of nitric oxide signaling. *Eur J Pharmacol*, 721: 373-381.
- Qu M, Nan X, Gao Z, Guo B, Liu B, Chen Z. 2013. Protective effects of lycopene against methylmercury-induced neurotoxicity in cultured rat cerebellar granule neurons. *Brain Res*, 1540: 92-102.
- Qu M, Zhou Z, Chen C, Li M, Pei L, Chu F, Yang J, Wang Y, Li L, Liu C, Zhang L, Zhang G, Yu Z, Wang D. 2011. Lycopene protects against trimethyltin-induced neurotoxicity in primary cultured rat hippocampal neurons by inhibiting the mitochondrial apoptotic pathway. *Neurochem Int*, 59: 1095-1103.
- Rao AV, Argawal S. 1999. Role of lycopene as antioxidant carotenoid in the prevention of chronic diseases: A review. *Nutr Res*, 19: 305-323.
- Rao AV, Waseem Z, Agarwal S. 1998. Lycopene content of tomatoes and tomato products and their contribution to dietary lycopene. *Food Res Intern*, 31: 737-41.
- Reich P, Shwachman H, Craig JM. 1960. Lycopopenia: A variant of carotenemia. *N Engl J Med*, 262: 263-269.
- Rodriguez-Amaya DB. 2001. A Guide to Carotenoid Analysis in Foods; ILSI Press: Washington, USA, pp: 1-45.
- Rodriguez-Amaya DB, Kimura M. 2004. Carotenoids in foods. In *Harvestplus Handbook for Carotenoid Analysis*; IFPRI and CIAT: Washington, DC, USA, pp: 2-7.
- Sabbağ Ç, Sürücüoğlu MS. 2011. Likopen: İnsan sağlığında vazgeçilmez bir bileşen. *Gıda Teknolojileri Elektronik Dergisi*, 6: 27-41.
- Sachdeva AK, Chopra K. 2015. Lycopene abrogates A β (1-42)-mediated neuroinflammatory cascade in an experimental model of Alzheimer's disease. *J Nutr Biochem*, 26: 736-744.
- Sahin K, Orhan C, Sahin N, Küçük O. 2019. Anticancer Properties of Lycopene. In: Méridon JM, Ramawat K. Editors. *Bioactive molecules in food. reference series in phytochemistry*. Springer, London, UK, pp: 935-969.
- Sahin K, Yenice E, Tuzcu M, Orhan C, Mizrak C, Ozercan IH, Sahin N, Yilmaz B, Bilir B, Ozpolat B, Kucuk O. 2018. Lycopene protects against spontaneous ovarian cancer formation in laying hens. *J Cancer Prev*, 23: 25-36.
- Saini RK, Rengasamy KR, Mahomoodally FM, Keum Y-S. 2020. Protective effects of lycopene in cancer, cardiovascular, and neurodegenerative diseases: An update on epidemiological and mechanistic perspectives. *Pharmacol Res*, 155: 104730.
- Saltveit ME, Mencarelli F. 1988. Inhibition of ethylene synthesis and action in ripening tomato fruit by ethanol vapors. *J Am Soc Hort Sci*, 113: 572-576.
- Schierle J, Bretzel W, Buhler I, Faccin N, Hess D, Steiner K, Schuep W. 1996. Content and isomeric ratio of lycopene in food and human blood plasma. *Food Chem*, 59: 459-465.
- Schunck CA. 1903. The xanthophyll group of yellow colouring matters. *Proc R Soc London*, 72: 165-176.
- Selgas MD, Garcva ML, Calvo MM. 2009. Effects of irradiation and storage on the physico-chemical and sensory properties of hamburgers enriched with lycopene. *International J Food Sci Technol*, 44: 1983-1989.
- Shah H, Mahajan SR. 2014. Screening of topical gel containing lycopene and dexamethasone against UV radiation induced photoaging in mice. *Biomed Aging Pathol*, 4: 303-308.
- Shakeri A, Hashempur MH, Mojibian M, Aliasl F, Bioos S, Nejatbakhsh F. 2018. A comparative study of ranitidine and quince (*Cydonia oblonga* Mill) sauce on gastroesophageal reflux disease (GERD) in pregnancy: A randomised, open-label, active-controlled clinical trial. *J Obstet Gynaecol*, 38: 899-905.
- Sharma SK, Le Maguer M. 1996. Lycopene in tomatoes and tomato pulp fractions. *Ital J Food Sci*, 2: 107-113.
- Sheehy RE, Kramer M, Hiatt W. 1988. Reduction of polygalacturonase activity in tomato fruit by antisense RNA. *Proc Natl Acad Sci USA*, 85: 8805-8809.
- Shi J, Le Maguer M. 2010. Lycopene in Tomatoes: Chemical and Physical. *Crit Rev Food Sci Nutr*, 40: 1-42.
- Shi, J, Le Maguer M, Bryan M. 2002. Lycopene from tomatoes. In Shi J, Mazza G, Le Maguer M, editors. *Functional foods-biochemical and processing aspects*. CRC Press, New York, USA, pp: 135-168.
- Shoji T. 2007. Polyphenols as natural food pigments: changes during food processing. *Am J Food Technol*, 2: 570-581.
- Simpson DJ, Baqar MR, Lee TH. 1977. Chemical regulation of plastid development. III. Effect of light and CPTA on chromoplast ultrastructure and carotenoids of *Capsicum annum*. *Z Pflanzenphysiol*, 82: 189-209
- Stah W, Sies H. 1996. Lycopene: A biologically important carotenoid for humans? *Arch Biochem Biophys*, 336: 1-9.
- Stahl W, Sies H. 1992. Uptake of lycopene and its geometrical isomers is greater from heat-processed than from unprocessed tomato juice in humans. *J Nutr*, 122: 2161-66.
- Stahl W, Sundquist AR, Hamusch M, Schwarz W, Sies H. 1993. Separation of β -catonene geometrical isomers in biological samples. *Clin Chem*, 39: 810-814.
- Story EN, Kopec RE, Schwartz SJ, Harris, GK. 2010. An update on the health effects of tomato lycopene. *Annu Rev Food Sci Technol*, 1: 189-210.
- Su Q, Rowley KG, Balazs NDH. 2002. Carotenoids: Separation methods applicable to biological samples, *J Chromatogr B*, 781: 393-418
- Tonucci LH, Holden JM, Beecher GR, Khachik F, Davis C.S, Mulokon G. 1995. Carotenoid content in thermally processed tomato-based food products. *J Agric Food Chem*, 43: 579-586.
- Trumbo P, Yates AA, Schlicker S, Poos M. 2001. Dietary reference intakes: Vitamin A, vitamin K, arsenic, boron, chromium, copper, iodine, iron, manganese, molybdenum, nickel, silicon, vanadium, and zinc. *J Acad Nutr Diet*, 101: 294.
- Trumbo PR. 2005. Are there adverse effects of lycopene exposure? *J Nutr*, 135: 2060s-2061s.
- Tyssandier V, Cardinault N, Caris-Veyrat C, Amiot MJ, Grolier P, Bouteloup C, Azais-Braesco V, Borel P. 2002. Vegetable-borne lutein, lycopene, and beta-carotene compete for incorporation into chylomicrons, with no adverse effect on the medium-term (3-wk) plasma status of carotenoids in humans. *Am J Clin Nutr*, 75: 526-34.
- Ukai N, Lu Y, Etoh H, Yagi A, Ina K, Oshima S, Ojima F, Sakamoto H, Ishiguro Y. 1994. Photosensitized oxygenation of lycopene. *Biosci Biotechnol Biochem*, 58: 1718-1719.
- Unlu NZ, Bohn T, Clinton SK, Schwartz SJ. 2005. Carotenoid absorption from salad and salsa by humans is enhanced by the addition of avocado or avocado oil. *J Nutr*, 135: 431-36.
- Unlu NZ, Bohn T, Francis D, Clinton SK, Schwartz SJ. 2007. Carotenoid absorption in humans consuming tomato sauces obtained from tangerine or high- β -carotene varieties of tomatoes. *J Agric Food Chem*, 55: 1597-1603.
- Veeramachaneni S, Ausman LM, Choi SW, Russell RM, Wang XD. 2008. High dose lycopene supplementation increases hepatic cytochrome P4502E1 protein and inflammation in alcohol-fed rats. *J Nutr*, 138: 1329-1335.
- Wang X-D. 2004. Carotenoid Oxidative/Degradative Products

- and Their Biological Activities. Marcel Dekker; New York, NY, USA.
- Xianquan S, Shi J, Kakuda Y, Yueming J. 2005. Stability of lycopene during food processing and storage. *J Med Food*, 8: 413-22
- Xu F, Yuan QP, Dong HR. 2006. Determination of lycopene and beta-carotene by high-performance liquid chromatography using sudan I as internal standard. *J Chromatogr B*, 838: 44-49.
- Yılmaz T. 2011. Domates İşleme Atıklarından Ultrason Destekli Likopen Ekstraksiyonu İşleminin Optimizasyonu. Yüksek Lisans Tezi, Ege Üniversitesi, Fen Bilimleri Enstitüsü, İzmir, pp: 128.
- Zeng Z, He W, Jia Z, Hao S. 2017. Lycopene improves insulin sensitivity through inhibition of STAT3/Srebp-1c-mediated lipid accumulation and inflammation in mice fed a high-fat diet. *Exp Clin Endocrinol Diabetes*, 125: 610-617.
- Zengin F, Kurt Ş. 2018. Likopen ve likopenin insan sağlığı açısından önemi. *ADYÜTAYAM*, 6: 30-45.
- Zhang F, Fu Y, Zhou X, Pan W, Shi Y, Wang M, Zhang X, Qi D, Li L, Ma K, Tang R, Zheng K, Song Y. 2016. Depression-like behaviors and heme oxygenase-1 are regulated by lycopene in lipopolysaccharideinduced neuroinflammation. *J Neuroimmunol*, 298: 1-8.
- Zumbrunn A, Uebelhart P, Eugster CH. 1985. HPLC of carotenes with γ -end groups and (Z)-configuration at terminal conjugated double bonds, isolation of (5Z)-lycopene from tomatoes. *Helv Chim Acta*, 68: 1540-1542.
- Zuorro A, Lavecchia R, Medici F, Piga L. 2012. Enzyme-assisted production of tomato seed oil enriched with lycopene from tomato pomace. *Food Bioproc Technol*, 6: 3499-3509.